INTERAGENCY MONITORING OF PROTECTED VISUAL ENVIRONMENTS

# IMPROVE

ISSN No. 0737-5352-26

# SPATIAL AND TEMPORAL PATTERNS AND THE CHEMICAL COMPOSITION OF THE HAZE IN THE UNITED STATES:

## An Analysis of Data from the IMPROVE Network, 1988-1991

CIRA Cooperative Institute for Research in the Atmosphere

Colorado State University

February, 1993

ISSN No. 0737-5352-26

# SPATIAL AND TEMPORAL PATTERNS AND THE CHEMICAL COMPOSITION OF THE HAZE IN THE UNITED STATES:

## An Analysis of Data from the IMPROVE Network, 1988 - 1991

by

James F. Sisler
Dale Huffman
Cooperative Institute for Research in the Atmosphere
CIRA-Foothills Campus
Colorado State University
Fort Collins, CO 80523

Douglas A. Latimer
Latimer and Associates
679 Quince Circle
Boulder, CO 80304

Principal Investigators

William C. Malm
National Park Service
CIRA-Foothills Campus
Colorado State University
Fort Collins, CO 80523

Marc L. Pitchford
Environmental Protection Agency
Environmental Monitoring & Systems Laboratory
944 E. Harmon
Las Vegas, NV 89193

February, 1993

DISCLAIMER

The assumptions, findings, conclusions, judgements, and views presented herein are those of the authors and should not be interpreted as necessarily representing official National Park Service policies.

## ACKNOWLEDGEMENTS

This report is the result of a collaborative effort involving the authors and a number of individuals from several institutions. We thank Drs. Thomas Cahill and Robert Eldred of the University of California at Davis for their efforts in developing the IMPROVE aerosol monitoring network, managing the aerosol database, and providing input to the report concerning aerosol sampling and analysis. Also, we thank Dr. Judith Chow and associates at Desert Research Institute, University of Nevada Systems at Reno for their input on the analysis of carbonaceous species. We also wish to acknowledge Mr. John Molenar and Dr. David Dietrich of Air Resource Specialists in Fort Collins, Colorado for developing and managing the IMPROVE visibility monitoring network, supplying the optical and relative humidity data, and for their input to this report.

We would like to recognize Dr. Marc Pitchford of the U. S. Environmental Protection Agency's Environmental Monitoring Support Laboratory in Las Vegas, Nevada for his efforts in establishing, designing, and managing the IMPROVE program and for his comments on the draft of this report.

We are also indebted to the following reviewers for their useful input to this report: Drs. Peter Mueller and Pradeep Saxena of the Electric Power Research Institute, Mr. John Core of WESTAR, Mr. Rich Poirot of the Vermont Air Program, Drs. Warren White and Ed Macias of CAPITA, and Mr. Robert Kellam and staff at the Office of Air Quality Planning and Standards, U. S. Environmental Protection Agency.

TABLE OF CONTENTS

# LIST OF FIGURES

# LIST OF TABLES

7 MEASURED LIGHT EXTINCTION

## LIST OF APPENDICES

# OVERVIEW AND SUMMARY

This report describes data obtained from the first three years, March 1988 through February 1991, of the IMPROVE measurement program (Interagency Monitoring of Protected Visual Environments). IMPROVE is a cooperative visibility monitoring effort between the U.S. Environmental Protection Agency, federal land management agencies, and state air agencies.

The objectives of IMPROVE are:

(1) To establish current background visibility in Class I areas;

(2) To identify chemical species and emission sources responsible for existing man-made visibility impairment; and

(3) To document long-term trends.

Due to resource and funding limits, IMPROVE was not able to measure visual air quality in all 156 mandatory Class I areas that are afforded visibility protection by the Clean Air Act. Instead, 36 IMPROVE and NPS/IMPROVE protocol sites were selected to represent the distribution of visibility and aerosol concentrations over the United States. Each site has aerosol monitoring and scene monitoring (automated cameras) equipment. However, only 20 sites have optical monitoring equipment (transmissometers) to measure light extinction. Figure S.1 shows the locations of these sites. On the basis of regional similarities, the sites were grouped into 19 regions as shown in Table S.1.

## S.1 Monitoring Methodologies

Aerosol monitoring in the IMPROVE network is accomplished by a combination of particle sampling and sample analysis. The sampler was designed specifically for IMPROVE. It collects four simultaneous samples: one $PM_{10}$ sample (particles less than 10 $\mu$m in diameter) on a Teflon filter and three $PM_{2.5}$ samples on Teflon, nylon, and quartz filters. The IMPROVE sampler is programmed to collect two 24-hour duration samples per week (i.e., 26 per season, 104 per year). The $PM_{10}$ filter is used to determine total $PM_{10}$ mass. The $PM_{2.5}$ Teflon filter is used to measure total fine aerosol mass, individual chemical species using Proton Induced X-ray Emission (PIXE) and Proton Elastic Scattering Analysis (PESA), and light absorption coefficient using the Laser Integrating Plate Method (LIPM). The nylon filter is used to measure nitrate and sulfate aerosol concentrations with Ion Chromatography (IC). Finally, the quartz filters are analyzed for organic and elemental carbon using the Thermal Optical Reflectance (TOR) method.

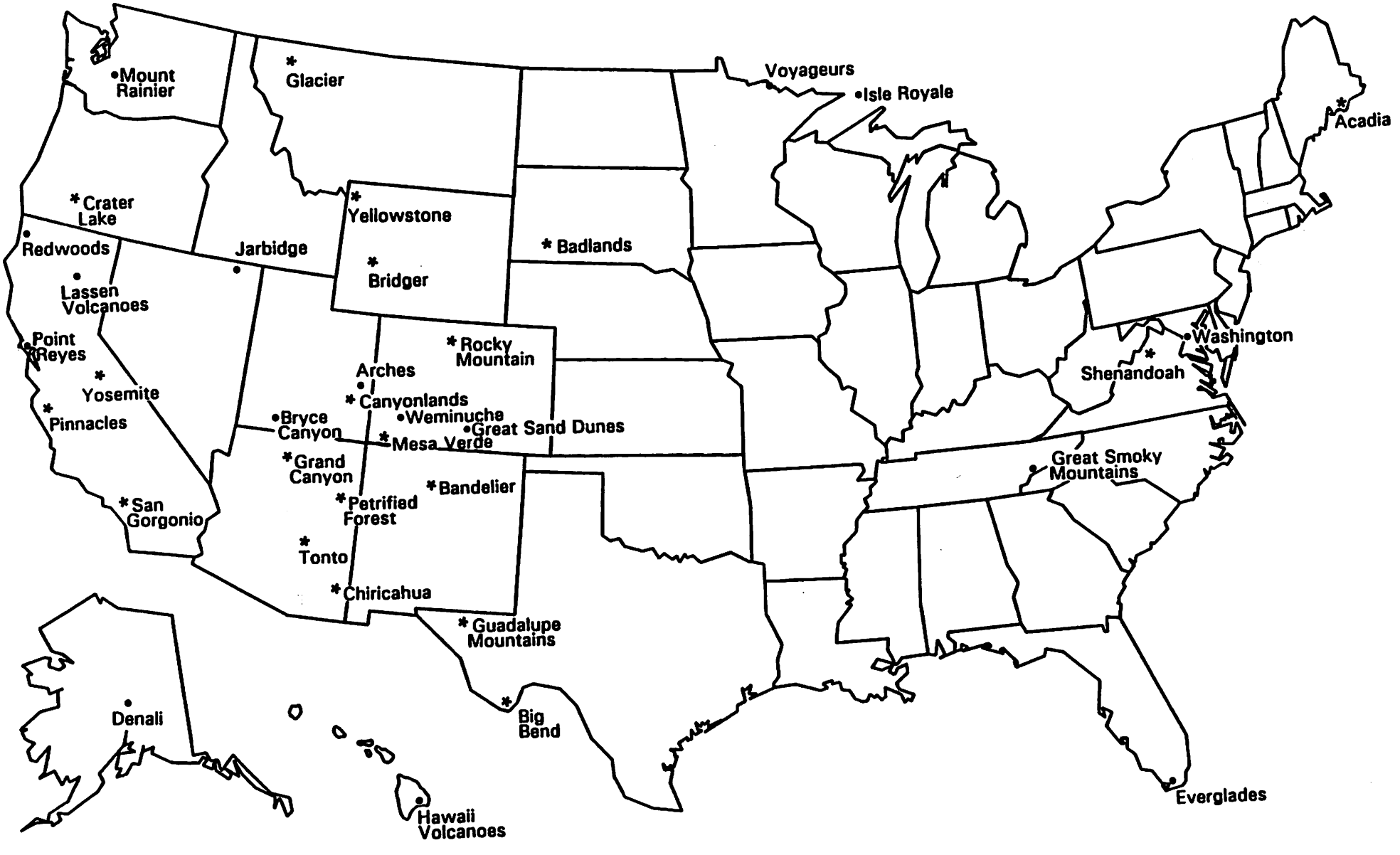


Figure S.1. The 36 IMPROVE sites included in the report. Sites designated by an asterisk have both aerosol and visibility monitoring.

Table S.1 IMPROVE and NPS/IMPROVE protocol sites according to region.

**Alaska (AKA)**
- Denali National Park (DENA)

**Appalachian Mountains (APP)**
- Great Smoky Mountains National Park (GRSM)
- Shenandoah National Park (SHEN)

**Boundary-Waters (BWA)**
- Isle Royale National Park (ISRO)
- Voyageurs National Park (VOYA)

**Cascade Mountains (CAS)**
- Mount Rainier National Park (MORA)

**Central Rocky Mountains (CRK)**
- Bridger Wilderness Area (BRID)
- Great Sand Dunes National Monument (GRSA)
- Rocky Mountain National Park (ROMO)
- Weminuche Wilderness Area (WEMI)
- Yellowstone National Park (YELL)

**Coastal Mountains (CST)**
- Pinnacles National Monument (PINN)
- Point Reyes National Seashore (PORE)
- Redwood National Park (REDW)

**Colorado Plateau (CPL)**
- Arches National Park (ARCH)
- Bandelier National Monument (BAND)
- Bryce Canyon National Park (BRCA)
- Canyonlands National Park (CANY)
- Grand Canyon National Park (GRCA)
- Mesa Verde National Park (MEVE)
- Petrified Forest National Park (PEFO)

**Florida (FLA)**
- Everglades (EVER)

**Great Basin (GBA)**
- Jarbidge Wilderness Area (JARB)

**Hawaii (HAW)**
- Hawaii Volcanoes National Park (HAVO)

**Northeast (NEA)**
- Acadia National Park (ACAD)

**Northern Great Plains (NGP)**
- Badlands National Monument (BADL)

**Northern Rocky Mountains (NRK)**
- Glacier National Park (GLAC)

**Sierra Nevada (SRA)**
- Yosemite National Park (YOSE)

**Sierra-Humboldt (SRH)**
- Crater Lake National Park (CRLA)
- Lassen Volcanoes National Park (LAVO)

**Sonoran Desert (SON)**
- Chiricahua National Monument (CHIR)
- Tonto National Monument (TONT)

**Southern California (SCA)**
- San Gorgonio Wilderness Area (SAGO)

**Washington, D.C. (WDC)**
- Washington, D.C. (WASH)

**West Texas (WTX)**
- Big Bend National Park (BIBE)
- Guadalupe Mountains National Monument (GUMO)

Transmissometers were employed to measure the light extinction coefficient at 20 of the IMPROVE sites. These instruments measure the light transmitted through the atmosphere over a distance of one to fifteen kilometers. The light transmitted between the light source (transmitter) and the light monitoring component (receiver) is converted to the path-averaged light extinction coefficient ($b_{ext}$). Relative humidity was measured continuously at the transmissometer sites.

## S.2 Assessing Aerosol Measurement Quality

The self-consistency and overall quality of the aerosol mass and chemical composition measurements were evaluated by intercomparing independent measurements.

Simultaneous measurements of elemental sulfur and of sulfate ions, on the Teflon and nylon filters respectively, were compared to assess their quality. The two sets of measurements agreed very well, indicating that almost all sulfur was due to sulfate species. The more precise elemental sulfur measurements on the Teflon filters were used to estimate sulfate concentrations in all of the studies, including reconstructions of fine mass and light extinction, acidity, and organic mass calculations.

Organic mass (OM) was estimated two different ways: From hydrogen mass measured on the Teflon filter (OMH); and from organic carbon mass measured on the quartz filter (OMC). Estimation of the organic mass by hydrogen also involved knowing or assuming the aerosol sulfate acidity. The two estimates of organic mass agreed well except for the third year of data, when a positive artifact affected the OMH estimate. This artifact was identified as resulting from problems associated with a batch of Teflon filters. This problem did not affect reconstructed extinction estimates; therefore, extinction calculations were reported for all three years. However, because hydrogen was used in estimates of acidity, only the first two years of data were used to estimate aerosol acidity. The quartz-filter based organic carbon measurements were used to estimate organics in reconstructions of fine mass and light extinction.

Elemental (light-absorbing) carbon, measured on the quartz filters using the Thermal Optical Reflectance method (TOR), was compared to the light absorption coefficient ($b_{abs}$), measured on the Teflon filters using the Laser Integrating Plate Method (LIPM). $b_{abs}$ should agree very well with the elemental carbon TOR measurements and less well with the organic carbon TOR measurements. However, the portion of elemental carbon extracted at high temperature (ECHT) showed little or no correlation with $b_{abs}$. Also, $b_{abs}$ correlated well with both low-temperature-extracted elemental carbon (ECLT) and high-temperature-extracted organic carbon (OCHT). Further, the form of the correlation between $b_{abs}$ and ECLT (as shown in scatter plots) follows the form of the correlation between OCHT and ECLT. Finally, the ratio of $b_{abs}$ to elemental carbon mass was approximately twice as large as literature values. These comparisons were all unexpected, and indicated possible errors in the estimation of elemental and organic carbon. A systematic error in the measurement of $b_{abs}$ is possible but less likely, since the correlations noted above would still require explanation. Nevertheless, to be consistent with other studies, light-absorbing carbon was assumed to be the sum of ECLT and ECHT as measured from the quartz filters by the TOR method.

## S.3 Aerosol Acidity

Aerosol sulfate can be fully neutralized as ammonium sulfate [$(NH_4)_2SO_4$], partially neutralized as in ammonium bisulfate [$NH_4HSO_4$], or fully acidic as sulfuric acid [$H_2SO_4$]. Hydrogen is associated with sulfate, nitrate, and organic carbon. However, the Teflon filters are analyzed in a vacuum during which nitrate aerosol is assumed to volatilize. Therefore, one should be able to estimate the acidity of the sulfate aerosol by using the measured aerosol concentrations of hydrogen, sulfate, and organic carbon in a statistical analysis to determine the hydrogen-sulfate ratio which is indicative of acidity. Sites identified as acidic by this procedure include Hawaii Volcanoes in Hawaii; Mount Rainier in the Pacific Northwest; Point Reyes, Redwoods, and Pinnacles in Northern California; Shenandoah in the East; and Tonto in southeastern Arizona. The uncertainties in the statistical approach used to derive aerosol acidity are significant. However, these results appear to be consistent with the fact that ammonia may not be present in sufficient quantities at coastal sites and in the Appalachian Mountains to neutralize sulfuric acid, and that sites with relatively fresh sulfate (such as Shenandoah, which is near power plants, and Tonto, which is near copper smelters) may not have had time for neutralization.

## S.4 Spatial and Seasonal Distribution of Aerosol Concentration and Chemical Composition

Fine aerosol concentrations are highest in the eastern United States (in the Appalachian Mountains and in Washington, D.C.). Concentrations are also relatively high in Southern California. The lowest concentrations occur in the Great Basin in Nevada, the Colorado Plateau in the Four Corners states, and in Alaska.

The largest single component of the fine aerosol in the East is sulfate, while in the Pacific Northwest it is organics and in Southern California it is nitrate. In general, the largest mass fractions of the fine aerosol are sulfate and organics. Of the 19 regions in the IMPROVE network, organic carbon is the largest single component in nine regions (Alaska, Cascades, Colorado Plateau, Central Rockies, Coast Mountains, Great Basin, Northern Rockies, Sierra Nevada, and Sierra-Humboldt). Sulfate is the largest single component of fine aerosol in six regions, primarily in the East (Appalachian Mountains, Florida, Hawaii, Northeast, Northern Great Plains, and Washington, D.C.). The contributions of organic carbon and sulfate are approximately equal in three regions (Boundary Waters, Sonoran Desert, and West Texas). Soil is the next largest contributor, followed by nitrate and light-absorbing carbon. Nitrate is the largest component of fine aerosol in Southern California only.

With few exceptions, average fine mass concentrations, as well as the sulfate, organic carbon, and light-absorbing carbon components of fine mass, are highest in summer. Soil concentrations are highest in spring or summer. Nitrate concentrations are generally highest in winter or spring.

## S.5 Spatial and Seasonal Distribution of Reconstructed Light Extinction and Species Contributions

The light extinction coefficient ($b_{ext}$) is calculated from the measured aerosol species concentrations by multiplying the concentration of a given species by its light extinction efficiency, and summing over all species. Since sulfates and nitrates, as well as some organics, are hygroscopic, their light extinction efficiencies increase with relative humidity; therefore, extinction efficiencies for soluble species must be adjusted according to the seasonal and annual average relative humidity at each site.

Figures S.2a through S.2f summarize the spatial distribution of reconstructed light extinction (in $Mm^{-1}$), as well as the contributions to the total extinction from coarse particles and fine soil, sulfate, organics, nitrate, and light-absorbing carbon, averaged over the first three years of IMPROVE (March 1988 through February 1991).

Reconstructed light extinction varies throughout the United States in a way analogous to fine aerosol concentrations. The greatest light extinction occurs in the eastern United States and in Southern California, while the least light extinction occurs in the nonurban West (e.g., the Great Basin of Nevada and the Colorado Plateau) and in Alaska. However, since relative humidity (and hence the light scattering efficiency of sulfate, nitrate, and some organics) is higher in the East than in the West, the difference between eastern and western light extinction is even more pronounced than the difference in aerosol concentrations.

Fine aerosols are the most effective in scattering light and are the major contributors to light extinction. In most cases, the sulfate component of fine aerosol is the largest single contributor to light extinction. This is because sulfate, being hygroscopic, generally has a higher light extinction efficiency than other species due to associated liquid water. This is especially true in the eastern United States, where relative humidity is high. In the Appalachian Mountains (Shenandoah and Great Smoky Mountains), sulfate accounts for 2/3 of the total aerosol light extinction throughout the year, and 3/4 of the total in summer. Sulfate is the largest single contributor to light extinction in 12 of the 19 regions, and is comparable with organics as the most significant contributor in two additional regions (Cascades and Central Rockies). Organic carbon is the largest single contributor to light extinction in four of the 19 regions (Great Basin, Northern Rockies, Sierra Nevada, and Sierra-Humboldt) and is a major contributor in the two previously mentioned regions. Smaller contributions come from windblown dust (coarse particles and fine soil) and nitrate. Nitrate is the single largest contributor to light extinction only in Southern California. Light-absorbing carbon is generally the smallest contributor.

Generally, reconstructed light extinction is highest in summer and lowest in winter; however, there are many exceptions to this general rule. Higher extinction occurs in summer generally because of elevated sulfate and carbonaceous aerosol concentrations. Also, higher average RH's occur in the East during the summer, which increases extinction.

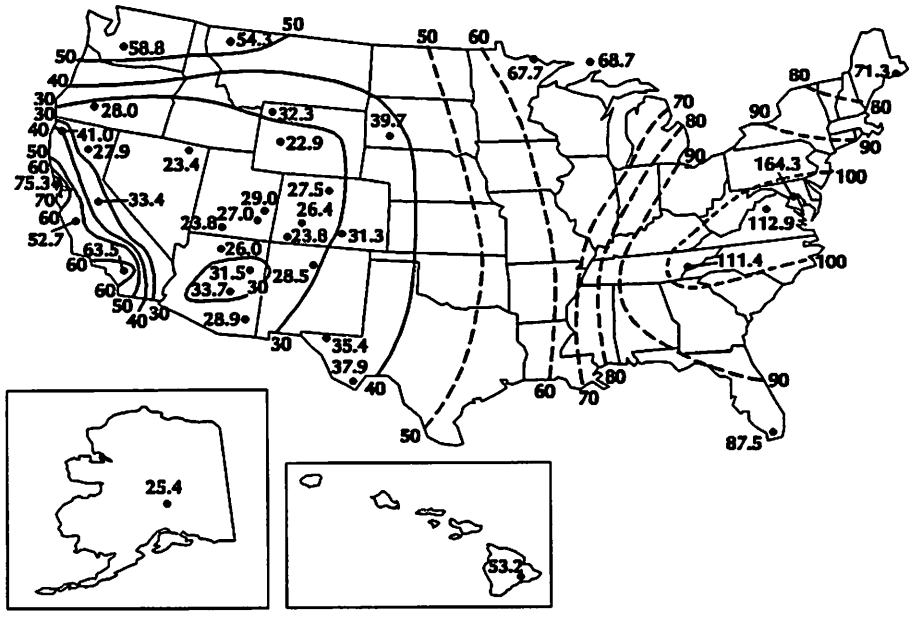


S.2 (a). Total light extinction $b_{ext}$ ($Mm^{-1}$)

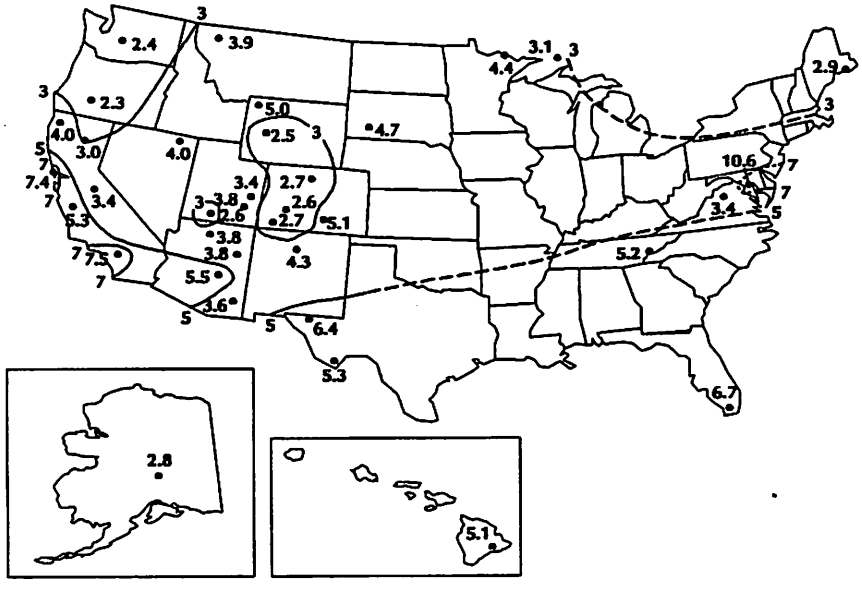


S.2 (b). Extinction due to coarse particles and fine soil ($Mm^{-1}$)

Figure S.2 Average reconstructed light extinction coefficient ($Mm^{-1}$) calculated from the aerosol concentrations measured during the first three years of IMPROVE, March 1988 through February 1991. The various panels of this figure show total extinction (including Rayleigh scattering due to air) and the contributions due to the various aerosol components: coarse particles and fine soil, sulfate, organic carbon, nitrate, and light-absorbing carbon.

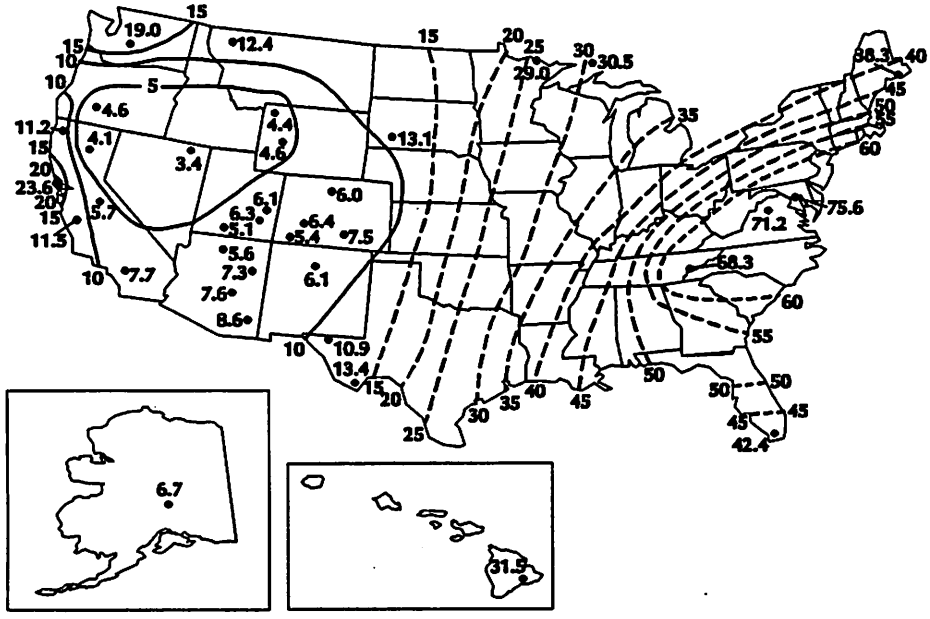


S.2 (c). Extinction due to sulfate ($Mm^{-1}$)

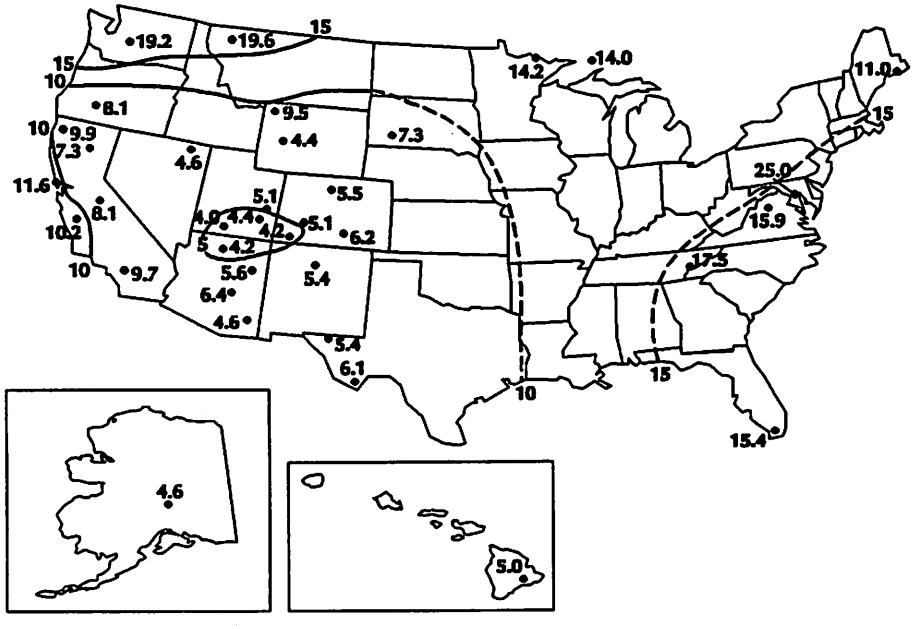


S.2 (d). Extinction due to organic carbon ($Mm^{-1}$)

Figure S.2 Continued.

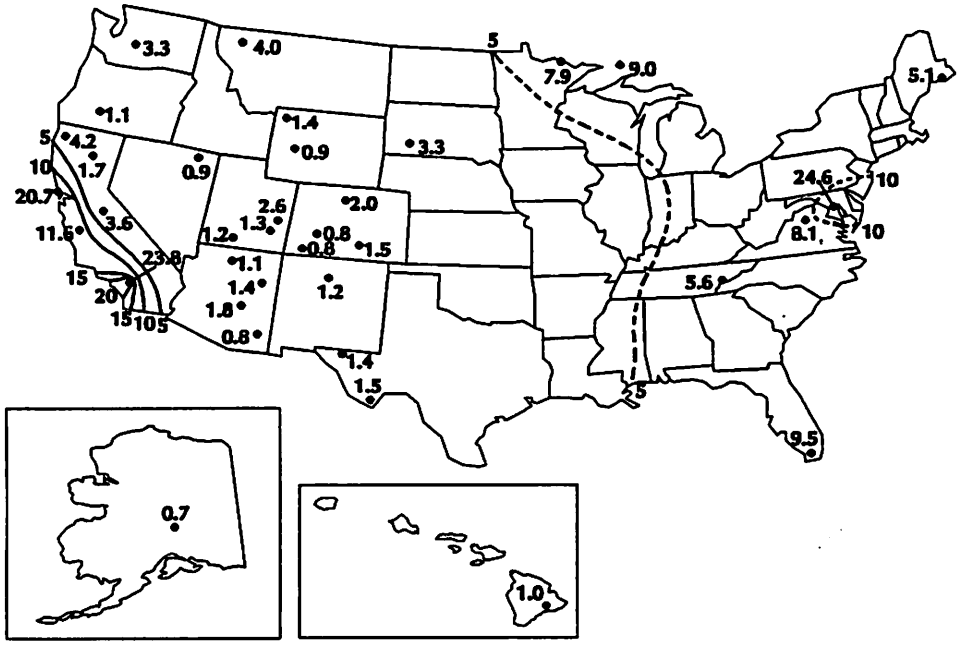


S.2 (e). Extinction due to nitrate ($Mm^{-1}$)

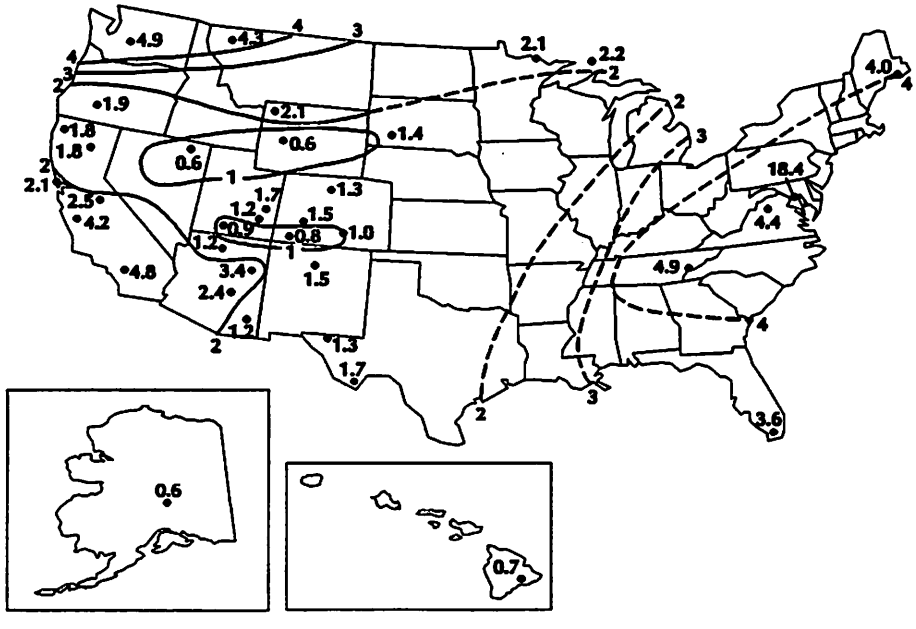


S.2 (f). Extinction due to light-absorbing carbon ($Mm^{-1}$)

Figure S.2. Continued.

## S.6 Spatial and Seasonal Trends in Visibility in the United States

To show the effect on visibility of aerosol extinction, the deciview (dv) scale is applied to the total (Rayleigh included) reconstructed aerosol extinction (see Chapter 1). By utilizing the dv scale, the effect of light extinction on visibility is portrayed in a way that is approximately linear with respect to perceived visual air quality.

Because higher extinction coefficients lead to higher dv numbers, the geographic trends in visibility follow the trends in reconstructed extinction. Pristine or Rayleigh conditions correspond to a dv of zero. A one or two dv change is usually associated with the minimal or just noticeable change (JNC) in visibility that is perceivable by an average individual.

Figure S.3 shows isopleths of deciviews averaged over the first three years of IMPROVE. The smallest dv or best visibility is reported at Bridger Wilderness with 8.3 dv. A broad region which includes the Great Basin, most of the Colorado Plateau, and portions of the Central Rockies has visibility impairment of less than 10 dv. Moving in any direction from this region generally results in increasing dv. West of the Sierra Range and including Southern California one finds dv values in excess of 15, with a maximum value of 20.2 dv at Point Reyes. The northwest United States and all of the eastern half of the United States have in excess of 15 dv of impaired visibility. The region east of the Mississippi and south of the Great Lakes has impairment in excess of 20 dv, with the Appalachian region exceeding 24 dv. The highest annual dv, 28 dv, is reported at Washington D.C.

The general spatial trend noted above for the annual average dv generally holds true for each season's average dv as well. Specifically, the least impairment occurs in all or part of the Great Basin, Colorado Plateau, and Central Rockies, with gradients of increasing dv in any direction. The best visibility occurs during the winter and the worst in the summer. Visibility impairment in the spring and autumn are comparable.

## S.7 Measured Light Extinction

Figure S.4 summarizes the light extinction measurements made with transmissometers during the first three years of IMPROVE. This figure shows both the seasonal and annual averages of measured light extinction for all periods, and for periods excluding fog, precipitation, and low clouds. As was the case for reconstructed light extinction, highest measured light extinction occurs in the eastern United States and, to a lesser extent, in Southern California.

Light extinction is significantly higher in the eastern United States when weather-related events are included. These events affect light extinction approximately two-thirds of the time at Shenandoah and Acadia National Parks.

When measured light extinction is compared to the reconstructed value calculated from the measured concentrations of the major aerosol species, good comparisons are formed (within 10%) for the Appalachian Mountains, Central Rockies, Colorado Plateau, Northeast, Northern

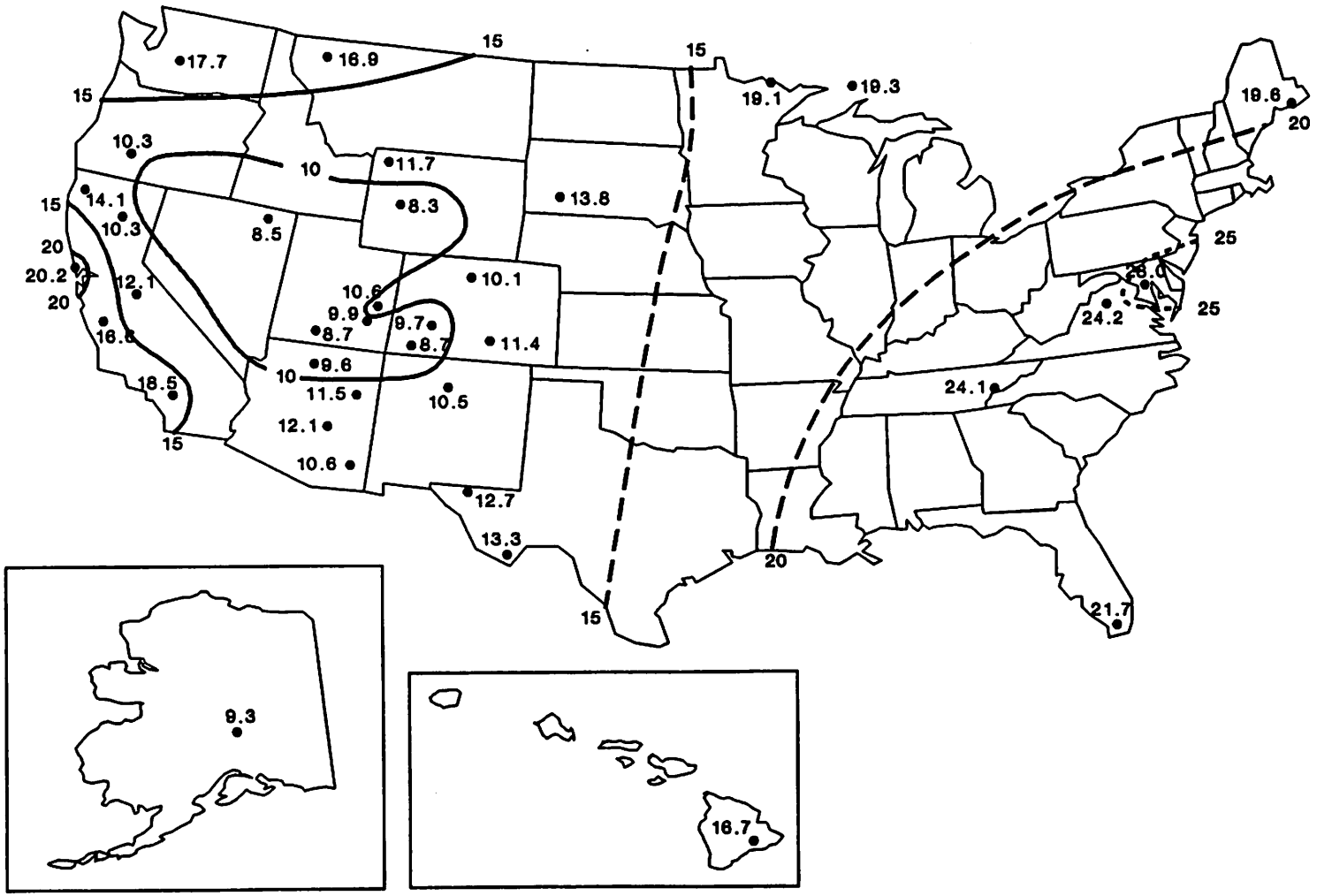


Figure S.3. Average visibility impairment in deciviews calculated from total (Rayleigh included) reconstructed light extinction for the first three years of IMPROVE, March 1988 through February 1991.

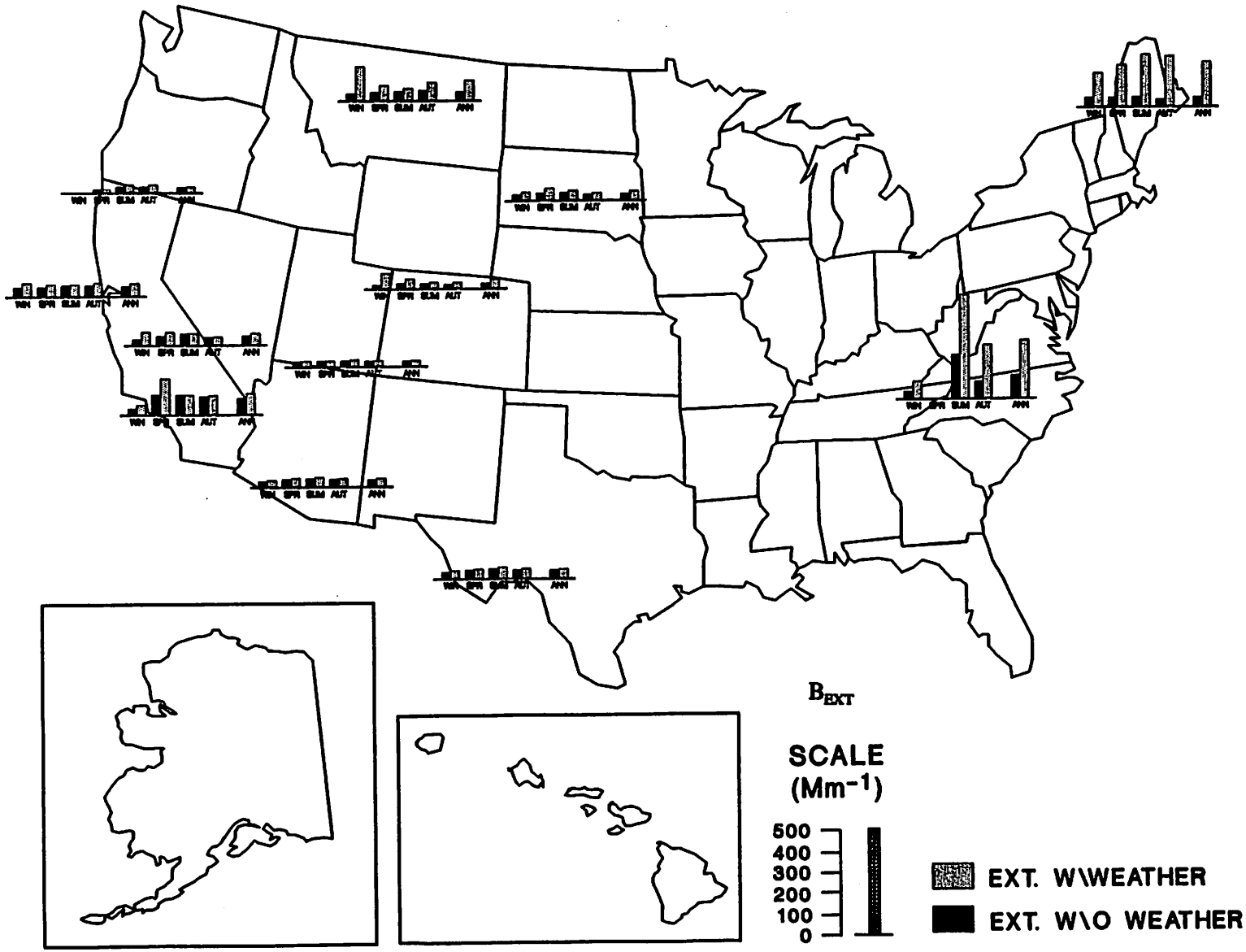


Figure S.4. Spatial and seasonal variation of measured light extinction coefficient ($Mm^{-1}$) in the U.S. for the three-year period, March 1988 through February 1991. From left to right, the bars show winter, spring, summer, autumn, and annual averages. Open bars include all time periods; dark bars exclude periods with fog, precipitation, and low clouds.

Great Plains, and Northern Rockies. However, reconstructed extinction is about 80% of measured light extinction in the Appalachian Mountains during summer and in the Pacific Coast, Southern California, Sonoran Desert, and West Texas regions. The worst comparison is at Yosemite in Sierra Nevada, where reconstructed light extinction is only 50% of the measured extinction. This may be because the aerosol monitor is above the mixed layer much of the time. The summertime Appalachian Mountains reconstructed extinction may be too low because of the assumption of fully-neutralized sulfate (ammonium sulfate). It is likely that the elevated sulfate concentrations in the Appalachian Mountains are acidic, and therefore have a higher light scattering efficiency than ammonium sulfate. Currently it is not clear why the reconstructed light extinction is less than measured light extinction in the other regions. One reason may be that the reconstructed light extinction is based on a 24-hour average, while measured extinction is hourly and often quite intermittent due to weather influences. Another possible explanation is that measured extinction is an average over the entire length of the transmissometer sight path, while aerosol measurements are at a point.

## S.8 Recommended Future Research

There are a number of uncertainties raised by the work described in this report that deserve additional study.

Organic Aerosol Measurement. Organic aerosol mass is calculated from the organic carbon mass collected on the quartz filters and measured by the TOR process. Adjustments are made to the organic carbon mass to correct for the adsorption of organic aerosols on the filter. However, this adjustment often results in negative concentrations. This area needs to be considered in future studies. Also, the mass fractions of hydrogen and carbon in organics are based on an assumption of the hydrocarbon type. Future research should evaluate these fractions on the basis of the most common organic molecules in the samples. The organic artifact seen on the Teflon filter in the third year should be carefully evaluated in future studies, when additional years of data are analyzed. Finally, the correlation between light absorption and organic carbon measured on the quartz filter with TOR was unexpected. Additional research should be directed toward determining whether all light-absorbing carbon is in fact elemental as determined by TOR, and in particular whether the TOR pyrolyzed carbon may be light-absorbing in the ambient aerosol.

Light-Absorbing Carbon Measurement. The work reported here shows that light absorption correlates equally well with organic carbon and elemental carbon. It may be instructive to study the sensitivity of the results presented in this report to the elemental carbon measurements. For example, the measurement of the light absorption coefficient $b_{abs}$ can be used directly to assess the light absorption contribution to the light extinction, and to calculate light-absorbing carbon aerosol concentrations (by dividing $b_{abs}$ by the light absorption efficiency).

Hygroscopicity of Aerosols. The relative humidity correction terms applied to the sulfate, nitrate, and organic aerosols need to be re-evaluated. The sulfate and nitrate RH factors are based on ammonium sulfate. Specific curves should be developed for ammonium nitrate, which has a different deliquescence point than sulfate. Also, acidic sulfates (e.g., sulfuric acid

and ammonium bisulfate) have higher water contents and higher light scattering efficiencies than ammonium sulfate. Finally, the humidity correction curve for organics is a very rough approximation based on aerosol measurements in Europe (Hanel, 1981). The hygroscopicity of organics is not currently well understood. Basic research is required in this area. Until such research is available, alternative assumptions regarding organic hygroscopicity should be tested.

Comparisons of Measured and Reconstructed Light Extinction. At many sites the light extinction estimated from concentrations of the major aerosol species underestimates measured light extinction. At some sites improved RH correction factors may provide better agreement. At other sites, it is currently not clear why reconstructed extinction underestimates measured light extinction. More work is required to resolve these differences and to improve the process of reconstructing light extinction.

Aerosol Acidity. The statistical analysis of aerosol acidity was based on a set of assumptions and on linear regression. More advanced variance-weighted regression techniques need to be applied. Physically incorrect results (e.g., overneutralization) are obtained at some sites. Sites with acidic aerosols should be flagged so that RH correction curves for acidic aerosols can be used.

In addition to the above refinements in the analyses conducted in this report, additional data analysis is recommended. For example, back trajectory analysis and spatial/temporal pattern analysis of episodes is recommended to determine the source region contributions to elevated concentrations. Also, the cleanest days should be studied to determine the source areas and meteorological causes of clean air.

# CHAPTER 1

# INTRODUCTION

In Section 169A of the Clean Air Act as amended August 1977, Congress declared, as a national goal, "the prevention of any future, and the remedying of any existing, impairment of visibility in mandatory Class I Federal areas which impairment results from manmade air pollution." Mandatory Class I Federal areas are national parks larger than 6000 acres, wilderness areas larger than 5000 acres, and international parks regardless of size, all of which were in existence on August 7, 1977. There are 158 Class I areas, of these areas 156 have been identified as having visibility related attributes that require protection.

This section of the Clean Air Act required the Environmental Protection Agency (EPA) to promulgate regulations requiring states to incorporate Class I area visibility protection in their State Implementation Plans (SIPs). These EPA regulations, promulgated on December 2, 1980, included a section requiring the states to develop a monitoring strategy for evaluating visibility in the mandatory Class I areas and to use monitoring data in decisions required by the visibility protection program. On July 12, 1985, EPA promulgated federal regulations for states that did not submit visibility SIPs.

The 1980 EPA regulations called for the establishment of a cooperative visibility monitoring effort between the EPA and several federal land management agencies: the National Park Service (NPS), the Fish and Wildlife Service (FWS), the Bureau of Land Management (BLM), and the Forest Service (FS). In 1991 several additional organizations joined the effort: State and Territorial Air Pollution Program Association (STAPPA), Western States Air Resources Council (WESTAR), and Northeast States for Coordinated Air Use Management (NESCAUM).

This cooperative visibility monitoring effort was named IMPROVE, for the Interagency Monitoring of Protected Visual Environments.

This report is the first in a series of annual reports that describe the data collected by the IMPROVE monitoring network. The objectives of this report are three-fold:

(1) To describe the spatial and temporal variation of visibility, as measured by the light extinction coefficient, and the chemical composition of the visibility-

degrading aerosol[1] for the first three years of operation of the network: Spring 1988 through Winter 1991;

(2) To provide a first estimate of the apportionment of visibility impairment to the fundamental chemical species, such as sulfates, nitrate, organics and elemental carbon, and soil dust; and

(3) To compare measurements of light extinction to calculations of light extinction reconstructed from the component chemical species.

## 1.1 Objectives of Visibility Monitoring

The primary objectives of IMPROVE are the following:

(1) To establish current background visibility levels in Class I areas;

(2) To identify chemical species and emission sources responsible for existing man-made visibility impairment; and

(3) To document long-term trends for assessing progress toward the national visibility goal.

By measuring visibility routinely over a network and over a sufficiently long period of time, the first and third objectives of IMPROVE can be met. The monitoring also meets a portion of the second objective: the identification of the chemical composition of the visibility-degrading aerosol.

Each of these IMPROVE objectives are discussed in greater detail below.

Establish Current Visibility. This is necessary for two reasons. First, visibility levels monitored at a Class I area, when compared to surrounding area visibility or area estimates for natural levels, may be sufficient to indicate man-made impairment. Second, knowledge of existing visibility levels is required to model the anticipated visibility effects of proposed emission sources, because increments of pollution are more noticeable in clear conditions.

Establishment of present visibility levels requires monitoring which is appropriate for both surface and elevated layer impairment distributions. Optical monitoring systems, such as the transmissometer, are appropriate for surface haze monitoring, while scene monitoring with photography is the only practical way to routinely monitor elevated layers.

---

[1]An aerosol is a suspension of fine and coarse solid and liquid particles in air. Particles, especially fine particles less than 2.5 $\mu$m, scatter light and degrade the visual information content of a scene (e.g., contrast, color, line, and texture). Fine particles consist of different chemical species either within the same particle (internally mixed) or in different particles (externally mixed). Significant chemical species found in particles include sulfates, nitrate, organic and elemental carbon, and soil dust. The sulfates, nitrate, and some hygroscopic organics absorb water from the atmosphere, thereby increasing significantly the light-scattering particle size and mass.

Visibility changes with time: diurnal, seasonal, and yearly variations all exist. Though five to eight years of data would be considered ideal for establishing present seasonal and annual averaged conditions, a minimum of one year is a reasonable compromise if that year is typical from a meteorological and source activity point of view.

Source identification. Identification of chemical species and emission sources responsible for man-made visibility impairment is necessary to protect Class I areas, as called for by Congress. Monitoring is the principal means of gathering information needed to identify the contribution to impairment by emission sources. Even to distinguish man-made from natural impairment, which is fundamental to the national visibility goals, requires information derived from monitoring data.

Aerosol and scene monitoring are the primary sources of emission source identification information. Photography of a plume emanating from its source and impacting a Class I area is sufficient to indicate impairment. Further, photographs can be evaluated to indicate the density or intensity of the visible plume. Unfortunately, most visibility impairment does not lend itself to this simple type of source attribution. Often sources are not visible from any line of sight that includes the Class I area, or their plumes disperse to a haze layer before reaching it.

Visibility impacts are often caused by aerosols formed over time from gaseous pollutants that are emitted without visibly noticeable plumes. Characteristics of the aerosol that are responsible for the haze provide valuable information that can be used in conjunction with other information to help identify the responsible emission sources. It is possible to statistically relate measured optical data to corresponding aerosol composition data to estimate the relative importance of the various major components of the aerosol. The result, known as an extinction budget, should narrow the list of possible sources responsible for large impacts. For example if organic carbon is shown to be responsible for 75% of the extinction coefficient, the major sources responsible must emit organic carbon.

Another related approach for source identification using aerosol data is known as receptor modeling. Instead of using only the major aerosol components that are directly responsible for the impairment, receptor models use relative concentrations of trace components which can more specifically identify the influence of individual sources (or source types).

Long-term trends. With the establishment of a long-term goal of no man-made visibility impairment in protected areas, Congress imposed the responsibility to show progress towards meeting that goal. Trends monitoring is an ideal approach for tracking the visibility conditions of Class I areas.

Optical and scene monitoring conducted to establish present visibility levels (described above), if conducted in perpetuity, will provide the data required to determine long-term visibility trends. In order to determine the effectiveness of individual concurrent emission reduction programs, it is necessary to conduct periodic aerosol monitoring to support extinction budget analysis as described above.

## 1.2 Overview of the IMPROVE Monitoring Network

The design of the IMPROVE monitoring network was resource and funding limited so that it was not practical to place monitoring stations at all 156 mandatory Class I areas where visibility is an important attribute. Instead, the IMPROVE Steering Committee selected a set of sites that were representative of the Class I areas. A total of 36 sites (20 IMPROVE and 16 NPS/IMPROVE protocol sites) are examined in this report. Each has aerosol monitoring and scene monitoring equipment (automated cameras); however, only 20 of the sites have optical monitoring equipment (e.g., transmissometers or nephelometers to measure visibility related parameters).

Figure 1.1 shows a map of the United States showing the locations of the 36 monitoring sites analyzed in this report. On the basis of regional similarities, the sites were grouped into 19 regions, listed in Table 1.1.

The routine IMPROVE monitoring approach involves aerosol, optical, and view monitoring. Aerosol monitoring measures the mass concentration (in micrograms per cubic meter, $\mu g/m^3$) and the chemical composition of the particles. Optical monitoring measures the light extinction coefficient ($b_{ext}$) using a transmissometer or the light scattering coefficient ($b_{scat}$) using a nephelometer. View monitoring documents the appearance of the scene by automated photography using color slide film.

Aerosol monitoring in the IMPROVE network is accomplished by a combination of particle sampling and sample analysis. The sampler employed was designed specifically for the program. It collects four simultaneous samples: one $PM_{10}$ sample (particles less than 10 micrometers, $\mu m$, in diameter) on a Teflon filter and three $PM_{2.5}$ samples (particles less than 2.5 $\mu m$ in diameter) on Teflon, nylon, and quartz filters. Each of the four samples is collected by a separate subsystem (or module) including everything from the inlet to the pump with only the support structure and controller/timer in common. The particle size segregation for the $PM_{10}$ module is accomplished by a wind insensitive inlet with a 10 $\mu m$ cutoff, while the $PM_{2.5}$ segregation is produced by passing the sampled air through a cyclone separator. Constant sample flow is maintained by a critical orifice in each module. The IMPROVE sampler is programmed to automatically collect two 24-hour duration samples per week.

Only mass analyses are conducted on the $PM_{10}$ samples. The $PM_{2.5}$ samples are analyzed for mass, elements, ions (including particulate nitrate sampled through a denuder), organic and elemental carbon, and optical absorption.

At most sites in the IMPROVE network, long-path transmissometers are employed for optical measurements. These instruments measure the amount of light transmitted through the atmosphere over a known distance, usually 0.5 to 10 kilometers, between the light source (transmitter) and the light monitoring component (receiver). Transmission measurements are converted electronically to the path-averaged light extinction coefficient ($b_{ext}$). At a few sites nephelometers are used which internally measure the light scattering coefficient ($b_{scat}$).

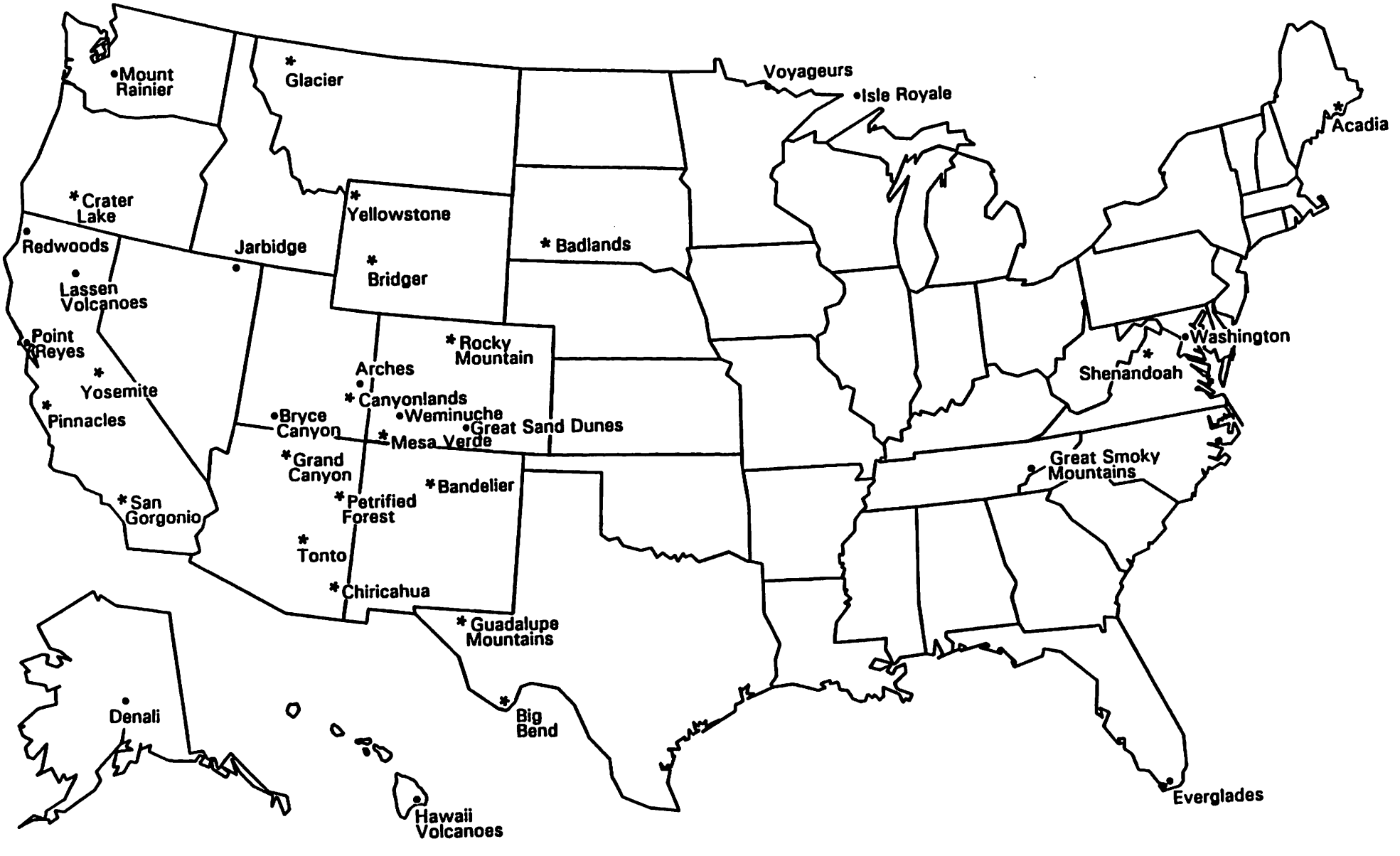


Figure 1.1. The 36 IMPROVE sites included in the report. Sites designated by an asterisk have both aerosol and visibility monitoring.

Table 1.1 IMPROVE and NPS/IMPROVE protocol sites according to region.

**Alaska (AKA)**
- Denali National Park (DENA)

**Appalachian Mountains (APP)**
- Great Smoky Mountains National Park (GRSM)
- Shenandoah National Park (SHEN)

**Boundary-Waters (BWA)**
- Isle Royale National Park (ISRO)
- Voyageurs National Park (VOYA)

**Cascade Mountains (CAS)**
- Mount Rainier National Park (MORA)

**Central Rocky Mountains (CRK)**
- Bridger Wilderness Area (BRID)
- Great Sand Dunes National Monument (GRSA)
- Rocky Mountain National Park (ROMO)
- Weminuche Wilderness Area (WEMI)
- Yellowstone National Park (YELL)

**Coastal Mountains (CST)**
- Pinnacles National Monument (PINN)
- Point Reyes National Seashore (PORE)
- Redwood National Park (REDW)

**Colorado Plateau (CPL)**
- Arches National Park (ARCH)
- Bandelier National Monument (BAND)
- Bryce Canyon National Park (BRCA)
- Canyonlands National Park (CANY)
- Grand Canyon National Park (GRCA)
- Mesa Verde National Park (MEVE)
- Petrified Forest National Park (PEFO)

**Florida (FLA)**
- Everglades (EVER)

**Great Basin (GBA)**
- Jarbidge Wilderness Area (JARB)

**Hawaii (HAW)**
- Hawaii Volcanoes National Park (HAVO)

**Northeast (NEA)**
- Acadia National Park (ACAD)

**Northern Great Plains (NGP)**
- Badlands National Monument (BADL)

**Northern Rocky Mountains (NRK)**
- Glacier National Park (GLAC)

**Sierra Nevada (SRA)**
- Yosemite National Park (YOSE)

**Sierra-Humboldt (SRH)**
- Crater Lake National Park (CRLA)
- Lassen Volcanoes National Park (LAVO)

**Sonoran Desert (SON)**
- Chiricahua National Monument (CHIR)
- Tonto National Monument (TONT)

**Southern California (SCA)**
- San Gorgonio Wilderness Area (SAGO)

**Washington, D.C. (WDC)**
- Washington, D.C. (WASH)

**West Texas (WTX)**
- Big Bend National Park (BIBE)
- Guadalupe Mountains National Monument (GUMO)

View monitoring is accomplished by automated 35-mm camera systems. These systems take three color slides per day to document the appearance of a selected scene at each of the IMPROVE sites. The slides are used to interpret measurements, to communicate perceived visual conditions, and, if needed, to derive quantitative estimates of light extinction by microdensitometry.

In addition to the aerosol, optical, and view monitoring, most sites have temperature and relative humidity instruments. Liquid water is a component of the hygroscopic sulfate, nitrate, and possibly organic carbon fractions, but it is not efficiently captured by filter sampling techniques. Relative humidity measurements are used to estimate the amount of liquid water associated with these particles.

## 1.3 Background Regarding Visibility Impairment and Aerosols

Visibility is usually characterized either by visual range (the greatest distance that a large dark object can be seen), or by the light extinction coefficient (the attenuation of light per unit distance due to scattering and absorption by gases and particles in the atmosphere). Under certain assumed conditions these two measures of visibility can be shown to be inversely related to each other. Visual range functions well as an aid in military operations and transportation safety. Issues of concern for such use include: the minimum distance required to land an aircraft, the distance to the first appearance of a military target or an enemy aircraft or ship, and safe maneuvering distances under impaired visibility conditions. Because of the use of familiar distance units, the simple definition, and the ability of any sighted person to characterize visual conditions with this parameter without instruments, visual range is likely to remain the most popular measure of atmospheric visibility.

Extinction coefficient is used most by scientists concerned with the causes of reduced visibility. There are direct relationships between the concentrations of the atmospheric constituents and their contribution to the extinction coefficient. Apportioning the extinction coefficient to atmospheric constituents provides a method to estimate the change in visibility caused by a change in constituent concentrations. This methodology, known as extinction budget analysis, is important for assessing the visibility consequences of proposed pollutant emission sources, or for determining the extent of pollution control required to meet a desired visibility condition. Interest in the causes of visibility impairment is expected to continue and the extinction coefficient will remain important in visibility research and assessment.

Neither visual range nor extinction coefficient is linear with visual scene changes caused by uniform haze (i.e., as opposed to elevated haze layers and plumes). For example, a given change in visual range or extinction coefficient can result in a scene change which is either unnoticeably small or very apparent depending on the baseline visibility conditions. Presentation of visibility measurement data or model results in terms of visual range or extinction coefficient can lead to misinterpretation by those who are not aware of the nonlinear relationship.

To rigorously determine the perceived visual effect of a change in extinction coefficient requires the use of radiative transfer modeling to determine the changes in light from the field of view arriving at the observer location, followed by the use of psychophysical modeling to

determine the response to the light by the eye-brain system. Results are dependent not only on the baseline and changes to atmospheric optical conditions, but also on the characteristics of the scene and its lighting. The complexity of employing such a procedure and the dependence of the results on non-atmospheric factors prevent its widespread use to characterize perceived visibility changes resulting from changes in air quality.

Parametric analysis methods have been used to suggest that a constant fractional change in extinction coefficient or visual range produces a similar perceptual change for a scene regardless of baseline conditions. Simplifying assumptions eliminate the need to consider the visibility effects of scene and lighting conditions. Using the relationship of a constant fractional change in extinction coefficient to perceived visual change, a new visibility index called deciview (dv) is defined as:

$$dv = 10\ln(b_{ext} / 0.01 km^{-1}), \tag{1.1}$$

where extinction coefficient is expressed in $km^{-1}$ (Pitchford and Malm, 1993). A one dv change is about a 10% change in extinction coefficient, which is a small but perceptible scenic change under many circumstances. The deciview scale is near zero for pristine atmosphere (dv = 0 for Rayleigh condition at about 1.8 km elevation) and increases as visibility is degraded. Like the decibel scale for sound, equal changes in deciview are equally perceptible.

### 1.3.1 Relationship Between Visibility and Aerosol Concentrations

Visibility is degraded by light scattered into and out of the line of sight and by light absorbed along the line of sight. Light extinction (the sum of light scattering and absorption) is usually quantified using the light extinction coefficient ($b_{ext}$), which may be thought of as the atmospheric concentration of light extinction cross-sectional area. Light extinction has units of $m^2/m^3$ or $m^{-1}$.

The light extinction coefficient ($b_{ext}$) is the sum of the light scattering coefficient ($b_{scat}$) and the light absorption coefficient ($b_{abs}$). Light scattering results from the natural Rayleigh scatter ($b_{Ray}$) from air molecules (which causes the blue sky) and the scattering caused by suspended particles in the atmosphere (aerosols). Particle scatter ($b_{sp}$) can be caused by natural aerosol (e.g., wind-blown dust and fog) or by man-made aerosols (e.g., sulfates, nitrates, carbonaceous aerosol and other fine and coarse particles). Light absorption results from gases ($b_{ag}$) and particles ($b_{ap}$). Nitrogen dioxide ($NO_2$) is the only major light absorbing gas in the lower atmosphere; its strong wavelength-dependent scatter causes yellow-brown discoloration if present in sufficient quantities. Soot (elemental carbon) is the dominant light absorbing particle in the atmosphere. Thus, the total light extinction is the sum of its components:

$$b_{ext} = b_{scat} + b_{abs} = b_{Ray} + b_{sp} + b_{ag} + b_{ap}. \tag{1.2}$$

The particle light scattering coefficient ($b_{sp}$), in turn, is composed of the contributions from individual species. Fine particles are much more efficient at light scattering (per unit mass) than larger particles. Thus, it makes sense to divide the contributions to $b_{sp}$ into the contributions from various species of fine and coarse particles. In this study, we specifically evaluated the

following components of fine particles (those with diameters less than 2.5 $\mu$m): sulfate ($SO_4^=$), nitrate ($NO_3^-$), organic carbon, elemental carbon (soot), and others. In addition to these chemical species, the effect of water associated with sulfate, nitrate, and some organics need to be considered in the overall assessment of light extinction. Finally, the coarse fraction of $PM_{10}$ (those with diameters between 2.5 and 10 $\mu$m) and giant particles (those with diameters greater than 10 $\mu$m) are separately considered.

The light extinction coefficient can be written as the sum of the products of the concentrations of individual species and their respective light extinction efficiencies:

$$b_{ext} = b_{Ray} + \sum \beta_i C_i, \tag{1.3}$$

where $\beta_i$ is the light extinction efficiency ($m^2/g$) of species $i$, $C_i$ is the atmospheric concentration of species $i$ ($\mu g/m^3$), and the summation is over all light-interacting species (i.e., sulfate, nitrate, organic carbon, elemental carbon, other fine particles, coarse particles, giant particles, and $NO_2$). The above units, when multiplied, yield units for $b_{ext}$ of $10^{-6}$ $m^{-1}$ or $(10^6$ $m)^{-1}$, or as we prefer to label it here, inverse megameters ($Mm^{-1}$).

## 1.3.2 Effect of Relative Humidity on Light Scattering

Sulfates, nitrates, and some organics can combine with water in the vapor phase to form solutions. Thus, at some humidity conditions, considerable water may be associated with these species. Although the overall light scattering efficiency is on the order of 3 $m^2/g$ for these solutions, if the light scattering efficiency is stated in terms of the mass of dry sulfate ($SO_4^=$), the efficiency must be larger than 3 $m^2/g$ to account for the additional mass (and volume) of the associated water. In addition, the associated cations ($H^+$ and $NH_4^+$) must also be included. As a result, light scattering efficiency per unit of dry sulfate can be much larger than 3 $m^2/g$. This hygroscopic effect can be described by the following equation:

$$\beta_{wet} = k f_{RH} \beta_{dry} \tag{1.4}$$

where $\beta_{wet}$ is the light extinction efficiency of the wet sulfate, nitrate, and/or organic solution, $k$ is the ratio in molecular weight of the neutralized species (e.g., ammonium sulfate or ammonium nitrate) to the anion (sulfate, nitrate), $f_{RH}$ is a factor that accounts for the liquid water associated with the aerosol at the given relative humidity ($RH$), and $\beta_{dry}$ is the light extinction efficiency of the dry particle.

## 1.4 Organization of the Report

This report is divided into eight chapters. Chapter 2 summarizes the methodologies, protocols, and uncertainties of aerosol and optical monitoring. The assumptions for determining the chemical composition of the particles are discussed in Chapter 3. Chapter 4 presents the results of various cross-checks and comparisons for quality assurance and validation of the parameters derived from the aerosol measurements. A discussion of the acidity of the sulfate component of the aerosols is also included. The spatial and seasonal patterns of aerosol mass and chemical composition are summarized in Chapter 5. Chapter 6 discusses the theory and

results of light extinction apportionment by aerosol chemical species and the spatial and seasonal patterns of light extinction and reconstructed light extinction. Chapter 7 compares the reconstructed with measured extinction and describes some regional characteristics of the measured extinction.

# CHAPTER 2

# MONITORING METHODOLOGIES

Visibility is reduced by the presence of aerosols, which are mixtures of fine particles in the air. In order to develop reasonable plans to maintain a given visibility level, we need to know the component species in these aerosols, their sources, their amounts, and their separate effects upon the visibility. Thus, monitoring of protected visibility areas denoted Class I by the Clean Air Act has been on the two parallel fronts of 1) monitoring the composition of the aerosols in these areas, and 2) monitoring the visibility in these areas. These two tasks are performed by the aerosol and visibility monitoring networks of IMPROVE.

The aerosol monitoring network has been operational since spring 1988. The visibility monitoring network coincides with this time frame, and a number of sites go back as far as 1986. This report deals with the first three full years of aerosol data, from spring 1988 through winter 1990/1991.

## 2.1 Aerosol Monitoring Network

The aerosol network is managed by scientists at the University of California at Davis (UCD), according to protocols of aerosol sampling and analysis established by them to meet the needs mentioned in the preceding paragraph. These protocols must therefore meet two goals that are quite independent and sometimes in conflict: 1) determination of not only the aggregate aerosol mass but also the masses of its major constituents, to aid in explaining changes in visibility; and 2) determination, within the smallest possible detection limits, of elements that can act as tracer species to aid in establishing the sources of those constituent particles, natural and man made, that degrade visibility. Finally, the accuracy and precision of all measurements must be assured through strict validation procedures involving continuous, independent field comparisons (of some species) using widely divergent techniques.

The standard IMPROVE sampling module, shown in Figure 2.1, is a filter sampler consisting of the following: 1) an inlet; 2) a cyclone to provide a particle size cutoff based on the flow rate; 3) alternate collection filters, housed in cassettes in the flow path, with each filter followed by a flow on/off solenoid switch; 4) a critical orifice set to provide the proper flow rate for the desired particle size cutoff; and 5) a vacuum pump which produces the flow. The flow rate is monitored by two independent gauges, a magnehelic and a small gauge, which measure the pressure drop due to the flow, across the cyclone and the filter, respectively. Sampling is performed in two 24-hour periods per week.

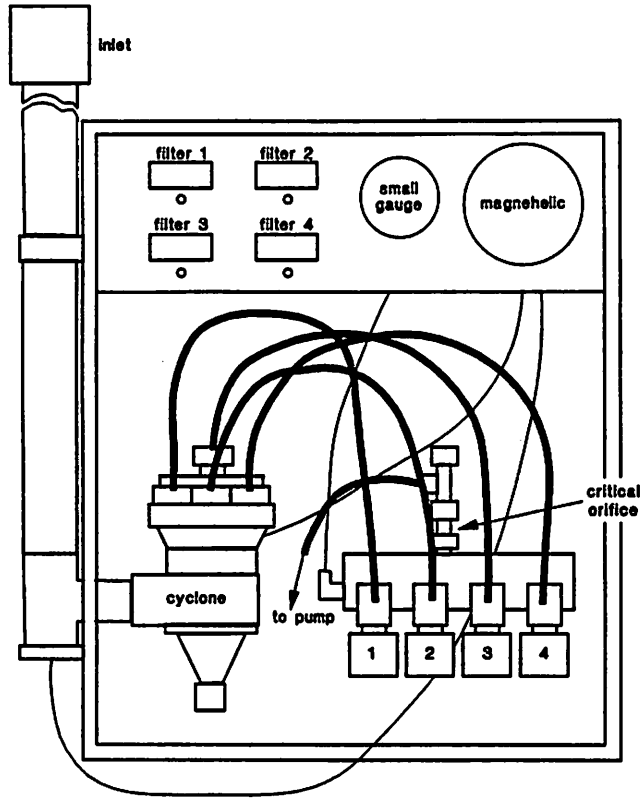


Figure 2.1 Schematic of fine particle aerosol sampling module.

## 2.1.1 Aerosol Sampling Protocol

In order to meet IMPROVE's disparate goals, a basic protocol has been established which calls for four independent sampling modules at each site. Three (denoted A,B and C) are fine particle samplers, with cyclone systems operated at a flow rate of 22.7 liters/minute, which collect particles up to 2.5 $\mu$m in diameter. The fourth (D) is a $PM_{10}$ collector, using an 18.9 liter/minute system that collects particles up to 10 $\mu$m. Each module is optimized for its specific purpose and matched to its analytical protocols as follows:

| MODULE | FILTER(S) | MEASURED VARIABLES |
|---|---|---|
| A ($\leq$2.5$\mu$m) | 25mm stretched Teflon | Fine Mass, absorption, H, Na to U (PIXE), (H,Li,Be,B,C,N,O) |
| B ($\leq$2.5$\mu$m) | Nitric acid denuder + 25mm Nylasorb filter | $NO_3^-$,$NO_2^-$,$Cl^-$,$SO_4^{2-}$ (Ion Chromatography) |
| C ($\leq$2.5$\mu$m) | Tandem, pre-fired quartz filters | Organic Carbon, Elemental Carbon |
| D/S ($\leq$10$\mu$m) | 25mm stretched Teflon, Impregnated quartz | Total Mass, $SO_2$ Gas(IC) |

It is often convenient to consider a particular module, its associated filter and the variables measured off that filter, as constituting a particular channel of measurement (e.g., "the Channel A filter" or "the Channel C carbon measurement"). The following paragraphs describe the measurements performed on the IMPROVE samples in each of the channels.

Gravimetric mass (Channel A fine mass, Channel D total mass) is measured as the difference between weighing of the filters before and after sampling, using an electromicrobalance.

The Channel A Teflon filters are analyzed for sulfur and other elements by Particle Induced X-ray Emission (PIXE), and simultaneously for hydrogen by Proton Elastic Scattering Analysis (PESA). Both PIXE and PESA involve subjecting the collected aerosol sample to a beam of 4.5 MeV protons, in vacuum, at the UCD cyclotron. In PIXE, each element present in the sample is induced by the proton beam to emit x-rays whose energy is characteristic of the element, and whose number is proportional to the mass of the element. In PESA, the protons in the cyclotron beam which are elastically scattered through a given angle (30°) by the hydrogen atoms in the sample are also easily discriminated and counted, to give an accurate measure of the amount of hydrogen.

The coefficient of light absorption for fine particles, $b_{abs}$, is also determined from the Channel A Teflon filters using a Laser Integrating Plate Method (LIPM). This involves direct measurement of the absorption of a laser beam by a sample, over the area of the sample. To obtain an ambient $b_{abs}$ value, the LIPM measurement must be corrected both for "shadowing" of some of the particles by others, due to the thickness of the sample, and for scattering effects. The LIPM measurement and its corrections are described more fully in Section 2.1.2.

The Channel B nylon filters are analyzed by Ion Chromatography (IC) for sulfate and nitrate ions, from which the sulfate and nitrate compounds are estimated. A sample is prepared for IC analysis by desorption of the collected material in 15 ml of an aqueous solution of sodium carbonate. This solution is applied to strips of filter paper and allowed to dry, and the various ion species are separated in the standard way according to their solubilities, by suspending the strips over a solvent and allowing it to pass up through the paper by capillary action. Ambient gaseous nitric acid ($HNO_3$) is subject to adsorption by the nylon filter and subsequent transformation to the solid nitrate form, which would bias measurements of the latter. Therefore, a gas denuder, consisting of a set of concentric cylindrical aluminum sheets coated with potassium carbonate ($K_2CO_3$), is placed in the Channel B inlet to remove $HNO_3$ before collection. (This denuder also removes $SO_2$ gas, which could possibly interact with collected particles and contribute falsely to the particulate sulfate measurement. The possibility of such a sulfate artifact, in either Channel A or Channel B, is a particular validation question which has arisen and is discussed in Section 4.1 and in Appendix B.)

The Channel C quartz filters are analyzed by Thermal Optical Reflectance (TOR) Combustion for organic and elemental carbon. A second quartz filter behind the first is used in estimating the artifact due to adsorption of organic gases. TOR involves: (1) heating a sample through a series of temperature increases or steps (in a pure Helium atmosphere to which oxygen is added in the later stages to enable the volatilization of elemental carbon); (2) converting the carbon evolved at each step into $CO_2$, using an oxidizer ($MnO_2$ at 912 °C); and (3) reducing the

$CO_2$ to methane, which is then quantified by passage through a flame ionization detector. Figure 2.2 is a graphical portrayal of the TOR process. Over the midrange of the TOR heating (between about 130 °C and 550 °C), charring of the sample occurs, due to pyrolysis of organic particles; this is monitored as a decrease in the reflectance from the sample surface. When the reflectance reaches a minimum, 2% oxygen is added to the atmosphere. This allows the elemental carbon in the sample, including the char produced by pyrolysis of organic matter, to oxidize; and the reflectance of the sample increases as the char is removed. All carbon measured up to the point where the reflectance reattains its initial value is interpreted as organic carbon. Carbon evolved beyond this point is reported as elemental carbon. Overall, the peaks in the carbon evolution from the sample (Figure 2.2) are conveniently divided into low- and high-temperature organic, and low- and high-temperature elemental, carbon--respectively OCLT, OCHT, ECLT AND ECHT. Organic carbon (OC) is the sum of the reported OCLT and OCHT. Elemental carbon is also known as light-absorbing carbon (LAC), and is the sum of ECLT and ECHT:

$$OC = OCLT + OCHT \tag{2.1}$$

$$LAC = ECLT + ECHT \tag{2.2}$$

The S, or secondary Channel D, filters are analyzed by ion chromatography for $SO_2$ gas. These filters are quartz impregnated with $K_2CO_3$, which changes $SO_2$ to solid $K_2SO_4$ on the filter. The $K_2SO_4$ is then analyzed by IC for $SO_4^{2-}$ to give a measure of the original gas.

## 2.1.2 Uncertainties

The amount of each aerosol species in a 24-hour sample is reported as an average ambient concentration, which is the collected mass of the species divided by the volume of air sampled. Both mass measurements and volume calculations have their uncertainties, as discussed below.

Uncertainty in an aerosol species measurement may be given in terms of a minimum detectable limit (MDL) for the species. The MDL is defined, for every species, in terms of the observed standard deviation $\sigma_{FB}$ in the measurement of the species off of supposedly blank filters (ones not subjected to sample flow, including laboratory controls and field blanks).

The general equation for the concentration ($C$) of a given species is

$$C=(M-A)/V, \tag{2.3}$$

where $M$ is the measured mass of the species, $V$ is the volume of air sampled, and $A$ is the artifactual mass (discussed below). The uncertainty in a measured concentration is the quadratic sum (the square root of the sum of the squares) of the uncertainties in $M$, $A$, and $V$: respectively, the analytical uncertainty, the artifact uncertainty and the volume uncertainty.

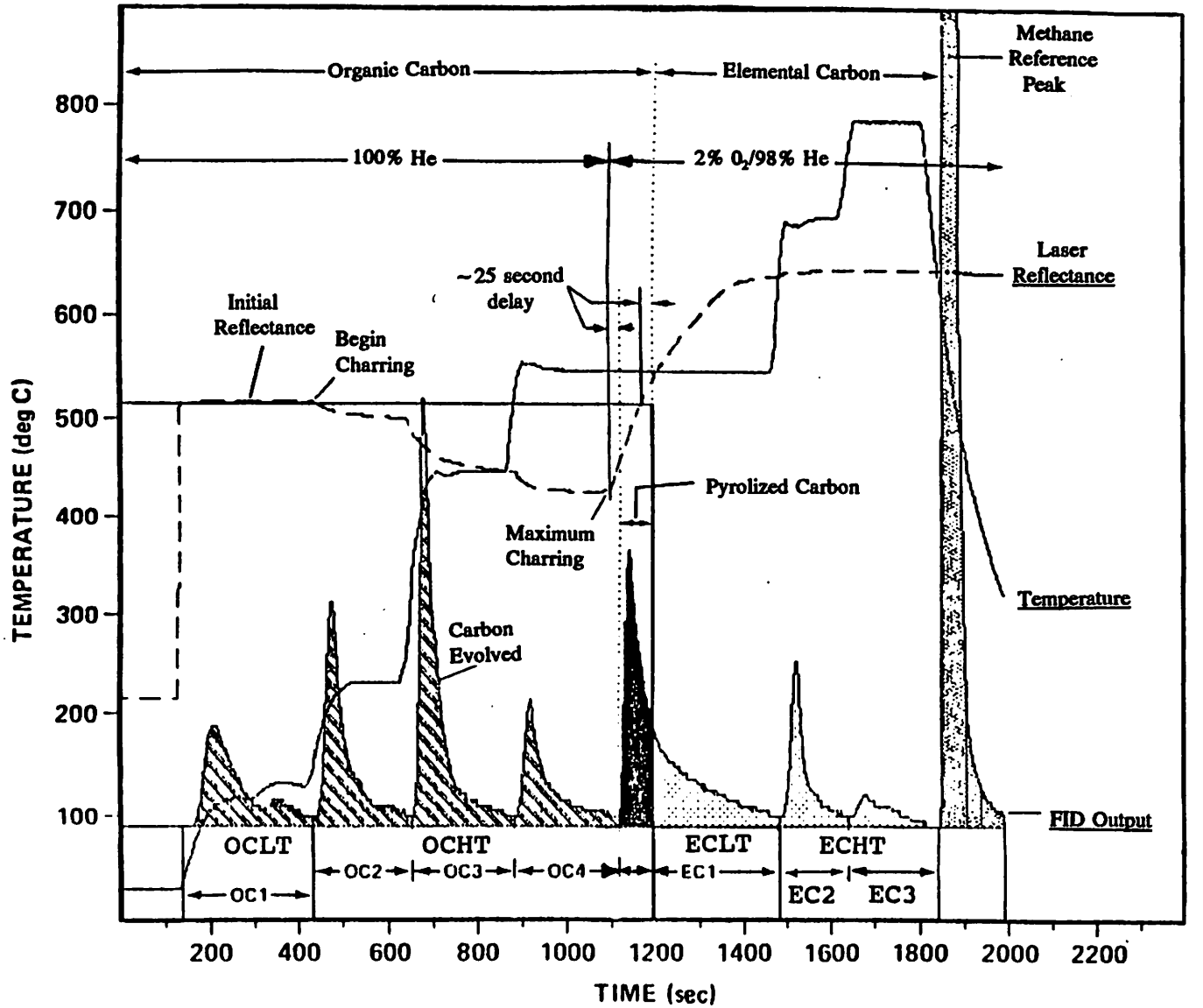


Figure 2.2 Time development of TOR carbon analysis. Area of shaded peaks are the amount of carbon evolved at successive steps in temperature (stepped solid line). Pyrolysis changes some organics to elemental carbon (charring), decreasing the sample reflectance (broken line); reattainment of initial reflectance marks the end of the pyrolyzed organic carbon. There is a 25 second delay between the sample chamber and the detector. (Modified after Chow et al., 1992.)

The artifact A may be positive, due to accrued nonaerosol mass, or negative, due to a failure to collect some portion of the considered aerosol species or to volatilization of particles that are collected (especially nitrates). The artifact may be produced by contamination in the filter material, by handling, and/or by adsorption of gases during collection. It is determined from secondary quartz filters for the Channel C carbon, and from designated field blank filters for all other measurements. These secondary or field blank measurements also contribute to the analytical uncertainty, particularly when the artifact is negligible.

The artifact has been found to be negligible for all measurements off the Teflon filters (Channels A and D), including PIXE, PESA, LIPM absorption, gravimetric analysis, and $SO_2$. General uncertainty considerations for the sample volume and the measured aerosol species follow.

Volume--The volume is the product of the average flow rate and the sample duration. The average flow rate is calculated from the magnehelic and small gauge readings taken at the beginning and end of the sampling period. The fractional uncertainty in volume equals the fractional uncertainty in flow rate, since the sample duration is well defined. The precision of the magnehelic and small gauge flow measurement system is as good as the precision of most audit devices. At present, the best estimate of internal precision of average flow rate is that it is better than 1%; and the best estimate of total uncertainty is that it is better than 3%. All calculations are based on a volume uncertainty of 3%.

Gravimetric Mass--The uncertainty in mass concentration is

$$\sigma_C = [(\sigma_{FB}/V)^2 + (f_V C)^2]^{1/2} , \qquad (2.4)$$

where $\sigma_{FB}$ is the standard deviation of the mass measured in the controls and field blanks, $V$ is volume, and $f_v$ is the fractional uncertainty in volume. The artifact is generally negligible, and the MDL ($=2\sigma_{FB}/V$), which is due to analytic uncertainty alone, is a constant 300 ng/m$^3$. In the third year, an organic artifact is associated with a small proportion (about 7%) of the Teflon filters being used. This artifact is discussed in Section 4.3 of this report.

PIXE and PESA Analysis--A PIXE measurement is performed by counting the x-rays in the element's spectral peak, normalizing to the number of protons passing through, and calibrating the system using known elemental standards. A background is subtracted, using the spectrum of a blank Teflon filter. PESA works the same way as PIXE, only counting the protons scattered by hydrogen rather than the x-rays emitted by it.

The artifact concentrations for the elements measured by PIXE and PESA are zero. The uncertainty in the concentration is thus the square root of the sum of the squares of the analytical uncertainties and the volume uncertainty. The analytical uncertainties are the uncertainty in calibration, which is about 4% over the long term, and the statistical uncertainty, which is proportional to the square root of the number of counts in the spectral peak. The 3% volume uncertainty and the 4% PIXE/PESA calibration uncertainty combine to give an uncertainty of 5%; and the total uncertainty is thus 5% plus counting statistics (again, combined quadratically).

A PIXE or PESA measurement actually determines the areal density of a given element, which is the mass of the element per unit area of the sample. To determine concentration, the areal density is multiplied by *SA/V*, where *SA* is the sample area on the filter. PIXE/PESA analysis can be performed on deposit areas smaller than 2 $cm^2$, so some filters are masked to limit the deposit area, thus concentrating the particles and reducing the minimum detectable limits of the tracer elements to as low as 0.05 $ng/m^3$.

Optical Absorption--The coefficient of absorption, $b_{abs}$, for the particles on the Channel A filter, depends on the initial and final LIPM measurements, the volume, and the filter sample area. A LIPM measurement gives the intensity of laser light transmitted through a sample (through a blank filter for the initial measurement). The intensity measurement is basically related to $b_{abs}$ through the relation

$$L_f = L_i \, e^{-b_{abs}t} \, , \tag{2.5}$$

or

$$b_{abs} = (1/t)\ln(L_i / L_f) \, , \tag{2.6}$$

where $t$ is the thickness of the sample, and $L_i$ and $L_f$ are the LIPM measurements before and after particle collection, respectively. The $b_{abs}$ value thus obtained must be corrected for the portion of light loss that is due to scattering by the particles rather than absorption. This correction, amounting to a reduction of 3%, has been determined by comparing the LIPM measurements with those using Laser Integrating Sphere Analysis (LISA), pictured in Figure 2.3. (In LISA, the absorption by the sample is basically the incident light energy minus the sum of the total reflected and transmitted energies over all scattering angles, as collected by the sphere.) Also, particles on the filter overlay and thus shadow one another in the measurement; so it is necessary to divide the measured coefficient by a factor $R$ that depends on the areal density of the particles on the filter, to obtain the true value of $b_{abs}$ for the atmosphere. (The function of $R$ has been established experimentally by studying the variation of $b_{abs}$ with areal density, as shown in Figure 2.4.) The coefficient of absorption in the atmosphere is thus given by

$$b_{abs} = (SA/V)\ln(L_i / L_f)(0.97/R) \, , \tag{2.7}$$

where $SA/V = 1/t$ is the sample area divided by the sample air volume. The average uncertainty in $b_{abs}$ is 13%.

Ion Chromatography--IC analysis of field blanks indicates that there is artifact formation during the period in the cassettes in the sampling module. The standard deviation in the measurement off the field blanks provides an estimate of the artifact uncertainty. The analytical uncertainty, based on data from replicate samples, is not a constant, but varies directly with the measured value. The uncertainty in concentration $C$ is given by:

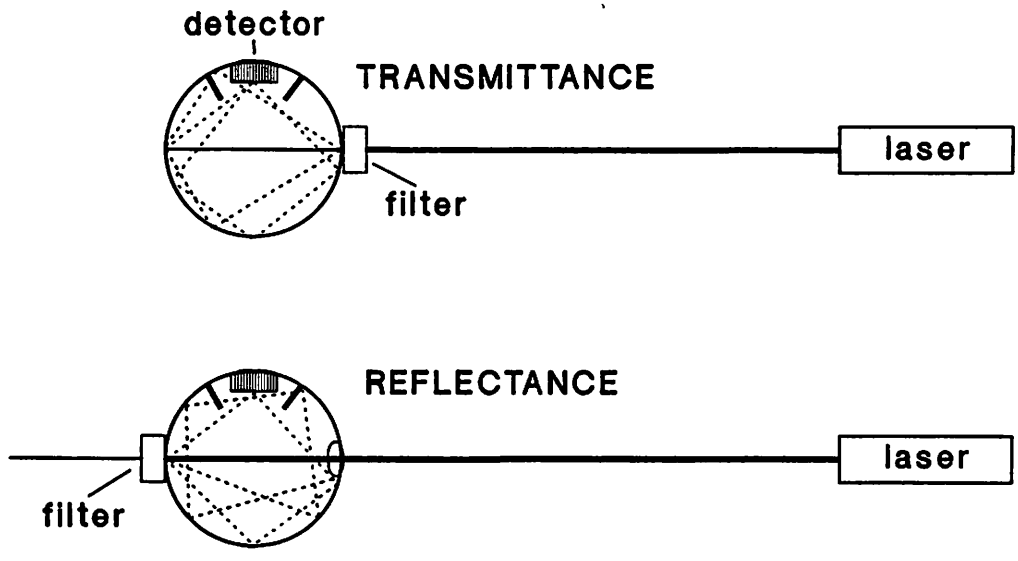


Figure 2.3 LISA configuration. Transmitted energy $E_T$ is measured with filter sample on front side of sphere; reflected energy $E_R$, with sample on back side. Absorption is then $E_A = E - (E_T + E_R)$, where $E$ is the energy in the incident beam. Coefficient of absorption is $\alpha = E_A/E = 1 - (T+R)$, with $T$=transmittance and $R$=reflectance.

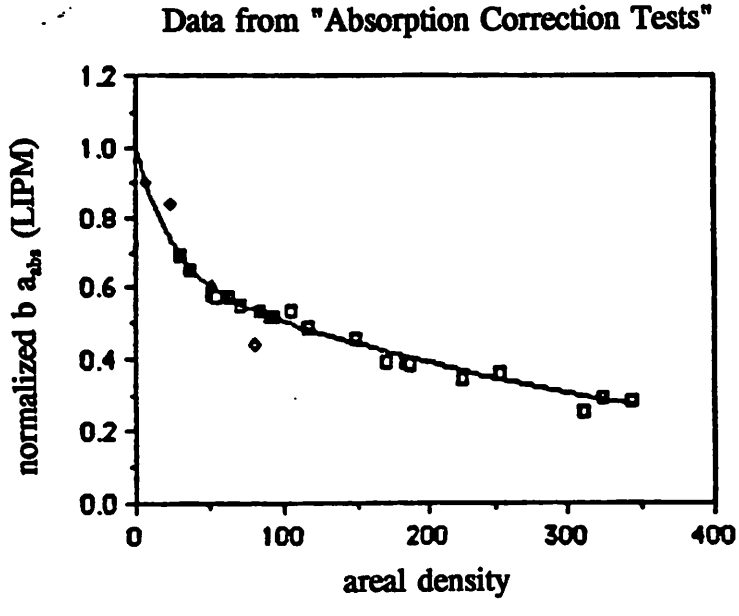


Figure 2.4 Variation of $b_{abs}$ with areal density, $\gamma$. Normalized $b_{abs}$ is $R(\gamma)$, where $R = ke^{(\gamma/A)} + (1-k)e^{(\gamma/B)}$, with constants $k$, $A$, $B$.

$$\sigma_C = [(f_A M/V)^2 + (\sigma_{FB}/V)^2 + (f_V C)^2]^{1/2} , \quad (2.8)$$

where $M$ is the mass measured by the ion analysis and $f_A$ is the fractional analytic uncertainty. The MDL is equal to twice the uncertainty measured on field blanks: MDL = $2(\sigma_{FB}/V)$ .

Carbon Analysis--Artifacts in the carbon measurements are based on measurements on secondary quartz filters placed behind the primary C filters in the sample flow. Organic carbon artifact is caused by contamination in the filter material, by contact with the cassette, and by the adsorption of organic gases during collection. The quartz filters are pre-fired to eliminate filter contamination; however, this process itself may produce surface sites on the filter material that will enhance later organic adsorption. Elemental carbon artifact is caused by contamination in the filter material and by contact with the cassette. (See Chapter 4, "Validation," on carbon measurements.) Uncertainties associated with the TOR analysis are shown in Table 2.1.

The carbon artifacts are constants, and are consistent with their values as derived from designated field blanks. Unfortunately, these carbon artifacts appear to be too large, since approximately 21% of the carbon measurements for the first two years were negative, and comparisons with other measurements give a negative carbon intercept. The reasons for this problem have not yet been determined, so correcting these negatives as yet simply involves adding a constant to the reported carbon concentrations. In this report, carbon corrections have been performed by finding the minimum concentration for each season at each site, and subtracting this, if it is negative, from every concentration in that season (thus adding a positive number to the concentrations). For the comparisons performed for this report, involving one or another sum of the individually reported varieties of carbon (for example, finding the total organic carbon from the reported high- and low-temperature forms), the appropriate sum has been taken before applying the correction.

Overall percentage uncertainties for the average concentrations of measured species are given in Table 2.2. The uncertainties of the composite variables (cf. Chapter 3 for their definitions) are estimated by quadratically adding the uncertainties of the components, assuming those uncertainties are independent. Since this is not quite valid, the uncertainties for composites formed by adding (SOIL, OMC, LAC) may be slightly larger than as given in Table 2.2 (5% for SOIL, rather than 4%, for example). The composite formed by subtraction (OMH) may have a slightly smaller uncertainty than reported.

The measured concentrations may be less than the MDL of the analytical system used, and therefore not quantifiable. This is generally not a problem with the ion chromatography and carbon combustion variables, because the presence of artifact means that some material is always measured. The problem for these variables is that the concentrations after removing artifact may have a large fractional uncertainty, and for this reason not be statistically reliable. For the $PM_{10}$ mass and the Channel A variables, the situation is different. Here there is no significant artifact, and the concentration may be so low that nothing can be determined because of statistical noise. In such a case, the concentration reported is just the MDL for the given species. When calculating averages and composite variables, when the value is below the MDL, it is dropped

Table 2.1. Specifications of the DRI Thermal/Optical Reflectance Carbon Analyzer.

| SUBJECT | SPECIFICATION |
|---|---|
| Sample Requirements | Substrate: Quartz-fiber filter, Pallflex 2500QAT-UP or equivalent |
| | Substrate pretreatment: Pre-fired at 900 °C for at least 3 hours (before sampling) |
| | Sample size: 0.5 $cm^2$ punch (uniform deposit) |
| | Sample storage: Store below 4 °C |
| Analysis Time | 880 to 4,890 seconds (15 to 82 minutes) |
| Measurement Range | 0.2 to 750 $\mu g$ carbon/$cm^2$ |
| Detection Limit | 0.2 $\mu g$ carbon/$cm^2$ |
| FID Precision | 0.1% of full scale |
| Reflectance Signal Precision | 0.2% of full scale |
| Sample Oven Temperature Precision | $\pm$ 10 °C at temperatures $<$ 450 °C |
| | $\pm$ 3 °C at temperatures $\geq$ 450 °C |
| Oxidation Oven Temperature | 912 $\pm$ 5°C |
| Methanator Oven Temperature | 550 $\pm$ 5°C |
| Lower Quantifiable Limits | Organic carbon: 0.5 to 1.0 $\mu g$ carbon/$cm^2$ |
| | Elemental carbon: 0.0 to 0.2 $\mu m$ carbon/$cm^2$ |
| | Carbonate carbon: 0.0 to 0.4 $\mu g$ carbon/$cm^2$ |
| Total Carbon Accuracy | $\pm$5% |
| Total Carbon Precision | For sample loading $<$ 10 $\mu g$ carbon/$cm^2$: $\pm$0.5 $\mu g$ carbon/$cm^2$ |
| | For sample loading $\geq$ 10 $\mu g$ carbon/$cm^2$: $\pm$3% |
| OC/EC Split Precision: | 5% of the total carbon measurement |
| OC/EC Split Accuracy | To be determined* |

* Probably 10% of the total carbon, by inference from the similar DRI instrument (Johnson et al., 1981).

Table 2.2 Precisions for average concentration of measured and composite variables.

| | | | | | | | |
|---|---|---|---|---|---|---|---|
| MASS | 4% | Fe | 5% | Pb | 14% | NHSO | 6% |
| $PM_{10}$ | 4% | Mn | 25% | Na | 10% | LAC | 25% |
| H | 6% | V | 30% | $CL^-$ | 39% | OMC | 18% |
| S | 5% | Ni | 14% | OCLT | 80% | OMH | 12% |
| $SO_2$ | 9% | Cu | 11% | OCHT | 25% | SOIL | 4% |
| Si | 6% | Zn | 7% | ECLT | 21% | RCMC | 7% |
| K | 6% | As | 16% | ECHT | 81% | RCMA | 5% |
| Ca | 6% | Se | 20% | $b_{abs}$ | 13% | | |
| Ti | 15% | Br | 11% | KNON | 14% | | |

and reported as simply one half of the MDL. And in such a case for a composite variable, one half the MDL is also used as the uncertainty.

## 2.2 Visibility Monitoring Network

The NPS Visibility Monitoring Network currently consists of 20 IMPROVE and IMPROVE Protocol sites. Each site contains an Optec, Inc., LPV-2 long path transmissometer system, a Handar data collection platform (DCP), a Handar Air Temperature/Relative Humidity sensor and a Primeline two-pen strip chart recorder. The data collection platform automatically transfers collected data through the GOES satellite to the visibility network manager, Air Resource Specialists, Inc.

The transmissometer, shown in Figure 2.5, consists of a transmitter (housing a light source) and a receiver (with light detector). The transmissometer system measures the ambient light loss (or extinction) from the transmitter to the receiver. These two individually-housed components are generally separated by a sight path distance of 0.5 to 10 kilometers, a long path length being required in order to accurately measure extinctions near the Rayleigh limit (which is the extinction due to particle-free, pristine air).

Given the exact amount of light emitted from the light source ($I_0$) and the amount reaching the receiver ($I$), the receiver computer can calculate the atmospheric transmission coefficient, $T$, as the ratio $I/I_0$. (See Equation 2.8 and the discussion of Section 2.2.1.) Given the sight path distance $r$, $T$ can be converted to the atmospheric extinction coefficient $b_{ext}$ according to

$$b_{ext} = -\ln(T)/r \ . \qquad (2.9)$$

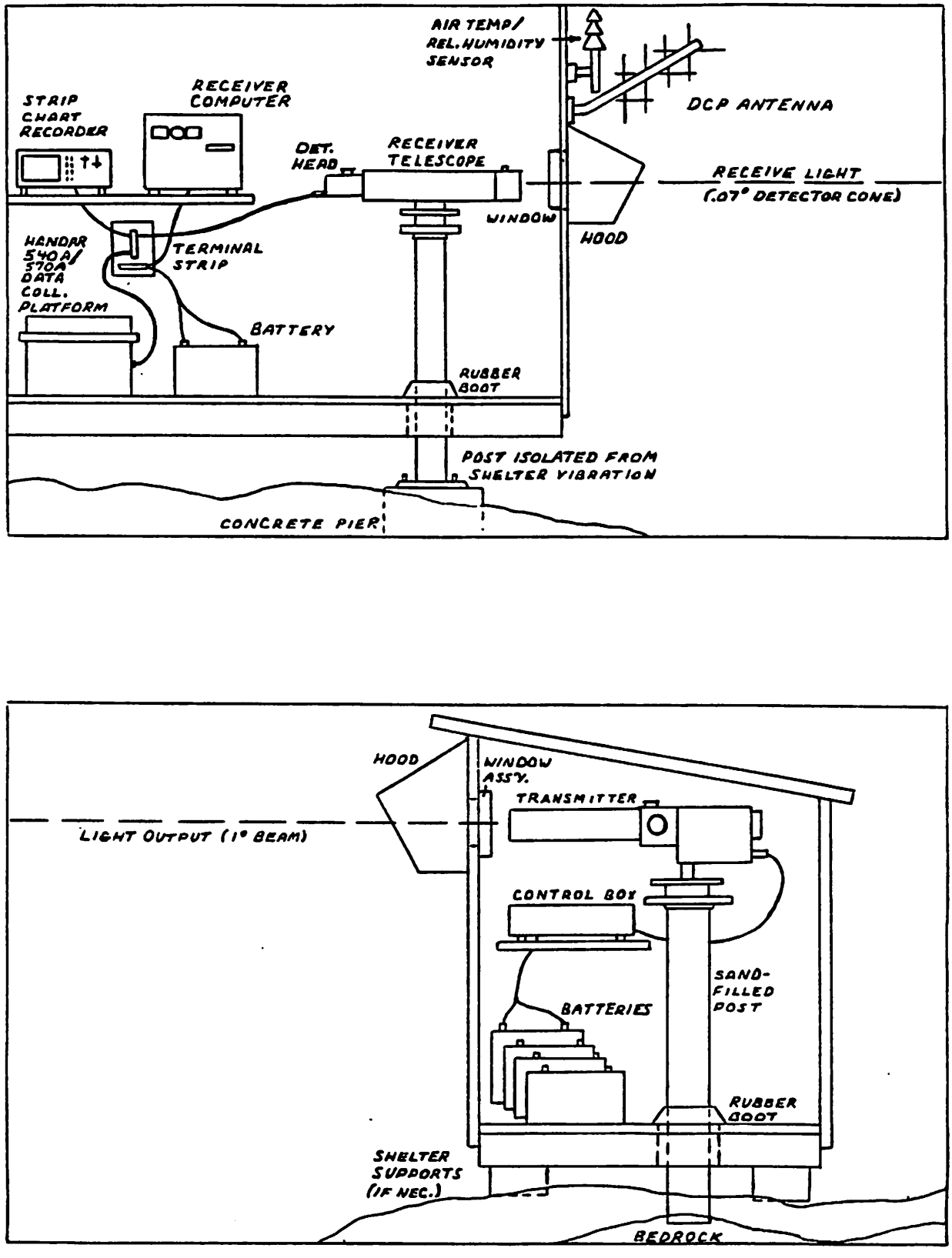


Figure 2.5 Transmissometer receiver (top) and transmitter (bottom).

A standard visual range may also be defined, as that distance over which the transmission coefficient is reduced to 2%, which from Equation 2.9 becomes

$$SVR = 3.91/b_{ext} \ . \qquad (2.10)$$

The transmission $T$ is calculated for each hour, based on a ten-minute sample (which is itself composed of ten successive one-minute samples over a ten minute period). Temperature and relative humidity averages are simultaneously collected. The strip chart recorder allows the site operator to verify system operational performance, and provides data backup in case of DCP or GOES system failure.

## 2.2.1 Uncertainties

Transmissometer--The basic equation used to calculate path transmission is:

$$T = I_r \ / \ (F_{lamp} \cdot I_{cal}) \ , \qquad (2.11)$$

where: $I_r$ = Intensity of light measured at distance $r$,
$I_{cal}$ = Calibration value of transmissometer,
$F_{lamp}$ = Variability function of lamp output.

The relative uncertainty ($U_x$) of any measured quantity $X$ is:

$$U_x = \sigma_x \ / \ \overline{X} \qquad (2.12)$$

where $\overline{X}$ = arithmetic mean of all $X$ measurements, and $\sigma_x$= precision (S.D.) of measurements of $X$. The relative uncertainty of the transmission is calculated from the relative uncertainties of the measured variables as:

$$U_T = (U_{Ir}^2 + U_{Ical}^2 + U_{lamp}^2)^{1/2} \ . \qquad (2.13)$$

$I_{cal}$ is the value that would be measured by the transmissometer detector if the atmospheric path were a vacuum. $I_{cal}$ incorporates the path distance, the transmission of all windows in the path, and the size of the working aperture used, according to

$$I_{cal} = (CP/WP)^2(WG/CG)^2(WA/CA)^2(WT)(1/FT)(1/T)(CR) \qquad (2.14)$$

and the relative uncertainty is

$$U_{Ical}=(2U_{CP}^2 + 2U_{WP}^2 + 2U_{WG}^2 + 2U_{CG}^2 + 2U_{WA}^2 + 2U_{CA}^2 + U_{WT}^2 + U_{FT}^2 + U_{CR}^2)^{1/2}. \quad (2.15)$$

The parameters in Equations (2.14) and (2.15) are given in Table 2.3. Path distances are measured using a laser range finder. Apertures are measured with a precision micrometer. Gain settings are measured with a precision voltmeter. Window and neutral density filter transmittances are measured with a reference transmissometer by differencing techniques; thus, they do not require absolute calibration. The standard deviation of the raw readings (CR) are calculated at each calibration. From the typical values given in Table 2.3, the predicted relative uncertainty in $I_{cal}$ is $U_{Ical}$=0.008. Experimentally, $U_{Ir}$ is a function of the extinction of the path. Typically, for weather-affected data, $U_{Ir}$=0.15, otherwise, $U_{Ir}$=0.006.

The transmissometer lamp brightness is continually adjusted by an optical feedback circuit. However, the lamp brightness still increases with usage, typically by 2% per 500 hours of lamp life, according to precise measurements. $U_{lamp}$ is simply the precision of those measurements, which is 0.002. The transmissometer data is corrected to fully account for the time drift.

Table 2.3 Transmissometer parameters.

| | Parameter | Value | Precision | Relative Uncertainty |
|---|---|---|---|---|
| CP | Calibration Path | 0.3 km | $1 \times 10^{-6}$ km | $3.3 \times 10^{-6}$ |
| WP | Working Path | 5.0 km | $1 \times 10^{-6}$ km | $2.0 \times 10^{-7}$ |
| CG | Calibration Gain | 100 km | $1 \times 10^{-2}$ km | $1.0 \times 10^{-4}$ |
| WG | Working Gain | 500 km | $1 \times 10^{-2}$ km | $2.0 \times 10^{-5}$ |
| CA | Calibration Aperture | 100 mm | $1 \times 10^{-2}$ mm | $1.0 \times 10^{-4}$ |
| WA | Working Aperture | 110 mm | $1 \times 10^{-2}$ mm | $9.1 \times 10^{-5}$ |
| WT | Window Transmission | 0.810 mm | 0.001 mm | $1.2 \times 10^{-3}$ |
| FT | NDF Transmission | 0.274 mm | 0.001 mm | $3.6 \times 10^{-3}$ |
| T | CP Transmission | 0.975 mm | 0.005 mm | $5.1 \times 10^{-3}$ |
| CR | Raw Readings | 900 mm | 4.5 mm | $5.0 \times 10^{-3}$ |

From the above analysis, typical values for the relative uncertainty in path transmission $T$, for each 10-minute transmission measurement, can be calculated using Equation (2.13):

$U_T$ = 0.01, with no optical interference,
$U_T$ = 0.20, with optical interference.

The extinction over the distance $r$ is given by Equation 2.16:

$$b_{ext} = -\ln(T)/r \ , \tag{2.16}$$

and since $r$ is measured to an extremely high precision with a laser range finder, the uncertainty in $b_{ext}$ is:

$$\sigma_{bext} = U_T \ /r, \ dependent \ upon \ r \ . \tag{2.17}$$

For $r$ between 0.5 and 10 kilometers, then, and $b_{ext}$ given in $Mm^{-1}$, the minimum uncertainty in $b_{ext}$ is

$$\sigma_{bext} = 0.01/(10 km) = 0.01/(0.01 Mm) = 1 Mm^{-1} \ , \tag{2.18}$$

so that $b_{ext}$ should be reported only to the nearest $Mm^{-1}$ (as done in Chapter 7). In addition, a bias in $b_{ext}$ can occur if the transmission of the windows is altered, by staining, pitting, collecting dirt, fogging, or breakage. This bias is of the same form as that of $\sigma_{bext}$ above, that is:

$$\text{bias} = (\text{relative change in window transmission})/r.$$

The uncertainties and limits for air temperature and relative humidity are obtained form the manufacturer's literature:

$U_{temp}$ = 1°C
$U_{RH}$ = 5%, for Handar sensors
2%, for Rotronics sensors
Maximum temperature = 60°C
Minimum temperature = -50°C
Maximum rel. humid. = 100%
Minimum rel. humid. = 0%

Figure 2.6 is a scatter plot (with one-to-one line indicated) of hourly extinction data collected by two short-path transmissometers during a summer 1991 study at Shenandoah National Park (Molenar et al., 1992). Figure 2.7 is a similar plot of data collected by two long-path transmissometers during a similar intercomparison study at Tonto National Monument in Arizona. Both figures indicate the extremely high precision of transmissometers to replicate extinction measurements when operating over identical paths. Figure 2.8 is a scatter plot of extinction by short-path vs. long-path transmissometers during the Shenandoah summer 1991 study. The correlation is again outstanding. Analysis of the extinction data from the short- and long-path transmissometers, shown in Table. 2.4, indicate that the predicted uncertainties ($U_T$) of 0.01 and 0.20, for weather and nonweather affected data, respectively, agree very well with the actual calculated uncertainties.

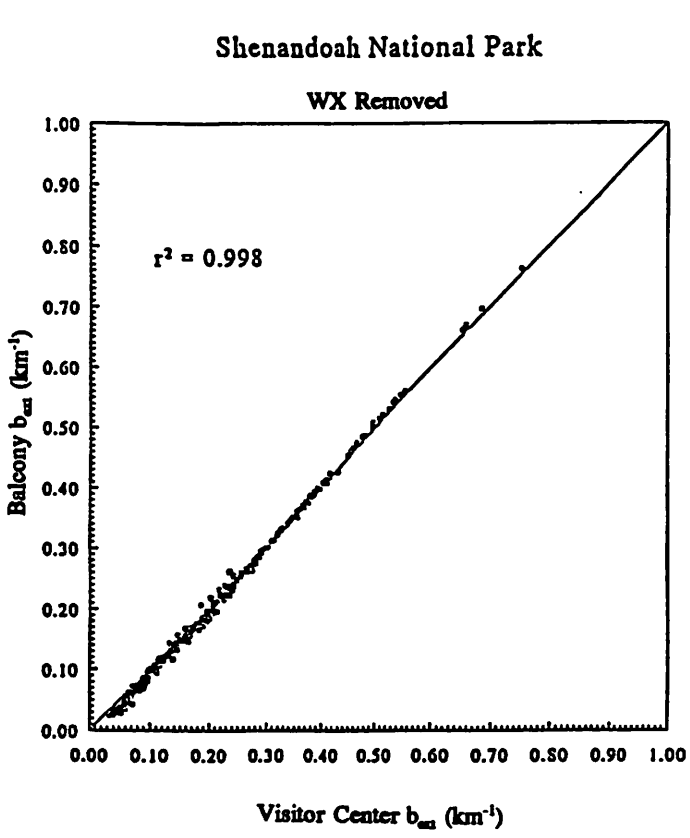


Figure 2.6 Comparison of $b_{ext}$ measured by two transmissometers operating side-by-side over a short path (0.67 km). (Molenar et al., 1992)

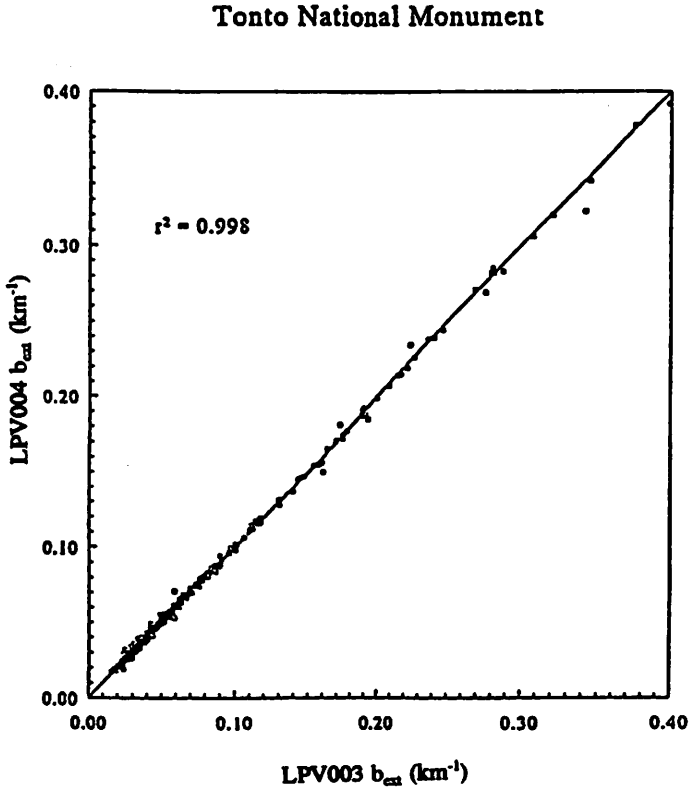


Figure 2.7 Comparison of $b_{ext}$ measured by two transmissometers operating side-by-side over a long path (7.2 km). (Molenar et al., 1992)

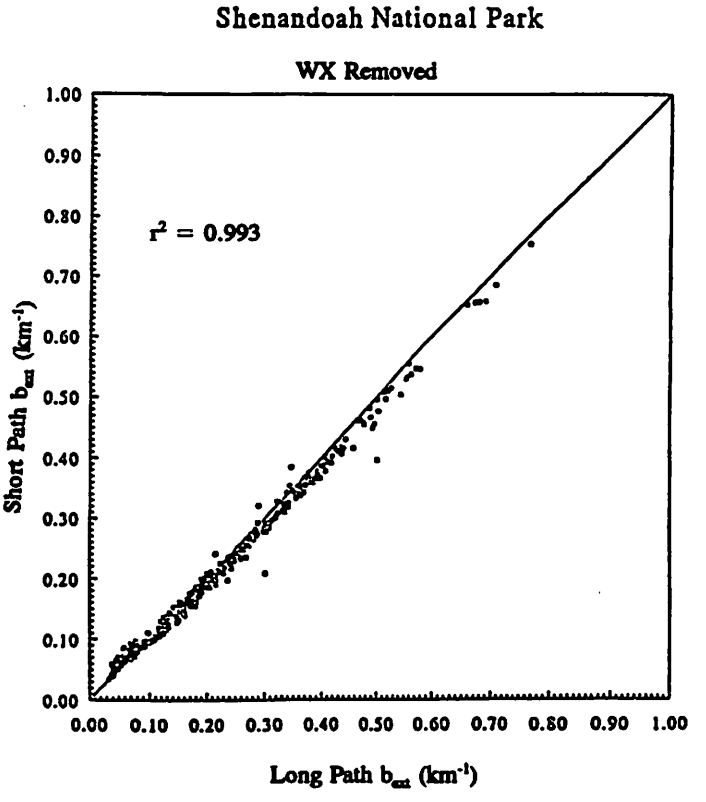


Figure 2.8 Comparison of $b_{ext}$ measured by two transmissometers, one operating over a short path (0.67 km), the other over a long path (1.41 km). (Molenar et al., 1992)

Table 2.4 Calculated $U_T$, Shenandoah summer 1991 study. (Molenar et al., 1992.)

| | Uncertainty $U_T$ | |
|---|---|---|
| **Path** | **Weather** | **No Weather** |
| 1.41 km | 0.14 $km^{-1}$ | 0.007 $km^{-1}$ |
| 0.67 km | 0.30 $km^{-1}$ | 0.015 $km^{-1}$ |

RH Sensor--The importance of the effect of relative humidity (RH) on the scattering properties of aerosols cannot be overstated. Accurate RH measurements are mandatory for a proper understanding and comparison of ambient optical measurements and ambient aerosol extinction apportionments. Recent advances in the design and manufacture of low-power thin film capacitive RH sensors provide the means to obtain accurate measurements of RH. Sensors of this type have historically been plagued by nonlinear response, hysteresis, creep and instability, particularly at high humidity levels.

Ambient temperature and relative humidity measurements were made with three RH sensor systems during the summer 1991 Shenandoah study. The first was an old-style capacitive

sensor, a Campbell 207 essentially the same as the Handar RH sensor used up to that point in IMPROVE. The second was a new model by Rotronics (model MP-100MF). This sensor featured temperature compensation and a new polymer engineered to minimize hysteresis and creep. The third system was an Assman model 5230 psychrometer modified for continuous, unattended operation. Modifications included a large water reservoir, type E fine-wire thermocouple affixed to each bulb, and a low-power ventilation fan. Wet and dry bulb temperatures were logged with a Campbell Scientific 21X micrologger equipped with an internal thermocouple reference junction.

Figure 2.9 shows scatter plots comparing the wet/dry bulb standard with the Rotronics and Campbell 207 systems. The Rotronics RH sensor is clearly superior to the Campbell 207, which deviates strongly from the wet/dry bulb system for RH greater than 90%. The RH data for the first three years of IMPROVE aerosol monitoring is from a (Handar) sensor like the Campbell 207, and is suspect above 90% RH; as discussed in the next section, transmissometer data taken when RH is greater than 90% is routinely deleted from the data base. The Rotronics system is now replacing the older system in the IMPROVE visibility monitoring network, which will allow retaining extinction data taken with RH above 90%.

## 2.2.2 Meteorological and Optical Interferences

The transmissometer directly measures the irradiance of a light source after the light has travelled over a finite atmospheric path. The average extinction coefficient of the sight path is calculated from this measurement, and is attributed to the average concentration of atmospheric gases and ambient aerosols along the sight path. The intensity of the light, however, can be modified not only by intervening gases and aerosols, but also by:

- the presence of condensed water vapor in the form of fog, clouds and precipitation along the sight path;
- condensation, frost, snow or ice on the shelter windows;
- reduction in light intensity by insects, birds, animals or vegetation along the sight path, or on the optical surfaces of the instrumentation or shelter windows; or
- fluctuations in light intensity, both positive and negative, due to optical turbulence, beam wander, atmospheric lensing, and miraging caused by variations in the atmospheric optical index of refraction along the sight path.

A major effort was undertaken to develop an algorithm to identify transmissometer extinction data that may be affected by the interferences described above. This algorithm contains five major tests:

1) Relative Humidity--The transmissometer measurement is flagged as having a possible interference when the relative humidity measured at the receiver is greater than 90%. This is because inferring the precise meteorological conditions along the sight path from a single point measurement is very difficult, and when RH is above 90% at one end of the path, small random

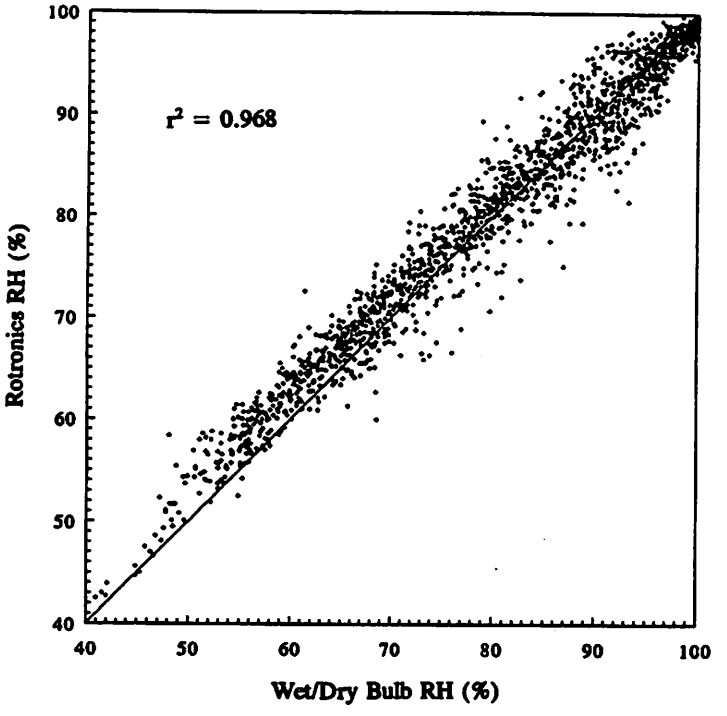


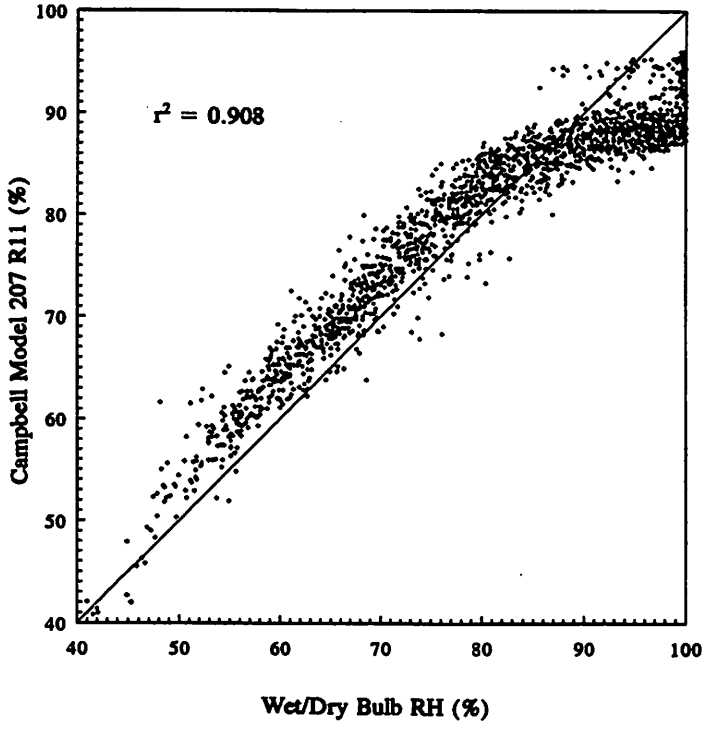


Figure 2.9 Comparisons of Rotronics MP-100MF and Campbell 207 RH sensors against Wet/Dry Bulb standard. (Molenar et al., 1992)

temperature or absolute humidity fluctuations along the path can lead to condensation of water vapor, causing meteorological interference to the transmissometer beam.

2) Maximum Extinction--Transmissometer measurements of $b_{ext}$ greater than a calculated maximum for the sight path are flagged. This maximum corresponds to a 2% transmission for the path, and, based on historical visibility data, this maximum $b_{ext}$ occurs less than 1% of the time. Beyond this maximum, it is assumed that meteorological or optical interferences are involved, not ambient aerosols.

3) Uncertainty Threshold--The normal procedure for the transmissometer is to take ten one-minute measurements of transmissometer irradiance each hour, and report the average and standard deviation of the ten values. In remote, rural areas the ambient aerosol concentration typically varies quite slowly, with time constants on the order of a few hours, not minutes. Thus, any measurement with a standard deviation, or uncertainty, above a selected threshold implies variation beyond that due to ambient aerosols, and is flagged as interference.

4) Rate of Change of Extinction--Transmissometer data collected before September 1, 1990 did not include standard deviation of measured irradiance values. For this data, periods of interferences were identified by comparing the hourly extinction to the preceding and succeeding hours, and calculating a rate of change in each direction. The hourly $b_{ext}$ value is flagged as being affected by interferences when this rate of change exceeds an assigned delta threshold.

5) Isolated Data Points--After the above four thresholds are applied to the hourly extinction data, those data points that are isolated between $b_{ext}$ data that have failed the above thresholds are also flagged as due to interference.

# CHAPTER 3

# DETERMINATION OF AEROSOL TYPES

The fine aerosol species at most continental sites can be classified into five major types: sulfates, nitrates, organics, elemental carbon, and soil. Other fine species such as nonsoil potassium, or sea spray and other trace elements, are less important from a visibility standpoint at the majority of the monitoring sites presented here. The value of many of the trace species lies, in part, in their use in identifying origins of different air masses. The fine aerosol types are estimated from the elements and ions measured in IMPROVE samplers based on their presumed or probable aerosol composition. The purpose of this chapter is to define and discuss the compositions assumed for the fine aerosol types and coarse particles. The adequacy and validity of these assumptions are addressed in greater detail in Chapter 4, "Validation".

## 3.1 Sulfate

Most fine sulfates are the result of chemical processes which convert $SO_2$ gas into sulfate species. In moist atmospheres, a major process involves the oxidation of $SO_2$ gas to sulfuric acid in water droplets. If there is inadequate ammonia in the atmosphere to fully neutralize sulfuric acid, as is sometimes the case, then the resulting aerosols are acidic. Under these circumstances solutions of continuously varying acidity are formed. The extremes of this continuum are ammonium sulfate (neutral) and sulfuric acid.

In this report sulfate represents the total concentration associated with elemental sulfur, not just the ion. The multiplicative molar correction factor[2] (mcf) for elemental sulfur depends on the degree of neutralization of the sulfuric acid produced by conversion of $SO_2$.

| SULFATE FORM | EQUATION | NEUTRALIZATION |
|---|---|---|
| $(NH_4)_2SO_4$: | [SULFATE]=4.125[S] | 100% |
| $(NH_4)HSO_4$: | [SULFATE]=3.594[S] | 50% |
| $H_2SO_4$: | [SULFATE]=3.063[S] | 0% |

The brackets indicate the mass of the aerosol species or element.

[2]The mcf is determined by an accounting of the total molar weight of a sulfate species then dividing by the molar weight of sulfur. For example, the mcf for ammonium sulfate is: ((14 + 4)2 + 32 + (16)4)/32 = 4.125.

Based on analysis of high volume filters, many authors have noted the acidity of aerosols in the eastern U.S. (Malm et al., 1991). It is recognized that scattering efficiencies of acidic aerosols in the presence of high RH can be quite different from the scattering characteristics of pure ammonium sulfate (Malm et al., 1990; Tang et al., 1981). However, because acidity was not explicitly measured, all elemental sulfur is presumed to be from ammonium sulfate, as a first approximation. Thus, all elemental sulfur concentrations are multiplied by 4.125. However, a more detailed analysis of assumptions regarding aerosol acidity is presented in Section 4.2.1.

## 3.2 Nitrates

Nitrate particles are collected on nylon filters. The input stream is denuded to remove nitric acid. The mass of the nitrate ion is determined by ion chromatography. Assuming, as is the case for sulfate, that the collected nitrates are fully neutralized (forming $NH_4NO_3$), the nitrate mass is estimated by using a mcf of 1.29:

$$[NITRATE]=1.29[NO_3]. \tag{3.1}$$

## 3.3 Carbons

Both elemental carbon, also called light absorbing carbon (LAC), and the mass of organic species (OM) can be estimated from either Channel A or Channel C (see the discussion in Chapter 2). The LAC and OM are indirectly inferred from Channel A fine aerosols collected on Teflon. LAC is inferred from an absorption coefficient ($b_{abs}$) as measured using the Laser Integrated Plate Method (LIPM); and OM is inferred from hydrogen (PESA) and sulfur (PIXE) concentrations.

Alternatively, the analysis of Channel C filters attempts to directly quantify the carbon mass from the material collected on quartz filters using the Thermal Optical Reflectance (TOR) combustion method (Chow et al., 1992). The results of the TOR method are the OCLT, OCHT, ECLT, and ECHT variables which depend primarily on the temperature of combustion:

OCLT = Low temperature organic carbon (25°C to 120°C);
OCHT = High temperature organic carbon (120°C to 550°C);
ECLT = Low temperature elemental carbon (550°C to 700°C); and,
ECHT = High temperature elemental carbon (above 700°C).

Because Channel C carbon determinations represent direct estimates of carbon mass they will be used to describe the ambient aerosol concentrations used in Chapters 6 and 7. The Channel A determinations will be used as quality control variables or checks on the validity of the assumptions used. One assumption that will be examined in detail in Chapter 4 on Validation is the association of ECLT and ECHT with LAC.

### 3.3.1 Organic Carbon

OM calculated from the concentrations of H and S measured on the Channel A Teflon filter will be denoted as OMH. An average ambient organic particle is assumed to contain constant fractions of carbon ($f_{OC}$) and hydrogen ($f_{OH}$) by weight. Furthermore, it is assumed that during exposure to the vacuum of Channel A PIXE and PESA analyses, all nitrates and water volatilize and do not contribute to the mass of H. By assuming a level of neutralization of the sulfate ion, OMH is calculated by:

| SULFATE FORM | EQUATION FOR OMH | NEUTRALIZATION |
|---|---|---|
| $(NH_4)_2SO_4$: | $[OMH]=(1/f_{OH})([H]-0.250[S])$ | 100% |
| $(NH_4)HSO_4$: | $[OMH]=(1/f_{OH})([H]-0.156[S])$ | 50% |
| $H_2SO_4$: | $[OMH]=(1/f_{OH})([H]-0.063[S])$ | 0% |

The sulfur factors are derived from the H/S ratio for each form of sulfate; for example ammonium sulfate has a ratio of 8/32, or 0.25. The value of the factor $f_{OH}$ will be examined in Chapter 4. To be consistent with the assumption of fully neutralized sulfate the top equation would apply; however, Section 4.2.1 will address the ramifications of this assumption.

Organics from Channel C (OMC) is simply the sum of OCLT and OCHT adjusted by the molar correction factor $1/f_{OC}$:

$$[OMC]=(1/f_{OC})([OCLT]+[OCHT]). \quad (3.2)$$

For this report, a value for $f_{OC}$ of 0.71 is used which gives a reciprocal factor of 1.4 (Watson et al., 1988).

### 3.3.2 Light Absorbing Carbon (LAC)

LAC, derived from the Channel C TOR analysis is simply the sum of the two elemental fractions:

$$[LAC]=[ECLT]+[ECHT]. \quad (3.3)$$

If the only light absorbing species is elemental carbon, then LAC should compare to Channel A $b_{abs}$ as measured by LIPM.

On Channel A, $b_{abs}$ is quantified directly by the LIPM analysis and is stated in units of $10^{-8}m^{-1}$. To compare the mass of LAC with $b_{abs}$ requires assuming an absorption efficiency. For this report, the relationship used for comparison purposes is:

$$[LAC]=[b_{abs}]/\beta, \quad (3.4)$$

where $\beta$, the absorption efficiency, is assumed to be 10 $m^2/g$.

## 3.4 Soil

The soil mass concentration is estimated by summing the elements predominantly associated with soil, plus oxygen for the normal oxides ($Al_2O_3$, $SiO_2$, CaO, $K_2O$, FeO, $Fe_2O_3$, $TiO_2$), plus a correction for other compounds, such as MgO, $Na_2O$, water, and $CO_2$. The final factors are based on the following observations:

(1) The soil mass can be calculated from the sum of the masses due to the constituent oxides. The mass due to each oxide is seen to be the corresponding measured elemental mass multiplied by the appropriate mcf for that oxide.

(2) Fe is present as both FeO and $Fe_2O_3$. It is assumed that the two forms are equally abundant (in molar concentrations), giving a mcf of 1.36. This differs from that obtained with average sediment by 1%.

(3) A complicating factor for fine soil particles is that K has a nonsoil component from smoke. Therefore, Fe was used as a surrogate for soil K. Based on the average K/Fe ratio for coarse particles of $0.6 \pm 0.2$ (Cahill et al., 1986), the following equation was used:

$$[K]=0.6[Fe], \tag{3.5}$$

which yielded a mcf of 2.08 for Fe.

The final equation for fine soil after dividing by 0.86 to account for other compounds (MgO, $Na_2O$, water, and $CO_2$) is:

$$[SOIL]=2.20[Al]+2.49[Si]+1.63[Ca]+2.42[Fe]+1.94[Ti]. \tag{3.6}$$

## 3.5 Nonsoil K (KNON)

KNON usually results from combustion processes that produce smoke and can be estimated by the equation:

$$[KNON]=[K]-0.6[Fe]. \tag{3.7}$$

The use of KNON as a tracer for smoke is problematic. This is because the particulate K is probably produced by transformation of volatilized K, while most smoke mass is from primary emissions. In addition, the resulting K is probably smaller than most of the other smoke particles and will have a lower settling velocity. For both reasons, the ratio of K/(smoke mass) will increase with transport time. When close to the source, the particulate K may not have time to form. For long transport, most mass other than K may settle out.

## 3.6 Salt

In general, NaCl is a significant factor in the reconstructed mass only in marine environments. A significant problem with Teflon filters is that chlorine can be volatilized from the filter during collection. Thus, the relationship:

$$[SALT]=2.5[Na], \tag{3.8}$$

is used rather than the simple sum of [Na] and [Cl].

## 3.7 Coarse Mass (CM)

Coarse mass is estimated gravimetrically by subtracting fine mass $PM_{2.5}$ from total aerosol mass $PM_{10}$:

$$[CM]=[PM_{10}]-[PM_{2.5}]. \tag{3.9}$$

No further chemical analysis is available on the individual coarse species. It is assumed that coarse mass consists primarily of insoluble airborne soil particles.

## 3.8 Reconstructed Fine Mass (RCFM)

The sum of the above fine composites should provide a reasonable estimate of the fine mass measured on the Teflon filter. However, a significant fraction of the nitrate particles can volatilize from the Teflon filter during collection and is not measured by gravimetric analysis. Therefore, nitrate collected on nylon filters is not included in RCFM when comparing RCFM to the gravimetric mass derived from the Teflon filter.

Salt will not be included in RCFM since most of the sites are continental. Moreover, because KNON due to smoke usually exits in trace amounts, and since smoke is measured by its contribution to OM or LAC, KNON will not be included in RCFM. On the other hand, when comparing RCFM to visibility, nitrates are included in RCFM because nitrates can be a significant fraction of fine mass. The equation for RCFM is therefore:

$$[RCFM]=[SULFATE]+[NITRATE]+[LAC]+[OM]+[SOIL]. \tag{3.10}$$

As discussed previously, the intent of the design of the IMPROVE sampler was to use Channel C (TOR) measurements to directly quantify both LAC and OM as opposed to using Channel A (PESA, PIXE, and LIPM) to indirectly estimate LAC and OM. Therefore, Channel C determinations of LAC and OM will be used to summarize aerosol conditions. However, in Chapter 4, it will be shown that there are unresolved issues in using Channel C estimates of the carbonaceous species.

# CHAPTER 4

# VALIDATION

The self-consistency and overall quality of the aerosol component measurements are assured by redundancy and intercomparisons between independently measured species. As discussed in Chapter 2, IMPROVE aerosol sampling and aerosol component species measurements proceed in four channels, labelled A through D, with each channel characterized by 1) the type of collection filter used, 2) the measuring technique(s) performed on the collected sample, 3) the species measured, and 4) the particle size range. Validation is a matter of comparing physically or chemically related species that have been measured in different channels. The comparisons discussed in the following sections are the primary ones.

## 4.1 Sulfur and Sulfate

Sulfur-containing aerosols are measured twice, following the IMPROVE philosophy of redundancy and independent quality assurance for important parameters. Channel A provides a measure of the concentration of elemental sulfur (S), by Proton-Induced X-ray Emission (PIXE) from the aerosol sample collected on a Teflon filter. Channel B provides a measure of the concentration of sulfate ion ($SO_4^{2-}$), by ion chromatography (IC) of the sample collected on a nylon filter placed behind a gas denuder. The denuder, described in Section 2.1.1, removes gaseous $HNO_3$ and $SO_2$ from the sample flow, because they can add artifacts to the particulate nitrate and sulfate measurements. Comparisons of the sulfur and sulfate measurements, presented below, indicate that the Channel A sulfur measurement is not particularly vulnerable to such an $SO_2$-related artifact. The results of a special study, discussed below and in Appendix B, support this view. Thus, while Channels A and B are independent of each other in both sampling and analysis, the sulfur and sulfate measurements are of the same physical species, ambient particulate sulfate.

The molecular weight of the sulfate ion (96) is three times that of sulfur (32). Therefore, the Channel B measure of sulfate should agree well with 3.0 times the Channel A measure of sulfur. Figure 4.1 shows a typical plot, which indicates generally excellent agreement between these independent measurements. However, the Channel A sulfur measurement is more precise, with a 5% uncertainty, and is therefore used in reconstructions involving the sulfates.

The assumption of no significant artifacts in the above measurements has been questioned. In two studies performed at Canyonlands National Park by Eatough et al. (1991),

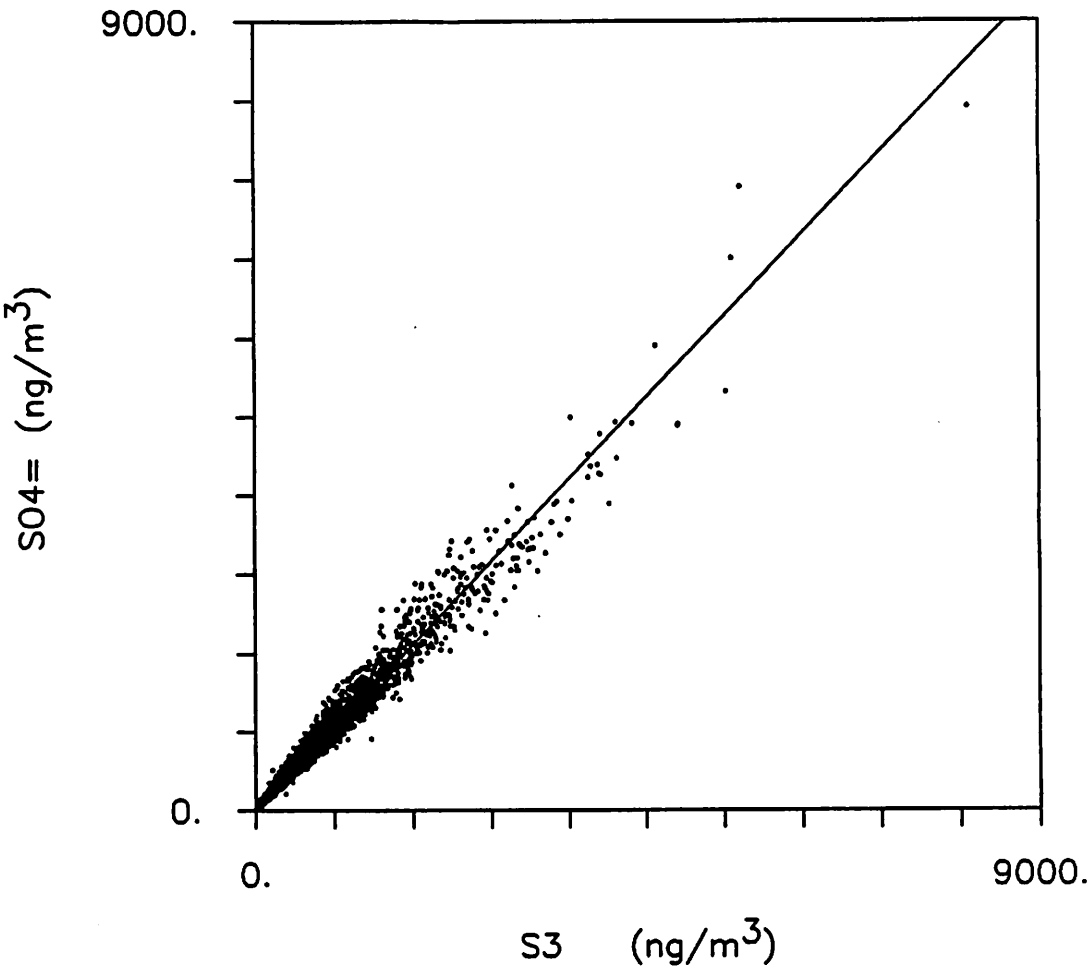


Figure 4.1 Comparison of sulfate on nylon and sulfur (times 3) on Teflon.

a difference in sulfate concentrations of 100 to 300 ng/m$^3$ was observed between their aerosol sampler modules and ones similar to the IMPROVE modules (but with about five times the flow rate). Eatough hypothesized that $SO_2$ gas was interacting with alkaline desert fine particles collected on the filter of the IMPROVE type sampler and was being changed to sulfate to produce a significant increase in the measured sulfate concentrations, and a corresponding decrease in the measured $SO_2$ concentrations. That this artifact was not seen in the samples from their own modules was attributed to their use of a gas diffusion denuder which they believed to be more effective in removing $SO_2$ than the IMPROVE Channel B denuder.

A comparison study to resolve this issue, involving IMPROVE samplers and samplers constructed by Eatough et al., was performed at Meadview (Lake Mead National Recreational Area, AZ) during the period 20-24 November, 1991. Appendix B is a full report of that study and its results. Table 4.1, excerpted from the report, shows that no $SO_2$-related artifact was found, regardless of the type of denuder used in sampling. (If there had been such an artifact, measured sulfur concentrations from samples collected without a denuder would have been larger than those from samples collected with a denuder. The "no denuder" samples actually showed slightly smaller sulfur concentrations, on average, than did the samples collected with a denuder,

as indicated in Table 4.1 by the negative differences in the last column. However, as reported in Appendix B, these differences are insignificant, being generally below the 5% minimum uncertainty in the measurement of sulfur by PIXE.) Also, the IMPROVE Channel B denuder was found to remove at least 60% of the $SO_2$. Thus Channel A must be subject to at least 2.5 times as much artifact as Channel B; however, the comparisons between sulfur and sulfate show no difference. The Meadview study provided overall support and additional validation of IMPROVE aerosol sampling protocols. However, the aerosol conditions during the study were sufficiently in doubt that no final judgement has been made regarding the size of a possible $SO_2$-related sulfur artifact in IMPROVE. Definitive tests are planned.

Table 4.1 Means and standard errors of sulfur by UCD PIXE in ng/m$^3$, for samples with and without a denuder. The difference is the "no denuder" value minus the "all denuders" value, and shows the sign of the "artifact".

| | Period | Duration | No Denuder | UCD Denuder | EPA Denuder | All Denuders | Difference no - all |
|---|---|---|---|---|---|---|---|
| 1 | 11/20 AM | 6.8h | 46±4 | 47±1 | 57 | 50±4 | -4±6 |
| 2 | 11/20 PM | 13.0h | 55±3 | 59±2 | 58 | 59±2 | -4±4 |
| 3 | 11/21 AM | 9.5h | 64±1 | 68±1 | 66 | 67±1 | -3±2 |
| 4 | 11/21 PM | 13.0h | 72±3 | 74±2 | 81 | 76±1 | -4±3 |
| 5 | 11/22 AM | 9.5h | 79±2 | 80±2 | 73 | 78±2 | +1±3 |
| 6 | 11/22 PM | 13.0h | 49±3 | 48±2 | 55 | 50±2 | -1±4 |
| 7 | 11/23 | 30.5h | 94±1 | 90±1 | 89 | 89±1 | +4±2 |
| 8 | 11/24 | 24.0h | 105±1 | 106±3 | 111 | 108±2 | -3±3 |

## 4.2 Carbon

Historically, carbon in atmospheric aerosols has been divided into organic and elemental forms, which are currently believed to contribute to light extinction through scattering and absorption, respectively. Elemental carbon is considered the major contributor to light absorption in the atmosphere, with an approximate absorption efficiency of 10 m$^2$/g. However, analysis of the IMPROVE carbon data, which is also reported in terms of organic and elemental carbon, suggests that significant light-absorbing carbon (LAC) resides in the organic portion. Section 4.2.2 develops this idea.

Carbon in IMPROVE is measured off the Channel C fine quartz filter by the Thermal/Optical Reflectance method (TOR), described in Section 2.1.1. The IMPROVE data provides validation measures for both the organic carbon and the light-absorbing carbon.

## 4.2.1 Organic Carbon and Hydrogen

Validation of the carbon measurement can be performed by comparing the total organic mass calculated from the Channel C organic carbon (OMC, for Organic Mass by Carbon) with the organic mass calculated from the Channel A hydrogen (OMH). As discussed in Section 3.3.1, OMC and OMH are calculated from:

$$OMC = 1.4(OCLT + OCHT) \tag{4.1}$$

$$OMH = 11(H - 0.250 \cdot S) \tag{4.2}$$

for fully neutralized aerosols. Figure 4.2 shows a plot of OMC vs. OMH for all sites for the first two years of data. The agreement between the two measures of organics is good across all sites. Negative values of OMH are due to acidity at some sites and seasons. Dispersion in the data may be due to uncertainty in the organics measured (see Sec. 2.1.2), as well as acid episodes at some sites or variation in the hydrogen fraction of organics from one site to another.

A major artifact problem associated with the data in the third year, which particularly affected the OMC-OMH comparison in the last year of the data reported on here, is discussed in Section 4.3.

OMC can further be used to investigate the acidity at each site, by studying the variation of H with S and OMC. In the study of acidity, OMC is assumed (on the basis of the comparisons with OMH just presented) to be an appropriate estimate of organic mass, and it is written simply as OM.

Acid aerosols are created by the oxidation of gaseous $SO_2$ into sulfuric acid ($H_2SO_4$) under humid conditions. The particulate sulfuric acid scavenges ambient ammonia ($NH_3$) and is neutralized to the extent that such ammonia is present, to produce either a partially neutralized form such as ammonium bisulfate, $(NH_4)HSO_4$, or fully neutralized ammonium sulfate, $(NH_4)_2SO_4$.

It is assumed that the measured hydrogen is comprised only of portions associated with the sulfates and organics (nitrates and water are volatilized in the vacuum conditions of the hydrogen measurement). Since the sulfates account for all of the measured sulfur, we may write

$$[H] = [H_S] + [H_{OM}] = H_s/S[S] + H_{om}/OM[OM], \tag{4.3}$$

where [H], [S] and [OM] are the concentrations of hydrogen, sulfur and organic matter, respectively; and $H_s$ and $H_{om}$ are the portions of hydrogen associated with sulfur and with organic matter, respectively. The ratio $H_s/S$ depends upon the effective form of the ambient sulfates, and indicates the relative acidity, or neutralization, of the sulfates. $H_s/S$ is 8/32 (0.250) for $(NH_4)_2SO_4$, 5/32 (0.156) for $(NH_4)HSO_4$, and 2/32 (0.063) for $H_2SO_4$.

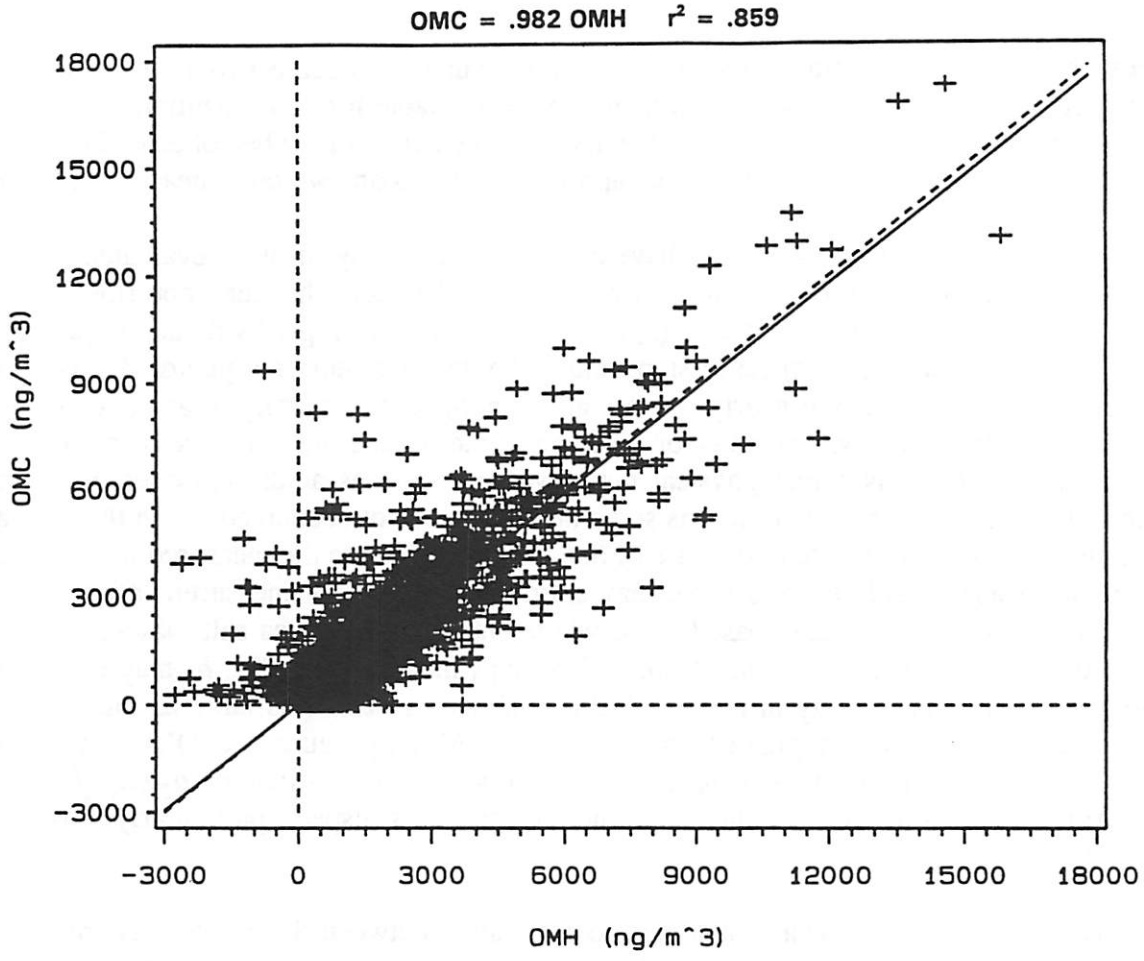


Figure 4.2 Comparison of organic mass on quartz by carbon (OMC) and organic mass on Teflon by hydrogen (OMH).

The $H_s/S$ ratio can be calculated through multivariate regression of H against S and OM over an extended period (generally longer than a single season). Alternatively, if a value for $H_{om}/OM$ is known, $H_{om}$ can be subtracted from H and the value of $H_s/S$ (and hence the acidity) can be studied on a short-term or even individual-sample basis:

$$H_s/S=([H]-H_{om}/OM[OM])/[S]. \qquad (4.4)$$

A value of $H_{om}/OM=0.09$ was used in the comparisons of OMC versus OMH, and gave very good overall results.

Table 4.2 shows the result of regressions of H against S and OM for every site, taken over the first two years of aerosol data. These regressions indicate an average $H_{om}/OM$ value of 0.067, smaller than the 0.09 value noted above; they also suggest that up to 60% of all sites are "over-neutralized", as indicated by the sulfur regression coefficient ($b_1$) being greater than the value of 0.250 corresponding to ammonium sulfate. Some sites show up as significantly acidic, including Hawaii Volcanoes in the Pacific; Mount Rainier, Point Reyes, Redwoods and Pinnacles in the Pacific West; Shenandoah in the East; and Tonto in the Sonoran Desert. These sites are expected to be acidic, for the following reasons: 1)The sites near the ocean lack marine

sources of ammonia to neutralize the sulfates; 2) Shenandoah is subject to a particularly large sulfate load that requires more ammonia than may be available for neutralization; and 3) Tonto is near smelters in Southern Arizona and Mexico, and the aerosol may be collected before it has had time to be neutralized. This may also apply to Shenandoah, which is near power plants.

While the regressions generally have good $r^2$ values, they must be evaluated critically, with consideration of the possible physical and analytical factors that may contribute to these results. For example, the intercept term ($b_0$) in Table 4.2 arises simply by default in performing an OLS (ordinary least squares) regression, and if the development of Equation 4.1 is correct, this intercept should be zero or nearly so. A significant $b_0$ term generally means one of several things: 1) that there is a systematic error involved in the measurement of one or more of H, S and OM; 2) that there is a real physical bias involved, such as acidic episodes occurring at higher sulfur loadings; or 3) that there is some other species not accounted for in the derivation of Equation 4.1, such as nitrate in the case of San Gorgonio (where the measured nitrate is about 3 times the measured sulfate, and some may survive the hydrogen measurement), or such as $Na_2SO_4$ at the coastal and near-coastal sites, where $Na^+$ ions from sea salt may combine with some of the sulfate ions in solution. Also, and perhaps most importantly, $b_0$ may be increased by the fact that the uncertainty in measured OM is about five times as large as the uncertainty in measured S. The much greater uncertainty in OM may cause the OLS regression to overestimate both of the coefficients $b_0$ and $b_1$ ($H_s$/S), while underestimating $b_2$ ($H_{om}$/OM). (In this regard, the variability in $b_2$ indicated in the regressions is suspect, particularly those values below 0.06). Why?

The regression method also assumes no correlation between S and OM. Therefore, bias toward higher sulfur coefficients might also arise from the presence of internally-mixed sulfate/organic aerosols causing a significant correlation of S with OM. Also, periods of fires affecting a number of western sites have undoubtedly skewed their data. The regression for Yellowstone was obtained only after the deletion of four outlying observations in organics and hydrogen during the massive fires at that site in the summer of 1988.

Performing variance-weighted regressions should nullify the effect of the excessive uncertainty in OM and substantially reduce the apparent overneutralization. However, even with variance-weighted regressions there is an analytical bias in the data that also has the effect of overestimating the sulfur coefficient. As discussed in Chapter 2, the organics measurement involves a correction for adsorption of organic gases by the collection filter; and this correction appears to have been systematically too large, frequently resulting in negative reported values of organic matter. These negatives have been removed by simply shifting each organics measurement by an amount equal to the largest negative value obtained, for every season of every year at each site. While this correction gives generally reasonable results, it can sometimes fail. This method is tantamount to assuming that the smallest organics measure in a season is zero, if there are negative values reported in the season; also, if no negative values are reported, there is no positive correction at all. In either case, the method allows for an occasional entire season of systematically underestimated organic matter, which can lead to large overestimation of $H_s$/S. This may be the cause of the high $H_s$/S value obtained for Denali, for example (see Figure 4.3).

units ?

Table 4.2. $H=b_o+b_1S+b_2$ OM regressions.

| REGION | SITE | $b_o$=int | $b_1=H_s/S$ | $b_2=H_{om}/OM$ | $r^2$ |
|---|---|---|---|---|---|
| Alaska | Denali | 2±4 | .302±.020 | .073±.003 | .848 |
| Appalachian | Great Smoky Mtns | 94±16 | .213±.010 | .061±.005 | .865 |
| | Shenandoah | 133±19 | .173±.012 | .068±.007 | .807 |
| Boundary Waters | Isle Royale | 41±8 | .232±.012 | .067±.003 | .929 |
| | Voyageurs | 26±5 | .255±.008 | .077±.001 | .964 |
| Cascades | Mount Rainier | 33±6 | .183±.014 | .077±.002 | .937 |
| Colorado Plateau | Arches | 15±5 | .273±.017 | .074±.004 | .854 |
| | Bandalier | 39±4 | .273±.012 | .059±.003 | .896 |
| | Bryce Canyon | 15±4 | .292±.017 | .062±.004 | .836 |
| | Canyonlands | 23±5 | .264±.017 | .055±.004 | .832 |
| | Grand Canyon | 11±4 | .281±.015 | .059±.004 | .889 |
| | Mesa Verde | 32±4 | .319±.013 | .026±.003 | .823 |
| | Petrified Forest | 38±5 | .270±.019 | .055±.004 | .809 |
| Central Rockies | Bridger | 11±4 | .334±.018 | .060±.004 | .855 |
| | Great Sand Dunes | 27±4 | .285±.018 | .065±.004 | .849 |
| | Rocky Mountains | 14±6 | .380±.023 | .042±.004 | .784 |
| | Weminuche | 13±5 | .349±.019 | .053±.004 | .834 |
| | Yellowstone | 25±6 | .229±.023 | .074±.003 | .823 |
| Pacific Coastal | Pinnacles | 13±9 | .186±.019 | .088±.003 | .853 |
| | Point Reyes | 3±9 | .155±.020 | .099±.003 | .890 |
| | Redwoods | 33±5 | .148±.016 | .068±.002 | .888 |
| Florida | Everglades | -13±13 | .231±.017 | .082±.003 | .903 |
| Great Basin | Jarbidge | 25±4 | .372±.032 | .051±.004 | .782 |
| Hawaii | Hawaii Volcanoes | 24±5 | .186±.004 | .038±.013 | .916 |
| Northeast | Acadia | 34±8 | .236±.009 | .067±.004 | .930 |

Table 4.2 Continued

| REGION | SITE | $b_0$=int | $b_1$=$H_s$/S | $b_2$=$H_{om}$/OM | $r^2$ |
|---|---|---|---|---|---|
| Northern Great Plains | Badlands | 27±5 | .247±.012 | .068±.003 | .890 |
| Northern Rockies | Glacier | 42±7 | .231±.025 | .066±.002 | .893 |
| Southern California | San Gorgonio | 30±17 | .298±.068 | .096±.010 | .791 |
| Sonoran Desert | Chiricahua | 16±5 | .296±.011 | .068±.004 | .912 |
| | Tonto | -55±24 | .157±.051 | .168±.010 | .668 |
| Sierra | Yosemite | 17±5 | .312±.018 | .071±.002 | .932 |
| Sierra Humboldt | Crater Lake | 15±6 | .443±.045 | .048±.004 | .786 |
| | Lassen Volcanoes | 23±4 | .303±.028 | .062±.003 | .851 |
| Washington DC | Washington | 8±10 | .291±.012 | .074±.007 | .953 |
| West Texas | Big Bend | 32±6 | .257±.011 | .056±.004 | .896 |
| | Guadalupe Mtns | 38±7 | .309±.012 | .029±.005 | .835 |

At the heart of the regression method is the fact that, aside from analytical or measurement biases and the possibility of unaccounted species at some sites, the quality of the long-term regression depends upon there being an actual value of $H_s$/S (and of $H_{om}$/OM) about which the ratio varies randomly and by only a limited amount, for all samples during the period of the regression. This means that the sulfate should have about the same average form (and the organics should have about the same average fraction of hydrogen) throughout. This should be the case at sites with periods during which the sulfates are fully neutralized, for example; and, while $H_s$/S would change during acid episodes, $H_{om}$/OM may be stable in such epsodes. Cases of a nearly constant value of $H_s$/S could allow an accurate determination of $H_{om}/OM$, according to:

$$H_{om}/Om=([H]-H_s/S[S])/[OM]. \qquad (4.5)$$

From this value of $H_{om}$/OM, changes in $H_s$/S that occur in other periods might be followed.

In general, there are a number of uncertainties involved in the calculation of acidity, whose separate effects are not easily discriminated. More detailed studies are being performed,

however, and the method discussed herein may hold some promise both as a measure of aerosol acidity and a check on the ambient organic forms in aerosols.

### 4.2.2 Elemental Carbon and Light Absorption

The carbon measurements can also be compared with the light absorption measurement, $b_{abs}$. Based on the previous discussion of light-absorbing and organic carbon, $b_{abs}$ should correlate well with elemental carbon, but not with OCLT or OCHT (unless the elemental and organic carbons are well correlated with each other). However, this is not the case.

Figures 4.4a and 4.4b show scatter plots of $b_{abs}$ vs. each of the four carbons at selected sites. (Scatter plots for all of the sites are presented in Appendix C.) It can be seen that ECHT often shows little or no correlation with $b_{abs}$, except at sites (particularly in the West) where the amount of ECHT is comparable to the ECLT; and even then, ECLT and ECHT show little correlation with one another. Instead, surprisingly, $b_{abs}$ is well correlated with both ECLT and OCHT. (There is sometimes even an indication of correlation between $b_{abs}$ and OCLT). These results suggest the possibility that light-absorbing carbon may be primarily divided between OCHT and ECLT.

At many sites, OCHT and ECLT are well correlated, and it might be supposed that the correlation of $b_{abs}$ with OCHT could be entirely explained as due to the ECLT associated with the OCHT, and not because OCHT itself absorbs light. However, if ECLT is responsible for most of the light absorption, then theory would suggest that the ratio $b_{abs}$/ECLT--the absorption efficiency of the ECLT--should be between about 8 and 12 $m^2/g$. However, many sites have ratios of $b_{abs}$/ECLT that are twice the expected value. This suggests that OCHT could contribute approximately half of the light absorption.

Furthermore, at other sites, particularly in a number of the western regions, there is a good deal more scatter between OCHT and ECLT, yet it is OCHT that correlates better with $b_{abs}$ than does ECLT (Figure 4.4b). Also, the scatter plots of $b_{abs}$ vs. ECLT at these sites (which show a limiting, minimum $b_{abs}$/ECLT ratio of about 20 $m^2/g$, with dispersion above that line) are quite similar to the corresponding scatter plots of OCHT vs ECLT (which also show a limiting, minimum OCHT/ECLT ratio, of about 3 or 4, with dispersion above that line). These plots do not rule out the possibility that other absorbing species exist which happen to correlate with OCHT. However, they suggest that $b_{abs}$ fails to correlate with ECLT precisely to the extent and in the same manner that OCHT does not correlate with ECLT, and therefore, that OCHT contains much or most of the light-absorbing carbon not accounted for by ECLT.

In fact, the scatter plots, and hence the correlations, of both ECLT and ECHT with $b_{abs}$ tend to mimic the forms of their respective scatter plots with OCHT. Thus, for example, what little correlation is shown at some sites between $b_{abs}$ and ECHT appears to depend upon the corresponding correlation between OCHT and ECHT at those sites. The conclusion is that even at sites where ECHT is comparable to ECLT, OCHT may contain approximately as much light-absorbing carbon as do ECLT and ECHT put together.

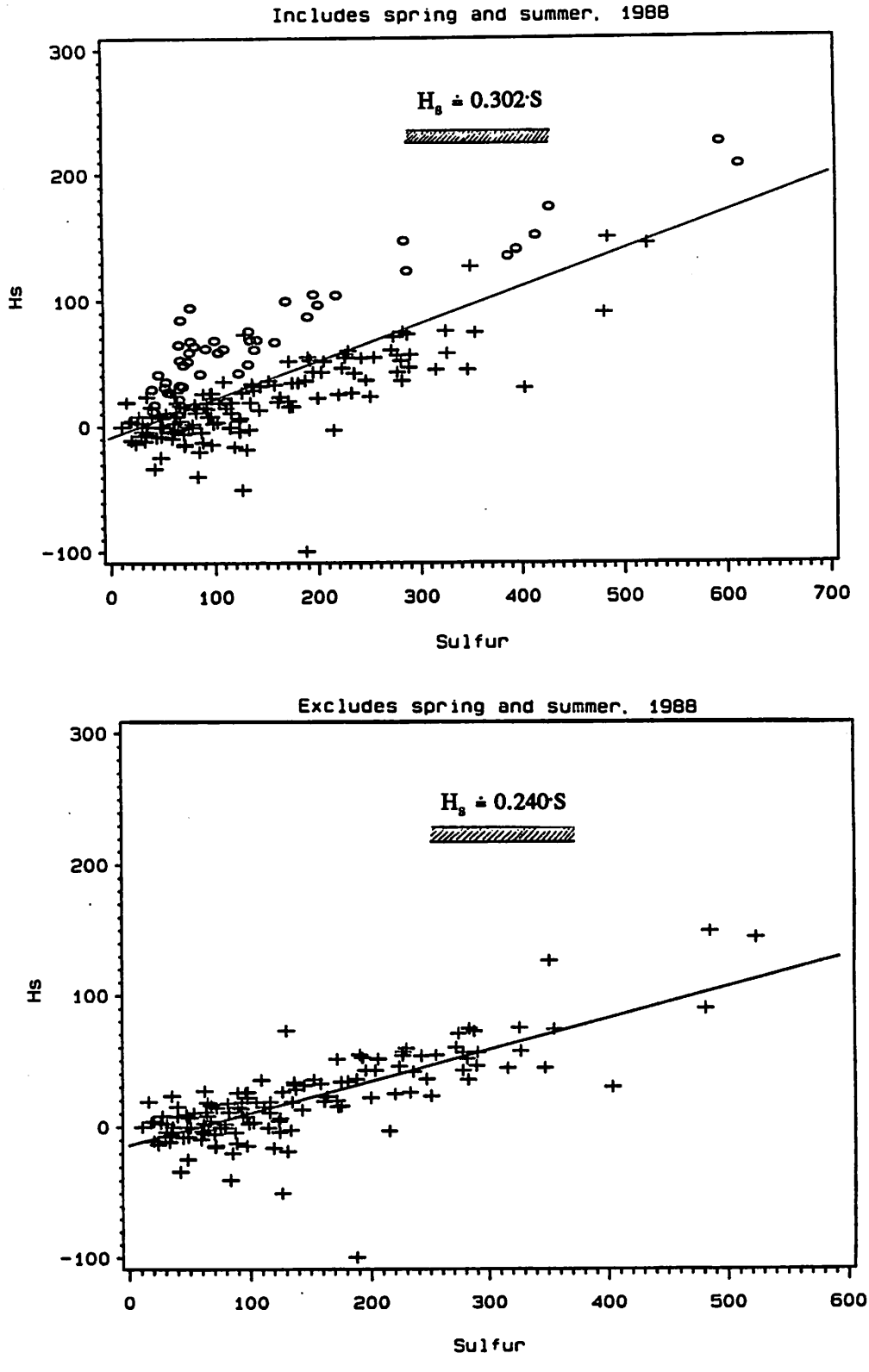


Figure 4.3 Plots of $H_s$ vs. S for Denali. Upper plot includes spring and summer, 1988 (circles), which cause the site to appear overneutralized.

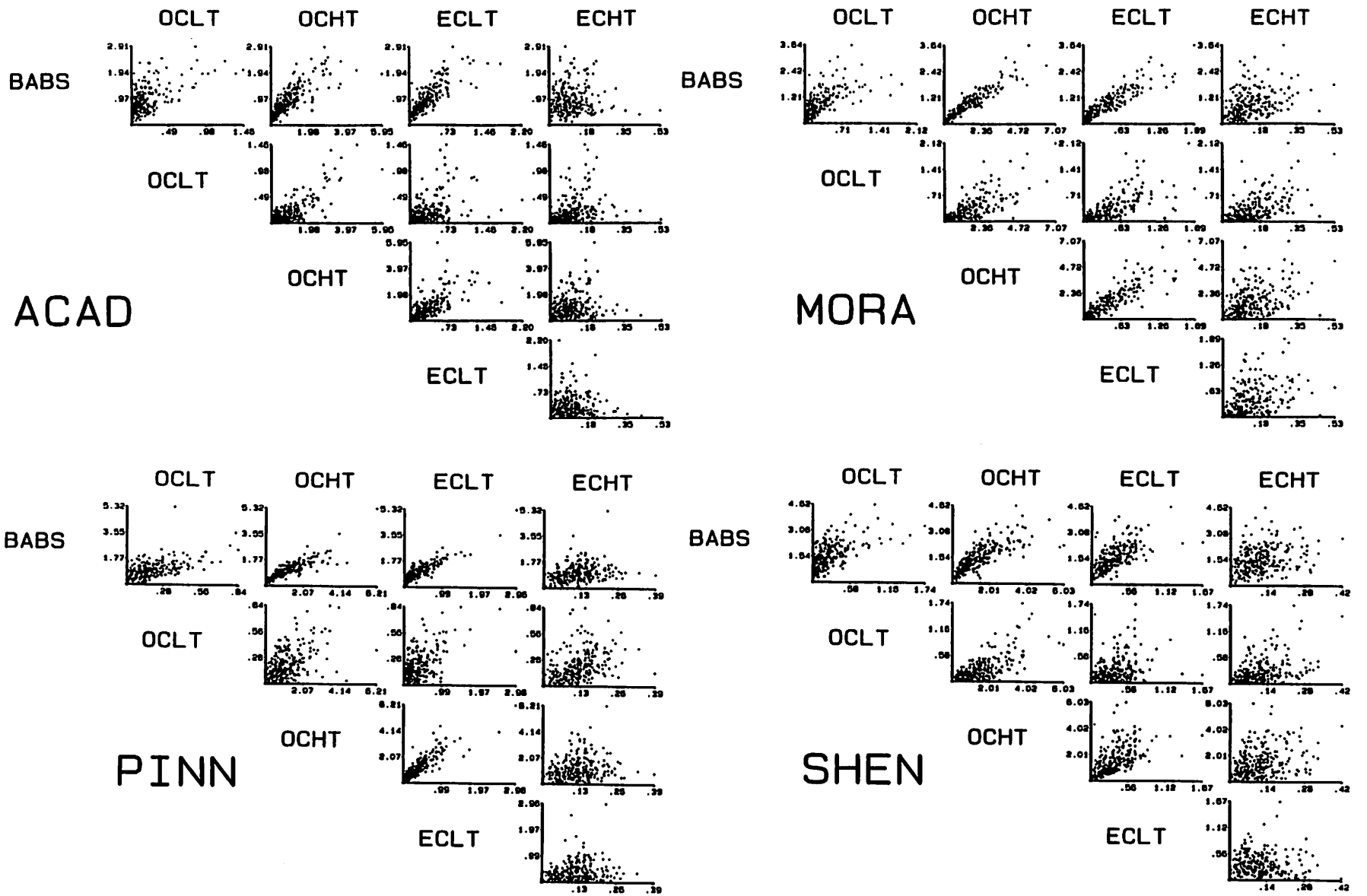


Figure 4.4a Scatter plots of $b_{abs}$ and carbons (OCLT, OCHT, ECLT, ECHT), showing correlation of OCHT and ECLT with $b_{abs}$ and each other, and lack of correlation of ECHT with other species. Units of $b_{abs}$ are $10^{-5}$/m; of carbons, $\mu g/m^3$.

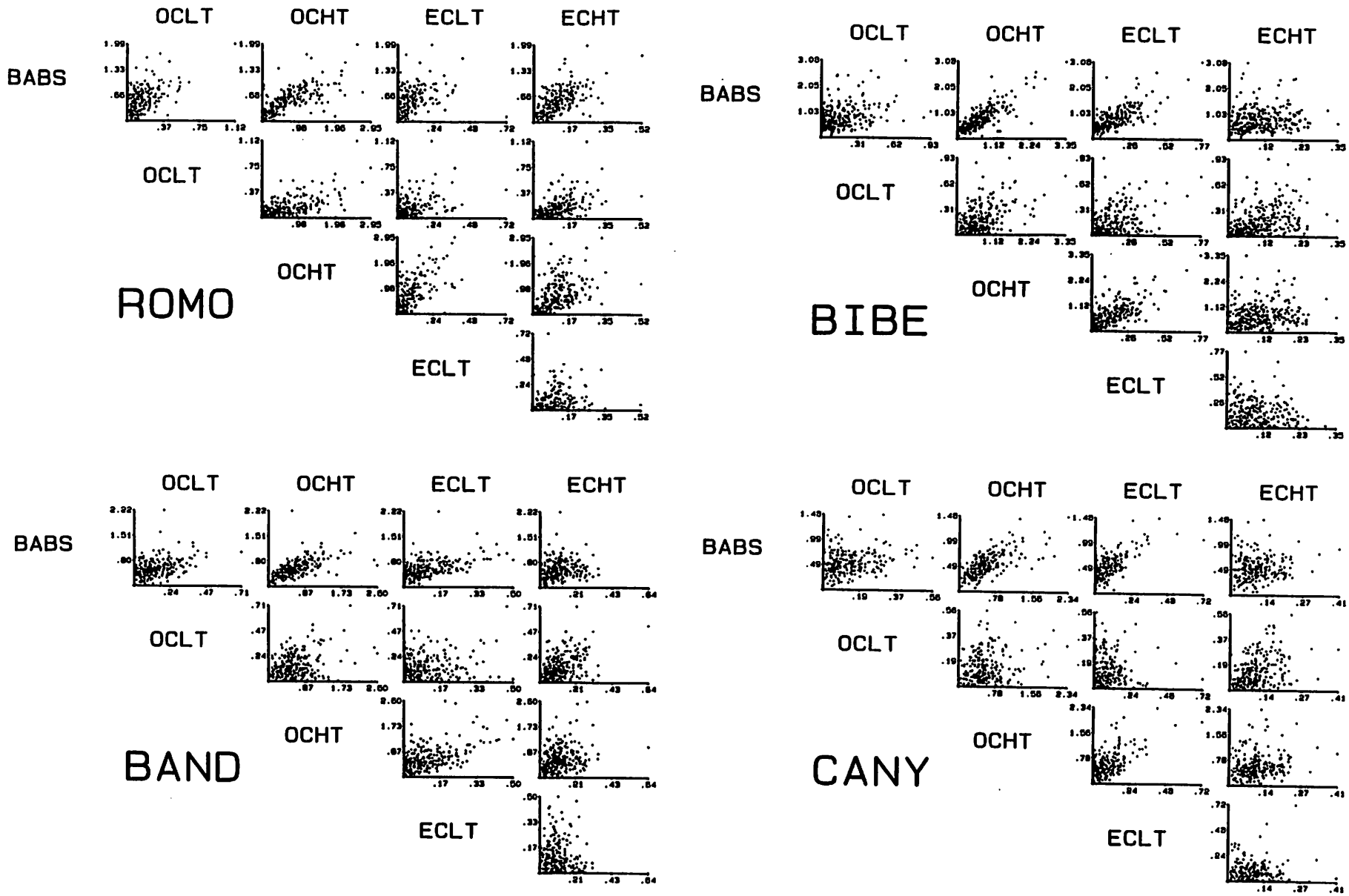


Figure 4.4b. Scatter plots of $b_{abs}$ and carbon species, showing lesser correlation between OCHT and ECLT, and similarity of $b_{abs}$ vs. ECLT and OCHT vs. ECLT plots. Units of $b_{abs}$ are $10^{-5}$/m; of carbons, $\mu g/m^3$.

The assignment of approximately half of the light-absorbing carbon to the OCHT at sites such as those represented in Figure 4.4b would reduce the observed absorption efficiency of the carbon approximately from 20 $m^2/g$ to the widely-accepted value of 10 $m^2/g$. Since the light-absorbing carbon appears to be principally divided between OCHT and ECLT, and the underlying ratio of these two species is about 4 to 1, it follows that approximately 25% of the TOR-reported OCHT at these sites may be light-absorbing carbon.

These results are best explained as due to systematic error in the TOR carbon analysis. (The alternatives, of systematic error in $b_{abs}$ or in the presumed absorption efficiency of carbon, would not explain the correlations noted above.) Consideration of the probable nature of the TOR error is necessary here, in order to clarify the current state of carbon analysis, and to contrast the measurements provided by carbon analysis with those demanded by visibility research. Previous analyses have assumed that the division of carbon into organic and elemental forms coincides with the division between light-absorbing and non-light-absorbing carbon. Considering this, the error in TOR indicated by the present analysis is appropriately explained as the misidentification of substantial elemental carbon as organic carbon. Such an error in the demarcation between organic and elemental carbon, the so-called "OC/EC split", might appear to be the most likely explanation for the present results. However, the possibility of such an error is particularly addressed in comparisons of various carbon analysis methods.

TOR has been directly compared with other carbon analysis methods (Chow et al., 1992), including: Thermal/Optical Transmittance (TOT, which differs from TOR only in using transmittance monitoring instead of reflectance to correct for the charring); Thermal Manganese Oxidation (TMO, in which the oxidizing agent, $MnO_2$, is present and in contact with the sample throughout the analysis); carbon spiking experiments (in which precisely controlled amounts of organic or elemental carbon are injected onto a clean filter using a microsyringe); and optical absorption. TOT, and hence indirectly TOR, has also been compared with photoacoustic spectroscopy (Turpin et al., 1990), which tracks the light absorption of an ambient aerosol sample. (In this analysis, the sample's absorption of a modulated laser beam produces heating effects in the sample which can be monitored as an acoustic signal.)

It should be noted that as far as the thermal carbon analysis methods (TOR, TOT, TMO, etc.) are concerned, there is no common definition of organic or elemental carbon (Chow et al., ibid.). Each of the methods divides the analyzed carbon into segments which are defined by 1) temperature, 2) rate of temperature increase, 3) composition of atmosphere surrounding the sample, and 4) method of optical correction for the observed charring. All of the carbon analysis methods, including photoacoustic spectroscopy, divide the carbon into organic and elemental forms, and identify the light-absorbing carbon as primarily elemental carbon. They tend to agree well in analyses of standard compounds of elemental or organic carbon, and of diesel fuel emissions, but not so well in analyses of various natural, and apparently more complex, woodsmoke sources of carbon.

The results of the comparisons of TOR with other carbon analysis methods indicate that TOR compares fairly well, and is therefore as good as any other method. However, where the agreement is not so good, TOR is considered more likely to <u>overestimate</u> the elemental carbon than to underestimate it, with respect to some other analysis methods (Chow et al., ibid.). Furthermore, evidence for elemental carbon misidentified as organic is expected to be seen

during the TOR analysis in either the optical reflectance monitoring or in observed coloration of the evolved material, and it is generally not. Therefore, a systematic error in the OC/EC split by TOR, in the context of other carbon analysis methods and their assumptions regarding carbon, is not particularly indicated.

However, if the light-absorbing carbon in OCHT is in fact not elemental but organic, the situation is changed. TOR is then not necessarily in error at all (as its comparisons with other methods indicate); its reported measurements are simply not directly interpretable as light-absorbing and non-light-absorbing carbon. If the light-absorbing portion of OCHT were identified primarily with the TOR pyrolyzed carbon (see Figure 2.2 and the related discussion in Section 2.1.1), every difficulty might be overcome. This is the one portion of evolved carbon which, if it were light-absorbing in the original state, would nevertheless not be observed as such in the TOR analysis. (It is interpreted as being light-absorbing only as a result of pyrolysis during the TOR analysis.) It is also the portion that emerges as most problematical in the comparisons of various carbon analysis methods, and the portion present in woodsmokes but absent from diesel fuel emissions (Chow et al., ibid.). Therefore, the TOR pyrolyzed carbon is the most probable candidate for additional light-absorbing carbon. The pyrolyzed carbon area indicated in Figure 2.2 (which is an analysis performed on a sample from Yellowstone) has been evaluated as 25% of the total carbon area denoted as OCHT in that figure. This agrees remarkably well with the quantitative conclusion presented above concerning the light-absorbing carbon which may be contained in OCHT at many rural western sites.

The extinction reconstructions calculated in Chapter 6 follow the traditional approach and assume that all absorption is due to LAC=ECLT+ECHT, with an efficiency of 10 $m^2/g$. However, the above discussion suggests that a better estimate for light absorption is $b_{abs}$ itself, and that a better estimate for LAC is the use of $b_{abs}/(10\ m^2/g)$.

## 4.3 Fine Mass

Another validation check is performed by comparing the measured fine mass to a reconstructed fine mass composed of sulfates, organics, light-absorbing carbon and soil, according to the formula:

$$FM = SO_4 + OMC + LAC + SOIL, \tag{4.6}$$

where the variables on the right side of the equation are derived from reported IMPROVE variables, according to the following equations (explained in Chapter 3):

$$\begin{aligned} SO_4 &= 4.125[S], \\ OMC &= 1.4[OCLT + OCHT], \\ LAC &= [ECLT + ECHT], \end{aligned} \tag{4.7}$$

and

$$SOIL = 2.20[Al] + 2.49[Si] + 1.63[Ca] + 2.42[Fe] + 1.99[Ti]. \quad (4.8)$$

The measurements of S, OC and LAC by IMPROVE have been discussed previously. The soil elements are measured in Channel A by PIXE analysis of the Teflon filter. The reconstructed fine mass thus involves Channels A and C, and it is compared with the Channel A fine mass measurement. Nitrates are not included in the reconstructed fine mass used in this comparison with the Channel A fine mass measurement, because they are volatile and not efficiently collected on Teflon. Also, nitrates (as properly measured off Channel B) comprise less than 15% of the total reconstructed fine mass at all sites outside of California (see Chapter 5).

Figure 4.5 shows typical scatter plots comparing measured and reconstructed fine mass. Scatter plots for all sites are given in Appendix D. The difference between the measured and reconstructed fine mass is denoted as unexplained mass. Measured mass is generally larger than reconstructed, and the unexplained mass is positive. The unexplained mass is thought to be residual water on the filter at the time the filter is weighed. It is greatest at sites with higher relative humidities. In the fine mass reconstruction, LAC could be replaced by $b_{abs}/(10\ m^2/g)$. Similarly, OMC could be replaced by OMH, particularly where the organic mass is small and the hydrogen measurement would be more accurate than the carbon. Time lines of the ratio of measured fine mass to reconstructed are provided in Appendix E for all sites, and Figure 4.6 gives typical examples.

It was discovered that the ratio of measured to reconstructed fine mass exhibits anomalously large values and swings in value at many sites in the middle to latter part of 1990. Data analysis was performed at the National Park Service, Colorado State University, including organics-by-carbon vs. organics-by-hydrogen plots and $H_s$ vs. S studies of acidity. This analysis suggested a possible excess hydrogen problem, which might be due to water or an organic artifact. A typical example of the observed effect of the artifact upon data plots is shown in Figure 4.7 for the Bandelier site.

An extensive study of the problem at all sites was performed by University of California (UCD). From March 1988 to September 1990, they reported, there was excellent agreement between the OMH measured off the Channel A Teflon filters and the OMC measured off the Channel C quartz filters (Figure 4.2). However, from September 1990, the Teflon measurements showed occasional but large positive offsets relative to the quartz measurements (Figure 4.8). During this latter period, the sulfur concentrations on Teflon maintained excellent agreement with the sulfate from corresponding nylon filters (Figure 4.9). The other IMPROVE data indicated the artifact was strictly organic and affected only the hydrogen (thus OMH) and fine mass measurements on the Channel A Teflon filter. Extensive tests, at Desert Research Institute and UCD, of the Channel C TOR organic carbon analysis of the quartz filter, supported the OMC measurement and indicated the problem was not analytical.

The problem began with a shipment of Teflon filters used between September 1990 and November 1991. An earlier batch, in April 1990, also had a problem--a bowing of the filter due to the support ring--and had been returned to the manufacturer. This batch had serious quality

control problems, such as occasional small holes, debris, and shiny flecks (the last evidently caused by improper maintenance of the die). The organic artifact was difficult to define because it was not readily observable on clean filters, but became evident after interaction with the air. It appeared on a relatively small fraction of filters, and it appears to have been associated with the manufacturing of the ringed filter, although UCD could not rule out the possibility of problems with the Teflon filter material itself.

Scanning electron microscope analysis of filters with the identified artifact showed the artifact to be a relatively flat material that blocks out all view of the Teflon substrate in the region of the artifact. Some of the artifact was seen on the back side of the filter.

One result of this discovered artifact was a decision to discontinue using recycled polyolephin in the filter support rings. The filter manufacturer's quality control procedures have been improved, and a new batch of Teflon material was produced. A prototype batch was scheduled to arrive in April 1992, and the first filters from the production run of this material were due to be received in May 1992.

Because of this artifact in the third year of data, only the data for the first two years were used in those areas of study affected by the artifact, including estimations of acidity and the reconstruction of fine mass by principal aerosol species.

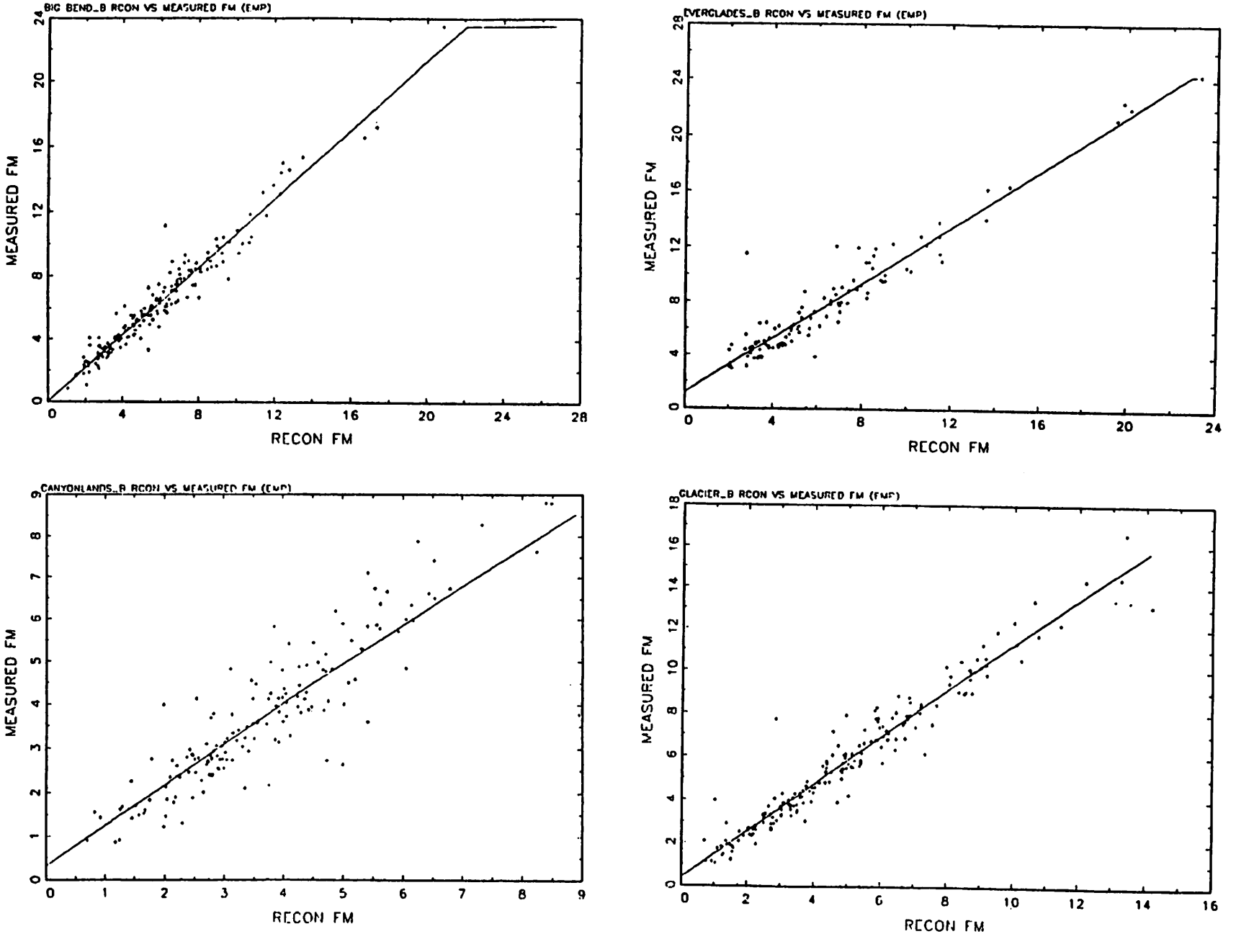


Figure 4.5 Comparisons of measured and reconstructed fine mass.

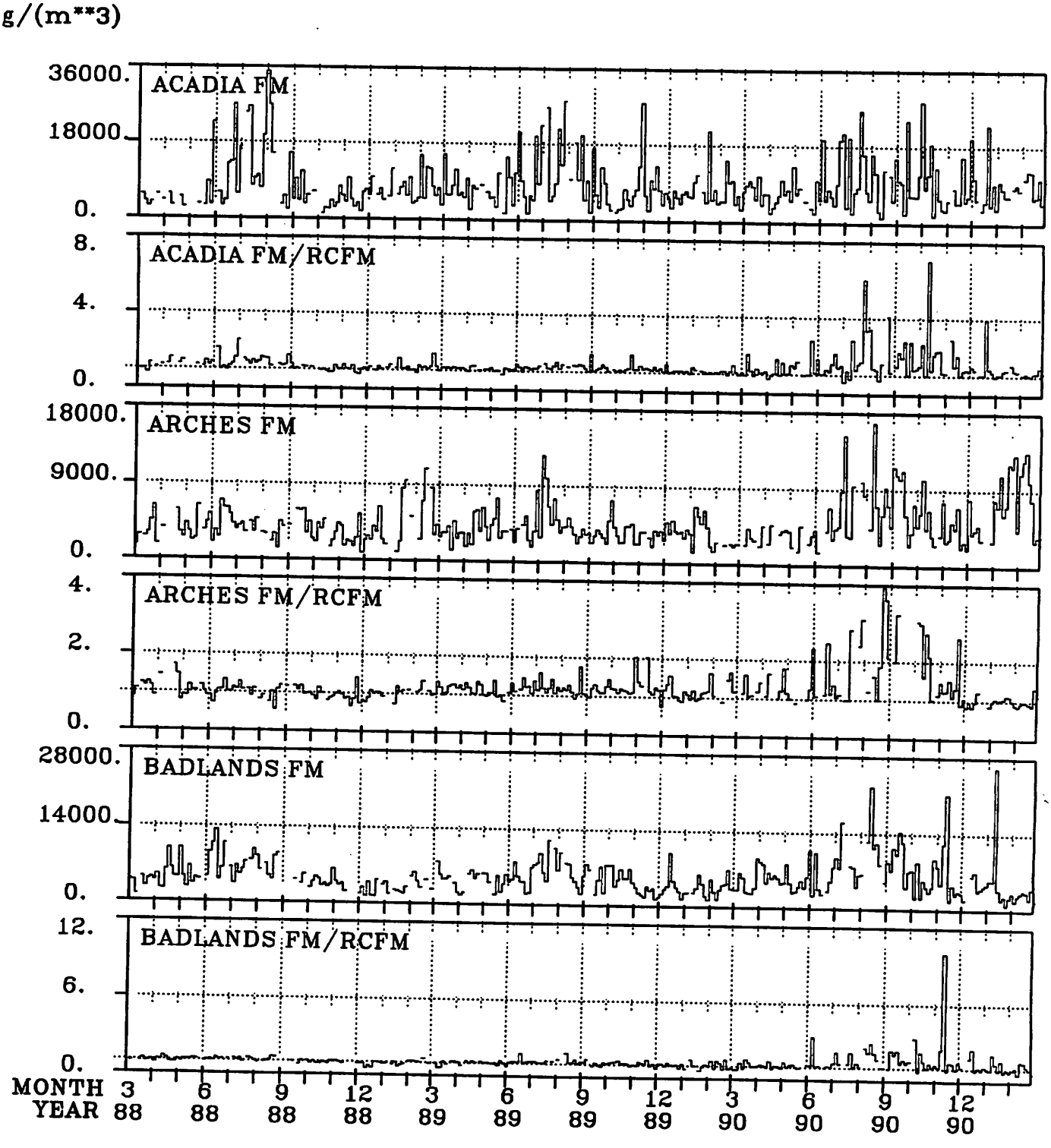


Figure 4.6 Selected fine mass time lines. There are two timelines for each site; the top one in each pair is the measured fine mass, the lower one is the ratio of measured to reconstructed fine mass.

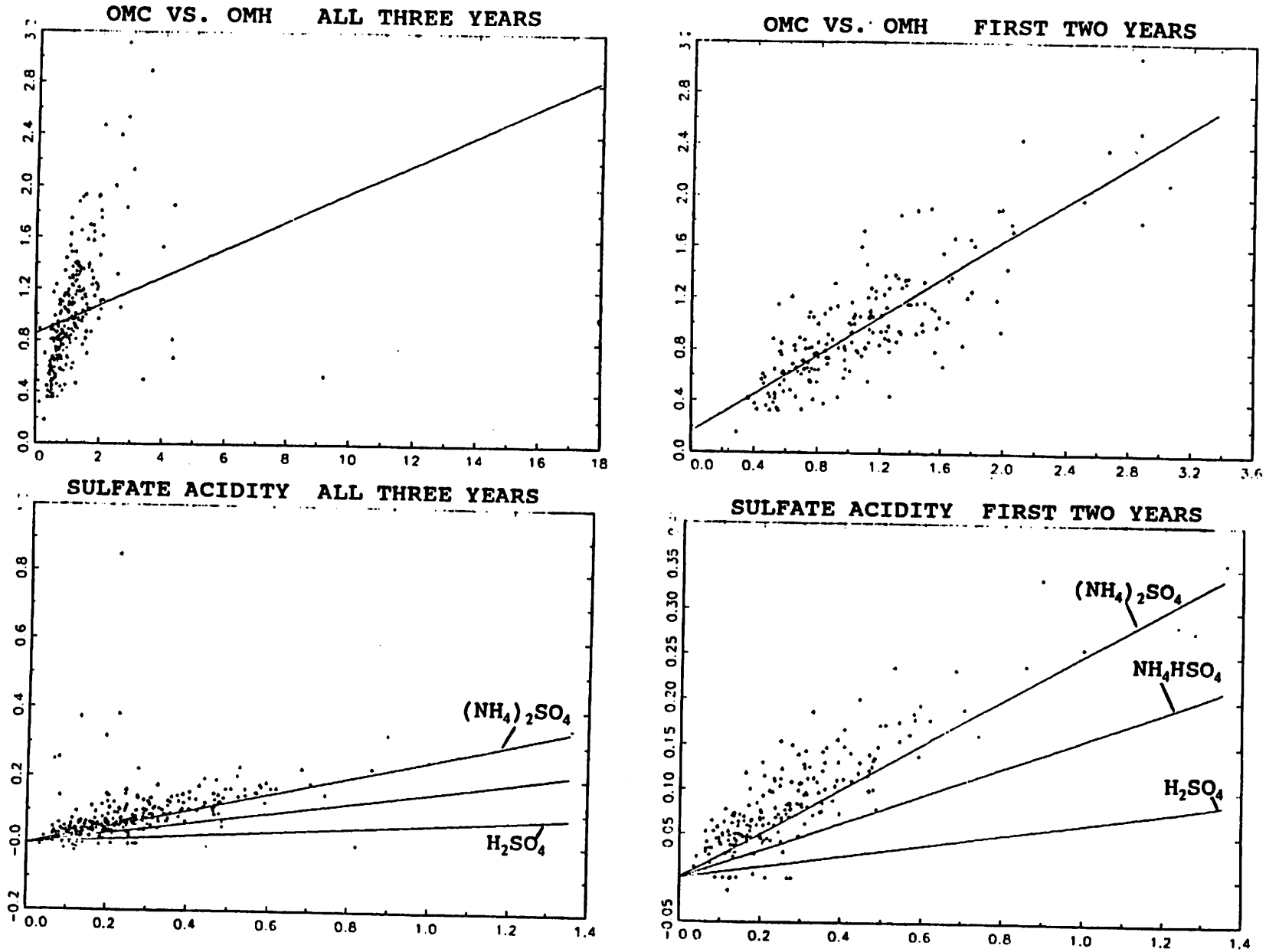


Figure 4.7 Typical effects of the artifact in the third year. The upper pair of plots are OMC vs. OMH; the lower, sulfate acidity. Left-hand plots include data from the third year; right-hand plots do not. Deviations are few, and indicate elevated hydrogen.

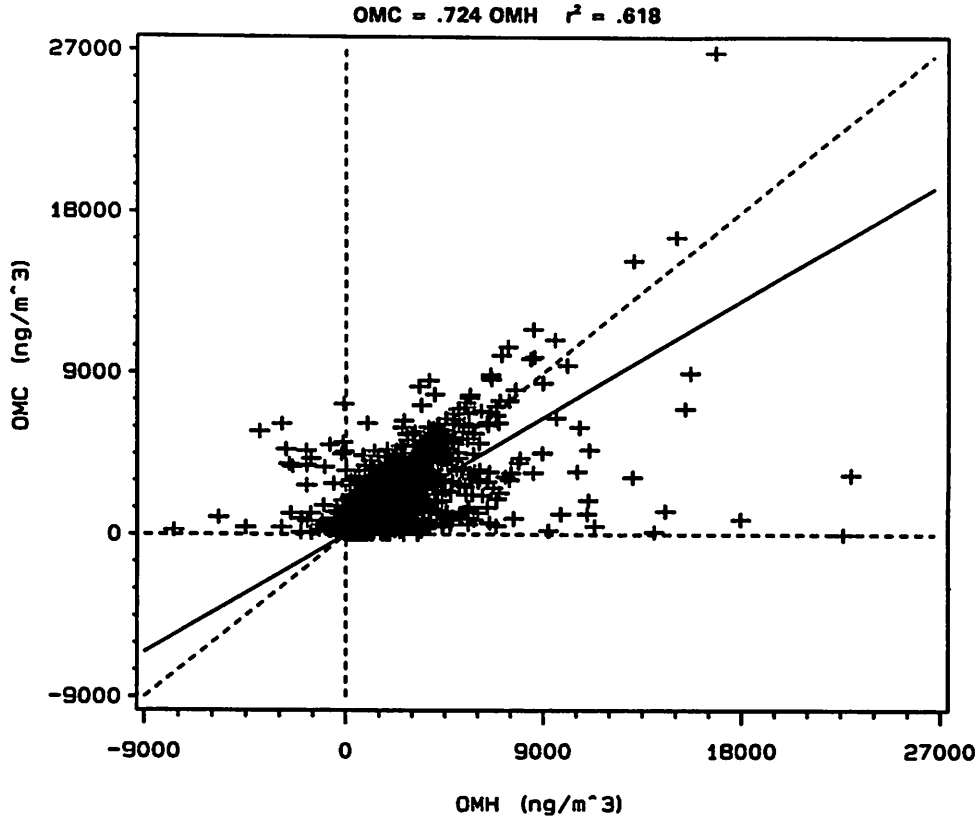


Figure 4.8 OMC versus OMH for the period of the Teflon artifact.

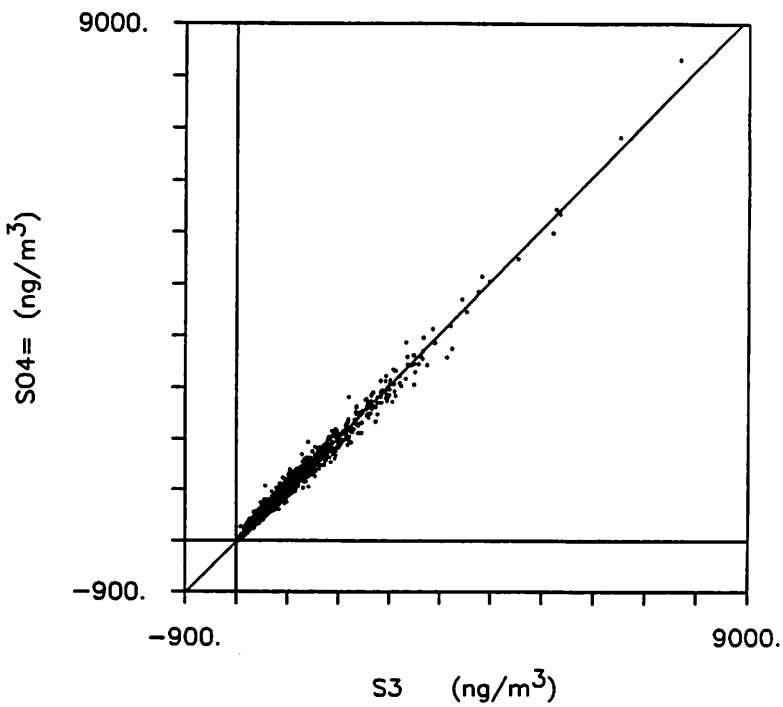


Figure 4.9 $SO_4$ versus 3·S for the period of the Teflon artifact.

# CHAPTER 5

# SPATIAL AND SEASONAL DISTRIBUTION OF AEROSOL CONCENTRATION

This chapter discusses the observed spatial and temporal variations in aerosol concentration and chemical composition throughout the United States on the basis of the IMPROVE measurements (see Chapter 3) for the three-year period, March 1988 through February 1991.

Aerosol concentrations and chemical composition vary because of a number of factors, including the spatial distribution of natural and anthropogenic emission sources and the meteorological conditions of the area. Highest aerosol concentrations tend to occur in significant urban or industrialized areas where emission densities are high. Also, concentrations are highest when atmospheric dilution is minimal such as what occurs in stagnation periods or periods of limited mixing. In addition, since sulfate and nitrate aerosols are formed from $SO_2$ and $NO_x$ emissions and chemical reactions in the atmosphere, these aerosols are highest when photochemistry is strongest.

For example, concentrations of sulfates tend to be highest in areas of significant sulfur dioxide ($SO_2$) emissions such as the eastern United States where $SO_2$ is emitted from coal-fired power plants, and in the Southwest due to copper smelter and Mexican $SO_2$ emissions. Organic carbon concentrations tend to be highest in regions such as the Pacific Northwest due to forests and forest-products industries and in areas such as Southern California from motor vehicle emissions. Nitrates tend to be most prevalent in California where both $NO_x$ emissions from motor vehicles and industry are high.

Spatial and temporal variations in aerosol composition and concentrations can be qualitatively examined through the use of annual and seasonal descriptive statistics of the three years of measurements (Appendix F), time lines of the individual measurements as shown in (Appendix G), and mass budgets. Mass budgets are the contribution of individual aerosol species to the reconstructed fine particle mass (see Chapter 3). Mass budgets are calculated by dividing the average concentration of each species by the average reconstructed fine particle mass for each region and time period of interest.

In this chapter, the observed spatial and seasonal trends in aerosol concentrations and chemical composition from the first three years of the IMPROVE network are presented. The 36 IMPROVE sites are grouped into regions according to their relative location, climatology, sulfate acidity, and similarities in concentrations and seasonal trends (see Chapter 1 for a list of the sites in each region). Average concentrations and chemical composition are calculated on

the basis of the measurements for each region. Tables 5.1 and 5.2 show the mass concentrations of fine and coarse aerosol and the chemical composition (mass budgets) of the fine aerosol for each of the 19 regions in the United States. These concentrations and mass budgets are averaged over the entire three-year period to provide the annual average and over the three years for each of the four seasonal averages. Figures 5.1 and 5.2 present these data in graphical form. The seasonal and annual averages of concentrations and mass budgets are presented as bar charts for each region and overlaid on maps of the United States.

Figures 5.3 and 5.4 show isopleth maps of measured three-year averages of fine and coarse particle concentrations, respectively. Figures 5.5 through 5.9 show isopleth maps of the three-year average concentrations and mass budgets for all the sites in the United States for the sulfate, nitrate, organic carbon, light-absorbing carbon, and soil fractions of the fine aerosol, respectively. The top map in each figure shows the concentration, and the bottom map shows the percentage contribution (mass budget) of the given species to total reconstructed fine-particle mass.

First, the characteristics of each of the regions (in alphabetic order) is discussed, followed by the spatial and temporal trends of the fine and coarse mass concentrations and the constituents of the fine-particle mass.

## 5.1 Characteristics of the Regions

Alaska. The Alaska region has only one monitoring site at Denali National Park. The average concentrations of fine and coarse aerosol over the three-year period were 1.9 and 4.2 $\mu g/m^3$, respectively. The fine aerosol concentration was the lowest measured anywhere in the United States during this period. Both fine and coarse aerosol concentrations are largest in summer and smallest in autumn. Organic carbon is the largest contributor of fine particle mass (at 44%), followed by sulfate (33%), soil (17%), and nitrate and light-absorbing carbon (each at 3%). The concentrations of organic and light-absorbing carbon are largest in summer, perhaps due to the prescribed burning and forest fires that usually occur during that season.

Appalachian Mountains. This region has monitors at two sites: Great Smoky Mountains and Shenandoah National Parks. The average concentrations of fine and coarse aerosol over the three-year period were 10.9 and 6.2 $\mu g/m^3$, respectively. The fine aerosol concentration was the second largest in the entire United States, exceeded only by the concentration of 16.2 $\mu g/m^3$ measured in Washington, D.C. Both fine and coarse aerosol concentrations are maximum in summer and minimum in winter. Sulfate is by far the largest component of the fine particle mass. At 58 percent, it is more than twice that of the next largest contributor, organic carbon (27%). Other contributors include nitrate (6%), soil (5%), and light-absorbing carbon (4%). Except for nitrate that has its largest concentration in the winter, the other components of fine aerosol all have maximum concentrations in summer. The seasonal variation in sulfate concentrations is particularly strong with summer concentrations of 10.5 $\mu g/m^3$ more than three times winter concentrations.

Table 5.1 Measured fine and coarse aerosol concentrations (in $\mu g/m^3$) for the 19 regions in the IMPROVE network, averaged over the three-year period, March 1988 through February 1991.

| Season | Fine mass | Sulfate | Nitrate | Organics | Elemental carbon | Soil | Coarse mass |
|---|---|---|---|---|---|---|---|
| **ALASKA** | | | | | | | |
| Winter | 1.6 | 0.7 | 0.1 | 0.6 | 0.1 | 0.2 | 4.0 |
| Spring | 2.4 | 0.9 | 0.1 | 0.7 | 0.1 | 0.6 | 3.9 |
| Summer | 2.7 | 0.5 | 0.0 | 1.5 | 0.1 | 0.4 | 5.4 |
| Autumn | 1.2 | 0.4 | 0.1 | 0.6 | 0.1 | 0.1 | 3.2 |
| ANNUAL | 1.9 | 0.6 | 0.1 | 0.9 | 0.1 | 0.3 | 4.2 |
| **APPALACHIAN** | | | | | | | |
| Winter | 6.5 | 3.0 | 0.8 | 2.0 | 0.4 | 0.3 | 3.1 |
| Spring | 10.6 | 6.0 | 0.8 | 2.7 | 0.5 | 0.6 | 4.5 |
| Summer | 16.6 | 10.5 | 0.3 | 4.4 | 0.5 | 0.8 | 11.2 |
| Autumn | 9.7 | 5.6 | 0.5 | 2.7 | 0.5 | 0.4 | 5.5 |
| ANNUAL | 10.9 | 6.3 | 0.6 | 3.0 | 0.5 | 0.5 | 6.2 |
| **BOUNDARY WATERS** | | | | | | | |
| Winter | 5.2 | 2.0 | 1.4 | 1.4 | 0.2 | 0.2 | 3.2 |
| Spring | 5.4 | 2.6 | 0.4 | 1.8 | 0.2 | 0.4 | 5.1 |
| Summer | 6.2 | 2.2 | 0.1 | 3.1 | 0.3 | 0.5 | 8.2 |
| Autumn | 4.3 | 1.6 | 0.4 | 1.8 | 0.2 | 0.3 | 5.8 |
| ANNUAL | 5.3 | 2.0 | 0.6 | 2.1 | 0.2 | 0.3 | 5.7 |
| **CASCADES** | | | | | | | |
| Winter | 3.8 | 0.6 | 0.1 | 2.6 | 0.5 | 0.1 | 2.9 |
| Spring | 5.2 | 1.4 | 0.2 | 2.7 | 0.5 | 0.3 | 3.1 |
| Summer | 6.7 | 2.4 | 0.4 | 3.0 | 0.5 | 0.3 | 4.6 |
| Autumn | 5.3 | 1.3 | 0.2 | 3.1 | 0.5 | 0.2 | 3.9 |
| ANNUAL | 5.1 | 1.3 | 0.2 | 2.8 | 0.5 | 0.2 | 3.5 |
| **COLORADO PLATEAU** | | | | | | | |
| Winter | 2.9 | 0.9 | 0.5 | 1.1 | 0.2 | 0.3 | 3.2 |
| Spring | 3.4 | 0.9 | 0.2 | 1.0 | 0.1 | 1.1 | 5.3 |
| Summer | 4.1 | 1.3 | 0.2 | 1.6 | 0.2 | 0.9 | 6.4 |
| Autumn | 3.2 | 1.2 | 0.1 | 1.2 | 0.2 | 0.5 | 3.7 |
| ANNUAL | 3.4 | 1.1 | 0.2 | 1.2 | 0.2 | 0.7 | 4.7 |
| **CENTRAL ROCKIES** | | | | | | | |
| Winter | 2.0 | 0.5 | 0.2 | 0.9 | 0.1 | 0.3 | 3.0 |
| Spring | 3.4 | 0.9 | 0.3 | 1.1 | 0.1 | 1.1 | 4.3 |
| Summer | 4.8 | 1.0 | 0.1 | 2.4 | 0.2 | 0.9 | 7.5 |
| Autumn | 2.9 | 0.8 | 0.1 | 1.3 | 0.1 | 0.5 | 4.0 |
| ANNUAL | 3.3 | 0.8 | 0.2 | 1.5 | 0.1 | 0.7 | 4.8 |
| **CENTRAL COAST** | | | | | | | |
| Winter | 5.6 | 0.9 | 1.9 | 2.3 | 0.4 | 0.2 | 7.7 |
| Spring | 4.2 | 1.4 | 0.8 | 1.5 | 0.2 | 0.3 | 9.3 |
| Summer | 4.5 | 1.9 | 0.8 | 1.4 | 0.1 | 0.2 | 10.7 |
| Autumn | 5.7 | 1.4 | 1.0 | 2.7 | 0.4 | 0.3 | 7.8 |
| ANNUAL | 5.0 | 1.4 | 1.1 | 1.9 | 0.3 | 0.2 | 8.9 |

Table 5.1 Continued

| Season | Fine mass | Sulfate | Nitrate | Organics | Elemental carbon | Soil | Coarse mass |
|---|---|---|---|---|---|---|---|
| **FLORIDA** | | | | | | | |
| Winter | 5.5 | 2.4 | 0.7 | 1.9 | 0.4 | 0.2 | 8.5 |
| Spring | 7.7 | 3.8 | 0.9 | 2.1 | 0.3 | 0.7 | 8.0 |
| Summer | 9.1 | 2.5 | 0.5 | 3.0 | 0.3 | 2.7 | 13.6 |
| Autumn | 6.9 | 3.1 | 0.5 | 2.3 | 0.4 | 0.5 | 8.6 |
| ANNUAL | 7.1 | 2.9 | 0.7 | 2.3 | 0.4 | 0.9 | 9.6 |
| **GREAT BASIN** | | | | | | | |
| Winter | 1.1 | 0.3 | 0.1 | 0.5 | 0.0 | 0.1 | 1.0 |
| Spring | 2.4 | 0.5 | 0.1 | 0.9 | 0.0 | 0.9 | 3.7 |
| Summer | 4.5 | 0.7 | 0.1 | 1.7 | 0.1 | 1.9 | 8.2 |
| Autumn | 3.1 | 0.6 | 0.1 | 1.4 | 0.1 | 1.0 | 5.1 |
| ANNUAL | 2.8 | 0.5 | 0.1 | 1.1 | 0.1 | 1.0 | 5.0 |
| **HAWAII** | | | | | | | |
| Winter | 4.0 | 2.8 | 0.1 | 0.9 | 0.1 | 0.1 | 3.0 |
| Spring | 3.6 | 2.5 | 0.1 | 0.8 | 0.1 | 0.2 | 7.4 |
| Summer | 1.6 | 0.9 | 0.1 | 0.5 | 0.0 | 0.1 | 10.3 |
| Autumn | 3.4 | 2.5 | 0.1 | 0.8 | 0.1 | 0.1 | 9.3 |
| ANNUAL | 3.2 | 2.2 | 0.1 | 0.7 | 0.1 | 0.1 | 8.2 |
| **NORTHEAST** | | | | | | | |
| Winter | 6.6 | 3.3 | 0.8 | 1.8 | 0.5 | 0.2 | 3.1 |
| Spring | 6.1 | 3.6 | 0.4 | 1.5 | 0.3 | 0.3 | 4.1 |
| Summer | 8.6 | 4.5 | 0.3 | 3.0 | 0.4 | 0.3 | 6.7 |
| Autumn | 5.6 | 3.0 | 0.4 | 1.6 | 0.4 | 0.2 | 4.1 |
| ANNUAL | 6.7 | 3.6 | 0.5 | 2.0 | 0.4 | 0.2 | 4.5 |
| **NORTHERN GREAT PLAINS** | | | | | | | |
| Winter | 3.4 | 1.2 | 0.6 | 1.1 | 0.1 | 0.5 | 3.9 |
| Spring | 5.0 | 1.9 | 0.6 | 1.3 | 0.1 | 1.0 | 6.0 |
| Summer | 5.6 | 1.8 | 0.2 | 2.2 | 0.2 | 1.2 | 9.7 |
| Autumn | 4.0 | 1.2 | 0.2 | 1.5 | 0.1 | 1.0 | 5.8 |
| ANNUAL | 4.5 | 1.5 | 0.4 | 1.5 | 0.1 | 0.9 | 6.3 |
| **NORTHERN ROCKIES** | | | | | | | |
| Winter | 5.3 | 1.0 | 0.6 | 3.0 | 0.5 | 0.3 | 2.5 |
| Spring | 4.6 | 1.1 | 0.2 | 2.4 | 0.3 | 0.6 | 4.2 |
| Summer | 5.4 | 0.9 | 0.2 | 3.0 | 0.3 | 1.0 | 9.2 |
| Autumn | 6.7 | 0.9 | 0.3 | 4.3 | 0.6 | 0.6 | 5.7 |
| ANNUAL | 5.5 | 1.0 | 0.3 | 3.1 | 0.4 | 0.6 | 5.5 |
| **SOUTHERN CALIFORNIA** | | | | | | | |
| Winter | 4.6 | 0.5 | 2.2 | 1.2 | 0.2 | 0.4 | 4.2 |
| Spring | 13.6 | 1.7 | 6.9 | 3.2 | 0.6 | 1.2 | 9.8 |
| Summer | 13.8 | 2.4 | 4.6 | 4.2 | 0.8 | 1.8 | 15.2 |
| Autumn | 8.1 | 1.1 | 3.1 | 2.0 | 0.4 | 1.5 | 13.2 |
| ANNUAL | 9.8 | 1.4 | 4.2 | 2.5 | 0.5 | 1.2 | 10.4 |

Table 5.1 Continued

| Season | Fine mass | Sulfate | Nitrate | Organics | Elemental carbon | Soil | Coarse mass |
|---|---|---|---|---|---|---|---|
| SONORA | | | | | | | |
| Winter | 3.2 | 1.2 | 0.3 | 1.1 | 0.2 | 0.4 | 3.3 |
| Spring | 4.4 | 1.2 | 0.3 | 1.3 | 0.1 | 1.5 | 7.5 |
| Summer | 5.6 | 2.1 | 0.2 | 1.8 | 0.2 | 1.2 | 7.6 |
| Autumn | 4.5 | 1.7 | 0.2 | 1.7 | 0.2 | 0.8 | 5.8 |
| ANNUAL | 4.4 | 1.5 | 0.3 | 1.5 | 0.2 | 0.9 | 6.0 |
| SIERRA | | | | | | | |
| Winter | 2.5 | 0.4 | 0.7 | 1.1 | 0.1 | 0.2 | 2.1 |
| Spring | 4.3 | 1.0 | 0.6 | 1.7 | 0.2 | 0.8 | 4.8 |
| Summer | 7.2 | 1.7 | 0.6 | 3.6 | 0.5 | 0.9 | 7.0 |
| Autumn | 4.4 | 0.9 | 0.6 | 2.1 | 0.3 | 0.5 | 5.3 |
| ANNUAL | 4.5 | 1.0 | 0.6 | 2.1 | 0.3 | 0.6 | 4.7 |
| SIERRA/HUMBOLDT | | | | | | | |
| Winter | 1.7 | 0.2 | 0.1 | 1.0 | 0.1 | 0.3 | 2.9 |
| Spring | 3.0 | 0.6 | 0.2 | 1.4 | 0.1 | 0.6 | 2.9 |
| Summer | 4.0 | 0.7 | 0.2 | 2.2 | 0.3 | 0.6 | 5.6 |
| Autumn | 2.8 | 0.4 | 0.1 | 1.7 | 0.2 | 0.4 | 2.7 |
| ANNUAL | 2.9 | 0.5 | 0.2 | 1.6 | 0.2 | 0.5 | 3.7 |
| WASHINGTON DC | | | | | | | |
| Winter | 16.3 | 5.4 | 3.4 | 4.9 | 2.0 | 0.6 | 30.1 |
| Spring | 16.8 | 7.3 | 2.6 | 4.2 | 1.7 | 1.0 | 10.2 |
| Summer | 16.7 | 8.6 | 1.2 | 4.4 | 1.6 | 0.9 | 13.5 |
| Autumn | 15.3 | 6.6 | 1.6 | 4.4 | 2.0 | 0.8 | 8.4 |
| ANNUAL | 16.2 | 6.9 | 2.2 | 4.5 | 1.8 | 0.8 | 16.4 |
| WEST TEXAS | | | | | | | |
| Winter | 3.6 | 1.5 | 0.2 | 1.1 | 0.1 | 0.6 | 5.1 |
| Spring | 6.4 | 2.2 | 0.3 | 1.7 | 0.2 | 2.1 | 10.4 |
| Summer | 6.6 | 2.5 | 0.3 | 1.7 | 0.1 | 1.9 | 7.4 |
| Autumn | 4.8 | 2.3 | 0.2 | 1.4 | 0.2 | 0.8 | 7.0 |
| ANNUAL | 5.4 | 2.1 | 0.3 | 1.5 | 0.1 | 1.4 | 7.5 |

Table 5.2 Measured aerosol mass budgets (in percent) for the 19 regions in the IMPROVE network, averaged over the three-year period, March 1988 through February 1991.

| Season | Sulfate | Nitrate | Organics | Elemental carbon | Soil |
|---|---|---|---|---|---|
| **ALASKA** | | | | | |
| Winter | 42.1 | 6.2 | 36.5 | 3.4 | 11.8 |
| Spring | 39.5 | 3.1 | 30.5 | 2.3 | 24.6 |
| Summer | 20.7 | 1.2 | 57.9 | 3.2 | 16.9 |
| Autumn | 32.1 | 4.3 | 49.2 | 4.9 | 9.5 |
| ANNUAL | 32.6 | 3.3 | 43.9 | 3.3 | 17.0 |
| **APPALACHIAN** | | | | | |
| Winter | 45.8 | 12.8 | 31.3 | 6.2 | 3.8 |
| Spring | 56.8 | 7.9 | 25.1 | 4.4 | 5.8 |
| Summer | 63.5 | 2.0 | 26.5 | 2.9 | 5.1 |
| Autumn | 58.0 | 4.9 | 28.1 | 5.0 | 4.0 |
| ANNUAL | 58.0 | 5.7 | 27.2 | 4.2 | 4.8 |
| **BOUNDARY WATERS** | | | | | |
| Winter | 38.0 | 27.4 | 27.0 | 3.8 | 3.9 |
| Spring | 48.7 | 6.8 | 32.6 | 3.6 | 8.3 |
| Summer | 35.8 | 2.1 | 50.6 | 4.2 | 7.3 |
| Autumn | 37.9 | 10.1 | 40.9 | 4.6 | 6.6 |
| ANNUAL | 38.9 | 11.0 | 39.5 | 4.1 | 6.5 |
| **CASCADES** | | | | | |
| Winter | 14.6 | 3.5 | 67.2 | 12.0 | 2.7 |
| Spring | 26.7 | 4.7 | 53.2 | 8.8 | 6.7 |
| Summer | 35.7 | 6.1 | 45.1 | 8.1 | 5.0 |
| Autumn | 24.6 | 3.7 | 58.7 | 9.7 | 3.3 |
| ANNUAL | 25.7 | 4.5 | 55.7 | 9.5 | 4.5 |
| **COLORADO PLATEAU** | | | | | |
| Winter | 33.0 | 13.1 | 37.3 | 6.1 | 10.5 |
| Spring | 27.9 | 7.0 | 29.9 | 2.6 | 32.6 |
| Summer | 31.9 | 4.3 | 39.0 | 4.2 | 20.6 |
| Autumn | 36.3 | 4.6 | 38.4 | 5.0 | 15.7 |
| ANNUAL | 31.9 | 7.2 | 36.3 | 4.3 | 20.3 |
| **CENTRAL ROCKIES** | | | | | |
| Winter | 27.8 | 11.2 | 45.1 | 3.8 | 12.2 |
| Spring | 27.6 | 7.8 | 32.0 | 2.1 | 30.5 |
| Summer | 24.0 | 3.2 | 48.7 | 4.6 | 19.4 |
| Autumn | 27.9 | 4.5 | 45.4 | 4.3 | 18.0 |
| ANNUAL | 25.8 | 5.9 | 43.7 | 3.9 | 20.7 |
| **CENTRAL COAST** | | | | | |
| Winter | 16.8 | 29.3 | 44.7 | 6.3 | 2.9 |
| Spring | 33.6 | 18.7 | 36.5 | 4.1 | 7.1 |
| Summer | 43.4 | 17.1 | 31.5 | 2.9 | 5.0 |
| Autumn | 24.2 | 16.3 | 47.9 | 6.9 | 4.7 |
| ANNUAL | 28.5 | 21.1 | 40.3 | 5.2 | 4.8 |

Table 5.2 Continued.

| Season | Sulfate | Nitrate | Organics | Elemental carbon | Soil |
|---|---|---|---|---|---|
| **FLORIDA** | | | | | |
| Winter | 43.3 | 12.5 | 34.0 | 6.9 | 3.2 |
| Spring | 48.5 | 11.2 | 27.4 | 3.7 | 9.2 |
| Summer | 27.1 | 5.9 | 33.3 | 3.4 | 30.2 |
| Autumn | 45.8 | 7.8 | 33.3 | 6.2 | 6.9 |
| ANNUAL | 40.9 | 9.2 | 31.9 | 5.0 | 13.0 |
| **GREAT BASIN** | | | | | |
| Winter | 25.9 | 12.3 | 48.0 | 1.4 | 12.3 |
| Spring | 22.1 | 5.9 | 35.6 | 1.1 | 35.3 |
| Summer | 14.9 | 2.5 | 38.8 | 2.2 | 41.6 |
| Autumn | 17.7 | 4.6 | 44.5 | 2.6 | 30.6 |
| ANNUAL | 18.3 | 4.7 | 40.1 | 2.0 | 34.9 |
| **HAWAII** | | | | | |
| Winter | 70.8 | 1.6 | 22.9 | 2.4 | 2.4 |
| Spring | 67.8 | 2.2 | 22.1 | 1.8 | 6.1 |
| Summer | 56.7 | 5.3 | 30.6 | 2.6 | 4.8 |
| Autumn | 72.0 | 1.6 | 22.1 | 2.0 | 2.3 |
| ANNUAL | 68.5 | 2.2 | 23.4 | 2.1 | 3.7 |
| **NORTHEAST** | | | | | |
| Winter | 50.6 | 11.4 | 27.8 | 7.2 | 3.0 |
| Spring | 58.5 | 7.1 | 24.4 | 5.3 | 4.6 |
| Summer | 52.4 | 4.0 | 35.1 | 4.9 | 3.6 |
| Autumn | 53.5 | 7.1 | 29.4 | 6.6 | 3.5 |
| ANNUAL | 53.5 | 7.2 | 29.8 | 5.9 | 3.7 |
| **NORTHERN GREAT PLAINS** | | | | | |
| Winter | 34.5 | 16.6 | 31.7 | 3.6 | 13.6 |
| Spring | 38.6 | 11.8 | 26.7 | 2.4 | 20.5 |
| Summer | 32.1 | 2.9 | 39.5 | 3.2 | 22.3 |
| Autumn | 30.0 | 5.2 | 37.1 | 3.6 | 24.1 |
| ANNUAL | 34.0 | 8.5 | 33.9 | 3.1 | 20.6 |
| **NORTHERN ROCKIES** | | | | | |
| Winter | 18.6 | 10.6 | 56.7 | 9.4 | 4.8 |
| Spring | 23.3 | 5.2 | 52.2 | 6.7 | 12.5 |
| Summer | 17.1 | 3.1 | 54.5 | 6.1 | 19.2 |
| Autumn | 12.8 | 4.3 | 64.7 | 9.4 | 8.8 |
| ANNUAL | 17.7 | 5.7 | 57.3 | 7.9 | 11.4 |
| **SOUTHERN CALIFORNIA** | | | | | |
| Winter | 11.3 | 47.8 | 26.2 | 5.3 | 9.4 |
| Spring | 12.2 | 51.1 | 23.5 | 4.2 | 8.9 |
| Summer | 17.2 | 33.4 | 30.6 | 5.7 | 13.1 |
| Autumn | 13.4 | 38.6 | 24.3 | 5.1 | 18.6 |
| ANNUAL | 13.9 | 43.0 | 25.9 | 4.9 | 12.3 |

Table 5.2 Continued.

| Season | Sulfate | Nitrate | Organics | Elemental carbon | Soil |
|---|---|---|---|---|---|
| SONORA | | | | | |
| Winter | 38.6 | 8.6 | 34.6 | 5.2 | 13.0 |
| Spring | 26.5 | 6.9 | 29.8 | 2.9 | 33.9 |
| Summer | 37.7 | 3.8 | 33.0 | 3.2 | 22.3 |
| Autumn | 37.5 | 3.7 | 37.1 | 5.1 | 16.5 |
| ANNUAL | 35.4 | 5.5 | 33.4 | 4.1 | 21.6 |
| SIERRA | | | | | |
| Winter | 14.9 | 27.1 | 46.7 | 4.2 | 7.2 |
| Spring | 24.2 | 14.3 | 39.4 | 4.0 | 18.1 |
| Summer | 23.4 | 8.0 | 49.6 | 6.7 | 12.2 |
| Autumn | 20.6 | 13.2 | 48.3 | 6.5 | 11.4 |
| ANNUAL | 21.7 | 13.6 | 46.4 | 5.6 | 12.7 |
| SIERRA/HUMBOLDT | | | | | |
| Winter | 14.2 | 7.2 | 56.6 | 6.6 | 15.4 |
| Spring | 18.6 | 8.2 | 48.5 | 4.8 | 19.9 |
| Summer | 18.2 | 4.7 | 55.1 | 6.5 | 15.5 |
| Autumn | 15.5 | 3.5 | 59.9 | 7.4 | 13.7 |
| ANNUAL | 17.1 | 5.7 | 54.7 | 6.3 | 16.2 |
| WASHINGTON DC | | | | | |
| Winter | 33.2 | 20.9 | 29.9 | 12.4 | 3.6 |
| Spring | 43.6 | 15.5 | 24.9 | 10.1 | 5.9 |
| Summer | 51.4 | 7.4 | 26.1 | 9.8 | 5.3 |
| Autumn | 43.3 | 10.5 | 28.5 | 12.8 | 4.9 |
| ANNUAL | 42.4 | 13.8 | 27.5 | 11.4 | 4.9 |
| WEST TEXAS | | | | | |
| Winter | 40.6 | 6.2 | 31.4 | 3.8 | 18.0 |
| Spring | 33.6 | 4.7 | 26.1 | 2.5 | 33.0 |
| Summer | 38.7 | 4.7 | 25.9 | 2.0 | 28.7 |
| Autumn | 46.8 | 3.4 | 29.1 | 3.5 | 17.2 |
| ANNUAL | 39.3 | 4.7 | 27.6 | 2.8 | 25.6 |

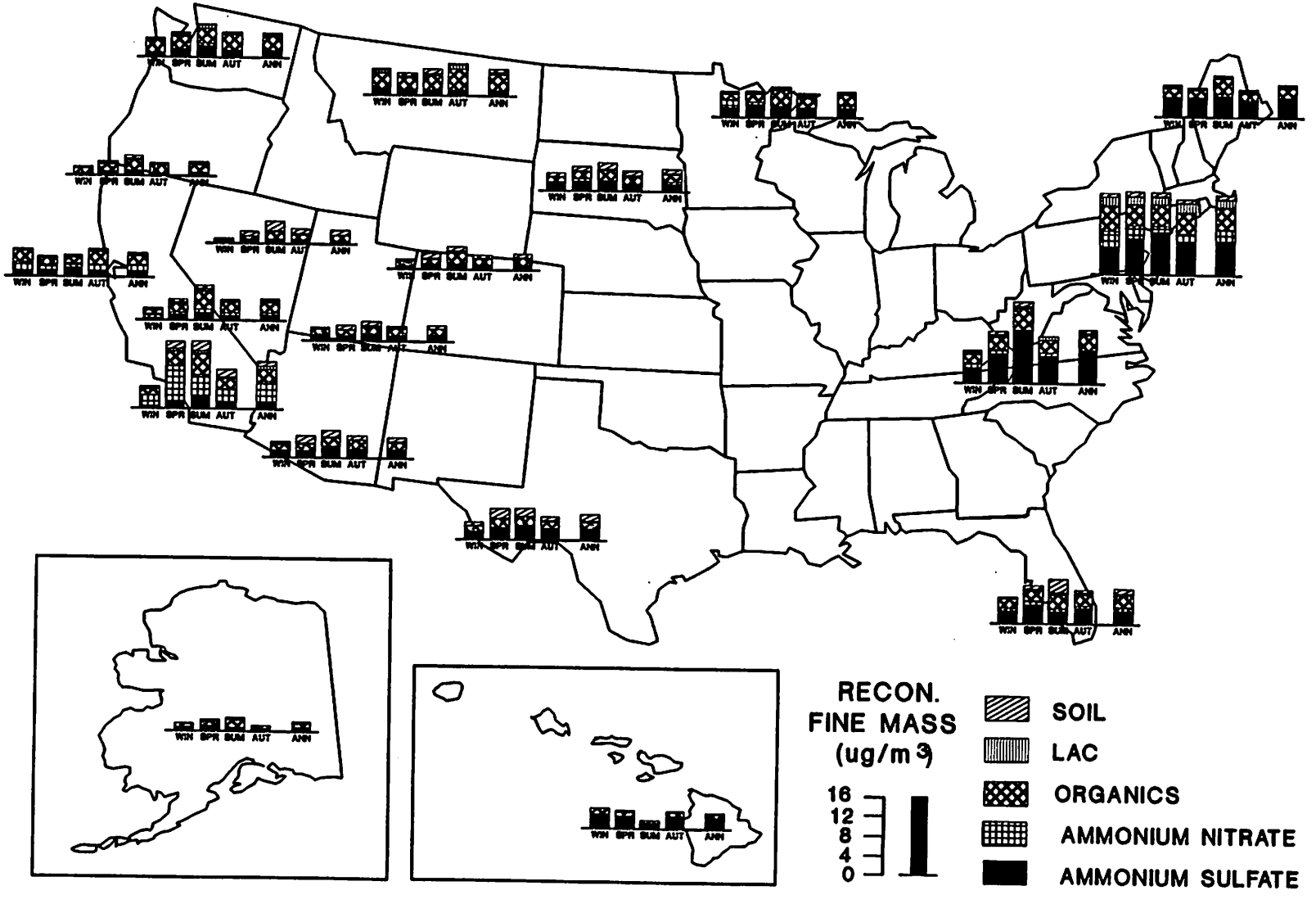


Figure 5.1 Seasonal and annual average concentrations of the fine particle mass and its components (in $\mu g/m^3$) for the 19 regions in the IMPROVE network in the United States for the three-year period, March 1988 through February 1991. For each region the bars from left to right are for winter, spring, summer, autumn, and annual averages.

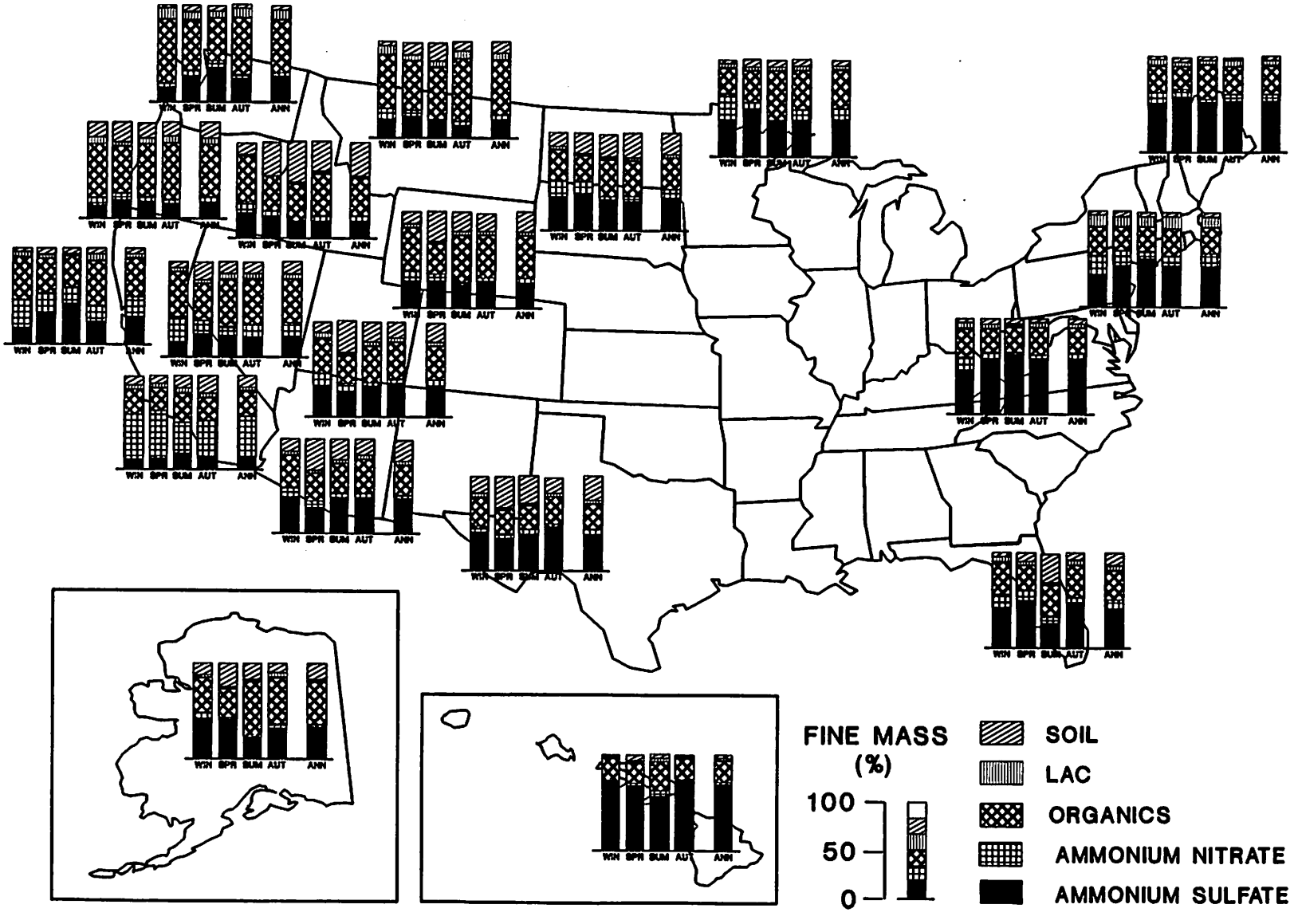


Figure 5.2 Seasonal and annual average fine particle mass budgets (in percent) for the 19 regions in the IMPROVE network in the United States for the three-year period, March 1988 through February 1991. For each region the bars from left to right are for winter, spring, summer, autumn, and annual averages.

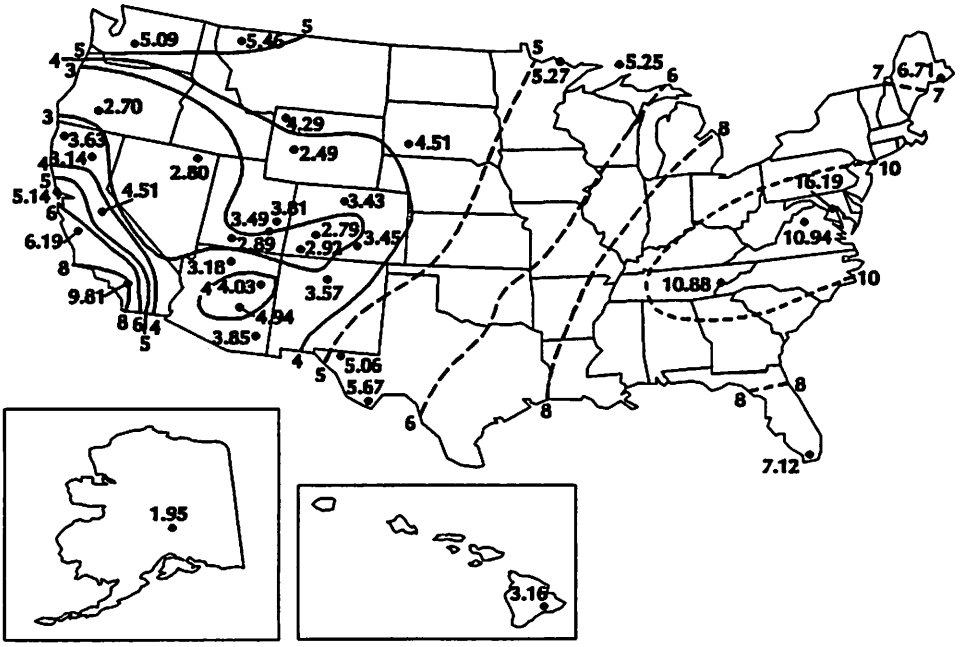


Figure 5.3 Three-year averages of fine particle mass concentrations (in $\mu m/m^3$) for each of the sites in the IMPROVE network in the U.S. for the three-year period, March 1988 - February 1991.

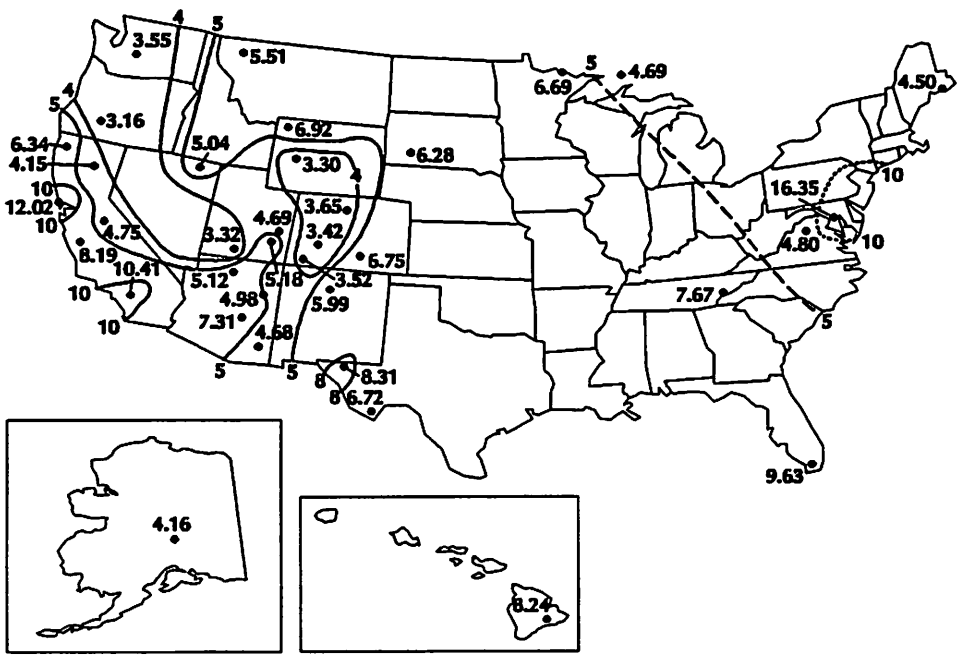


Figure 5.4 Three-year averages of coarse particle mass concentrations (in $\mu g/m_3$) for each of the sites in the IMPROVE network in the U.S. for the three-year period, March 1988 - February 1991.

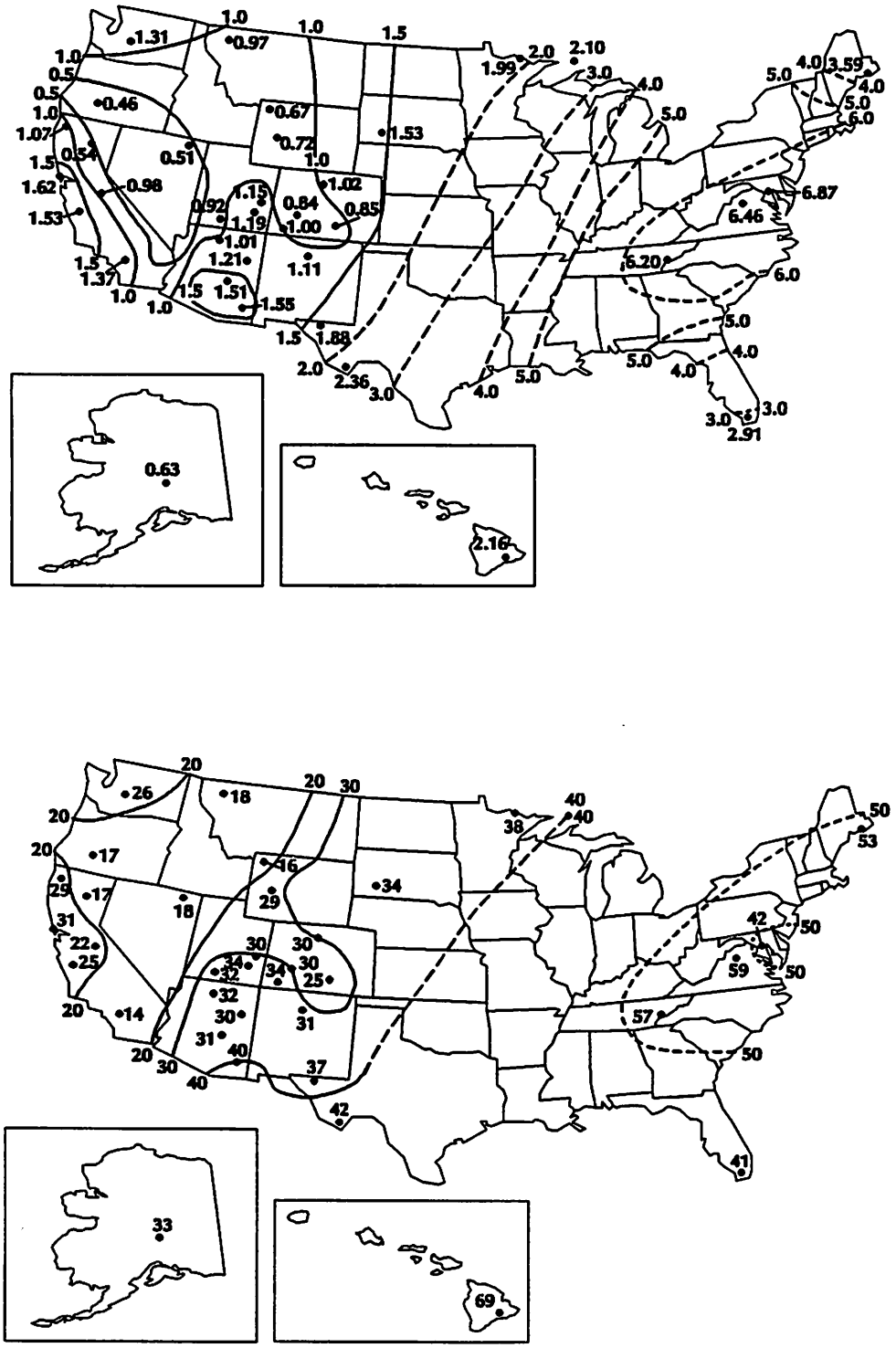


Figure 5.5 Three-year averages of fine sulfate aerosol concentrations (in $\mu g/m^3$) and sulfate fine mass fractions (in percent) for each of the sites in the IMPROVE network in the U.S. for the three-year period, March 1988 through February 1991.

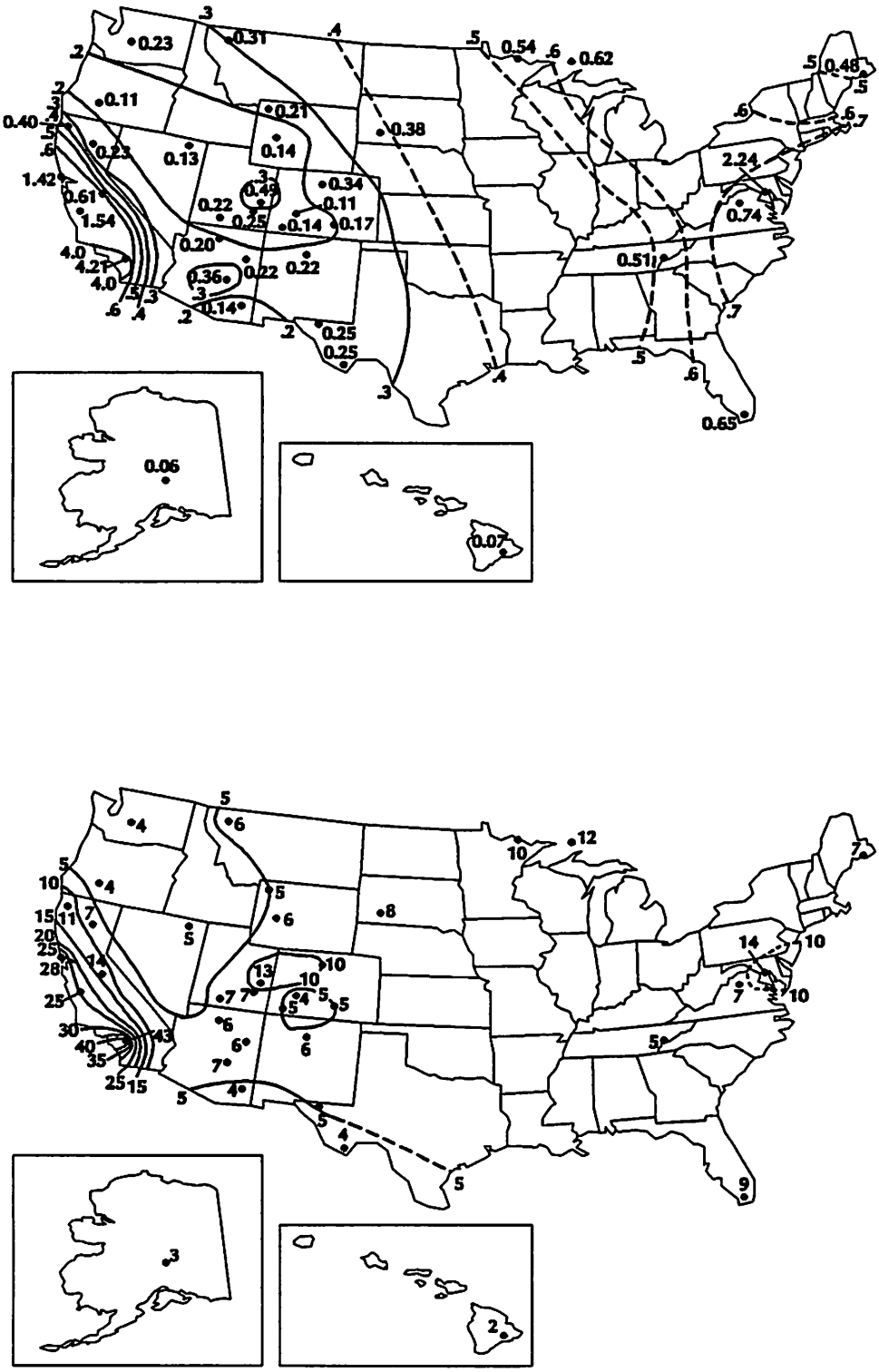


Figure 5.6 Three-year averages of fine nitrate aerosol concentrations (in $\mu g/m^3$) and nitrate fine mass fractions (in percent) for each of the sites in the IMPROVE network in the United States for the three-year period, March 1988 through February 1991.

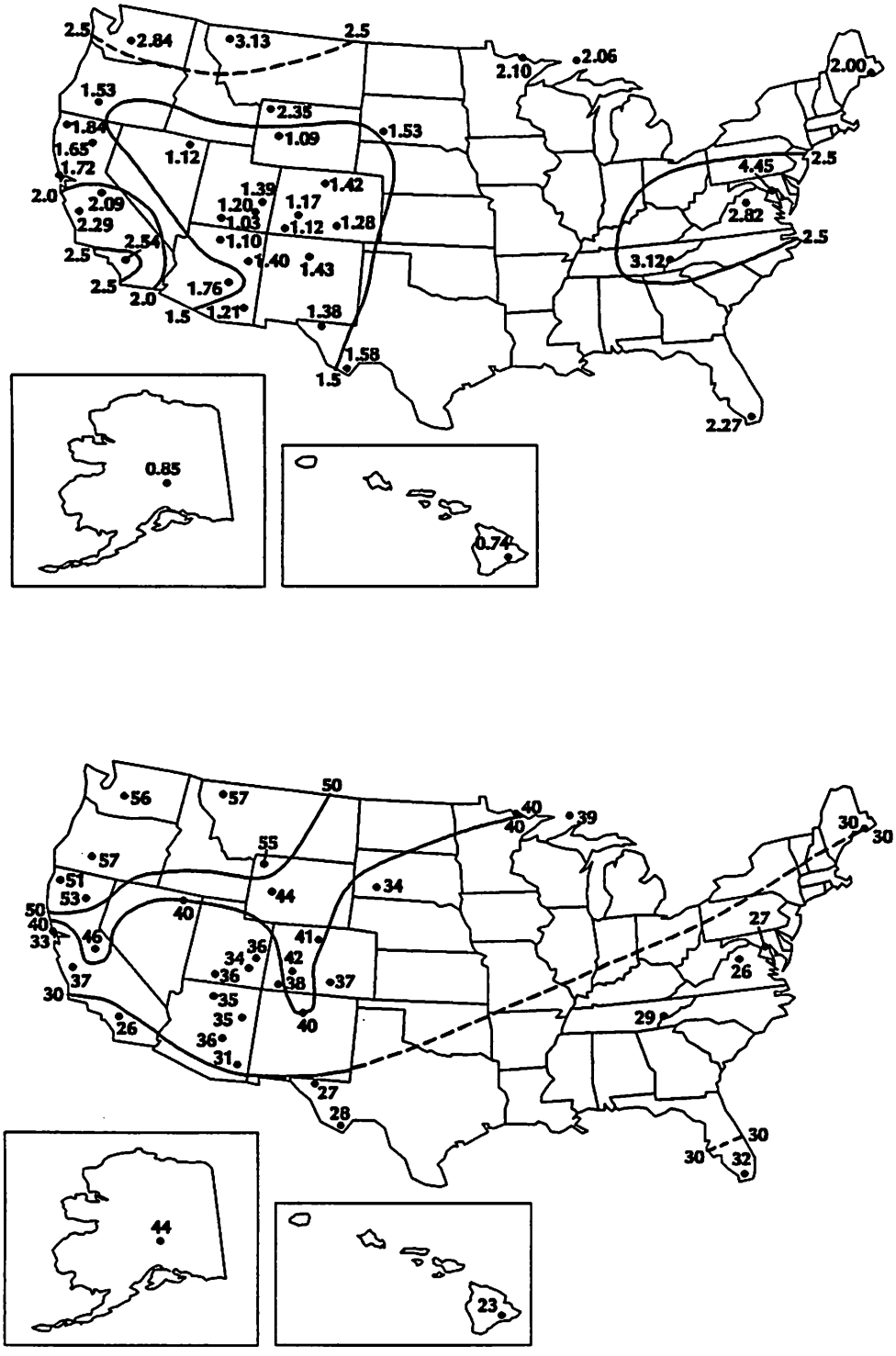


Figure 5.7 Three-year averages of fine organic carbon aerosol concentrations (in $\mu g/m^3$) and organic carbon fine mass fractions (in percent) for each of the sites in the IMPROVE network in the United States for the three-year period, March 1988 through February 1991.

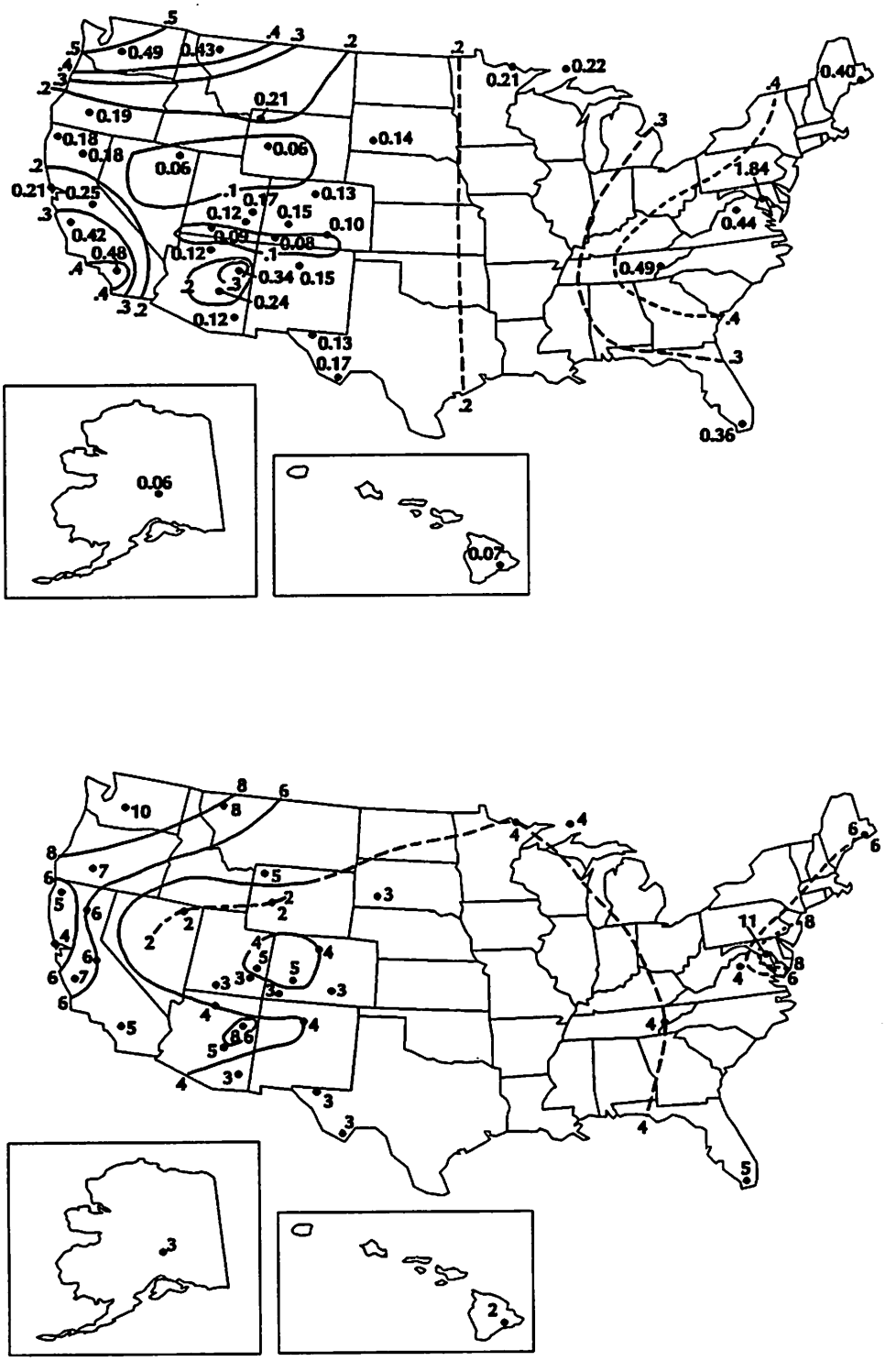


Figure 5.8 Three-year averages of fine light-absorbing carbon aerosol concentrations (in $\mu g/m^3$) and light-absorbing carbon fine mass fractions (in percent) for each of the sites in the IMPROVE network in the United States for the three-year period, March 1988 through February 1991.

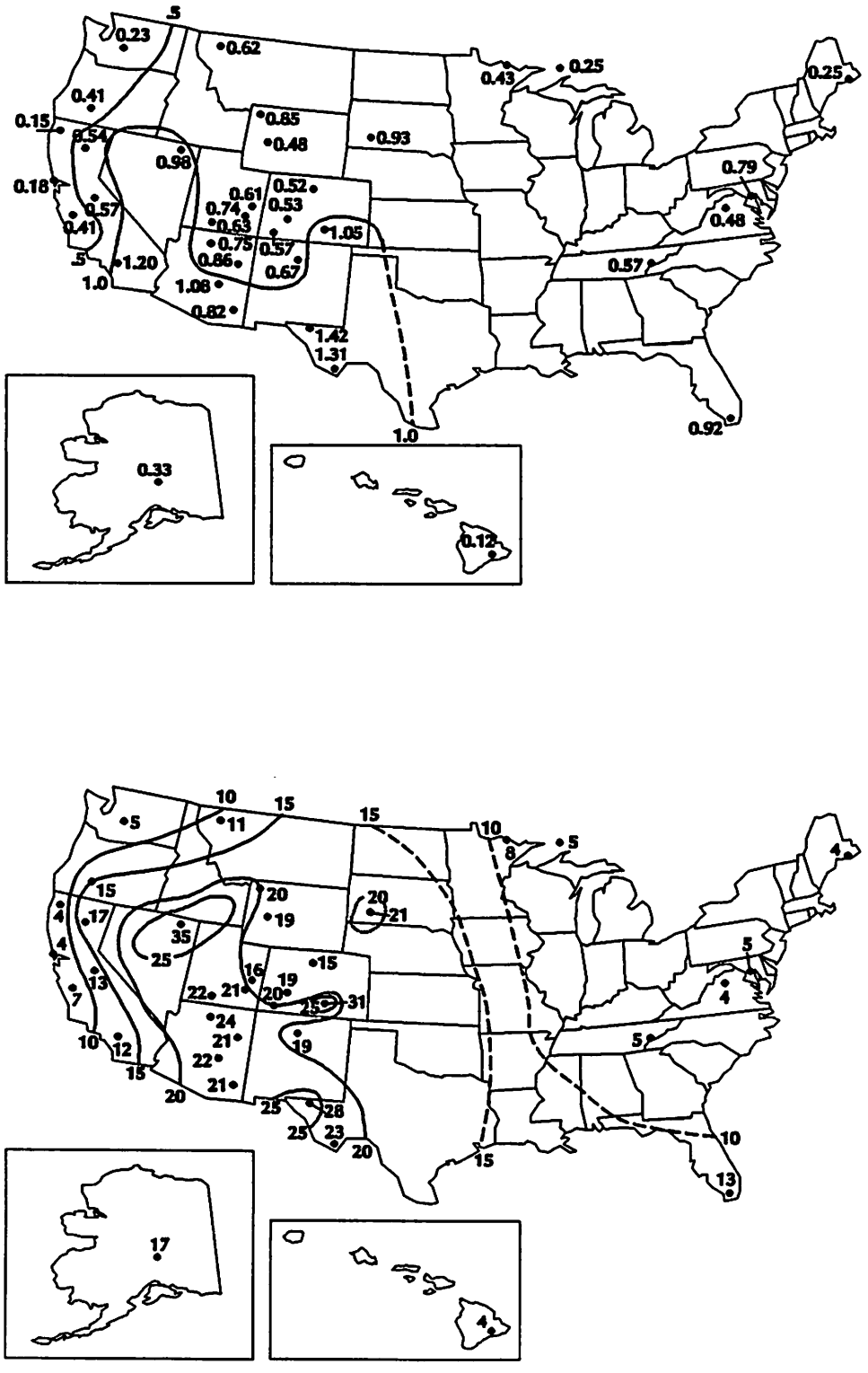


Figure 5.9 Three-year averages of fine soil aerosol concentrations (in $\mu g/m^3$) and soil fine mass fractions (in percent) for each of the sites in the IMPROVE network in the United States for the three-year period, March 1988 through February 1991.

Boundary Waters. This region, in Minnesota and Michigan, has two sets of measurements: in Isle Royale and Voyageurs National Parks. Over the three-year period, the average fine and coarse aerosol concentrations were 5.3 and 5.7 $\mu g/m^3$, respectively. Thus, the fine aerosol concentration is between the minimum measured in Alaska and the near maximumin the Appalachian Mountains. The highest fine and coarse aerosol concentrations occur during summer, but there is not as strong a seasonal variation as in Alaska and the Appalachian Mountains. In this region organic carbon is the largest fraction of fine particle mass at 40%, followed closely by sulfate (39%), and more distantly by nitrate (11%), soil (6%), and light-absorbing carbon (4%).

Cascade Mountains. This region in Washington State has only one set of measurements at Mount Rainier National Park, southeast of Seattle. Here the three-year average fine and coarse aerosol concentrations are 5.1 and 3.5 $\mu g/m^3$, respectively. Fine and coarse aerosol concentrations reach their maxima in summer and minima in winter. Sulfate and nitrate concentrations have strong seasonal variations, also with maxima in summer and minima in winter. This seasonal variation could be, in part, the result of seasonal variations in mixing and in photochemistry. In this region organic carbon is the single most significant contributor (at 56%) to fine particle mass. Sulfate (at 26%) is less than half the contribution of organics. Light-absorbing carbon contributes 10%, followed by soil (5%) and nitrate (4%).

Central Rocky Mountains. The measurements in this region are made at five locations in the mountainous Class I areas of Colorado and Wyoming, including the Bridger and Weminuche Wilderness areas, Rocky Mountain and Yellowstone National Parks, and Great Sand Dunes National Monument. Fine and coarse aerosol concentrations in this region averaged 3.3 and 4.8 $\mu g/m^3$ over the three-year period. Like many of the other regions, concentrations, especially of sulfate, organic carbon, light-absorbing carbon, and coarse aerosol, are highest in summer and lowest in winter. The largest contributor to fine particle mass in this region was organic carbon (44%), followed by sulfate and soil at 25% and 21%, nitrate (6%), and light-absorbing carbon (4%).

Coastal Mountains. This region includes three Class I areas along and near the coast of Northern California: Pinnacles National Monument, Point Reyes National Seashore, and Redwoods National Park. In this region the fine and coarse aerosol concentrations averaged 5.0 and 8.9 $\mu g/m^3$ over the three-year period. There was no strong seasonal variation in concentration, except for sulfate that had maxima and minima in summer and winter, respectively, and nitrate that showed the opposite trend, with maxima and minima in winter and summer, respectively. One would expect sulfate to reach its maximum concentrations in summer because of photochemistry. Nitrate would be expected to reach its peak during the colder months of winter because of the extreme thermal volatility of ammonium nitrate. Organic carbon in this region was the largest single component of fine aerosol (at 39%), followed by sulfate and nitrate (28%, 22%), and soil and light-absorbing carbon (5% each).

Colorado Plateau. This region in the Four Corners states of the Southwest is the most intensively monitored in the IMPROVE network. There are seven sites, most of them within the so-called Golden Circle of National Parks: Arches, Bandelier, Bryce Canyon, Canyonlands, Grand Canyon, Mesa Verde, and Petrified Forest National Parks. This region is of particular concern to the newly established Grand Canyon Visibility Transport Commission as required by

Congress in the 1990 amendments to the Clean Air Act. In this region fine and coarse aerosol concentrations averaged 3.4 and 4.7 $\mu g/m^3$, respectively. Fine and coarse aerosol concentrations here were greatest in summer and minimum in winter. Sulfate and organic carbon concentrations were also greatest in summer and smallest in winter. However, nitrate and light-absorbing carbon were both largest in winter. Here organic carbon and sulfate contributions are nearly equal (36% and 32%, respectively), followed by soil (20%), nitrate (7%), and light-absorbing carbon (5%).

Florida. This region has only one monitoring site, Everglades National Park. At Everglades the fine and coarse aerosol concentrations averaged 7.1 and 9.6 $\mu g/m^3$ over the three-year period of IMPROVE. Fine and coarse aerosol concentrations were highest in summer. Fine aerosol concentrations were smallest in winter, while coarse aerosol concentrations were smallest in spring. Sulfate was found to be the largest contributor to fine particle mass (41%), followed by organic carbon (32%), soil (13%), nitrate (9%), and light-absorbing carbon (5%).

Great Basin. The Great Basin of Nevada was represented by only one set of measurements at Jarbidge Wilderness Area in northeastern Nevada. Here the fine and coarse aerosol concentrations averaged 2.8 and 5.0 $\mu g/m^3$. The fine mass concentration was the lowest of any of the regions in the lower 48 states. Perhaps this is due to the fact that this site is relatively remote from high emission density areas and is generally well ventilated. Both fine and coarse aerosol concentrations, as well as all of the fine aerosol components except nitrate, experienced largest concentrations in the summer and lowest concentrations in the winter. The largest single contributors to fine particle mass at this site were organic carbon (40%) and soil (35%). Sulfate was a smaller contributor (18%), followed by nitrate (5%) and light-absorbing carbon (2%).

Hawaii. The Hawaiian Islands were represented by a single measurement site at Hawaii Volcanoes National Park. The fine and coarse aerosol concentrations were 3.2 and 8.2 $\mu g/m^3$, respectively. This site experienced quite a different seasonal pattern, with minimum fine aerosol concentrations in summer and maximum concentrations in winter. The sulfate, organic carbon, and light-absorbing carbon fractions of fine aerosol mass also exhibited this pattern. Coarse particle concentrations, however, had maximum concentrations in summer and minimum concentrations in winter. Sulfate was by far the largest contributor to fine particle mass, at 69%. Organic carbon contributed the next largest amount (23%). Soil, nitrate, and light-absorbing carbon were all minor contributors (4%, 2%, and 2%, respectively). Perhaps much of the sulfate measured in Hawaii is due to the natural emissions from the volcanic activity on this island.

Northeast. The northeastern United States is represented by the set of measurements at Acadia National Park on the coast of Maine. Here fine and coarse aerosol concentrations averaged 6.7 and 4.5 $\mu g/m^3$. Although fine and coarse aerosol concentrations were both largest in summer, there was not a strong seasonal variation. Sulfate, organic carbon, and soil concentrations were also largest in summer. Nitrate concentrations reached their maximum in winter. The contributors to fine particle mass included sulfate (53%), organic carbon (30%), nitrate (7%), light-absorbing carbon (6%), and soil (4%).

Northern Great Plains. Only one set of measurements was made in this region, at Badlands National Monument in South Dakota. Here fine and coarse aerosol concentrations averaged 4.5 and 6.3 $\mu g/m^3$ over the three-year IMPROVE monitoring period. Like many sites, the maximum and minimum fine and coarse aerosol concentrations occurred in summer and winter, respectively. All of the fine aerosol constituents except nitrate also exhibited this seasonal trend. Sulfate and organic carbon each contributed 34% of the fine particle mass, followed by soil (21%), nitrate (8%), and light-absorbing carbon (3%).

Northern Rocky Mountains. This region has measurements made at Glacier National Park in Montana, close to the Canadian border. Fine and coarse aerosol concentrations averaged 5.5 $\mu g/m^3$ each here. There were no strong seasonal variations except nitrate showed a strong winter peak. Organic carbon was by far the largest contributor to fine particle mass: 57%. Sulfate contributed 18%, soil 11%, light-absorbing carbon 8%, and nitrate 6%.

Sierra Nevada. The Sierra Nevada mountains in California were monitored at Yosemite National Park. Average fine and coarse aerosol concentrations were 4.5 and 4.7 $\mu g/m^3$. There was a strong seasonal variation, with maximum concentrations in summer and minimum concentrations in winter. The only exception was nitrate, which was relatively constant throughout the year. Organic carbon contributed more than twice what any other fine particle constituent contributed (46%). Its contribution was followed by sulfate (22%), nitrate (14%), soil (13%), and light-absorbing carbon (6%).

Sierra-Humboldt. The region further north in the Sierra Nevada and Humboldt mountain ranges was measured with sites at Crater Lake National Park in Oregon and Lassen Volcanoes National Park in Northern California. This region is relatively remote from high emission density areas. Its fine and coarse aerosol concentrations were relatively low, at 2.9 and 3.7 $\mu g/m^3$, respectively. Summer concentrations were generally about twice those during the winter. Organic carbon contributed most (55%) of the fine particle mass, with nearly equal contributions from sulfate and soil (17% and 16%) and from nitrate and light-absorbing carbon (6% each).

Sonoran Desert. This region in southeastern Arizona was monitored at two sites: Chiracahua and Tonto National Monuments. The three-year average fine and coarse mass concentrations in this region were 4.4 and 6.0 $\mu g/m^3$, respectively. These concentrations were highest in summer and lowest in winter. The sulfate, organic carbon, and soil components of fine particle mass also had maxima and minima in these seasons. The contributions to fine particle mass were distributed nearly equally between sulfate and organic carbon (35% and 34%), followed by soil (22%), nitrate (6%), and light-absorbing carbon (4%).

Southern California. Measurements in this region were made in San Gorgonio National Monument, east of the Los Angeles metropolitan area. Fine and coarse aerosol concentrations were highest of any western U.S. site here (9.8 and 10.4 $\mu g/m^3$); concentrations were only higher in the eastern United States. Like many sites in the IMPROVE network, concentrations are highest in summer and lowest in winter. This trend was also observed for nitrate: actually nitrate was highest in spring and lowest in winter, but concentrations in summer were twice those in winter. This site was the only site in the IMPROVE network in which nitrate was a larger contributor to fine particle mass than either sulfate or organic carbon. The contributions

were nitrate (43%), organic carbon (26%), sulfate (14%), soil (12%), and light-absorbing carbon (5%).

Washington, D.C. This is a single monitoring site in the nation's capital. Fine and coarse aerosol concentrations were higher here than anywhere in the IMPROVE network; they averaged 16.2 and 16.4 $\mu g/m^3$ over the three-year period from March 1988 through February 1991. There was not strong seasonal variation in fine aerosol concentrations; they only ranged from 15.3 $\mu g/m^3$ in autumn to 16.8 $\mu g/m^3$ in spring. However, the sulfate and nitrate components varied significantly by season: sulfate concentrations were largest in summer and smallest in winter, while nitrate concentrations were largest in winter and smallest in summer. The sulfate behavior could be caused by the seasonal variation in photochemistry. The nitrate behavior may be due to the extreme volatility of nitrate in warm weather. Over the entire three-year period, fine particle mass was constituted of sulfate (42%), organic carbon (27%), nitrate (14%), light-absorbing carbon (11%), and soil (5%).

West Texas. Two measurement sites in west Texas were included in the IMPROVE network: Big Bend and Guadalupe Mountains National Parks. Both sites are near the Mexico border in southwestern Texas. The fine and coarse aerosol concentrations averaged 5.4 and 7.5 $\mu g/m^3$ over the three-year period. Minimum concentrations generally occurred during winter, while maxima occurred in summer. The only exception was soil and coarse aerosols which peaked in spring, presumably during windy periods. The contributions to fine particle mass averaged 39% for sulfate, 28% for organic carbon, 25% for soil, 5% for nitrate, and 3% for light-absorbing carbon.

In general, the following observations can be made. With few exceptions, aerosol concentrations are highest in summer and lowest in winter. This is consistent with the fact that sulfate formation rates, natural organic carbon emissions, and mixing into mountainous regions are all maximum in summer and minimum in winter. With the notable exception of Southern California where nitrate is dominant, sulfate and organic carbon are the two principal components of the fine particle mass throughout the United States. Sulfate's contribution is much higher in the eastern United States and in Hawaii than in the western United States and in Alaska. Since most of the sulfate is anthropogenic in origin, regional $SO_2$ control would be a generally effective way to reduce fine aerosol concentrations in the United States.

## 5.2 Spatial Trends in Aerosol Concentrations in the United States

Because of the relatively large number of IMPROVE aerosol monitoring sites in the western United States, isopleth maps of the average aerosol concentrations measured over the three-year period from March 1988 through February 1991 could be drawn. Since there are relatively fewer sites in the eastern United States, isopleths there are much less accurate; this is indicated by dashed lines. Figures 5.3 through 5.9 show isopleth maps of the three-year average aerosol concentrations (fine mass, coarse mass, sulfate, nitrate, organic carbon, light-absorbing carbon, and soil). These figures provide us with information on how aerosol concentrations and mass budgets vary over the United States.

### 5.2.1 Fine Aerosol

Figure 5.3 shows isopleths of the three-year average fine aerosol concentrations measured during the first three-year period of the IMPROVE network. Note the strong gradient in fine particle concentrations from Southern California, a local maximum of 9.8 $\mu g/m^3$ to the 2.7-2.9 $\mu g/m^3$ minima observed in southern Oregon, Nevada, southern Utah, and southwestern Colorado. This is a factor of 3.5 variation in average fine aerosol concentration. Also note that fine aerosol concentrations increase again as one moves to the eastern United States with maxima of about 11 $\mu g/m^3$ in Shenandoah and Great Smoky Mountain National Parks and over 16 $\mu g/m^3$ in Washington, D.C. Thus, from the minima in the western United States to the maxima in the East, there is a factor of six variation in average concentration. Average fine aerosol concentrations in Denali National Park of 2.0 $\mu g/m^3$ in Alaska are lower than any measured in the lower 48. There is a factor of 8 variation between the average measured in Alaska and that measured in Washington, D.C.

### 5.2.2 Coarse Aerosol

Figure 5.4 shows isopleths of the three-year average coarse aerosol concentrations throughout the IMPROVE network. There are a few local maxima from 12 to 16 $\mu g/m^3$ that are noticeable near Los Angeles, San Francisco, and Washington, D.C. The lowest coarse aerosol concentrations occur in the swath from the Pacific Northwest through Nevada to southern Utah. Concentrations in this region average less than 4 $\mu g/m^3$. However, coarse aerosol concentrations are generally in the factor-of-two range from 4 to 8 $\mu g/m^3$. The patterns in the eastern United States are more difficult to discern. Coarse aerosol concentrations in Alaska and Hawaii are not significantly lower than in the lower 48 states. There is approximately a factor-of-five range from the lowest average concentrations measured in Oregon and Utah and the highest measured in Washington, D.C.

### 5.2.3 Fine Sulfate Aerosol

The average sulfate component of the fine aerosol measured over the first three-year period of the IMPROVE network is shown in Figure 5.5 Since sulfate is one of the two major components of fine particle mass, it is not surprising to observe similar gradients across the United States to what was observed for total fine particle mass. There is a strong gradient from the high concentrations in California urban areas to the low concentrations in southern Oregon and Nevada. There is also a strong gradient from the relatively low concentrations in the West to those in the East. There is a factor of 13.5 variation from the lowest concentration measured in Nevada to the highest concentration measured in Washington, D.C. This gradient is mostly likely indicative of the strong regional gradient in $SO_2$ emission density. The eastern United States has a concentration of power plants that burn high sulfur coal, while the western United States has relatively low $SO_2$ emission densities. A relative maximum in sulfate concentration is observed in southern Arizona, which is near copper smelters that emit large quantities of $SO_2$. The lower map in Figure 5.5 shows that sulfate constitutes as little as 14% of fine particle mass in Southern California to as much as 59% of total fine mass in Shenandoah National Park. In the Golden Circle of parks in the Four Corners states, sulfate is 30-34% of the fine particle mass.

In the eastern United States and in Hawaii, sulfate is the largest single component of fine particle mass. In the Boundary Waters, Sonoran Desert, and West Texas regions, sulfate is tied with organic carbon as the largest component of fine particle mass. Sulfate is the second largest component of fine mass in all other regions studied except Southern California and the Great Basin (where sulfate is the third largest component).

### 5.2.4 Fine Nitrate Aerosol

Figure 5.6 shows isopleth maps of the nitrate concentration and nitrate mass fraction of fine aerosol, averaged over the first three years of the IMPROVE measurement program. Note that the highest concentration of 4.2 $\mu g/m^3$ was measured in San Gorgonio Wilderness, just east of the Los Angeles metropolitan area. Other high concentrations occur in Washington, D.C. (2.2 $\mu g/m^3$), and near the San Francisco area (1.4-1.5 $\mu g/m^3$). There is a strong gradient from the high concentrations in the California urban areas to the minima of 0.1 $\mu g/m^3$ measured in Oregon, Nevada, Wyoming, and Colorado. There is a local maximum of 0.4 $\mu g/m^3$ near the Phoenix metropolitan area. The long swath of low nitrate concentrations ($<0.15$ $\mu g/m^3$) extending from Oregon, Nevada, and Idaho into Utah, Wyoming, and Colorado is interrupted by higher concentrations in southeastern Utah, including a local maximum of 0.5 $\mu g/m^3$ at Arches National Park. Nitrate mass fractions are typically 4-7 percent, except in California where they are 25 percent and higher in eastern Utah, western Colorado, Minnesota, Michigan, and in the Washington, D.C. area where they range from 10-14 percent. Nitrate concentrations generally reach their maxima in the winter when colder temperature favor the formation of ammonium nitrate aerosol from nitric acid vapor. Nitrate is the largest single component of fine aerosol mass in Southern California at San Gorgonio Wilderness.

### 5.2.5 Fine Organic Carbon Aerosol

Figure 5.7 shows isopleth maps of the organic carbon fraction of the fine aerosol concentration, averaged over the first three years of the IMPROVE measurement program. There is a significant spatial gradient from California and the Pacific Northwest with average concentrations of 2.0 to 3.1 $\mu g/m^3$ to the desert areas of the western United States with concentrations of 1.0 to 1.5 $\mu g/m^3$. In the eastern United States organics range generally from 2.0 to 4.5 $\mu g/m^3$. In Alaska and Hawaii organic aerosol concentrations are the lowest, from 0.7 to 0.9 $\mu g/m^3$.

Except in the northwestern United States where organic carbon is over half of the fine particle mass, organic carbon generally constitutes between 30-40 percent of the fine particle mass. Moreover, organic carbon is the largest single component of fine particle mass in most of the regions in the United States. Exceptions include the eastern United States and Hawaii where sulfate is the dominant component and Southern California where nitrate is the dominant component.

### 5.2.6 Fine Light-Absorbing Carbon Aerosol

Figure 5.8 shows isopleth maps of the light absorbing carbon concentration and mass fraction of the fine aerosol, averaged over the first three years of IMPROVE. Note that light

absorbing carbon concentrations are highest in the Northeast, Pacific Northwest, and Southern California, while concentrations are much lower in much of the West (Wyoming, Utah, and Nevada). Light absorbing carbon is the smallest contributor to fine particle mass, constituting generally 2-6 percent of the fine particle mass. Exceptions to this are the Pacific Northwest and Washington, D.C. areas, where light absorbing carbon contributes as much as 10-11 percent of the fine particle mass.

### 5.2.7 Fine Soil Aerosol

Figure 5.9 shows isopleth maps for fine soil. The contribution of soil to the fine aerosol in the United States is generally small, except for the elevated concentrations ($< 1\ \mu g/m^3$) in the desert areas of the Southwest. Soil contributes approximately 5-10 percent of the fine aerosol mass, except in the desert Southwest where contributions are generally greater than 20 percent.

## 5.3 Summary

The following are the major patterns observed in the first three years of IMPROVE:

1. Spatial Patterns. Concentrations of fine particles (those most important in determining visibility) are highest in the eastern U.S. and in Southern California and lowest in the relatively unpopulated areas of the West.

2. Major Contributions to Fine Aerosol. The most significant components of the fine particles are organic carbon and sulfate. Of the 19 regions studied, organic carbon was the largest component in nine regions (Alaska, Cascades, Colorado Plateau, Central Rockies, Coast Mountains, Great Basin, Northern Rockies, Sierra Nevada, and Sierra-Humboldt). Sulfate was the dominant component of fine particle mass in six regions, mainly in the East (Appalachian Mountains, Florida, Hawaii, Northeast, Northern Great Plains, and Washington, D.C.). The contributions of organic carbon and sulfate were approximately equal in three regions (Boundary Waters, Sonoran Desert, and West Texas). Nitrate was the largest component of the fine aerosol in Southern California.

3. Smaller Contributors. After the contributions of organic carbon and sulfate, soil is the next largest, followed by nitrate and light absorbing carbon.

4. Seasonality. With a few exceptions, average fine mass concentrations, and the sulfate and organic carbon components of fine mass are highest in summer. Soil concentrations are highest in spring or summer. On the other hand, nitrate concentrations are generally highest in winter or spring. Light absorbing carbon exhibits relatively little seasonal variation.

# CHAPTER 6

# SPATIAL AND SEASONAL DISTRIBUTION OF RECONSTRUCTED LIGHT EXTINCTION

In the previous chapter the measurements of aerosol concentrations and chemical composition during the first three years of IMPROVE were presented. In this chapter, these aerosol measurements and current understanding of the light extinction efficiencies of aerosol components are used to derive the reconstructed light extinction coefficient. In addition, the relative contribution of various aerosol components to total light extinction are combined into a light extinction budget. The next chapter presents the results of direct transmissometer measurements of the light extinction coefficient.

## 6.1 Reconstructing Light Extinction from Aerosol Measurements

To review the discussion presented in Chapter 1 (see Equation 1.2), the light extinction coefficient is the sum of several components:

$$b_{ext}=b_{scat}+b_{abs}=b_{Ray}+b_{sp}+b_{ag}+b_{ap} \qquad (6.1)$$

where

| | | | |
|---|---|---|---|
| | $b_{ext}$ | = | light extinction coefficient, |
| | $b_{scat}$ | = | light scattering coefficient, |
| | $b_{abs}$ | = | light absorption coefficient, |
| | $b_{Ray}$ | = | Rayleigh light scattering coefficient, |
| | $b_{sp}$ | = | light scattering coefficient due to particles, |
| | $b_{ag}$ | = | light absorption coefficient due to gases, and |
| | $b_{ap}$ | = | light absorption coefficient due to particles. |

The Rayleigh scattering coefficient ($b_{Ray}$) is the light scattered by molecules of gas in the natural atmosphere (i.e., oxygen and nitrogen, primarily). The Rayleigh scattering coefficient will vary with atmospheric pressure. For this report we assume the Rayleigh scattering coefficient is 10 $Mm^{-1}$ (inverse megameters) at all sites.

The light absorption coefficient due to gases ($b_{ag}$) is dominated in the atmosphere by the effect of nitrogen dioxide ($NO_2$) gas. For this report, we assume this component is negligible. This assumption may not be correct at locations close to significant $NO_x$ emission sources (e.g., urban areas or power plants).

In most instances, $b_{sp}$ and $b_{ap}$ are primarily responsible for visibility reduction. Single particle scattering and absorption properties can, with a number of limiting assumptions, be calculated theoretically using Mie theory (vandeHulst, 1981). However, before such calculations are carried out, suitable boundary conditions must be specified. Typically aerosol models assume:

- External mixtures - particles exist in the atmosphere as pure chemical species which are mixed without interaction;

- Multi-component aerosols - single particles are made up of two or more species. If the chemical species are combined in fixed proportions independent of particle size, the aerosol is referred to as internally mixed. Other models assume solid cores with deposited shells of various thickness and composition.

If an aerosol is mixed externally, or for an internally mixed aerosol if the index of refraction is not a function of composition or size, and the aerosol density is independent of volume, then aerosol extinction due to particles can be related in a linear fashion to particle mass concentration (Ouimette and Flagan, 1982).

The approach used here to estimate extinction assumes externally mixed aerosols. The light extinction coefficient can then be calculated (or reconstructed) from aerosol concentrations by taking Equation 6.1 and describing the light extinction contributed by aerosol component ($i$) as the product of the aerosol component's concentration ($C_i$) and its light extinction efficiency ($b_i$). Thus, the total light extinction coefficient is simply the sum of the light extinctions of each aerosol component:

$$b_{ext}=b_{Ray}+\sum \beta_i C_i. \tag{6.2}$$

The efficiencies used for the various components are discussed below. Any apportionment by this means can only be judged in the context of whether or not it is reasonable, and whether apportionment of mass to extinction is consistent with measurements of scattering and absorption (White et al., 1986).

Equation 6.2 can be cast into the following form for the aerosol components measured as part of the IMPROVE program:

$$\begin{aligned} b_{ext}=b_{Ray}+\beta_{sulfate}[SULFATE]+\beta_{NITRATE}[NITRATE]+\beta_{OC}[OCM] \\ +\beta_{LAC}[LAC]+\beta_{SOIL}[SOIL]+\beta_{CM}[CM] \end{aligned} \tag{6.3}$$

where $b_{ext}$ is the total light extinction coefficient (in $Mm^{-1}$), $b_{Ray}$ is the Rayleigh scattering coefficient (10 $Mm^{-1}$), the $\beta$'s are the light extinction coefficients for each component (in $m^2/g$), and the parameters in brackets ([ ]) are the concentrations of the aerosol components (in $\mu g/m^3$).

The values of light extinction efficiency (in $m^2/g$) used in this report are as follows:

| | |
|---|---|
| Sulfates and Nitrates | $3 f_T(RH)$ |
| Organic Carbon | $3 [1 + f_H(RH)]/2$ |
| Light Absorbing Carbon | 10 |
| Fine Soil | 1 |
| Coarse Particles | 0.6 |

The functions $f_T(RH)$ and $f_H(RH)$ are correction factors to account for the liquid water that may be part of the hygroscopic aerosol components (sulfate, nitrate, and some organic carbon). These functions are dependent on the relative humidity (RH) at the given site. These functions are discussed in Section 6.2 (a detailed exposition is given in Appendix H).

In this report, we assume that coarse particles and fine soil particles are from a single natural source, windblown dust. Thus, the extinction calculated for these two components were combined into a single category and is reported as coarse extinction.

Figure 6.1 shows schematically how the various aerosol components are used to reconstruct the total light extinction due to aerosols. Total light extinction is then the sum of aerosol light extinction, Rayleigh scattering, and nitrogen dioxide light absorption.

## 6.2 Effect of Relative Humidity on Extinction Efficiencies

A complicating factor is that soluble fine aerosol species absorb water from the atmosphere and grow in size. This behavior can be modeled as a function of relative humidity (RH) assuming thermodynamic equilibrium (Tsay et al., 1991). It is known that ammonium sulfate aerosols will abruptly go into solution at a specific RH. This process is known as deliquescence. The reverse phase change, crystallization, when the liquid evaporates from the droplets, occurs at a lower RH and a slower rate. The growth and phase change of the particles, of course, affects their light scattering efficiency. In general, the higher the RH, the greater the scattering by sulfate and nitrate aerosols. The relationship between RH and scattering efficiency for sulfate aerosols, referred to as $f_T(RH)$, is parameterized from curves published by Tang et al. (1981) and shown in Figure 6.2. Tang's curves, calculated theoretically for aerosols of different size distributions under conditions of increasing RH, have sharp discontinuities at 62% RH for ammonium nitrate, and at 80% for ammonium sulfate, the deliquescence points for these species.

Such aerosol mixtures exhibit the hysterisis effect (illustrated in Figure 6.3) in which more water is held in the aerosol phase then equilibrium considerations would dictate. In the atmosphere, the situation is further complicated by internally mixed soluble aerosols which may go through several stages of growth (Wexler and Seinfeld, 1991). The RHs at which these stages occur depend on the mixture, but in general are between 50% and 80% (Tang et al., 1981). Tang's curves were smoothed between the deliquescence point and 30% RH (see Figure 6.3) because: (1) mixtures of ammonium nitrate and ammonium sulfate species have been shown to be hygroscopic below single species values (Sloane, 1985; Stelson and Seinfeld, 1982); (2) it is not known whether the ascending or descending limb of the hysteresis curve applies for a particular aerosol sample (i.e.,whether aerosol water concentrations are at equilibrium or at

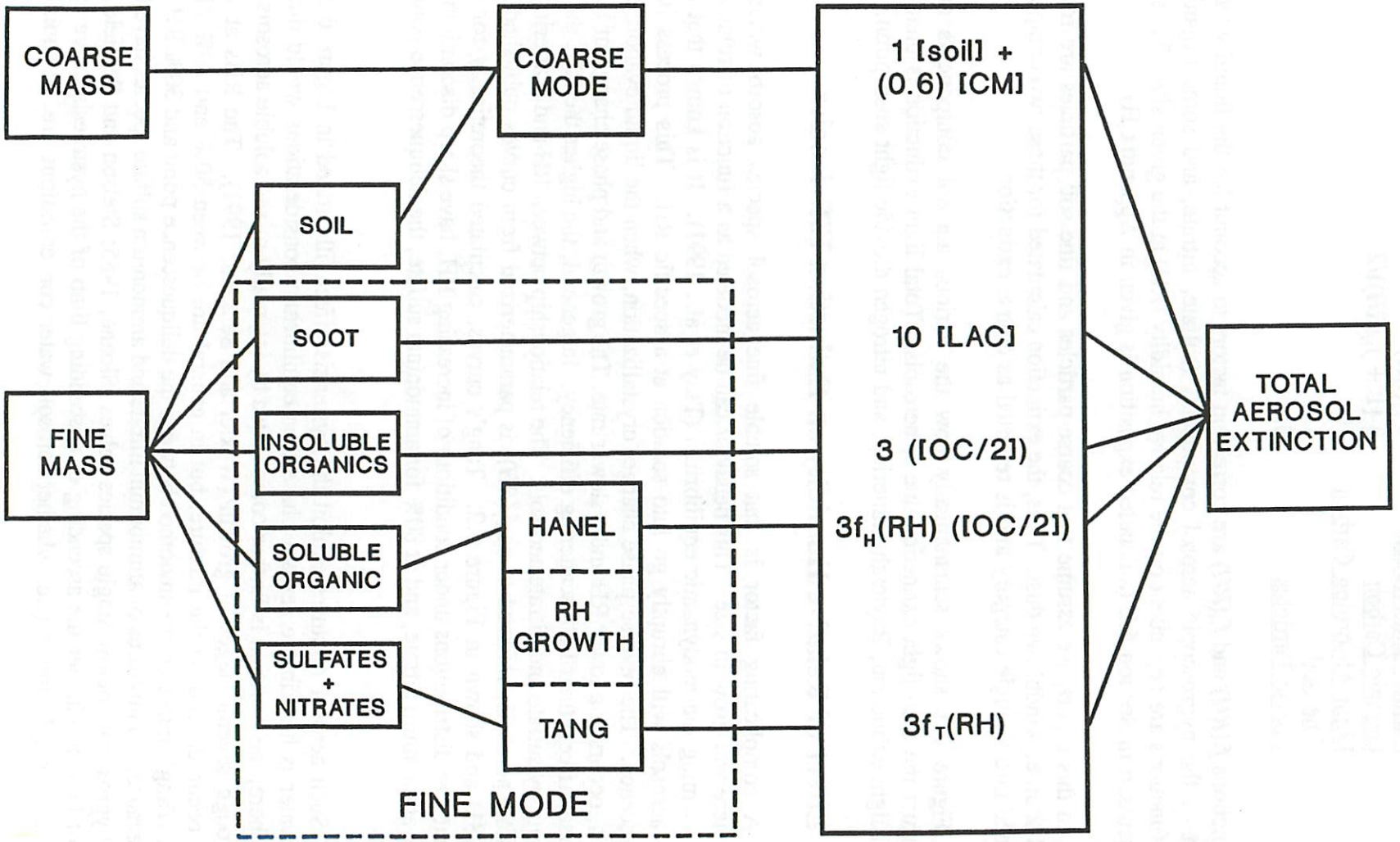


Figure 6.1. Schematic flow diagram showing how light extinction is reconstructed from measurements of aerosol concentration and relative humidity.

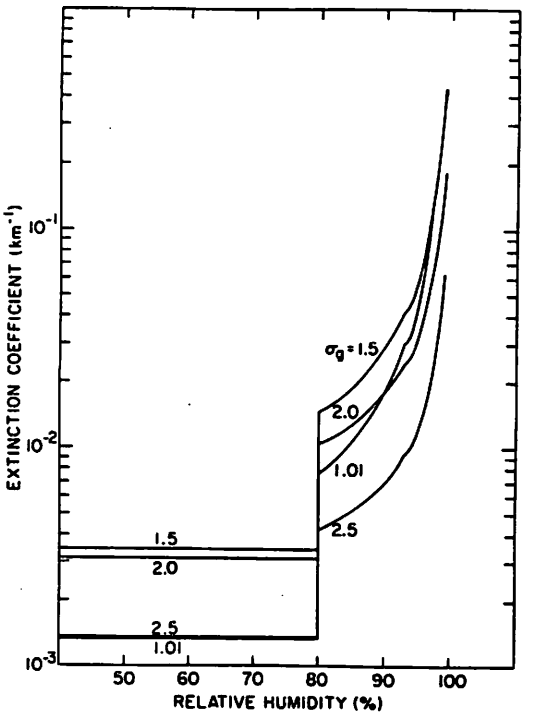


Figure 6.2. Dependence on relative humidity of light extinction coefficient for 1 $\mu g/m^3$ of ammonium sulfate (with size distributions characterized by the indicated geometric standard deviations ($r_g$). Note the deliquescence point at 80% relative humidity. Source: Tang (1980), Tang et al. (1981).

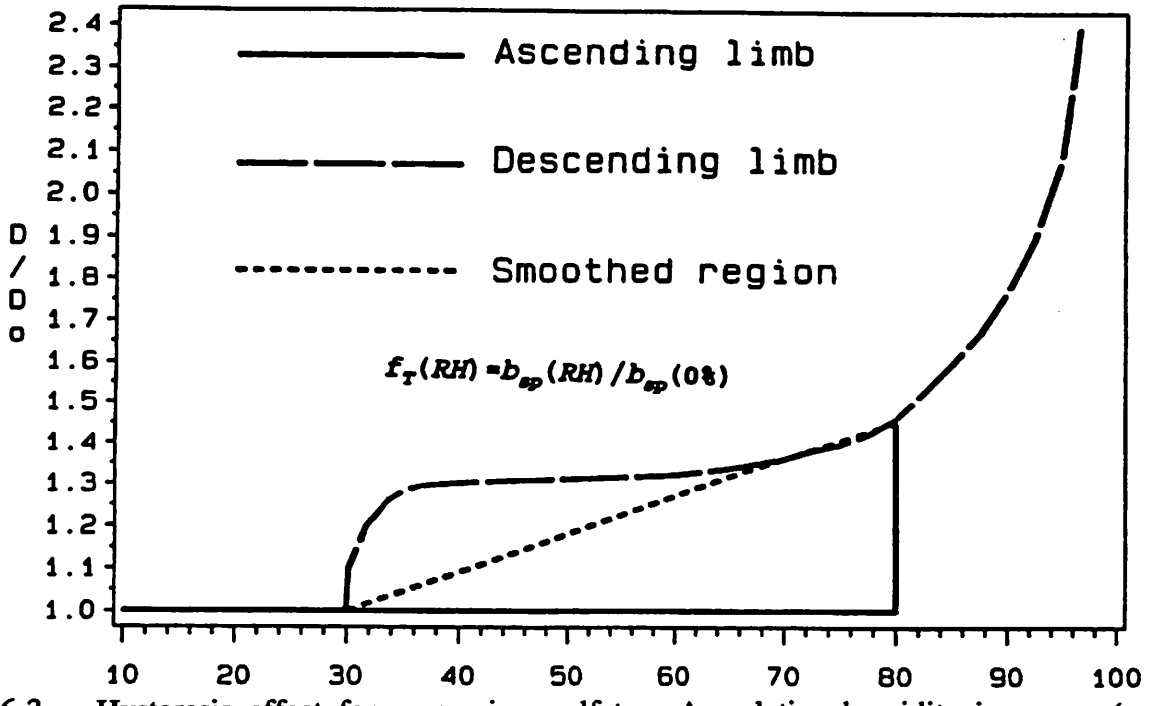


Figure 6.3. Hysteresis effect for ammonium sulfate. As relative humidity increases (see ascending limb), water is not taken up into the aerosol phase until 80% RH. However, for decreasing relative humidity (see descending limb), more water is retained in the aerosol phase than equilibrium considerations would indicate. The relationship between the ascending and descending limbs was used to model RH dependence of sulfate and nitrate light scattering efficiency.

super-equilibrium); and (3) the growth factor and light scattering efficiency for ambient aerosols has previously been observed to be rather smooth (Wexler and Seinfeld, 1991; Sloane, 1985).

The effect of relative humidity and aerosol water on sulfate and nitrate light scattering is accounted for with a RH correction factor, $f_T(RH)$:

$$f_T(RH)=b_{sp}(RH)/b_{sp}(0\%), \tag{6.4}$$

where $b_{sp}(0\%)$ and $b_{sp}(RH)$ are the dry and wet scattering, respectively.

Soluble organics are presumed to be less hygroscopic than ammonium sulfate and ammonium nitrate. Therefore, a correction factor parameterized to data published by Hanel (1982), $f_H(RH)$, was derived. $f_H(RH)$ produces a smaller correction per unit of soluble material and is used to model the influence of RH on soluble organic material. In this report, it is assumed that half the organics are water soluble and that half are not.

Light extinction budgets and mass budgets involve averaging samples collected over a time interval. The extinction/mass budget represents the average contribution of each aerosol species to the average extinction/mass for the time interval. When soluble aerosols dominate $PM_{2.5}$, the distribution of RH over the interval becomes an issue. Failure to consider the distribution of RH can have significant effects on the average extinction attributed to soluble aerosols.

Mass budgets, for a particular time interval, are calculated by finding the average concentrations of the individual species of fine mass, then dividing each by the sum of the averages. If the aerosol data can be time matched with RH data, then light extinction budgets can be calculated in a parallel fashion. Specifically, a light extinction for each species and each sample can be calculated. Thus, the average light extinction due to each species over the time interval can be estimated.

If collocated and time-matched RH data are not available, but reliable estimates of the average RH over the time interval are, then a first approximation of an average light extinction for a given species can be made. One initial approach would be to apply the RH correction factor associated with the average RH to estimate the average extinction due to a soluble species. However, it can be demonstrated that for sites where the average RH is high, this approach will seriously underestimate the average extinction of a soluble aerosol when the soluble aerosol concentration is independent of RH (see Appendix H). This is due to the convex and highly nonlinear nature of the aerosol growth curves and the subsequent functions, $f_T(RH)$ and $f_H(RH)$. In the case of Tang's or Hanel's function Equation 6.5 holds

$$f_T(RH) \leq \overline{f_T(RH)} . \tag{6.5}$$

Moreover, if the distribution of soluble species concentrations are independent of RH,

then

$$\overline{f_T(RH)c} \simeq \overline{f_T(RH)}(\bar{c}). \tag{6.6}$$

Equality would occur as a limiting value when the sample size increases without bound.

In this report, light extinction due to a soluble species at site $s$ is derived using hourly RH values less than or equal to 98% and the equation is

$$b_{ext}=\beta F_{T,s}\bar{c}, \tag{6.7}$$

where

$$F_{T,s} = \overline{f_T(RH_s)}. \tag{6.8}$$

$F_{H,s}$ is defined similarly. Using Equation 6.3, extinction budgets for a time interval may be calculated by replacing $f_T(RH_s)$ with $F_{T,s}$ and $f_H(RH_s)$ with $F_{H,s}$ and by using the average concentration of each species over the time interval as the mass concentration.

Using the data for the collocated sites, Figure 6.4 has the plot of Tangs's RH dependent factor, as defined by Equation 6.8, versus annual average RH for the 20 IMPROVE sites with RH and light extinction measurements. A quadratic curve was fitted to the annual and seasonal data as defined by,

$$F = b_0 + b_1(\overline{RH}) + b_2(\overline{RH})^2. \tag{6.9}$$

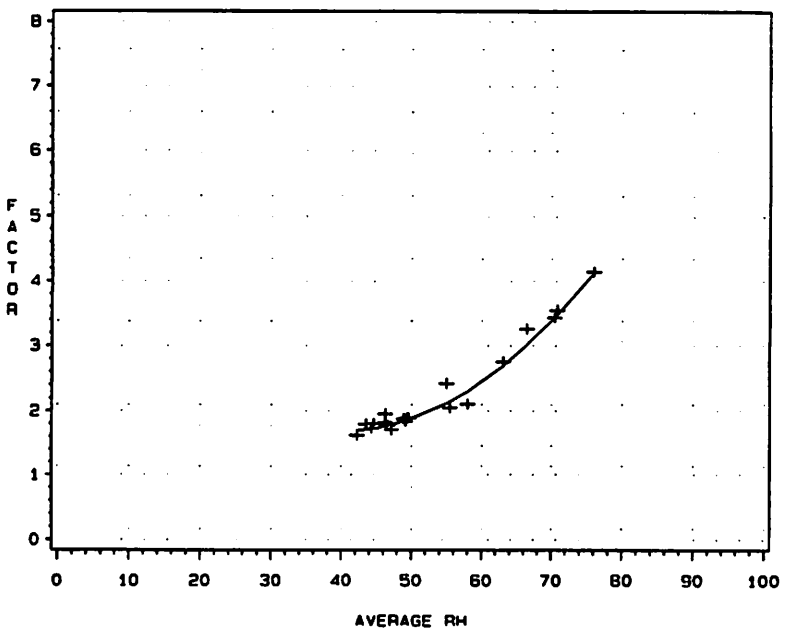


Figure 6.4. Dependence on average site relative humidity of the relative humidity correction factor for sulfate ($F_{T,s}$) for the IMPROVE sites with relative humidity measurements.

Tables 6.1a and 6.1b show the results of the regressions for Tangs's and Hanel's weighted correction factors. The high $r^2$ values arise from the fact that the noise in the relationship is due primarily to differences in the RH distributions between sites. More explicitly, if two sites had the same average RH, their weighted factors would be the same if their RH distributions were identical.

Table 6.1. Parameters of the best-fit quadratic equation relating the relative humidity light extinction correction factors ($F_T$ and $F_H$) to average site relative humidity ($F = b_o + b_1RH + b_2RH^2$).

(a) $F_T$ for Sulfates and Nitrates (Tang)

| Season | $b_o$ | $b_1$ | $b_2$ | $r^2$ |
|---|---|---|---|---|
| Annual | 4.63±0.93 | -0.148±0.033 | 0.0019±0.0003 | 0.98 |
| Autumn | 3.01±0.711 | -0.094±0.025 | 0.0014±0.0002 | 0.98 |
| Spring | 2.42±0.54 | -0.070±0.021 | 0.0012±0.0002 | 0.98 |
| Summer | 2.06±0.382 | -0.059±0.015 | 0.0011±0.0001 | 0.98 |
| Winter | 5.90±2.39 | -0.181±0.078 | 0.0021±0.0006 | 0.88 |

(b) $F_H$ for Soluble Organics (Hanel)

| Season | $b_o$ | $b_1$ | $b_2$ | $r^2$ |
|---|---|---|---|---|
| Annual | 3.93±0.702 | -0.119±0.025 | 0.001±0.0002 | 0.97 |
| Autumn | 2.69±0.527 | -0.078±0.019 | 0.001±0.0002 | 0.98 |
| Spring | 2.18±0.417 | -0.058±0.017 | 0.0009±0.0001 | 0.97 |
| Summer | 1.85±0.281 | -0.047±0.011 | 0.001±0.0002 | 0.98 |
| Winter | 5.20±1.96 | -0.154±0.061 | 0.002±0.0005 | 0.84 |

Using the results of the quadratic regressions, annual and seasonal weighted factors were calculated for 16 additional sites by estimating their annual and seasonal average RH from weather service RH contour maps (NOAA, 1978) (Figure 6.5a). Figure 6.5b shows a contour map showing the annual RH dependent factor isopleths for the continental United States.

## 6.3 Spatial Distributions of Reconstructed Light Extinction and Light Extinction Budgets

Spatial patterns in the reconstructed light extinction should be somewhat similar to those observed for aerosols since reconstructed light extinction is calculated from aerosol concentrations. However, since light extinction efficiencies of sulfates and nitrates are larger than other fine aerosols because of associated water, and since light absorbing carbon has a relatively high extinction efficiency, the extinction budgets should be different from fine aerosol budgets.

Figure 6.6 shows the magnitude of total reconstructed aerosol light extinction (non-Rayleigh) coefficient based on the three years of IMPROVE aerosol data for each of the 19 regions in the United States. In a series of five bar graphs for each region, the magnitude of reconstructed aerosol light extinction is shown for each season and for the entire period (annual). The portions contributed by ammonium sulfate, ammonium nitrate, organic carbon, light absorbing carbon, and windblown dust (the fine soil and coarse mass contributions) are shown by different bar shadings. Note that the highest reconstructed extinctions occur in the eastern U.S., while the lowest extinctions occur in the non-urban West. Significant seasonal variation in reconstructed light extinction can be observed, especially in the Appalachian Mountains and in Southern California.

Figure 6.7 shows the light extinction budget or the relative fraction of total aerosol (non-Rayleigh) extinction caused by the various aerosol components. Note that the contribution of sulfate to total aerosol extinction is usually the largest single contributor for all sites east of New Mexico plus Alaska and Hawaii. In the East, sulfates usually contribute more to extinction than all other species combined. At many of the sites in the Pacific Northwest, organic carbon is the largest single contributor.

Figure 6.8 shows isopleths of the total reconstructed light extinction coefficient (including Rayleigh) for the entire three-year period, March 1988 through February 1991. Because of the less dense coverage in the eastern U.S., the isopleths are dashed to indicate greater uncertainty in their placement. The highest light extinction ($>100$ $Mm^{-1}$) occurs in the eastern United States. The lowest light extinction ($<30$ $Mm^{-1}$) occurs in the non-urban Southwest. Extinctions are also relatively high near the Los Angeles and San Francisco metropolitan areas of California and, to a lesser extent, in the Pacific Northwest.

## 6.4 Characteristics of the Regions

Tables 6.2, 6.3, and 6.4 summarize the seasonal and annual averages of the reconstructed light extinction coefficients for each of the 19 regions in the United States, averaged over the first three years of the IMPROVE monitoring program, March 1988 through February 1991.

Table 6.2 shows the breakdown of extinction among fine and coarse particles scattering and light absorption. In addition, this table shows the percentage of total light extinction (including Rayleigh) that is caused by aerosol light extinction (both scattering and absorption).

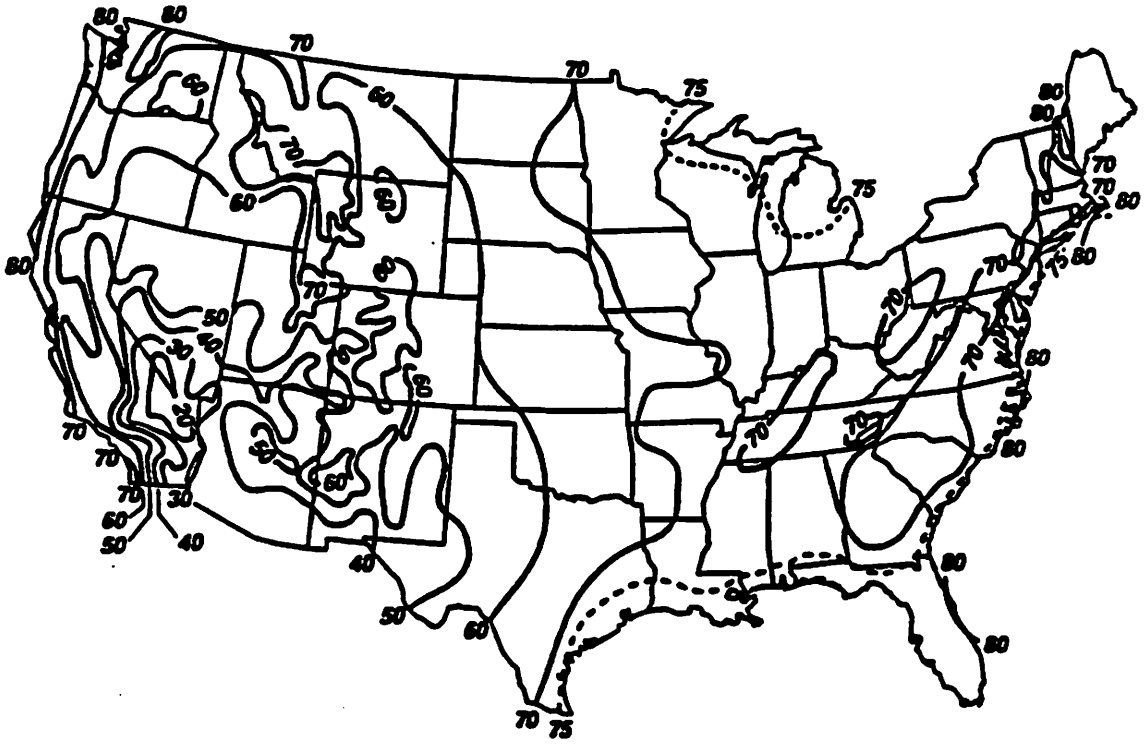

(a) Annual mean relative humidity.

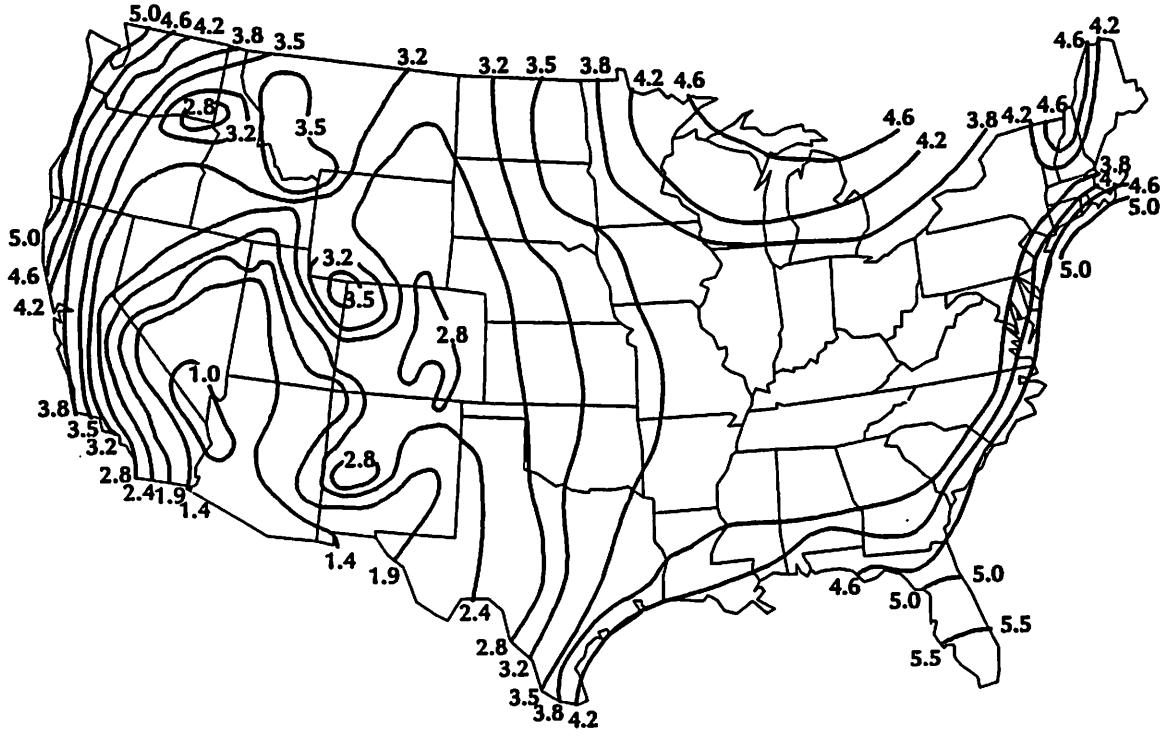

(b) $F_T$.

Figure 6.5. Spatial variation in average relative humidity (NOAA, 1978) and the sulfate *RH* correction factor $F_T$.

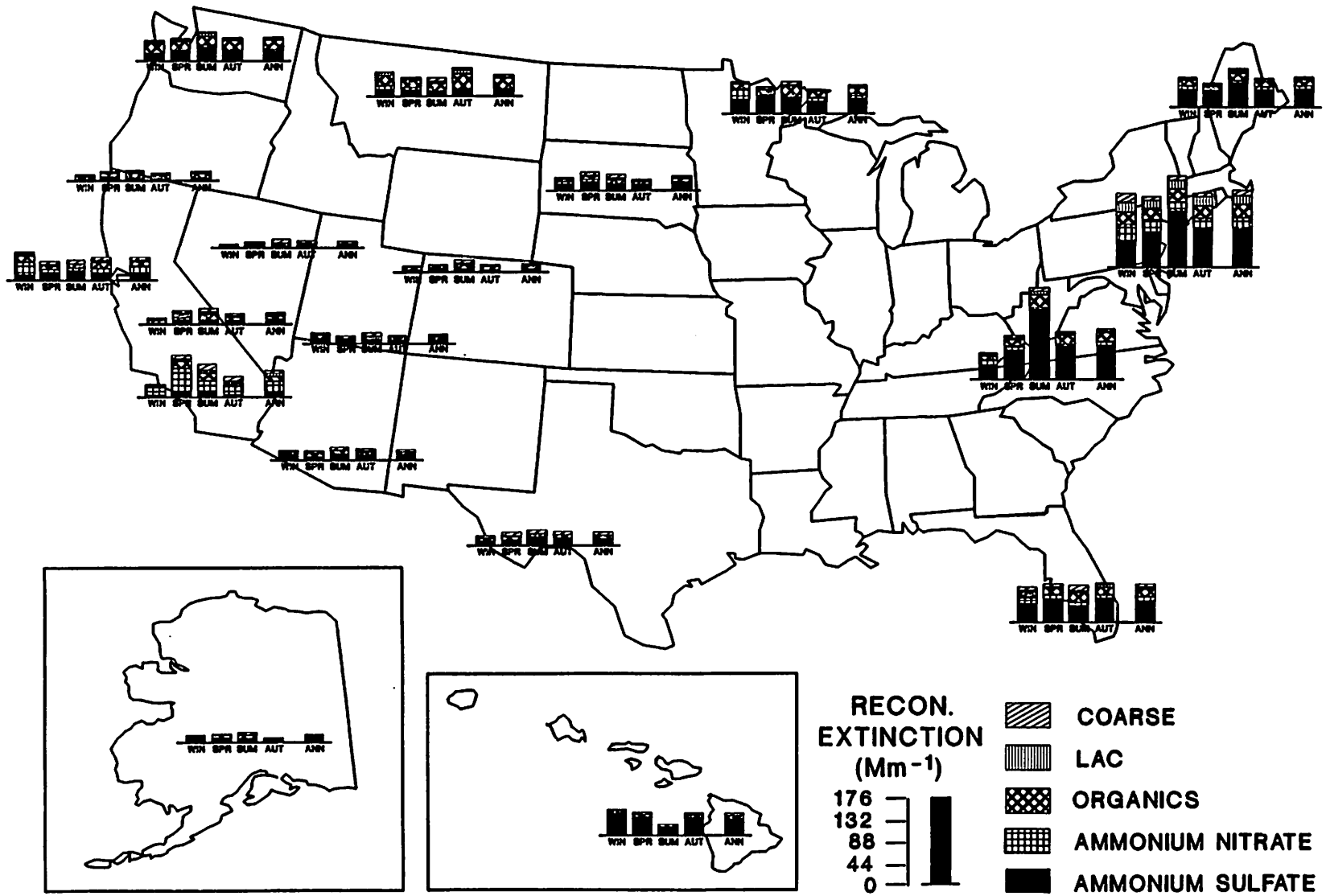


Figure 6.6. Spatial and seasonal distribution of reconstructed aerosol light extinction coefficient ($Mm^{-1}$) in the United States for the three-year period, March 1988 through February 1991. For each of the 19 regions, the bars show the contributions to aerosol light extinction of sulfate, nitrate, organic carbon, light absorbing carbon, and coarse particles and fine soil. From left to right the bars show winter, spring, summer, autumn, and annual averages.

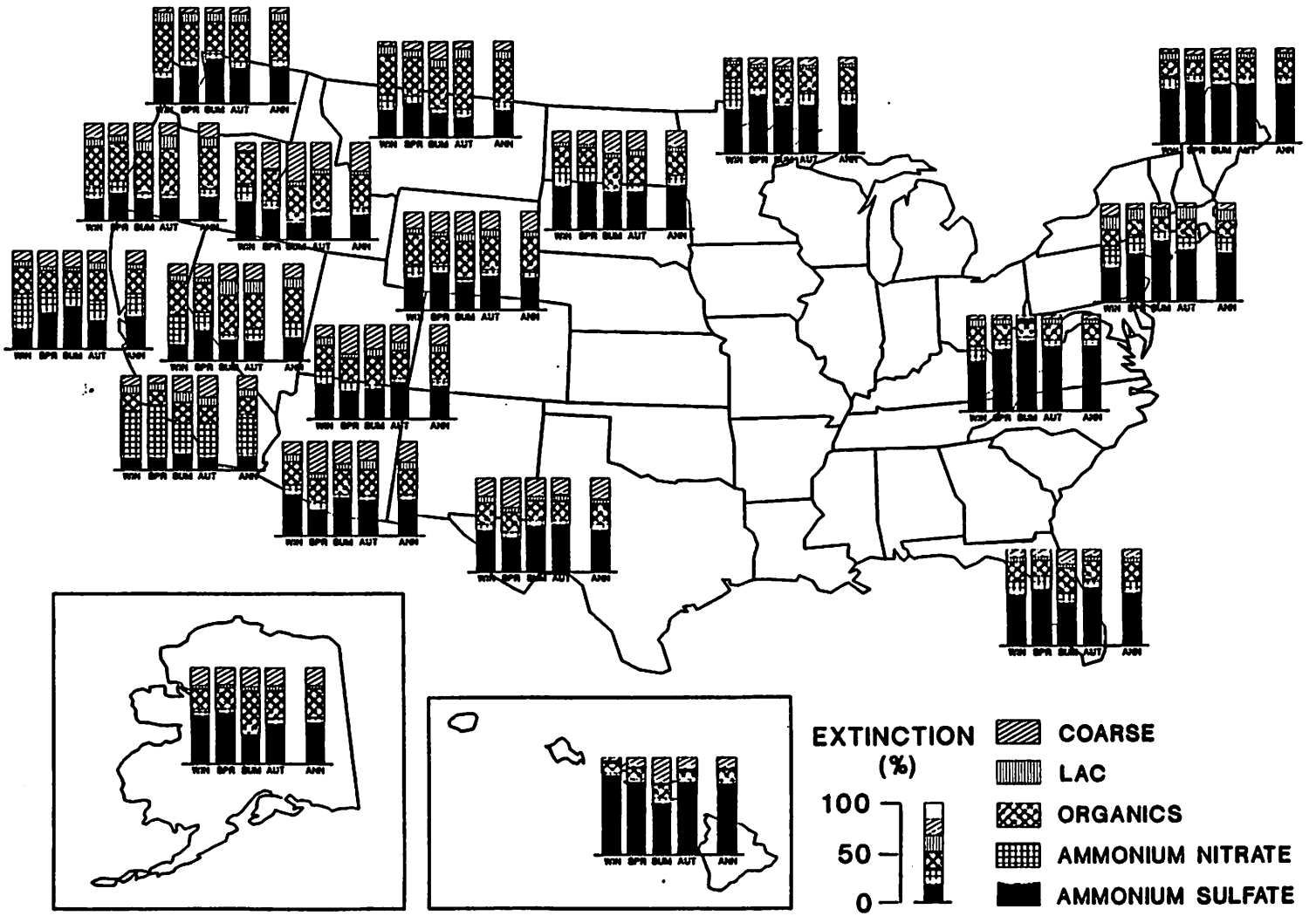


Figure 6.7. Spatial and seasonal distribution of the reconstructed light extinction budget in the United States for the three-year period, March 1988 through February 1991. For each of the 19 regions, the bars show the percentage contributions to aerosol light extinction of sulfate, nitrate, organic carbon, light absorbing carbon, and coarse particles and fine soil. From left to right the bars show winter, spring, summer, autumn, and annual averages.

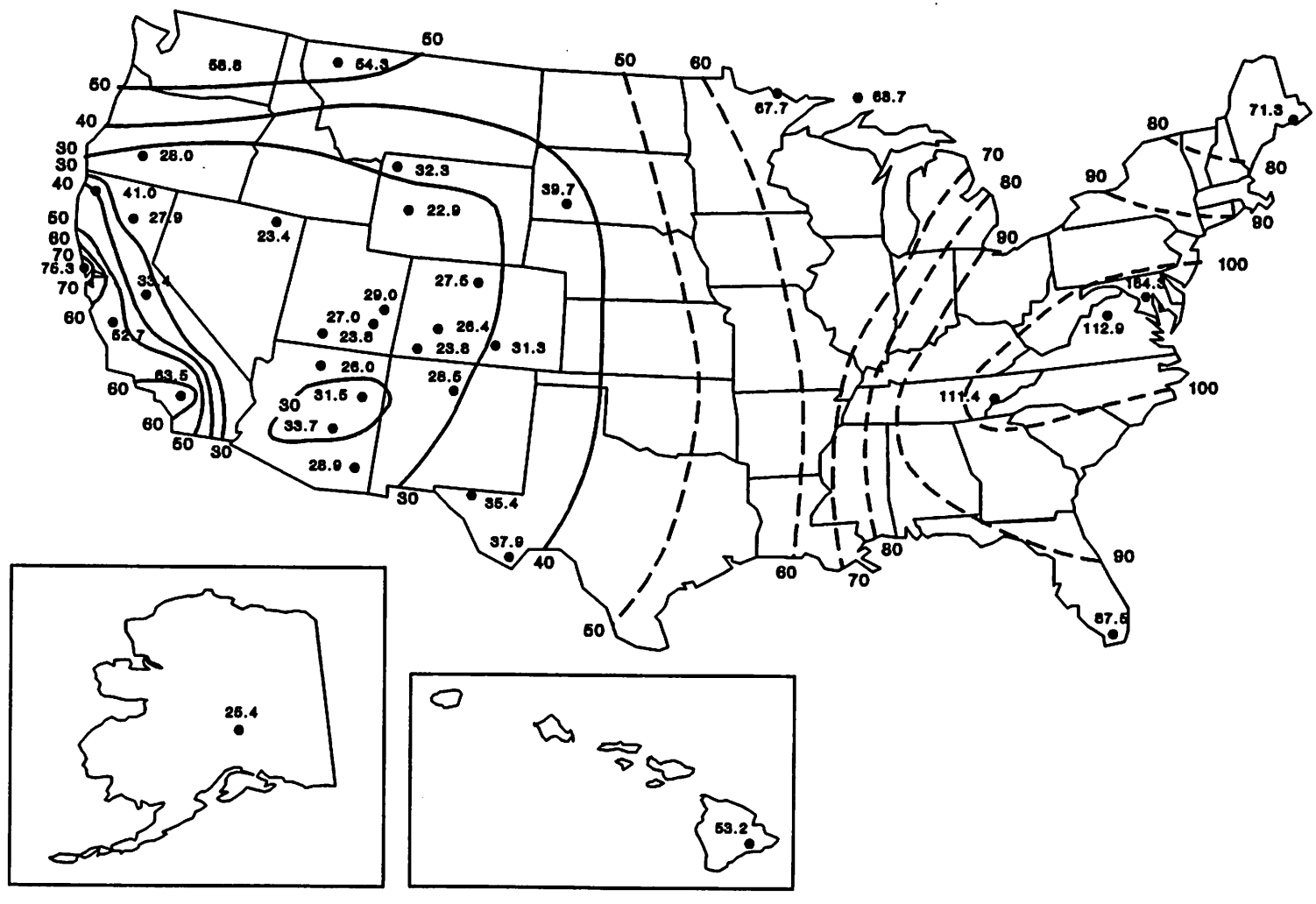


Figure 6.8. Three-year averages of total reconstructed light extinction coefficient ($Mm^{-1}$) for each of the sites in the IMPROVE network in the United States for the 3-year period, March 1988 through February 1991.

Also, the average relative humidity at each site is shown. Table 6.3 shows the aerosol light extinction as well as the contributions of sulfate, nitrate, organic carbon, light absorbing carbon, and coarse particles (including fine soil). Table 6.4 shows the aerosol light extinction budgets: the fractions (percent) of total aerosol (non-Rayleigh) light extinction contributed by sulfate, nitrate, organic carbon, light absorbing carbon, and coarse particles (including fine soil).

The characteristics of each region, in alphabetic order, are briefly discussed below.

Alaska. The Alaska region consists only of the measurements at Denali National Park. Here the three-year average reconstructed total light extinction coefficient was calculated to be 25 $Mm^{-1}$, of which aerosol extinction constituted 61 percent. There is a modest seasonal variation in total reconstructed light extinction, with highest extinction in summer and lowest in autumn. However, there is significant seasonal variation in the individual components of aerosol extinction. For example, organic carbon extinction is highest in summer (8.2 $Mm^{-1}$) and lowest in winter (2.8 $Mm^{-1}$). Nitrate is highest in winter (1.0 $Mm^{-1}$) and lowest in summer (0.3 $Mm^{-1}$). Sulfate is the largest single contributor to aerosol extinction at 43%, followed by organic carbon (30%), coarse particles and fine soil (18%), and nitrate and light absorbing carbon (at 4% each).

Appalachian Mountains. This region consists of measurements at two sites: Great Smoky Mountains and Shenandoah National Parks. The average reconstructed total light extinction coefficient in this region, averaged over the three-year period, of 112 $Mm^{-1}$ was close to the highest measured throughout the IMPROVE network (Washington, D.C. was highest). Virtually all of the extinction (91%) was due to aerosol light extinction. There is a very strong seasonal variation in total reconstructed light extinction with a summer average of 193 $Mm^{-1}$ and a winter average of 64 $Mm^{-1}$. This seasonal variation is largely due to the extreme seasonal variation in sulfate light extinction: summer sulfate extinction is nearly five times larger than extinction in winter. This can be attributed to the seasonal variation in sulfate concentrations (due to differences in photochemistry) and also to the fact that summer is the most humid season with an average relative humidity of 78%. Thus, sulfate aerosols contain much liquid water at such high humidities. Sulfate is the most dominant component of aerosol light extinction. It contributes more than two-thirds (68%), while in summer its contribution is more than three-fourths (76%). Organic carbon is the next largest contributor at 16%, followed by nitrate (7%), light absorbing carbon (5%), and coarse particles and fine soil (4%).

Boundary Waters. This region, in Minnesota, consists of two sets of measurements: in Isle Royale and Voyageurs National Parks. Over the three-year period, the average total reconstructed light extinction coefficient was 68 $Mm^{-1}$. There was very little seasonal variation in total light extinction; however, nitrate and organic carbon varied significantly. Nitrate extinction peaked strongly in the winter (20.9 $Mm^{-1}$) but was very small in summer (1.8 $Mm^{-1}$). Organic carbon extinction was highest in summer (21.2 $Mm^{-1}$) and lowest in winter (8.6 $Mm^{-1}$). Once again, sulfate was the dominant contributor: at 51%, sulfates contributed over half of the aerosol light extinction. Sulfate's contribution was followed by organic carbon (24%), nitrate (15%), coarse particles and fine soil (7%), and light absorbing carbon (4%).

Table 6.2 Seasonal and annual averages, averaged over the three-year period from March 1988 through February 1991, of reconstructed total light extinction coefficient ($Mm^{-1}$) for the 19 regions in the IMPROVE network. Also shown are the light scattering coefficients resulting from fine and coarse aerosols, light absorption for carbonaceous aerosol, percentage of total extinction resulting from aerosols, and the average region relative humidity.

| Season | Total extinction | Fine scattering | Coarse scattering | Absorption | Percent aerosol | Relative humidity |
|---|---|---|---|---|---|---|
| ALASKA | | | | | | |
| Winter | 23.9 | 10.8 | 2.6 | 0.5 | 58 | 68 |
| Spring | 27.0 | 13.5 | 2.9 | 0.5 | 63 | 67 |
| Summer | 28.8 | 14.2 | 3.7 | 0.9 | 65 | 70 |
| Autumn | 21.0 | 8.4 | 2.1 | 0.6 | 52 | 75 |
| ANNUAL | 25.4 | 11.9 | 2.8 | 0.6 | 61 | 70 |
| APPALACHIAN | | | | | | |
| Winter | 63.5 | 47.3 | 2.1 | 4.1 | 84 | 66 |
| Spring | 97.5 | 79.5 | 3.3 | 4.6 | 90 | 66 |
| Summer | 193.1 | 170.7 | 7.6 | 4.8 | 95 | 78 |
| Autumn | 105.8 | 87.3 | 3.7 | 4.9 | 91 | 73 |
| ANNUAL | 112.2 | 93.3 | 4.3 | 4.6 | 91 | 71 |
| BOUNDARY WATERS | | | | | | |
| Winter | 72.1 | 58.0 | 2.1 | 1.9 | 86 | 79 |
| Spring | 63.3 | 47.9 | 3.5 | 1.9 | 84 | 75 |
| Summer | 72.6 | 54.6 | 5.4 | 2.6 | 86 | 82 |
| Autumn | 58.6 | 42.9 | 3.7 | 2.0 | 83 | 84 |
| ANNUAL | 68.2 | 52.3 | 3.8 | 2.2 | 85 | 80 |
| CASCADES | | | | | | |
| Winter | 50.5 | 34.1 | 1.9 | 4.6 | 80 | 89 |
| Spring | 54.9 | 38.2 | 2.2 | 4.5 | 82 | 77 |
| Summer | 68.1 | 49.6 | 3.1 | 5.4 | 85 | 74 |
| Autumn | 57.0 | 39.4 | 2.5 | 5.1 | 82 | 80 |
| ANNUAL | 58.8 | 41.6 | 2.4 | 4.9 | 83 | 80 |
| COLORADO PLATEAU | | | | | | |
| Winter | 28.8 | 14.8 | 2.2 | 1.9 | 63 | 58 |
| Spring | 24.5 | 9.3 | 4.3 | 0.9 | 59 | 40 |
| Summer | 29.2 | 12.8 | 4.7 | 1.8 | 65 | 39 |
| Autumn | 25.9 | 11.5 | 2.7 | 1.6 | 61 | 46 |
| ANNUAL | 27.1 | 12.1 | 3.5 | 1.5 | 63 | 46 |
| CENTRAL ROCKIES | | | | | | |
| Winter | 22.7 | 9.8 | 2.1 | 0.8 | 55 | 63 |
| Spring | 27.4 | 13.0 | 3.6 | 0.7 | 63 | 58 |
| Summer | 34.9 | 17.2 | 5.4 | 2.3 | 70 | 53 |
| Autumn | 26.4 | 12.2 | 2.9 | 1.3 | 62 | 57 |
| ANNUAL | 28.1 | 13.2 | 3.6 | 1.3 | 64 | 58 |

Table 6.2 Continued.

| Season | Total extinction | Fine scattering | Coarse scattering | Absorption | Percent aerosol | Relative humidity |
|---|---|---|---|---|---|---|
| CENTRAL COAST | | | | | | |
| Winter | 67.8 | 49.4 | 4.8 | 3.6 | 82 | 73 |
| Spring | 48.9 | 31.2 | 5.9 | 1.9 | 79 | 68 |
| Summer | 50.8 | 32.7 | 6.7 | 1.4 | 80 | 65 |
| Autumn | 56.2 | 37.3 | 4.9 | 4.0 | 82 | 67 |
| ANNUAL | 56.3 | 38.1 | 5.6 | 2.7 | 81 | 68 |
| FLORIDA | | | | | | |
| Winter | 80.4 | 61.3 | 5.3 | 3.8 | 88 | 82 |
| Spring | 87.3 | 68.9 | 5.5 | 2.9 | 89 | 75 |
| Summer | 84.6 | 60.6 | 10.9 | 3.1 | 88 | 80 |
| Autumn | 90.2 | 70.3 | 5.6 | 4.3 | 89 | 83 |
| ANNUAL | 87.5 | 67.3 | 6.7 | 3.6 | 89 | 80 |
| GREAT BASIN | | | | | | |
| Winter | 18.7 | 7.8 | 0.8 | 0.2 | 47 | 73 |
| Spring | 21.5 | 8.2 | 3.1 | 0.3 | 54 | 55 |
| Summer | 27.1 | 9.4 | 6.8 | 1.0 | 63 | 38 |
| Autumn | 24.5 | 9.6 | 4 | 0.8 | 59 | 55 |
| ANNUAL | 23.4 | 8.8 | 4 | 0.6 | 57 | 55 |
| HAWAII | | | | | | |
| Winter | 62.3 | 49.4 | 1.9 | 1.0 | 84 | 80 |
| Spring | 55.9 | 40.7 | 4.6 | 0.7 | 82 | 80 |
| Summer | 33.4 | 16.7 | 6.3 | 0.4 | 70 | 80 |
| Autumn | 55.6 | 39.2 | 5.7 | 0.7 | 82 | 80 |
| ANNUAL | 53.2 | 37.5 | 5.1 | 0.7 | 81 | 80 |
| NORTHEAST | | | | | | |
| Winter | 70.2 | 53.4 | 2.1 | 4.7 | 86 | 70 |
| Spring | 59.0 | 43.1 | 2.7 | 3.2 | 83 | 65 |
| Summer | 87.9 | 69.4 | 4.3 | 4.2 | 89 | 72 |
| Autumn | 67.3 | 51.0 | 2.7 | 3.7 | 85 | 75 |
| ANNUAL | 71.3 | 54.4 | 2.9 | 4.0 | 86 | 70 |
| NORTHERN GREAT PLAINS | | | | | | |
| Winter | 37.4 | 23.4 | 2.8 | 1.2 | 73 | 70 |
| Spring | 45.3 | 29.5 | 4.6 | 1.2 | 78 | 64 |
| Summer | 42.1 | 23.2 | 7.1 | 1.8 | 76 | 58 |
| Autumn | 33.7 | 17.8 | 4.4 | 1.4 | 70 | 61 |
| ANNUAL | 39.7 | 23.6 | 4.7 | 1.4 | 75 | 63 |
| NORTHERN ROCKIES | | | | | | |
| Winter | 60.1 | 43.4 | 1.7 | 5.0 | 83 | 82 |
| Spring | 48.5 | 32.3 | 3.1 | 3.1 | 79 | 77 |
| Summer | 46.4 | 26.5 | 6.6 | 3.3 | 78 | 68 |
| Autumn | 66 | 45.7 | 4.0 | 6.3 | 85 | 79 |
| ANNUAL | 54.3 | 36 | 3.9 | 4.3 | 82 | 76 |

Table 6.2 Continued.

| Season | Total extinction | Fine scattering | Coarse scattering | Absorption | Percent aerosol | Relative humidity |
|---|---|---|---|---|---|---|
| SOUTHERN CALIFORNIA | | | | | | |
| Winter | 37.5 | 22.1 | 3.0 | 2.4 | 73 | 47 |
| Spring | 94.7 | 71.9 | 7.1 | 5.8 | 89 | 54 |
| Summer | 76 | 47.3 | 10.9 | 7.8 | 87 | 44 |
| Autumn | 50.6 | 27.1 | 9.4 | 4.1 | 80 | 40 |
| ANNUAL | 63.5 | 41.2 | 7.5 | 4.8 | 84 | 46 |
| SONORA | | | | | | |
| Winter | 28.9 | 14.8 | 2.4 | 1.7 | 65 | 53 |
| Spring | 28.4 | 11.1 | 6.0 | 1.3 | 64 | 35 |
| Summer | 36.1 | 18.5 | 5.8 | 1.8 | 72 | 41 |
| Autumn | 31.7 | 15 | 4.3 | 2.4 | 68 | 42 |
| ANNUAL | 31.3 | 14.9 | 4.5 | 1.8 | 68 | 43 |
| SIERRA | | | | | | |
| Winter | 23.7 | 11.2 | 1.5 | 1.0 | 58 | 50 |
| Spring | 36.6 | 21.2 | 3.7 | 1.7 | 73 | 62 |
| Summer | 40.6 | 20.8 | 5.1 | 4.8 | 75 | 42 |
| Autumn | 31.7 | 15.2 | 3.7 | 2.8 | 68 | 43 |
| ANNUAL | 33.4 | 17.5 | 3.4 | 2.5 | 70 | 49 |
| SIERRA/HUMBOLDT | | | | | | |
| Winter | 22.7 | 9.6 | 2.0 | 1.1 | 56 | 70 |
| Spring | 29.3 | 15.6 | 2.3 | 1.4 | 66 | 67 |
| Summer | 32.3 | 15.7 | 4.0 | 2.6 | 69 | 56 |
| Autumn | 25.4 | 11.4 | 2.0 | 2.0 | 61 | 60 |
| ANNUAL | 28.0 | 13.5 | 2.7 | 1.8 | 64 | 63 |
| WASHINGTON DC | | | | | | |
| Winter | 158.4 | 109.6 | 18.7 | 20.2 | 94 | 66 |
| Spring | 151.0 | 117.0 | 7.1 | 17.0 | 93 | 66 |
| Summer | 192.2 | 156.9 | 9.0 | 16.3 | 95 | 78 |
| Autumn | 157.3 | 121.9 | 5.8 | 19.6 | 94 | 73 |
| ANNUAL | 164.3 | 125.3 | 10.6 | 18.4 | 94 | 71 |
| WEST TEXAS | | | | | | |
| Winter | 29.4 | 14.3 | 3.7 | 1.4 | 66 | 50 |
| Spring | 37.3 | 17.4 | 8.4 | 1.6 | 73 | 39 |
| Summer | 41.9 | 24.2 | 6.3 | 1.3 | 76 | 53 |
| Autumn | 37.9 | 21.2 | 5.0 | 1.7 | 73 | 54 |
| ANNUAL | 36.7 | 19.3 | 5.9 | 1.5 | 73 | 49 |

Table 6.3 Seasonal and annual averages, averaged over the three-year period from March 1988 through February 1991, of reconstructed aerosol light extinction coefficient ($Mm^{-1}$) for the 19 regions in the IMPROVE network. Also shown are the light extinction coefficients ($Mm^{-1}$) resulting from sulfate, nitrate, organic carbon, light absorbing carbon, and coarse particles/fine soil.

| Season | Aerosol extinction | Sulfate | Nitrate | Organics | Elemental carbon | Soil and coarse |
|---|---|---|---|---|---|---|
| **ALASKA** | | | | | | |
| Winter | 13.9 | 6.9 | 1.0 | 2.8 | 0.5 | 2.6 |
| Spring | 17.0 | 9.1 | 0.7 | 3.8 | 0.5 | 2.9 |
| Summer | 18.8 | 5.6 | 0.3 | 8.2 | 0.9 | 3.7 |
| Autumn | 11.0 | 4.6 | 0.6 | 3.2 | 0.6 | 2.1 |
| ANNUAL | 15.4 | 6.7 | 0.7 | 4.6 | 0.6 | 2.8 |
| **APPALACHIAN** | | | | | | |
| Winter | 53.5 | 28.8 | 8.1 | 10.5 | 4.1 | 2.1 |
| Spring | 87.5 | 57.8 | 8.1 | 13.6 | 4.6 | 3.3 |
| Summer | 183.1 | 138.4 | 4.3 | 27.9 | 4.8 | 7.6 |
| Autumn | 95.8 | 65.7 | 5.6 | 16.0 | 4.9 | 3.7 |
| Annual | 102.2 | 69.7 | 6.9 | 16.7 | 4.6 | 4.3 |
| **BOUNDARY WATERS** | | | | | | |
| Winter | 62.1 | 28.5 | 20.9 | 8.6 | 1.9 | 2.1 |
| Spring | 53.3 | 32.6 | 4.5 | 10.8 | 1.9 | 3.5 |
| Summer | 62.6 | 31.5 | 1.8 | 21.2 | 2.6 | 5.4 |
| Autumn | 48.6 | 24.9 | 6.8 | 11.3 | 2.0 | 3.7 |
| Annual | 58.2 | 29.8 | 8.4 | 14.1 | 2.2 | 3.8 |
| **CASCADES** | | | | | | |
| Winter | 40.5 | 11.0 | 2.7 | 20.4 | 4.6 | 1.9 |
| Spring | 44.9 | 17.7 | 3.1 | 17.3 | 4.5 | 2.2 |
| Summer | 58.1 | 27.4 | 4.7 | 17.5 | 5.4 | 3.1 |
| Autumn | 47.0 | 18.1 | 2.7 | 18.6 | 5.1 | 2.5 |
| ANNUAL | 48.8 | 19.0 | 3.3 | 19.2 | 4.9 | 2.4 |
| **COLORADO PLATEAU** | | | | | | |
| Winter | 18.8 | 6.7 | 3.3 | 4.7 | 1.9 | 2.2 |
| Spring | 14.5 | 4.5 | 1.1 | 3.6 | 0.9 | 4.3 |
| Summer | 19.2 | 6.2 | 0.8 | 5.7 | 1.8 | 4.7 |
| Autumn | 15.9 | 6.2 | 0.8 | 4.6 | 1.6 | 2.7 |
| Annual | 17.1 | 6.0 | 1.4 | 4.7 | 1.5 | 3.5 |
| **CENTRAL ROCKIES** | | | | | | |
| Winter | 12.7 | 4.2 | 1.7 | 3.9 | 0.8 | 2.1 |
| Spring | 17.4 | 6.6 | 1.9 | 4.6 | 0.7 | 3.6 |
| Summer | 24.9 | 6.5 | 0.9 | 9.7 | 2.3 | 5.4 |
| Autumn | 16.4 | 5.8 | 0.9 | 5.5 | 1.3 | 2.9 |
| ANNUAL | 18.1 | 5.8 | 1.3 | 6.1 | 1.3 | 3.6 |

Table 6.3 Continued.

| Season | Aerosol extinction | Sulfate | Nitrate | Organics | Elemental carbon | Soil and coarse |
|---|---|---|---|---|---|---|
| CENTRAL COAST | | | | | | |
| Winter | 57.8 | 11.4 | 25.0 | 13.0 | 3.6 | 4.8 |
| Spring | 38.9 | 14.7 | 8.4 | 8.1 | 1.9 | 5.9 |
| Summer | 40.8 | 18.6 | 7.0 | 7.0 | 1.4 | 6.7 |
| Autumn | 46.2 | 14.3 | 9.8 | 13.1 | 4.0 | 4.9 |
| ANNUAL | 46.3 | 15.4 | 12.1 | 10.6 | 2.7 | 5.6 |
| FLORIDA | | | | | | |
| Winter | 70.4 | 37.9 | 10.9 | 12.5 | 3.8 | 5.3 |
| Spring | 77.3 | 45.6 | 10.5 | 12.8 | 2.9 | 5.5 |
| Summer | 74.6 | 33.5 | 7.2 | 19.8 | 3.1 | 10.9 |
| Autumn | 80.2 | 47.6 | 8.1 | 14.6 | 4.3 | 5.6 |
| ANNUAL | 77.5 | 42.4 | 9.5 | 15.4 | 3.6 | 6.7 |
| GREAT BASIN | | | | | | |
| Winter | 8.7 | 3.4 | 1.6 | 2.8 | 0.2 | 0.8 |
| Spring | 11.5 | 3.6 | 1.0 | 3.6 | 0.3 | 3.1 |
| Summer | 17.1 | 2.9 | 0.5 | 6.0 | 1.0 | 6.8 |
| Autumn | 14.5 | 3.5 | 0.9 | 5.2 | 0.8 | 4.0 |
| ANNUAL | 13.4 | 3.4 | 0.9 | 4.6 | 0.6 | 4.0 |
| HAWAII | | | | | | |
| Winter | 52.3 | 42.6 | 1.0 | 5.8 | 1.0 | 1.9 |
| Spring | 45.9 | 34.2 | 1.1 | 5.3 | 0.7 | 4.6 |
| Summer | 23.4 | 12.3 | 1.2 | 3.2 | 0.4 | 6.3 |
| Autumn | 45.6 | 33.9 | 0.7 | 4.5 | 0.7 | 5.7 |
| ANNUAL | 43.2 | 31.5 | 1.0 | 5.0 | 0.7 | 5.1 |
| NORTHEAST | | | | | | |
| Winter | 60.2 | 35.4 | 8.0 | 10.0 | 4.7 | 2.1 |
| Spring | 49.0 | 31.9 | 3.9 | 7.3 | 3.2 | 2.7 |
| Summer | 77.9 | 48.9 | 3.8 | 16.8 | 4.2 | 4.3 |
| Autumn | 57.3 | 36.3 | 4.8 | 9.9 | 3.7 | 2.7 |
| ANNUAL | 61.3 | 38.3 | 5.1 | 11.0 | 4.0 | 2.9 |
| NORTHERN GREAT PLAINS | | | | | | |
| Winter | 27.4 | 11.9 | 5.7 | 5.7 | 1.2 | 2.8 |
| Spring | 35.3 | 17.5 | 5.4 | 6.6 | 1.2 | 4.6 |
| Summer | 32.1 | 12.7 | 1.1 | 9.4 | 1.8 | 7.1 |
| Autumn | 23.7 | 9.4 | 1.6 | 6.7 | 1.4 | 4.4 |
| ANNUAL | 29.7 | 13.1 | 3.3 | 7.3 | 1.4 | 4.7 |
| NORTHERN ROCKIES | | | | | | |
| Winter | 50.1 | 14.4 | 8.2 | 20.8 | 5.0 | 1.7 |
| Spring | 38.5 | 14.0 | 3.1 | 15.2 | 3.1 | 3.1 |
| Summer | 36.4 | 9.2 | 1.7 | 15.6 | 3.3 | 6.6 |
| Autumn | 56.0 | 12.3 | 4.1 | 29.3 | 6.3 | 4.0 |
| ANNUAL | 44.3 | 12.4 | 4.0 | 19.6 | 4.3 | 3.9 |

Table 6.3 Continued

| Season | Aerosol extinction | Sulfate | Nitrate | Organics | Elemental carbon | Soil and coarse |
|---|---|---|---|---|---|---|
| SOUTHERN CALIFORNIA | | | | | | |
| Winter | 27.5 | 3.3 | 13.9 | 4.9 | 2.4 | 3.0 |
| Spring | 84.7 | 11.3 | 47.2 | 13.3 | 5.8 | 7.1 |
| Summer | 66.0 | 11.1 | 21.5 | 14.7 | 7.8 | 10.9 |
| Autumn | 40.6 | 5.2 | 14.9 | 7.0 | 4.1 | 9.4 |
| ANNUAL | 53.5 | 7.7 | 23.8 | 9.7 | 4.8 | 7.5 |
| SONORA | | | | | | |
| Winter | 18.9 | 8.1 | 2.0 | 4.6 | 1.7 | 2.4 |
| Spring | 18.4 | 5.1 | 1.4 | 4.6 | 1.3 | 6.0 |
| Summer | 26.1 | 10.7 | 1.0 | 6.7 | 1.8 | 5.8 |
| Autumn | 21.7 | 8.0 | 0.9 | 6.1 | 2.4 | 4.3 |
| ANNUAL | 21.3 | 8.1 | 1.3 | 5.5 | 1.8 | 4.5 |
| SIERRA | | | | | | |
| Winter | 13.7 | 2.3 | 4.2 | 4.7 | 1.0 | 1.5 |
| Spring | 26.6 | 8.4 | 5.0 | 7.8 | 1.7 | 3.7 |
| Summer | 30.6 | 6.8 | 2.3 | 11.7 | 4.8 | 5.1 |
| Autumn | 21.7 | 4.6 | 2.9 | 7.7 | 2.8 | 3.7 |
| ANNUAL | 23.4 | 5.7 | 3.6 | 8.1 | 2.5 | 3.4 |
| SIERRA/HUMBOLDT | | | | | | |
| Winter | 12.7 | 2.8 | 1.4 | 5.3 | 1.1 | 2.0 |
| Spring | 19.3 | 5.5 | 2.3 | 7.7 | 1.4 | 2.3 |
| Summer | 22.3 | 5.1 | 1.3 | 9.4 | 2.6 | 4.0 |
| Autumn | 15.4 | 3.4 | 0.8 | 7.2 | 2.0 | 2.0 |
| ANNUAL | 18.0 | 4.4 | 1.4 | 7.7 | 1.8 | 2.7 |
| WASHINGTON DC | | | | | | |
| Winter | 148.4 | 51.9 | 32.7 | 25.0 | 20.2 | 18.7 |
| Spring | 141.0 | 70.5 | 25.0 | 21.5 | 17.0 | 7.1 |
| Summer | 182.2 | 112.9 | 16.3 | 27.8 | 16.3 | 9.0 |
| Autumn | 147.3 | 77.6 | 18.8 | 25.6 | 19.6 | 5.8 |
| ANNUAL | 154.3 | 75.6 | 24.6 | 25.0 | 18.4 | 10.6 |
| WEST TEXAS | | | | | | |
| Winter | 19.4 | 8.6 | 1.3 | 4.4 | 1.4 | 3.7 |
| Spring | 27.3 | 10.0 | 1.4 | 5.9 | 1.6 | 8.4 |
| Summer | 31.9 | 15.6 | 1.9 | 6.7 | 1.3 | 6.3 |
| Autumn | 27.9 | 14.5 | 1.0 | 5.6 | 1.7 | 5.0 |
| ANNUAL | 26.7 | 12.2 | 1.4 | 5.7 | 1.5 | 5.9 |

Table 6.4 Seasonal and annual averages, averaged over the three-year period from March 1988 through February 1991, of percentage contributions to the reconstructed aerosol light extinction coefficient (light extinction budget) for the 19 regions in the IMPROVE network for sulfate, nitrate, organic carbon, light absorbing carbon, and coarse particles/fine soil.

| Season | Sulfate | Nitrate | Organics | Elemental carbon | Soil and Coarse |
|---|---|---|---|---|---|
| ALASKA | | | | | |
| Winter | 49.7 | 7.3 | 20.4 | 3.9 | 18.7 |
| Spring | 53.3 | 4.1 | 22.0 | 3.2 | 17.3 |
| Summer | 30.0 | 1.8 | 44.0 | 4.6 | 19.6 |
| Autumn | 41.5 | 5.6 | 28.8 | 5.4 | 18.7 |
| ANNUAL | 43.3 | 4.4 | 29.8 | 4.1 | 18.4 |
| APPALACHIAN | | | | | |
| Winter | 53.8 | 15.1 | 19.6 | 7.6 | 3.9 |
| Spring | 66.1 | 9.2 | 15.6 | 5.3 | 3.8 |
| Summer | 75.6 | 2.3 | 15.3 | 2.6 | 4.2 |
| Autumn | 68.6 | 5.8 | 16.7 | 5.1 | 3.8 |
| ANNUAL | 68.3 | 6.7 | 16.3 | 4.5 | 4.2 |
| BOUNDARY WATERS | | | | | |
| Winter | 46.2 | 33.0 | 14.1 | 3.2 | 3.4 |
| Spring | 60.9 | 8.6 | 20.2 | 3.6 | 6.6 |
| Summer | 50.4 | 2.9 | 33.9 | 4.2 | 8.6 |
| Autumn | 51.4 | 13.6 | 23.3 | 4 | 7.6 |
| ANNUAL | 51.1 | 14.5 | 24.2 | 3.7 | 6.5 |
| CASCADES | | | | | |
| Winter | 27.1 | 6.6 | 50.4 | 11.3 | 4.6 |
| Spring | 39.5 | 6.9 | 38.6 | 10.1 | 4.9 |
| Summer | 47.2 | 8.0 | 30.1 | 9.4 | 5.3 |
| Autumn | 38.4 | 5.7 | 39.6 | 10.9 | 5.4 |
| ANNUAL | 39.0 | 6.8 | 39.4 | 10.0 | 4.8 |
| COLORADO PLATEAU | | | | | |
| Winter | 37.7 | 14.8 | 25.5 | 9.5 | 12.4 |
| Spring | 31.5 | 7.9 | 25.1 | 6.0 | 29.5 |
| Summer | 32.3 | 4.4 | 29.9 | 8.9 | 24.4 |
| Autumn | 39.1 | 5.0 | 28.9 | 9.8 | 17.3 |
| ANNUAL | 35.3 | 7.9 | 27.6 | 8.6 | 20.5 |
| CENTRAL ROCKIES | | | | | |
| Winter | 33.8 | 13.1 | 31.0 | 6.0 | 16.1 |
| Spring | 38.2 | 10.6 | 26.6 | 4.2 | 20.4 |
| Summer | 28.5 | 3.8 | 37.4 | 8.9 | 21.3 |
| Autumn | 35.3 | 5.6 | 33.8 | 7.6 | 17.7 |
| ANNUAL | 32.7 | 7.3 | 33.6 | 7.1 | 19.3 |

Table 6.4 Continued.

| Season | Sulfate | Nitrate | Organics | Elemental carbon | Soil and coarse |
|---|---|---|---|---|---|
| CENTRAL COAST | | | | | |
| Winter | 21.5 | 35.6 | 26.9 | 6.8 | 9.3 |
| Spring | 37.4 | 20.9 | 21.7 | 4.9 | 15.1 |
| Summer | 44.2 | 17.2 | 18.2 | 4.0 | 16.4 |
| Autumn | 30.0 | 19.7 | 30.3 | 9.3 | 10.7 |
| ANNUAL | 33.0 | 24.0 | 24.5 | 6.2 | 12.2 |
| FLORIDA | | | | | |
| Winter | 53.8 | 15.5 | 17.7 | 5.4 | 7.5 |
| Spring | 59.0 | 13.6 | 16.6 | 3.7 | 7.1 |
| Summer | 44.9 | 9.7 | 26.5 | 4.2 | 14.6 |
| Autumn | 59.4 | 10.1 | 18.2 | 5.3 | 7.0 |
| Annual | 54.6 | 12.2 | 19.8 | 4.6 | 8.6 |
| GREAT BASIN | | | | | |
| Winter | 38.8 | 18.5 | 32.3 | 1.8 | 8.7 |
| Spring | 31.3 | 8.4 | 31.4 | 2.4 | 26.6 |
| Summer | 16.9 | 2.8 | 34.8 | 5.7 | 39.7 |
| Autumn | 24.4 | 6.4 | 35.9 | 5.7 | 27.7 |
| ANNUAL | 25.3 | 6.5 | 34.1 | 4.1 | 29.9 |
| HAWAII | | | | | |
| Winter | 81.5 | 1.8 | 11.2 | 1.8 | 3.6 |
| Spring | 74.4 | 2.5 | 11.6 | 1.4 | 10.1 |
| Summer | 52.8 | 5.0 | 13.7 | 1.8 | 26.8 |
| Autumn | 74.5 | 1.6 | 9.9 | 1.5 | 12.5 |
| ANNUAL | 72.8 | 2.4 | 11.6 | 1.6 | 11.7 |
| NORTHEAST | | | | | |
| Winter | 58.8 | 13.3 | 16.7 | 7.8 | 3.4 |
| Spring | 65.0 | 7.9 | 14.9 | 6.6 | 5.6 |
| Summer | 62.7 | 4.8 | 21.5 | 5.4 | 5.5 |
| Autumn | 63.3 | 8.4 | 17.2 | 6.4 | 4.7 |
| ANNUAL | 62.4 | 8.4 | 17.9 | 6.5 | 4.8 |
| NORTHERN GREAT PLAINS | | | | | |
| Winter | 43.5 | 21.0 | 20.8 | 4.5 | 10.2 |
| Spring | 49.6 | 15.2 | 18.8 | 3.4 | 13.1 |
| Summer | 39.4 | 3.5 | 29.4 | 5.6 | 22.1 |
| Autumn | 39.9 | 6.9 | 28.4 | 6.1 | 18.7 |
| ANNUAL | 44.0 | 11.0 | 24.5 | 4.8 | 15.8 |
| NORTHERN ROCKIES | | | | | |
| Winter | 28.8 | 16.3 | 41.5 | 9.9 | 3.5 |
| Spring | 36.3 | 8.1 | 39.4 | 8.1 | 8.1 |
| Summer | 25.4 | 4.7 | 42.7 | 9.2 | 18.0 |
| Autumn | 21.9 | 7.4 | 52.3 | 11.2 | 7.2 |
| ANNUAL | 28.0 | 9.0 | 44.3 | 9.8 | 8.9 |

Table 6.4 Continued.

| Season | Sulfate | Nitrate | Organics | Elemental carbon | Soil and coarse |
|---|---|---|---|---|---|
| SOUTHERN CALIFORNIA | | | | | |
| Winter | 12.0 | 50.6 | 17.8 | 8.8 | 10.8 |
| Spring | 13.3 | 55.7 | 15.7 | 6.8 | 8.4 |
| Summer | 16.8 | 32.5 | 22.3 | 11.8 | 16.5 |
| Autumn | 12.7 | 36.7 | 17.3 | 10.1 | 23.2 |
| ANNUAL | 14.4 | 44.4 | 18.2 | 9.0 | 13.9 |
| SONORA | | | | | |
| Winter | 44.6 | 9.7 | 24.4 | 8.8 | 12.5 |
| Spring | 28.0 | 7.3 | 25 | 7.0 | 32.8 |
| Summer | 40.8 | 4.0 | 25.7 | 7.0 | 22.5 |
| Autumn | 38.4 | 3.8 | 27.8 | 10.8 | 19.2 |
| ANNUAL | 38.8 | 5.9 | 25.7 | 8.4 | 21.1 |
| SIERRA | | | | | |
| Winter | 16.9 | 30.9 | 34.1 | 7.5 | 10.6 |
| Spring | 31.7 | 18.8 | 29.3 | 6.5 | 13.8 |
| Summer | 22.1 | 7.6 | 38.1 | 15.6 | 16.6 |
| Autumn | 21.0 | 13.4 | 35.6 | 13.0 | 16.9 |
| ANNUAL | 24.5 | 15.3 | 34.8 | 10.8 | 14.6 |
| SIERRA/HUMBOLDT | | | | | |
| Winter | 22.1 | 11.1 | 42.3 | 9.0 | 15.5 |
| Spring | 28.6 | 12.2 | 39.7 | 7.3 | 12.2 |
| Summer | 22.7 | 5.7 | 42.0 | 11.8 | 17.8 |
| Autumn | 22.1 | 4.9 | 46.9 | 13.1 | 13.0 |
| ANNUAL | 24.4 | 7.9 | 42.8 | 10.1 | 14.9 |
| WASHINGTON DC | | | | | |
| Winter | 34.9 | 22.0 | 16.9 | 13.6 | 12.6 |
| Spring | 50.0 | 17.7 | 15.2 | 12.0 | 5.0 |
| Summer | 62.0 | 8.9 | 15.2 | 8.9 | 4.9 |
| Autumn | 52.7 | 12.8 | 17.4 | 13.3 | 3.9 |
| ANNUAL | 49.0 | 16.0 | 16.2 | 11.9 | 6.9 |
| WEST TEXAS | | | | | |
| Winter | 44.2 | 6.8 | 22.7 | 7.0 | 19.3 |
| Spring | 36.6 | 5.1 | 21.6 | 5.8 | 30.9 |
| Summer | 49.0 | 6.0 | 21.1 | 4.1 | 19.8 |
| Autumn | 51.3 | 3.8 | 20.5 | 6.1 | 18.3 |
| ANNUAL | 45.5 | 5.4 | 21.4 | 5.6 | 22.2 |

Cascade Mountains. This region in Washington State consists of only the measurements at Mount Rainier National Park, southeast of Seattle. Here the three-year average reconstructed light extinction was 59 $Mm^{-1}$. There was a modest seasonality, with summer extinction being the largest and winter the lowest. Most of this seasonality is from sulfate light extinction which varies from 11 $Mm^{-1}$ in summer to 27.4 $Mm^{-1}$ in summer. At Mount Rainier sulfate and organic carbon contribute equally (each at 39% of the aerosol extinction). Together they account for over two-thirds of the aerosol extinction. Their contributions are followed by light absorbing carbon (10%), nitrate (7%), and coarse particles and fine soil (5%).

Central Rocky Mountains. The measurements in this region are made at five locations in the mountainous Class I areas of Colorado and Wyoming, including the Bridger and Weminuche wilderness areas, Rocky Mountain and Yellowstone National Parks, and Great Sand Dunes National Monument. The three-year average reconstructed total light extinction was fairly low at; 28 $Mm^{-1}$. Summer extinction is much higher than winter extinction. Although all the aerosol components, except nitrate, vary by season similarly, the greatest seasonal variation appears to be in the organic carbon and the light absorbing carbon contributions. As in the Cascades, organic carbon and sulfate are nearly equal contributors to light extinction at about one-third each (34%, 33%). Their contribution is followed by coarse particles and fine soil (19%) and light absorbing carbon and nitrate (at 7% each).

Coastal Mountains. This region includes three Class I areas along and near the coast of Northern California: Pinnacles National Monument, Point Reyes National Seashore, and Redwoods National Park. This region has an average reconstructed light extinction of 56 $Mm^{-1}$, twice that for the Central Rockies. Unlike most other regions, extinction is highest in winter and lowest in summer. Most of this seasonal variation is caused by the nitrate, organic carbon, and light absorbing carbon components, which all have peaks in winter. Perhaps the winter peaks for the carbon species are related to wintertime home heating with wood. The sulfate and coarse particle and fine soil components vary seasonally, with maxima in summer and minima in winter. The nitrate seasonality is strongest, in winter nitrate extinction averages 25 $Mm^{-1}$, while in summer it is only 7 $Mm^{-1}$. On average, sulfate contributes one-third of aerosol light extinction (33%), nitrate and organic carbon each one-quarter (24% each), followed by coarse particles and fine soil (12%), and light absorbing carbon (6%).

Colorado Plateau. This region in the Four Corners states of the Southwest is the most intensively monitored in the IMPROVE network. There are seven sites, most of them within the so-called Golden Circle of national parks: Arches, Bandelier, Bryce Canyon, Canyonlands, Grand Canyon, Mesa Verde, and Petrified Forest National Parks. The three-year average total reconstructed light extinction coefficient was relatively low for this region: 27 $Mm^{-1}$. There is very little seasonal variation in reconstructed light extinction; however, nitrate extinction is considerably higher in winter than in summer (3.3 $Mm^{-1}$ versus 0.8 $Mm^{-1}$). Here the largest single contributor to aerosol light extinction is sulfate (35%), followed by organic carbon (28%), coarse particles and fine soil (21%), light absorbing carbon (9%), and nitrate (8%).

Florida. This region consists of only one site, Everglades National Park. At Everglades the total reconstructed light extinction coefficient averaged 88 $Mm^{-1}$ over the first three years of IMPROVE. There is not much seasonal variation in light extinction there. Sulfate was, by

far, the largest contributor to aerosol light extinction (55%), followed by organic carbon (20%), nitrate (12%), coarse particles and fine soil (9%), and light absorbing carbon (5%).

Great Basin. The Great Basin of Nevada was represented by only one set of measurements at Jarbidge Wilderness Area in northeastern Nevada. Here the three-year average total reconstructed light extinction coefficient was the lowest of any of the regions in the United States (even lower than Alaska). It was 23 $Mm^{-1}$, only 13 $Mm^{-1}$ above the Rayleigh scattering coefficient. There is significant seasonal variability in extinction at this site, with highest extinction in summer and lowest extinction in winter. Most of this seasonal variation is due to the seasonal variations in organic carbon, light absorbing carbon, and coarse particles and fine soil. Sulfate and nitrate extinction actually was highest in winter and lowest in summer. Organic carbon contributed about one-third (34%) of aerosol extinction, while coarse particles/fine soil was 29% and sulfate was 25%. These contributions were followed distantly by nitrate (7%), and light absorbing carbon (4%).

Hawaii. The Hawaiian Islands were represented by a single measurement site at Hawaii Volcanoes National Park. The total reconstructed light extinction coefficient averaged 53 $Mm^{-1}$. There was a significant seasonal variation, with winter aerosol extinction more than twice that during the summer. This seasonality is contributed largely by the seasonal variations in sulfate extinction, by far, the largest contributor to light extinction. Sulfate extinction was nearly three-fourths (73%) of aerosol light extinction. Other contributions were relatively small: organic carbon (12%), coarse particles and fine soil (12%), nitrate (2%), and light absorbing carbon (2%).

Northeast. The northeastern United States is represented by the set of measurements at Acadia National Park on the coast of Maine. At Acadia the total reconstructed light extinction coefficient averaged 71 $Mm^{-1}$, with highest extinction in summer and lowest in autumn. Sulfate and organic carbon extinction were highest in summer and lowest in spring. Nitrate and light absorbing carbon extinction were highest in winter. Sulfate was the largest contributor to aerosol light extinction (62%), followed by organic carbon (18%), nitrate (8%), light absorbing carbon (7%), and coarse particles and fine soil (5%).

Northern Great Plains. Only one set of aerosol measurements was made in this region, at Badlands National Monument in South Dakota, where reconstructed light extinction averaged 40 $Mm^{-1}$. Unlike any other region, extinction was highest in spring and lowest in autumn. This seasonality was due primarily to the sulfate and nitrate components. Organic carbon and light absorbing carbon extinction were both maximum in summer and minimum in winter. Again, sulfate was the dominant component of aerosol light extinction, contributing 44%, followed by organic carbon (25%), coarse particles and fine soil (16%), nitrate (11%), and light absorbing carbon (5%).

Northern Rocky Mountains. This region consisted of the measurements made at Glacier National Park in Montana, close to the Canadian border, where the total reconstructed light extinction coefficient averaged 54 $Mm^{-1}$. Autumn extinction was highest, and summer extinction was lowest. This seasonal variation was due primarily to the effects of organic carbon and light absorbing carbon, which both had maximum extinction in autumn. Both sulfate and nitrate extinction had maxima in winter and minima in summer. Coarse particle and fine soil extinction

were maximum in summer and minimum in winter. Organic carbon was the largest single contributor to aerosol light extinction in Glacier (44%). Its contribution was followed by sulfate (28%), light absorbing carbon (10%), nitrate (9%), and coarse particles and fine soil (9%).

Sierra Nevada. The aerosol in the Sierra Nevada mountains in California were monitored at Yosemite National Park. The reconstructed total light extinction averaged 33 $Mm^{-1}$, with strong seasonal variation resulting in a summer average of 41 $Mm^{-1}$ and a winter average of 24 $Mm^{-1}$. This seasonality is due primarily to the strong seasonal variation in extinction due to organic carbon, light absorbing carbon, and coarse particles/fine soil. Organic carbon was the largest single contributor to aerosol extinction (35%), followed by sulfate (25%), nitrate (15%), coarse particles/fine soil (15%), and light absorbing carbon (11%).

Sierra-Humboldt. The region further north in the Sierra Nevada and Humboldt mountain ranges was measured at Crater Lake National Park in Oregon and Lassen Volcanoes National Park in Northern California. For this region, total reconstructed light extinction averaged 28 $Mm^{-1}$, with maximum extinction in summer and minimum extinction in winter. This seasonality was due primarily to the variations in extinction caused by organic carbon, light absorbing carbon, and coarse particles/fine soil. Organic carbon was, by far, the largest contributor to aerosol light extinction (43%), followed by sulfate (24%), coarse particles and fine soil (15%), light absorbing carbon (10%), and nitrate (8%).

Sonoran Desert. This region in southeastern Arizona was monitored at two sites: Chiracahua and Tonto National Monuments. The three-year average total reconstructed light extinction coefficient was 31 $Mm^{-1}$. There was minimal seasonal variation in extinction; however, extinction was highest in summer and lowest in spring. Sulfate extinction varied from a high of 10.7 $Mm^{-1}$ in summer to a low of 5.1 $Mm^{-1}$ in spring. Organic carbon extinction also varied from a summer high of 6.7 $Mm^{-1}$ to a spring low of 4.6 $Mm^{-1}$. Fine soil and coarse particle extinction was highest in spring when it was the largest single contributor to light extinction. In this region sulfate was the largest contributor to aerosol light extinction at 39%, followed by organic carbon (26%), coarse particles and fine soil (21%), light absorbing carbon (8%), and nitrate (6%).

Southern California. Measurements in this region were made in San Gorgonio National Monument, east of the Los Angeles metropolitan area. Total reconstructed light extinction averaged 64 $Mm^{-1}$. The maximum extinction occurred in spring and the minimum occurred in winter. This seasonal variation was caused largely by the seasonal variation in nitrate, and to a lesser extent by sulfate. Extinction caused by organic carbon, light absorbing carbon, and coarse particles/fine soil all peaked in summer and had minima in winter. Unlike any other region in the IMPROVE network, nitrate was the largest single component of aerosol light extinction. Nitrate contributed 44%, organic carbon 18%, sulfate 14%, coarse particles/fine soil 14%, and light absorbing carbon 9%.

Washington, D.C. The highest light extinction coefficient, reconstructed from aerosol concentration, was found in Washington. It averaged 164 $Mm^{-1}$ over the three-year period of IMPROVE. Extinction was somewhat higher in summer (192 $Mm^{-1}$) and lower in spring (151 $Mm^{-1}$). Sulfate extinction was considerably larger in summer (113 $Mm^{-1}$) than in the other seasons. Organic carbon's contribution was constant over the seasons. Nitrate extinction in

winter was twice what it was in summer. Sulfate was the dominant contributor to aerosol light extinction, contributing nearly half (49%), followed by nitrate and organic carbon each contributing 16%, light absorbing carbon (12%), and coarse particles and fine soil (7%).

West Texas. Total light extinction reconstructed from the aerosol measurements at Big Bend and Guadalupe Mountains National Parks averaged 37 $Mm^{-1}$. Highest extinction occurred in summer and lowest extinction occurred in winter. This seasonality was contributed primarily by sulfate, which was by far the largest contributor to aerosol light extinction (46%). Sulfate's contribution was followed distantly by coarse particles and fine soil (22%), organic carbon (21%), light absorbing carbon (6%), and nitrate (5%).

It is interesting to compare the light extinction budgets to the fine aerosol budgets. Organic carbon was the largest single contributor to fine aerosol mass in nine of the 19 regions and was tied with sulfate in three regions, and sulfate was the largest single contributor to fine aerosol mass in six regions. However, sulfate has a larger light extinction efficiency than organic carbon because of its hygroscopic nature; therefore, sulfate is generally the largest single contributor to light extinction, being the largest contributor in 12 of 19 regions and tied with organic carbon in two additional regions (Cascades and Central Rockies). Organic carbon is the largest single contributor to aerosol light extinction in four regions: Great Basin, North Rockies, Sierra Nevada, and Sierra-Humboldt. Only in Southern California is nitrate the largest contributor. In general, then, sulfate is the dominant contributor to light extinction, followed by organic carbon, and more distantly by nitrate and fine soil/coarse particles, and finally, light absorbing carbon.

## 6.5 Spatial Trends in Reconstructed Light Extinction in the United States

Figure 6.9 shows the sulfate light extinction coefficient averaged over the first three years of IMPROVE (March 1988 - February 1991). Note that the highest sulfate extinction occurs in the eastern United States, and the lowest sulfate extinction occurs in Oregon, Nevada, Idaho, and Wyoming. The major gradient in sulfate light extinction is from the eastern United States to the non-urban West. However, there is also a gradient from the San Francisco Bay Area and from the Pacific Northwest to the non-urban West. Sulfate extinction is more than half of total aerosol light extinction in the eastern and north central U.S. In the Appalachians, Middle Atlantic states, and the Northeast, sulfate contributes about two-thirds of aerosol light extinction. In the worst season for sulfate (summer), sulfate's share is even higher, reaching three-quarters in the eastern United States.

Figure 6.10 shows the nitrate light extinction. There is a gradient from the east to west, with relatively high nitrate contributions in the Washington, D.C. area. However, the strongest gradient is from the urban areas of California, especially the Los Angeles metropolitan area, to the California desert. Nitrate contributions to aerosol light extinction are generally less than 10 percent, except in California, where nitrate can contribute as much as 44 percent.

Figure 6.11 shows isopleths of the organic carbon light extinction throughout the United States, averaged over the first three years of IMPROVE. Note that extinction caused by organic

carbon is largest in the eastern United States and in the Pacific Northwest, and lowest in the Golden Circle of parks in southern Utah and northern Arizona. The fraction of aerosol light extinction contributed by organic carbon ranges from a high of more than 40 percent in the Pacific Northwest to less than 20 percent in the urban areas of California and in much of the eastern United States. The reason that organic carbon is a smaller share of aerosol extinction in the East is the much larger contribution of sulfate extinction there.

Figure 6.12 shows isopleths of the extinction caused by light absorbing carbon. Light absorbing carbon extinction is highest in the Pacific Northwest and in the eastern United States and lowest in the non-urban West. Light absorbing carbon contributes about 10 percent of aerosol light extinction in Northern California, the Pacific Northwest, and in Washington, D.C.; however, in most areas its contribution is much less.

## 6.6 Spatial Trends in Visibility in the United States

To show the effect on visibility of aerosol extinction the deciview (dv) scale is applied to the total (Rayleigh included) aerosol extinction (see Chapter 1). By utilizing the dv scale the effect of aerosol extinction on the human visual system is portrayed as a linear scale of visibility degradation. Pristine or Rayleigh conditions have a dv of zero. A one or two dv change is usually associated with the minimal or just noticeable change (JNC) in visibility perceived by the average individual.

Figure 6.13 shows isopleths of deciviews averaged over the first three years of IMPROVE. The smallest dv or best visibility is reported at Bridger Wilderness with 8.3 dv's. There is a broad region that includes the Great Basin, most of the Colorado Plateau and portions of the Central Rockies that has visibility impairment of less than 10 dv. Moving in any direction from this region generally results in a gradient of increasing dv. West of the Sierra Range and including Southern California are dv values in excess of 15 and a maximal value of 20.2 dv at Point Reyes. The northwest U.S. and all of the eastern half of the U.S. have in excess of 15 dv of impaired visibility and the region east of the Mississippi and south of the Great Lakes have impairment in excess of 20 dv with the Appalachian region exceeding 24 dv. The highest annual dv is reported at Washington D.C. with an impairment of 28 dv.

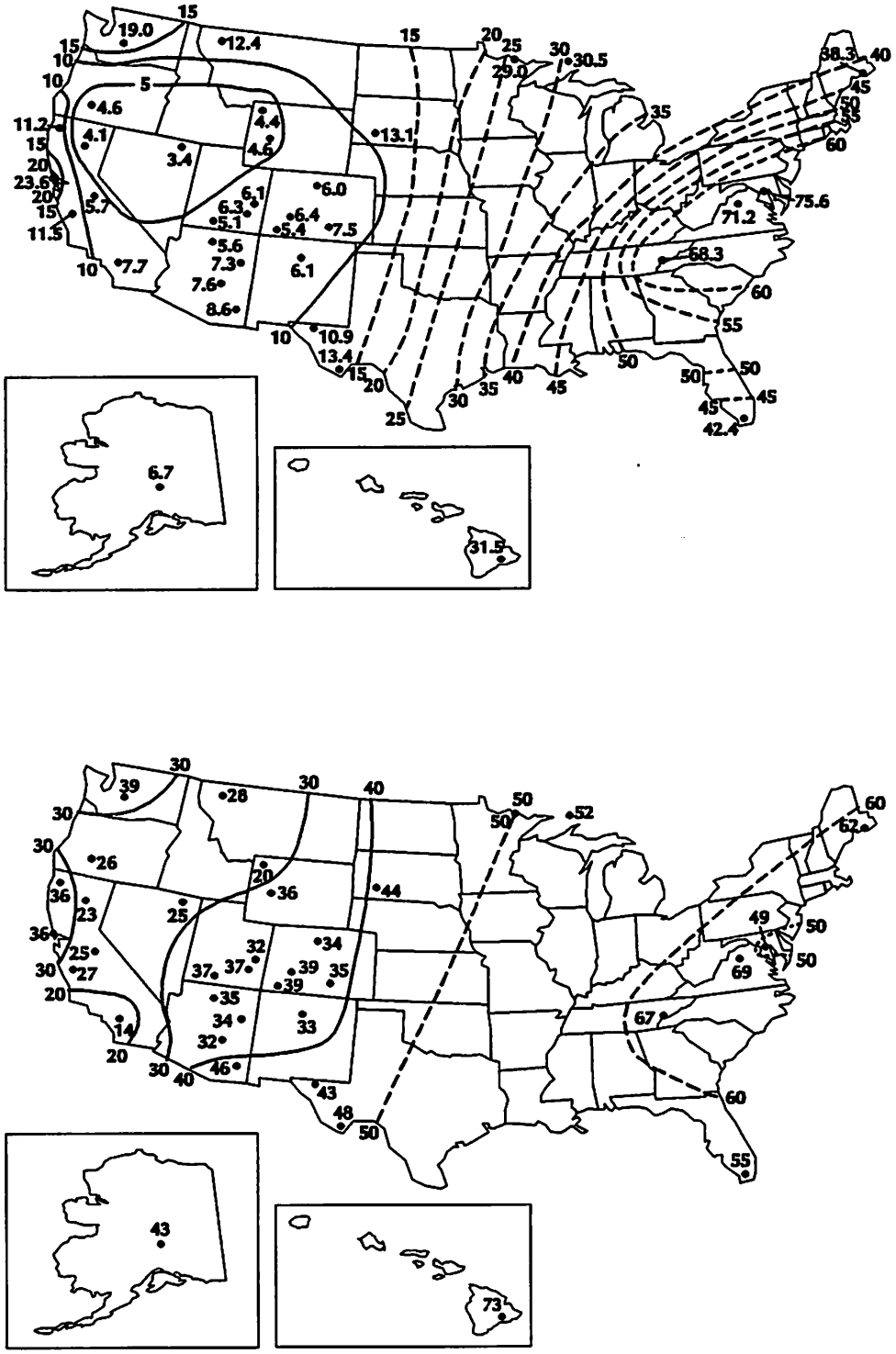





Figure 6.9. Three-year averages of reconstructed sulfate light extinction coefficient in $Mm^{-1}$ (top figure) and sulfate fraction in percent of aerosol light extinction (bottom figure), for each of the sites in the IMPROVE network in the United States for the three-year period, March 1988 through February 1991.

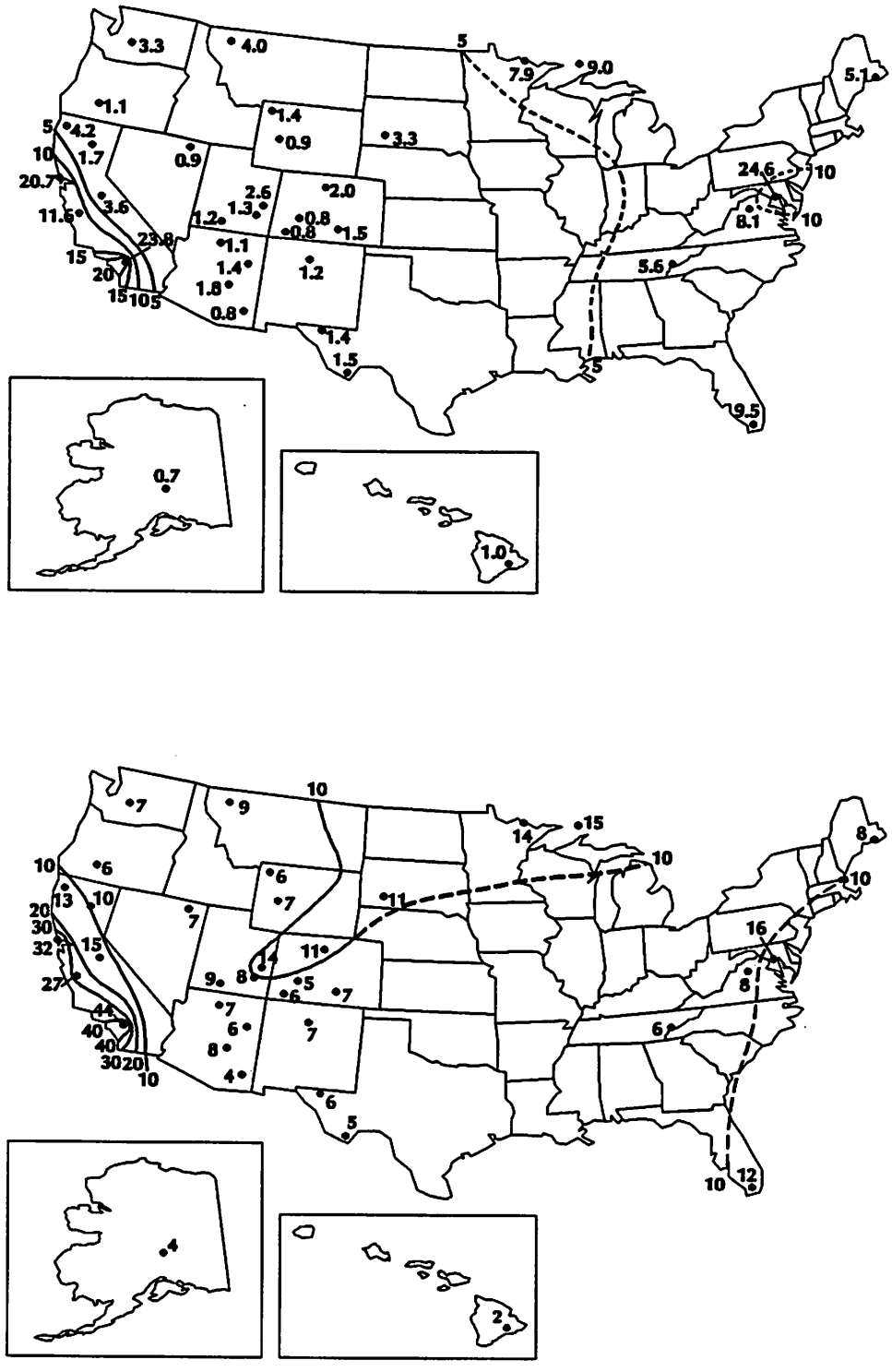


Figure 6.10. Three-year averages of reconstructed nitrate light extinction coefficient in $Mm^{-1}$ (top figure) and nitrate fraction in percent of aerosol light extinction (bottom figure), for each of the sites in the IMPROVE network in the United States for the three-year period, March 1988 through February 1991.

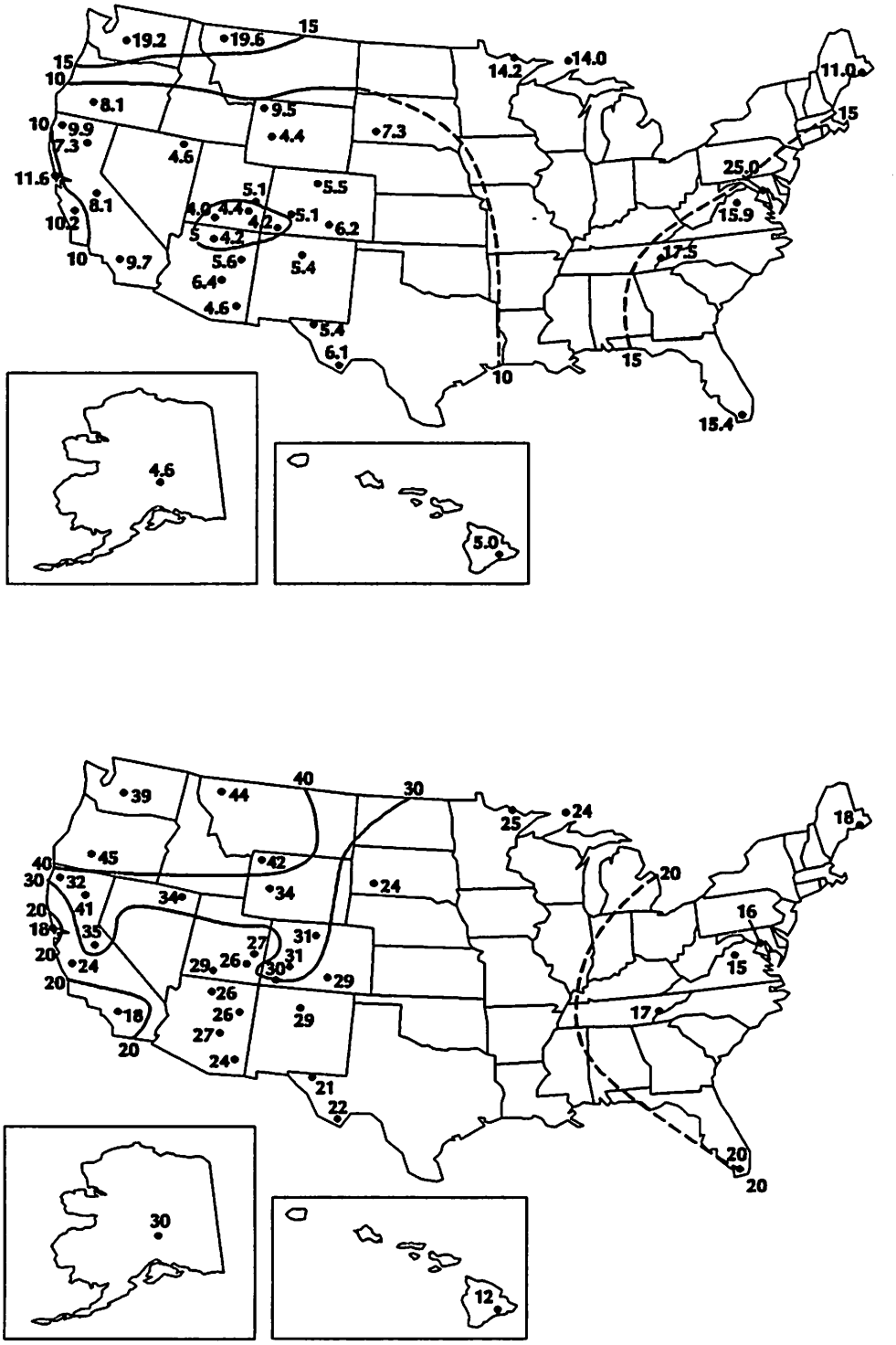


Figure 6.11. Three-year averages of reconstructed organic carbon light extinction coefficient in $Mm^{-1}$ (top figure) and organic carbon fraction in percent of aerosol light extinction (bottom figure), for each of the sites in the IMPROVE network in the United States for the three-year period, March 1988 through February 1991.

Isopleths of dv for the winter, spring, summer, and autumn are shown in Figure 6.14 through Figure 6.17, respectively. The general spatial trend noted above for the annual average generally holds true for each season's average dv trend. Specifically the least impairment or lowest dv's generally occur in all or part of the Great Basin, Colorado Plateau, and Central Rockies with gradients of increasing dv in any direction. One interesting exception to this occurs in the winter (Figure 6.14), which shows an "island" of impaired visibility in the middle of the Colorado Plateau region at Canyonlands and Arches with dv's of 11.2 and 14.7, respectively. It is also of interest to note the eastern U.S. is almost uniformly above 15 dv of impairment for all four seasons.

The best visibility occurs during the winter (Figure 6.14) with the minimum dv of 6 being reported at Bridger Wilderness followed by 6.3 dv at Jarbidge. The region of 10 or less dv's encompasses a broad expanse that covers the Sierra-Humboldt, Sierra Nevada, Great Basin, and almost all of the Colorado Plateau and the Central Rockies. In the eastern half of the U.S. the sites with more than 20 dv are Washington D.C. at 27.6 dv, the Everglades in Florida at 20.8 dv, and Isle Royale with 20.6 dv.

Summertime visibilities (Figure 6.16), except for the Coastal Range, are generally the worst. Only small portions of the Great Basin, Central Rockies, and Colorado Plateau regions have impaired visibilities slightly below 10 dv. In the East there is a broad region east of the Mississippi with more than 20 dv of impairment in visibility and a swath that covers the Appalachian and Washington D.C. regions with almost 30 dv of impairment.

Visibility impairment in the spring (Figure 6.15) and autumn (Figure 6.17) are quite comparable. The only significant difference is the shifting of the region with impairment of 10 dv or less from the southeast in the spring to the Northwest in the autumn. In the spring, most of the Great Basin and Central Rockies, all of the Colorado Plateau, and a portion of the Sonoran region have less than 10 dv of impaired visibility. During autumn the Sierra-Humboldt, Great Basin, Colorado Plateau, and the western fringe of the Central Rockies have less than 10 dv of impairment.

## 6.7 Summary

The following are the major patterns in light extinction reconstructed from aerosol measurements and relative humidity during the first three years of IMPROVE:

1. Spatial Patterns. Following the patterns observed in fine aerosol concentrations, reconstructed light extinction is highest in the eastern United States and in urban California and lowest in the non-urban West.

2. Major Contributors to Light Extinction. Fine aerosols are the principal contributors to light extinction in the United States. Sulfate is the largest single contributor to light extinction in 12 of 19 regions and is tied for first place in two additional regions. In the eastern United States and in Hawaii, sulfate is the overwhelming contributor. Organic carbon is the single largest contributor to light extinction in

four of 19 regions and is tied for first place in two additional regions. Nitrate was the largest single contributor to light extinction only in Southern California.

3. Smaller Contributors. After sulfate and organic carbon, nitrate and windblown dust (coarse particles and fine soil) generally contribute equal amounts. Light absorbing carbon is generally the smallest contributor.

4. Seasonality. Generally, reconstructed light extinction is highest in summer and lowest in winter; however, there are many exceptions to this general rule. Higher extinction occurs in summer generally because of relatively elevated sulfate and carbonaceous aerosol concentrations.

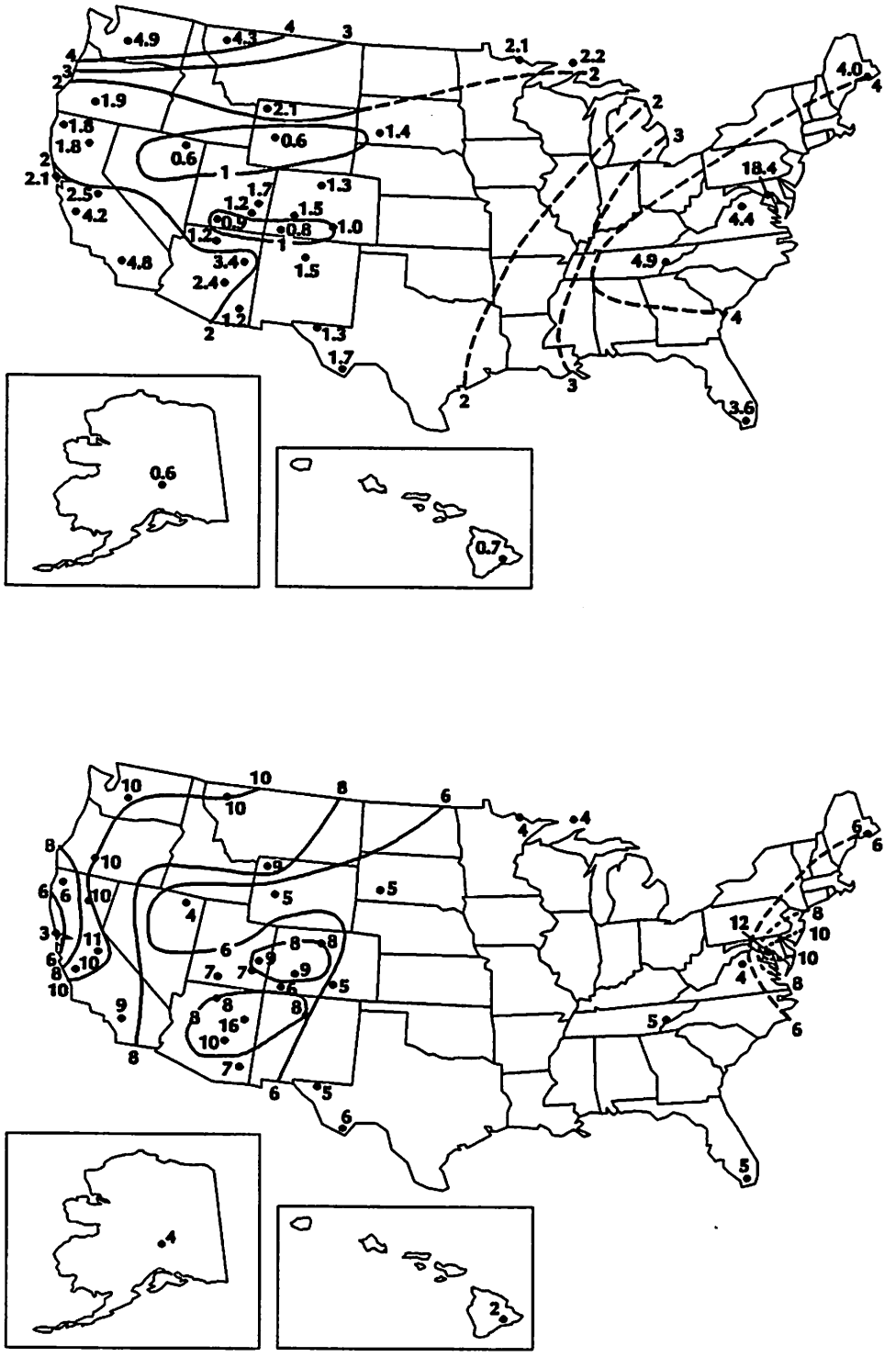


Figure 6.12. Three-year averages of reconstructed light absorbing carbon light extinction coefficient in $Mm^{-1}$ (top figure) and light absorbing carbon fraction in percent of aerosol light extinction (bottom figure), for each of the sites in the IMPROVE network in the United States for the three-year period, March 1988 through February 1991.

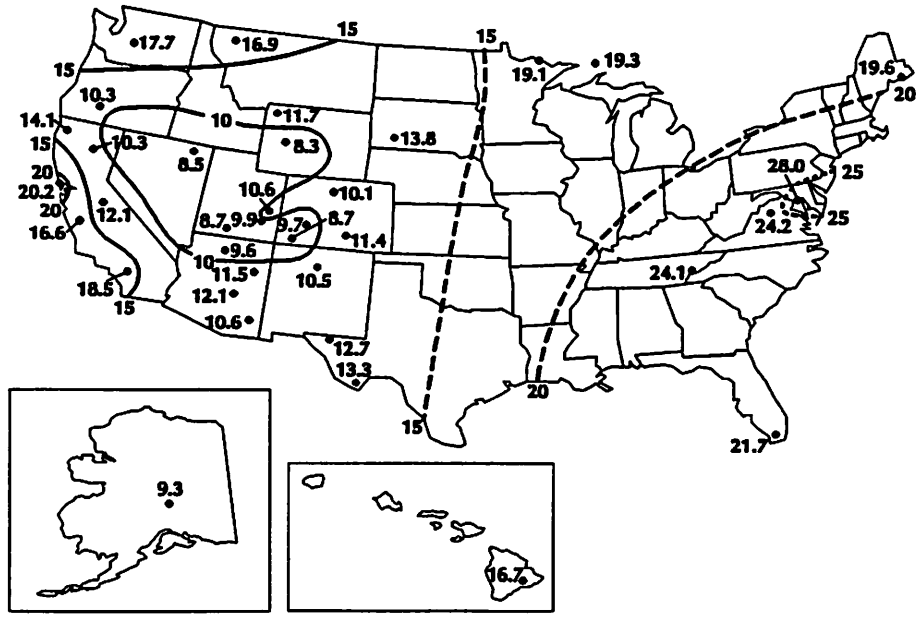


Figure 6.13. Average visibility impairment in deciviews calculated from total (Rayleigh included) reconstructed light extinction for the first three years of IMPROVE, March 1988 through February 1991.

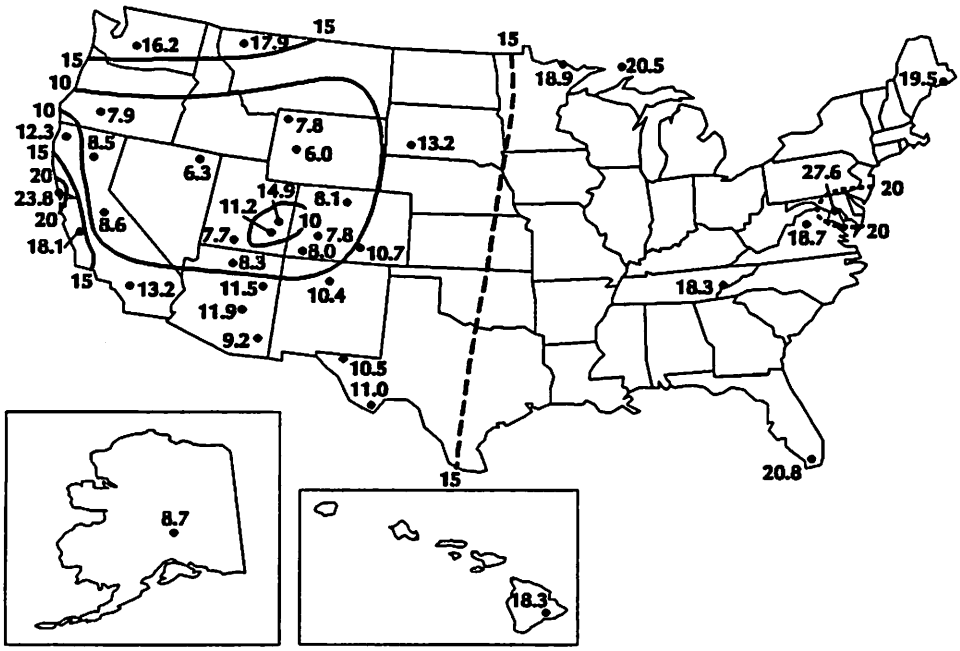


Figure 6.14. Average winter visibility impairment in deciviews calculated from total (Rayleigh included) reconstructed light extinction for the first three years of IMPROVE, March 1988 through February 1991.

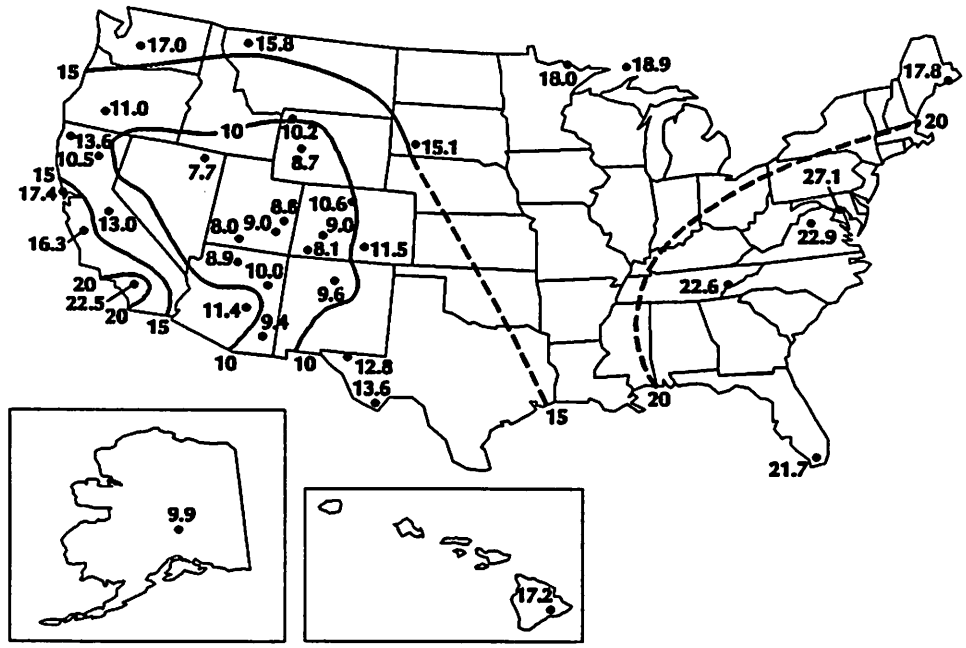


Figure 6.15. Average spring visibility impairment in deciviews calculated from total (Rayleigh included) reconstructed light extinction for the first three years of IMPROVE, March 1988 through February 1991.

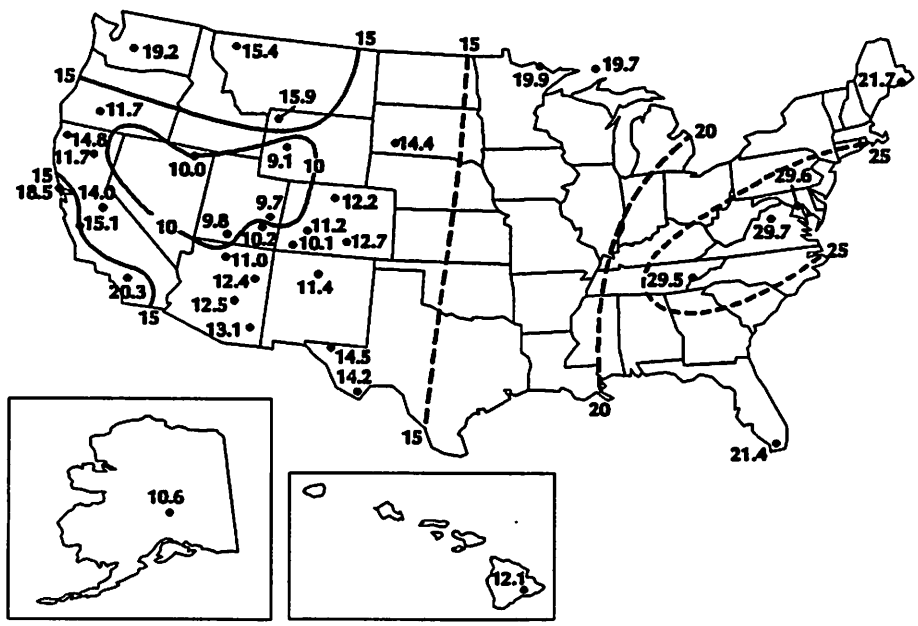


Figure 6.16. Average summer visibility impairment in deciviews calculated from total (Rayleigh included) reconstructed light extinction for the first three years of IMPROVE, March 1988 through February 1991.

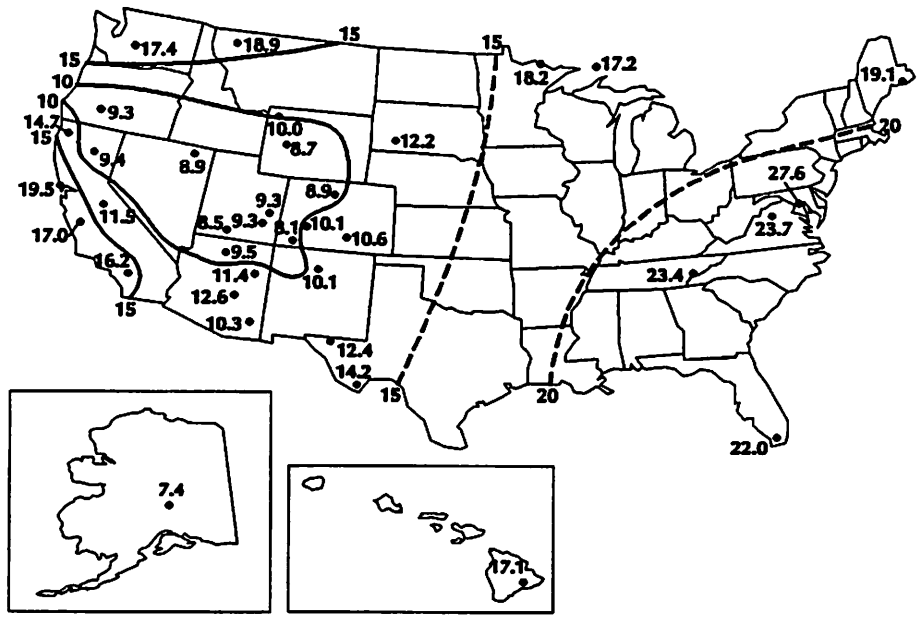


Figure 6.17. Average autumn visibility impairment in deciviews calculated from total (Rayleigh included) reconstructed light extinction for the first three years of IMPROVE, March 1988 through February 1991.

# CHAPTER 7

# MEASURED LIGHT EXTINCTION

Light extinction data from the 20 IMPROVE sites with transmissometers are summarized in Appendix I. A typical data summary for one season at one site, as shown in Figure 7.1, includes a time plot of extinction ($b_{ext}$) or standard visual range ($SVR=3.91/b_{ext}$), an accompanying time plot of relative humidity (RH), and a plot of the cumulative frequency distribution of $b_{ext}$ values occurring in the period, both for all the $b_{ext}$ values (points denoted by an "x") and for only those values which are not tagged as weather-affected (points denoted by an "o"). The meaning of weather-affected $b_{ext}$ values and the algorithm used to identify them are discussed in Section 2.2.2.

Stacked timelines of the extinction for the sites arranged by region are given in Appendix J. The average seasonal and annual extinction, both excluding and including weather-affected values, is presented by region in Figure 7.2. The measured and reconstructed extinctions are compared in Table 7.1 (where measured $b_{ext}$ excludes weather-related events), and values of the standard visual range calculated from these extinctions are compared in Table 7.2. The reconstructed light extinction, discussed in detail in Chapter 6, is based on twice-weekly 24-hour particle samples, while extinction is measured by transmissometer every hour of every day. Furthermore, extinction is not measured at all sites; and where it is measured, values that are deemed weather-affected are not used. Therefore, a detailed comparison of the measured and reconstructed light extinction values requires matching the time period of each 24-hour particle sample with the closest corresponding sequence of valid hourly measured extinction values for those sites having measured extinction. Time constraints prevent such a level of comparison in this report; and the values presented in Table 7.1 simply compare reasonably-defined seasonal averages of reconstructed and measured light extinction.

Table 7.1 shows good agreement (to better than about 10%) in the East, in the Central Rockies and Colorado Plateau, and in the Northern Great Plains. The other regions show underestimation of extinction by reconstruction. Reconstructed extinction is typically 70-80% of the measured extinction. The ratio of reconstructed to measured extinction is also about 80% at the Appalachian site (Shenandoah), during the summer season. This may be due to the fact that sulfate is acidic in this season and acidic sulfate has a higher light scattering efficiency then that of ammonium sulfate assumed here. The worst agreement is in Sierra Nevada (Yosemite), where the reconstructed extinction is only 50% of the measured value. This may be due to the fact that the aerosol monitor is located above the mixed layer much of the time. At this time it is not clear why reconstructed extinction is less then measured extinction in California and in southern Arizona and northwestern Texas.

CHIRICAHUA NATIONAL MONUMENT, ARIZONA
Transmissometer Data Summary
Fall Season: September 1, 1989 – November 30, 1989

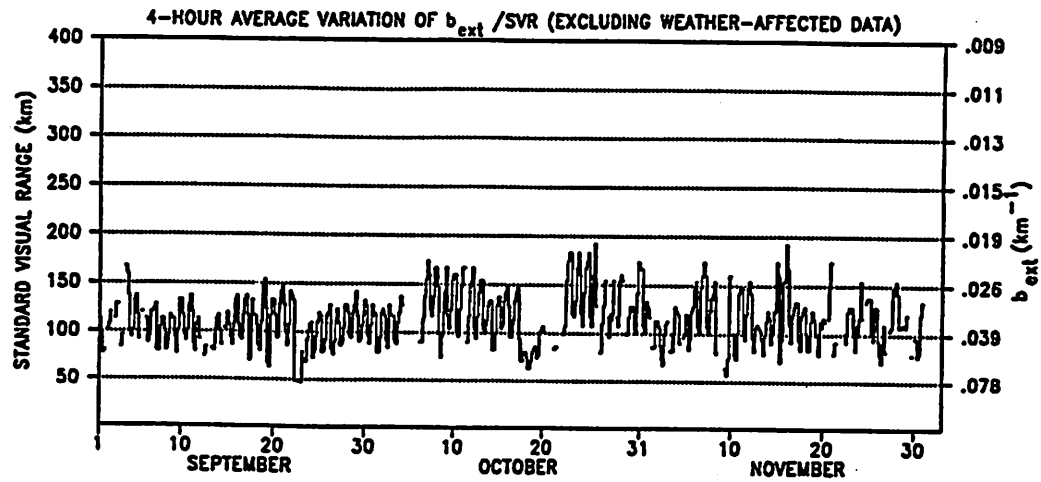


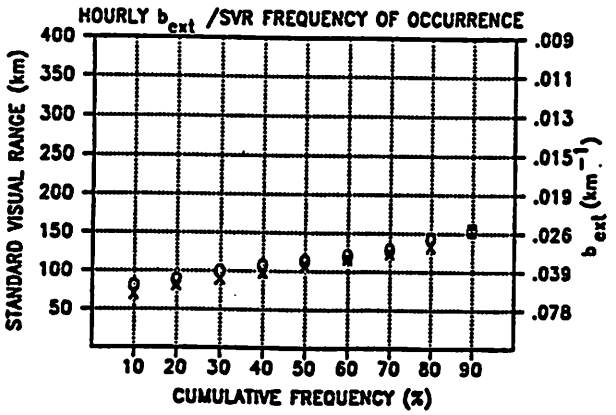


| % | Excluding Weather [O] $b_{ext}$ | Excluding Weather [O] SVR | Including Weather [X] $b_{ext}$ | Including Weather [X] SVR |
|---|---|---|---|---|
| 10 | .049 | 80 | .056 | 70 |
| 20 | .044 | 88 | .047 | 82 |
| 30 | .039 | 99 | .043 | 90 |
| 40 | .036 | 107 | .039 | 99 |
| 50 | .034 | 113 | .036 | 107 |
| 60 | .032 | 120 | .033 | 117 |
| 70 | .030 | 128 | .031 | 124 |
| 80 | .027 | 142 | .029 | 133 |
| 90 | .025 | 154 | .025 | 154 |

FOR A GIVEN % OF THE TIME THE SVR IS LESS THAN OR EQUAL TO THE CORRESPONDING SVR VALUE.

| TRANSMISSOMETER DATA RECOVERY | NUM | % |
|---|---|---|
| TOTAL POSSIBLE HOURLY AVERAGES IN THE TIME PERIOD | 2184 | 100 |
| TOTAL COLLECTED HOURLY AVERAGES IN THE TIME PERIOD | 2184 | 100 |
| VALID HOURLY AVERAGES INCLUDING WEATHER-AFFECTED DATA | 2069 | 95 |
| VALID HOURLY AVERAGES EXCLUDING WEATHER-AFFECTED DATA | 1568 | 72 |
| PERCENT OF ALL VALID AVERAGES NOT AFFECTED BY WEATHER | | 76 |

DATE PREPARED: 8/27/91

Figure 7.1 Example transmissometer data summary.

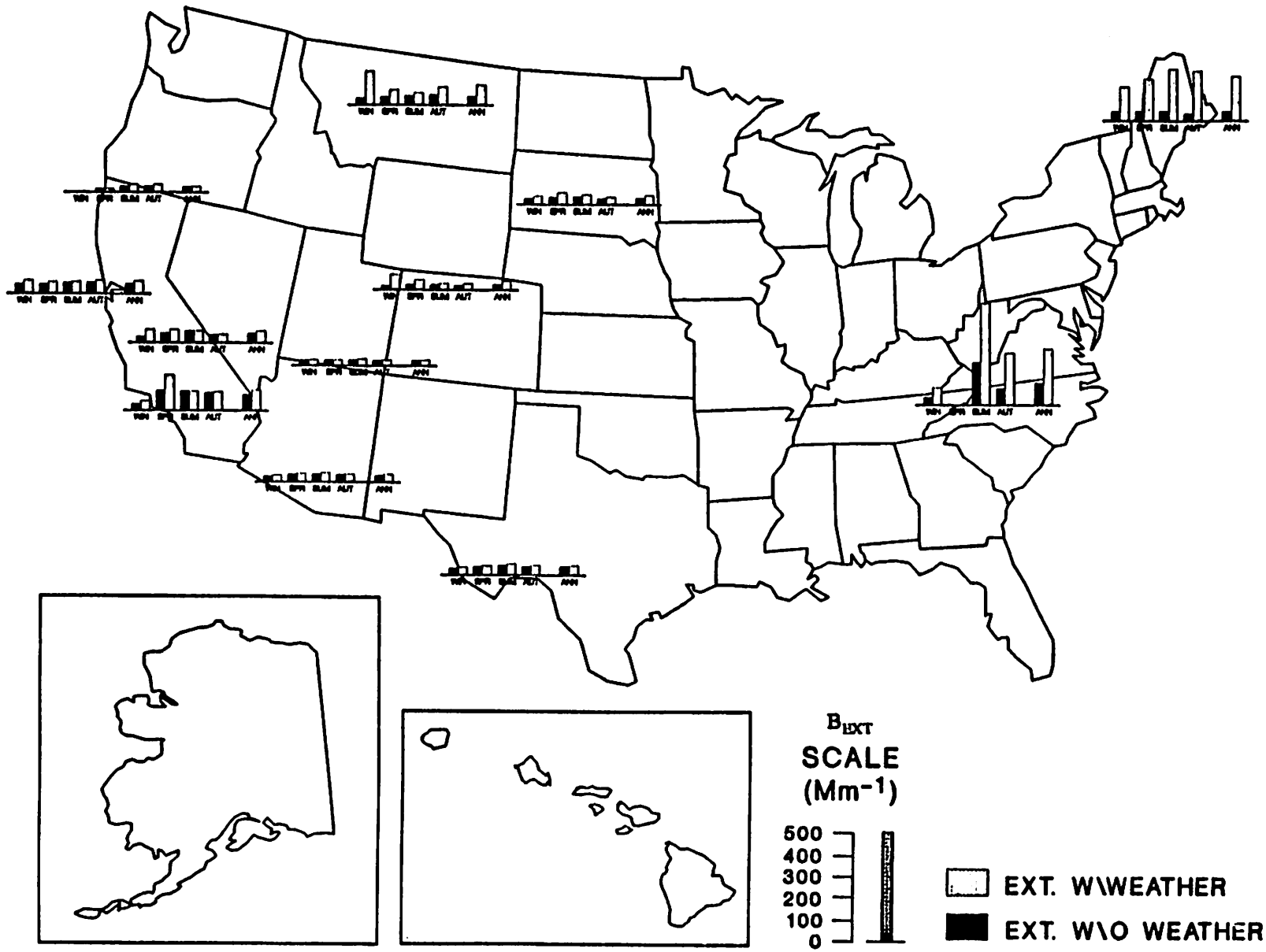


Figure 7.2 Spatial and seasonal variation of measured light extinction coefficient ($Mm^{-1}$) in the United States for the three-year period, March 1988 through February 1991. From left to right, the bars show winter, spring, summer, autumn, and annual averages. Open bars include all time periods; dark bars exclude periods with fog, precipitation, and low clouds.

Table 7.1 Comparison of measured and reconstructed light extinction coefficient ($Mm^{-1}$) averaged over the three-year period, March 1988 through February 1991, by region for every season. Measured values are averages of the daily median extinction, excluding weather-related events. The two versions of reconstructed extinction assume dry organics (D) and 50% wet organics (W), respectively.

| REGION | SEASON | MEASURED | RECON D | RECON W |
|---|---|---|---|---|
| Appalachian | winter | 48 | 49 | 51 |
| | spring | . | . | . |
| | summer | 182 | 144 | 151 |
| | autumn | 92 | 99 | 104 |
| | annual | 123 | 109 | 114 |
| Colorado Plateau | winter | 24 | 24 | 25 |
| | spring | 27 | 25 | 25 |
| | summer | 30 | 30 | 30 |
| | autumn | 27 | 25 | 25 |
| | annual | 27 | 26 | 26 |
| Central Rockies | winter | 18 | 19 | 19 |
| | spring | 24 | 23 | 23 |
| | summer | 28 | 29 | 30 |
| | autumn | 24 | 23 | 23 |
| | annual | 24 | 23 | 24 |
| Pacific Coast | winter | 48 | 42 | 42 |
| | spring | 47 | 37 | 38 |
| | summer | 54 | 41 | 41 |
| | autumn | 52 | 41 | 41 |
| | annual | 50 | 40 | 41 |
| Northeast | winter | 43 | 45 | 47 |
| | spring | 44 | 40 | 41 |
| | summer | 37 | 40 | 42 |
| | autumn | 37 | 39 | 40 |
| | annual | 41 | 42 | 43 |
| Northern Great Plains | winter | 32 | 31 | 32 |
| | spring | 37 | 32 | 32 |
| | summer | 38 | 34 | 35 |
| | autumn | 29 | 30 | 30 |
| | annual | 33 | 31 | 32 |

Table 7.1 Continued

| REGION | SEASON | MEASURED | RECON D | RECON W |
|---|---|---|---|---|
| Northern Rockies | winter | 32 | 35 | 38 |
| | spring | 45 | 39 | 42 |
| | summer | 48 | 36 | 39 |
| | autumn | 53 | 44 | 48 |
| | annual | 46 | 38 | 41 |
| Southern California | winter | 48 | 33 | 33 |
| | spring | 94 | 90 | 92 |
| | summer | 101 | 73 | 74 |
| | autumn | 83 | 56 | 57 |
| | annual | 79 | 61 | 62 |
| Sonoran Desert | winter | 29 | 26 | 27 |
| | spring | 39 | 27 | 27 |
| | summer | 44 | 34 | 34 |
| | autumn | 37 | 28 | 29 |
| | annual | 37 | 29 | 29 |
| Sierra Nevada | winter | 46 | 20 | 20 |
| | spring | 71 | 31 | 32 |
| | summer | 72 | 36 | 36 |
| | autumn | 45 | 31 | 31 |
| | annual | 59 | 29 | 30 |
| West Texas | winter | 34 | 27 | 28 |
| | spring | 48 | 33 | 34 |
| | summer | 54 | 35 | 35 |
| | autumn | 49 | 33 | 33 |
| | annual | 44 | 31 | 32 |

Table 7.2 Comparison of measured and reconstructed standard visual range (SVR) by region for every season, based on averages of the daily median extinction (Table 7.1). Units are kilometers (km).

| REGION | SEASON | MEASURED | RECON D | RECON W |
|---|---|---|---|---|
| Appalachian | winter | 82 | 79 | 77 |
| | spring | . | . | . |
| | summer | 21 | 27 | 26 |
| | autumn | 42 | 40 | 38 |
| | annual | 32 | 36 | 34 |
| Colorado Plateau | winter | 161 | 163 | 159 |
| | spring | 145 | 156 | 155 |
| | summer | 132 | 131 | 130 |
| | autumn | 146 | 156 | 154 |
| | annual | 145 | 151 | 149 |
| Central Rockies | winter | 213 | 208 | 204 |
| | spring | 160 | 170 | 167 |
| | summer | 138 | 134 | 131 |
| | autumn | 163 | 172 | 169 |
| | annual | 165 | 167 | 164 |
| Pacific Coast | winter | 82 | 94 | 92 |
| | spring | 84 | 105 | 104 |
| | summer | 73 | 95 | 94 |
| | autumn | 76 | 97 | 95 |
| | annual | 78 | 98 | 97 |
| Northeast | winter | 90 | 86 | 84 |
| | spring | 90 | 98 | 96 |
| | summer | 106 | 98 | 93 |
| | autumn | 106 | 100 | 97 |
| | annual | 96 | 94 | 91 |
| Northern Great Plains | winter | 123 | 128 | 123 |
| | spring | 106 | 123 | 121 |
| | summer | 102 | 116 | 112 |
| | autumn | 136 | 132 | 129 |
| | annual | 120 | 127 | 123 |

Table 7.2 Continued

| REGION | SEASON | MEASURED | RECON D | RECON W |
|---|---|---|---|---|
| Northern Rockies | winter | 121 | 112 | 103 |
| | spring | 87 | 101 | 93 |
| | summer | 81 | 108 | 101 |
| | autumn | 73 | 90 | 81 |
| | annual | 84 | 103 | 95 |
| Southern California | winter | 81 | 118 | 117 |
| | spring | 42 | 43 | 42 |
| | summer | 39 | 53 | 53 |
| | autumn | 47 | 69 | 69 |
| | annual | 49 | 64 | 63 |
| Sonoran Desert | winter | 136 | 149 | 147 |
| | spring | 100 | 145 | 144 |
| | summer | 90 | 116 | 115 |
| | autumn | 105 | 137 | 136 |
| | annual | 105 | 135 | 134 |
| Sierra Nevada | winter | 85 | 195 | 192 |
| | spring | 55 | 126 | 122 |
| | summer | 54 | 109 | 108 |
| | autumn | 87 | 126 | 124 |
| | annual | 66 | 133 | 131 |
| West Texas | winter | 116 | 143 | 141 |
| | spring | 82 | 117 | 116 |
| | summer | 72 | 113 | 111 |
| | autumn | 80 | 119 | 118 |
| | annual | 89 | 124 | 123 |

Figure 7.2 should also be compared with Figure 6.6 showing reconstructed extinction by region. The relative importance of sulfate in the East is easily noted, as well as that of nitrate in California. The effect of weather upon the extinction is marked in several regions, particularly in the East.

In fact, the measured extinction data can be classified into three broad-based categories, closely tied to the way the weather algorithm handles the data in each category: 1) Western States, 2) Eastern States, and 3) Sites Influenced by Diurnal Haze. These categories are discussed below.

## 7.1 Western Sites

The majority of sites are in this category; they are all located west of the Mississippi River. At these locations, the weather algorithm flags only 10%-20% of the data and has very little effect on the mean extinctions. Figure 7.3 shows a typical weather algorithm plot of western regional data. The most apparent exception to this is the in-canyon transmissometer at Grand Canyon National Park (Figure 7.4). During winter, the measured below-rim extinction is frequently five to ten times higher than the measured extinction above the canyon.

## 7.2 Eastern Sites

Ambient RH levels at Acadia and Shenandoah National Parks are much higher than those at the western monitoring sites (with the notable exception of the Glacier National Park site, whose transmissometer sight path is over Lake McDonald, and close to the water); and this increases the severity of the visual air quality impacts. The weather algorithm flags more data at these sites (up to 70% at Acadia, 80% at Shenandoah) due to a higher frequency of fog, precipitation, and relative humidity above 90%. Figure 7.5 presents a typical weather algorithm plot for data from these sites. Seasonal summaries of Acadia and Shenandoah extinction data are plotted with a different scale than the western sites, to allow for the much higher extinction levels.

## 7.3 Sites Influenced by Diurnal Hazes

Extinction data collected at San Gorgonio Wilderness and Yosemite National Park exhibit a strong diurnal pattern due to daily incursions of severe hazes from areas of high pollution west of the Sierra Nevadas. Large, rapid, and wildly varying fluctuations in measured extinction are caused by these hazes. Thus, the rate of change test in the weather identification algorithm is not used at these sites; only the humidity and maximum extinction flags are used. Figure 7.6 presents an example of this diurnally fluctuating data.

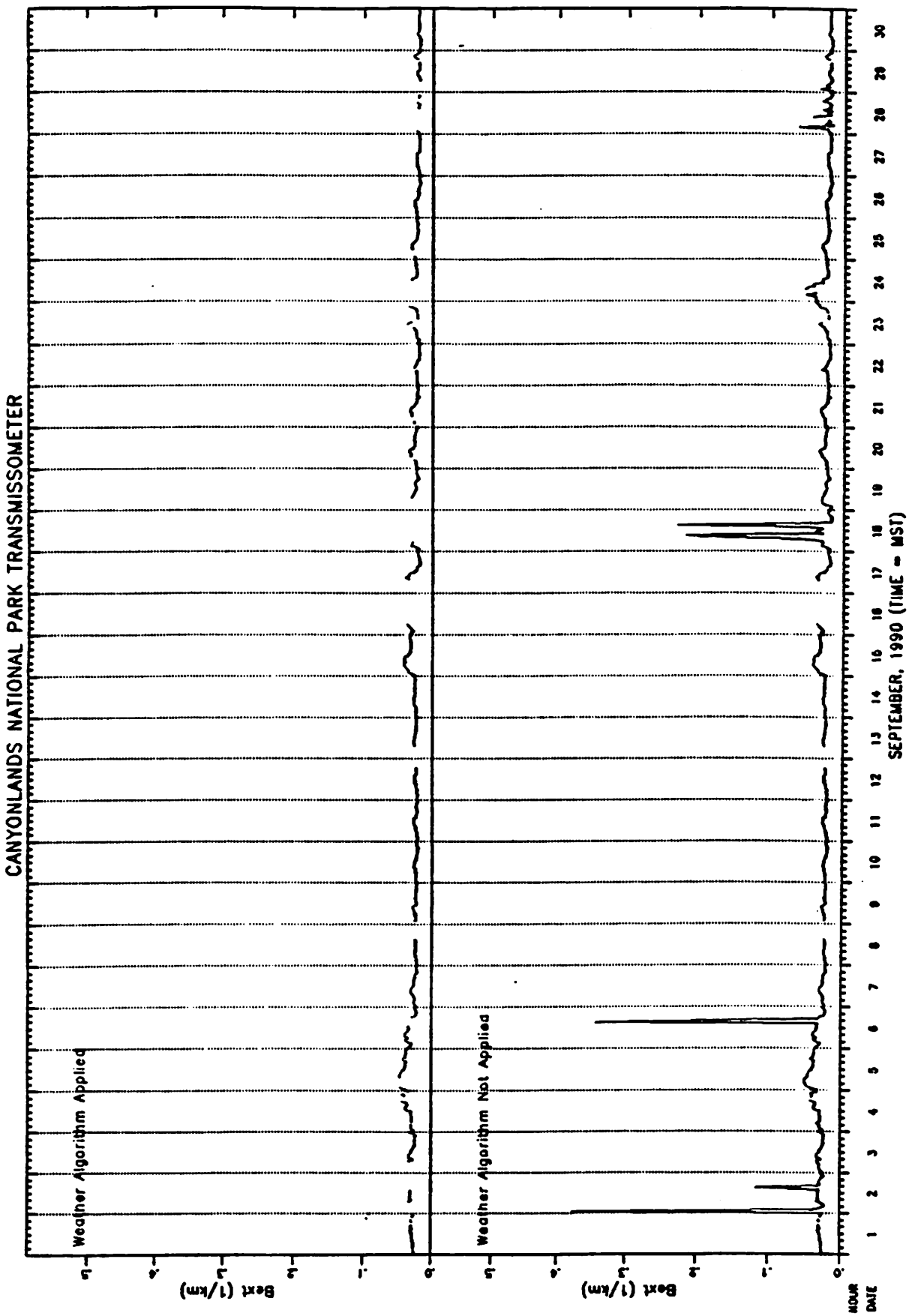


Figure 7.3 Example Weather-Algorithm Plot, Canyonlands National Park, September 1990.

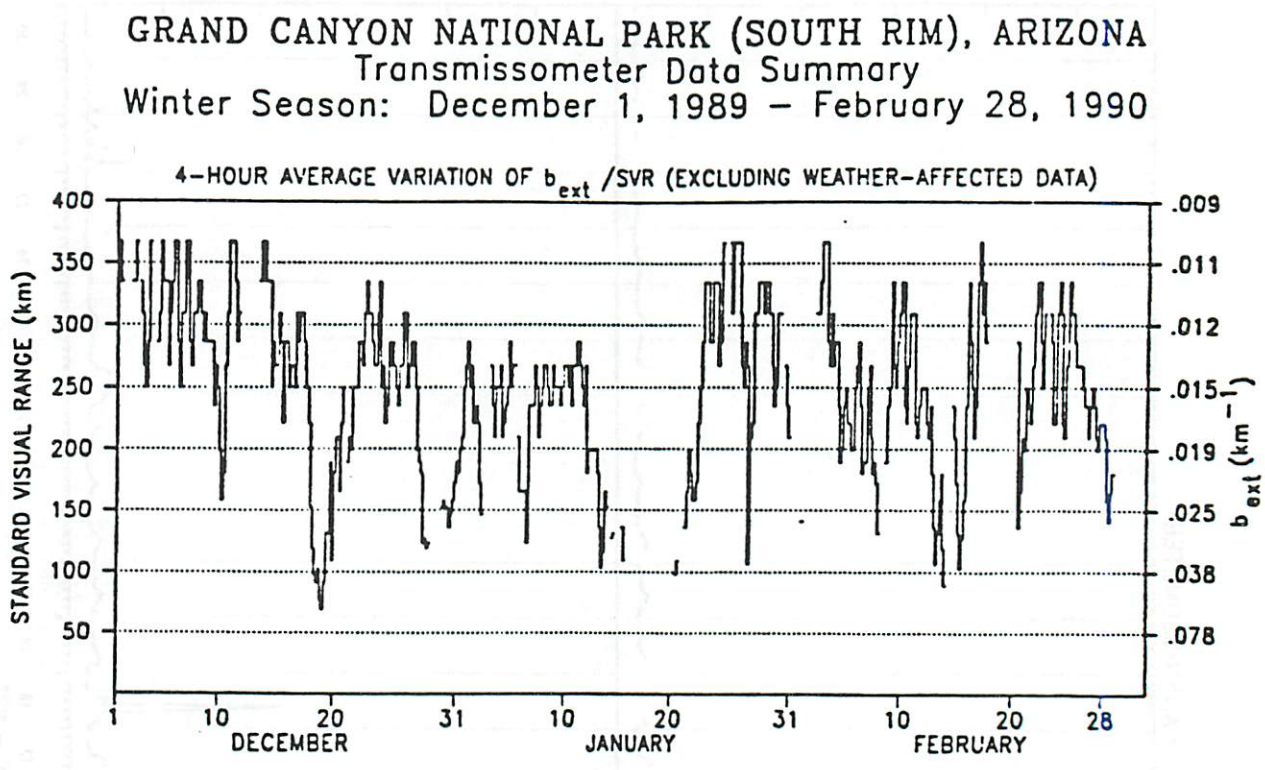


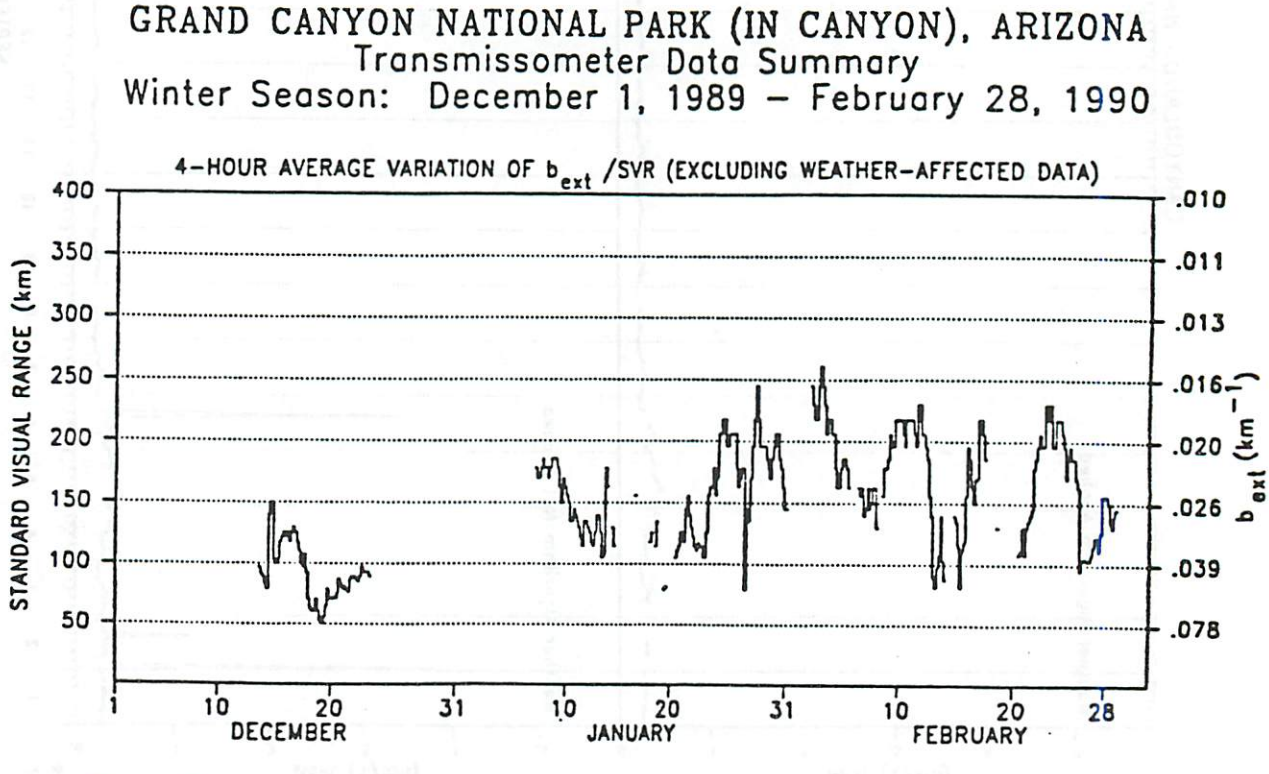


Figure 7.4 Comparison of $b_{ext}$ at Grand Canyon, on Rim vs. In-canyon.

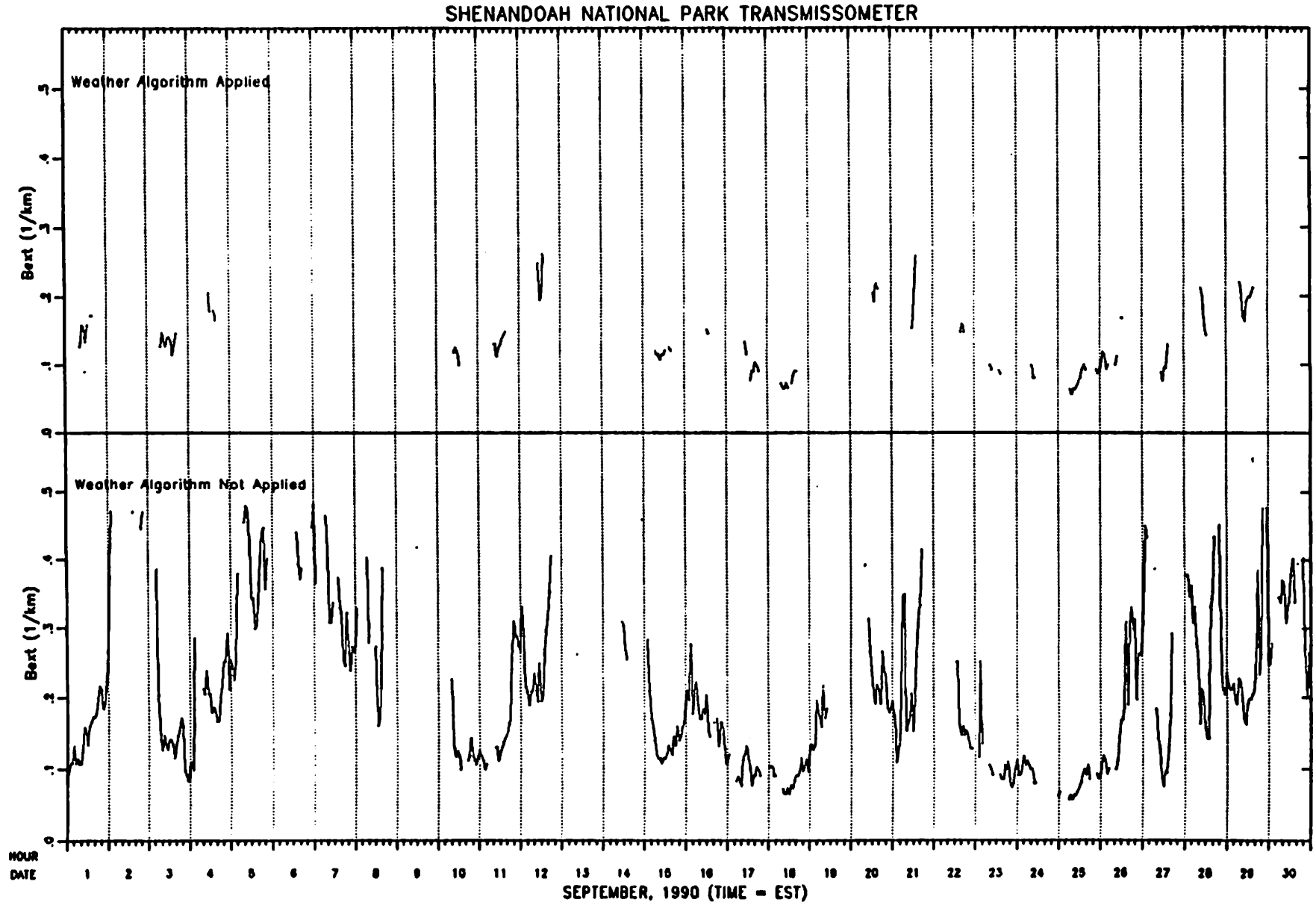


Figure 7.5 Example Weather-Algorithm Plot, Shenandoah National Park, September 1990.

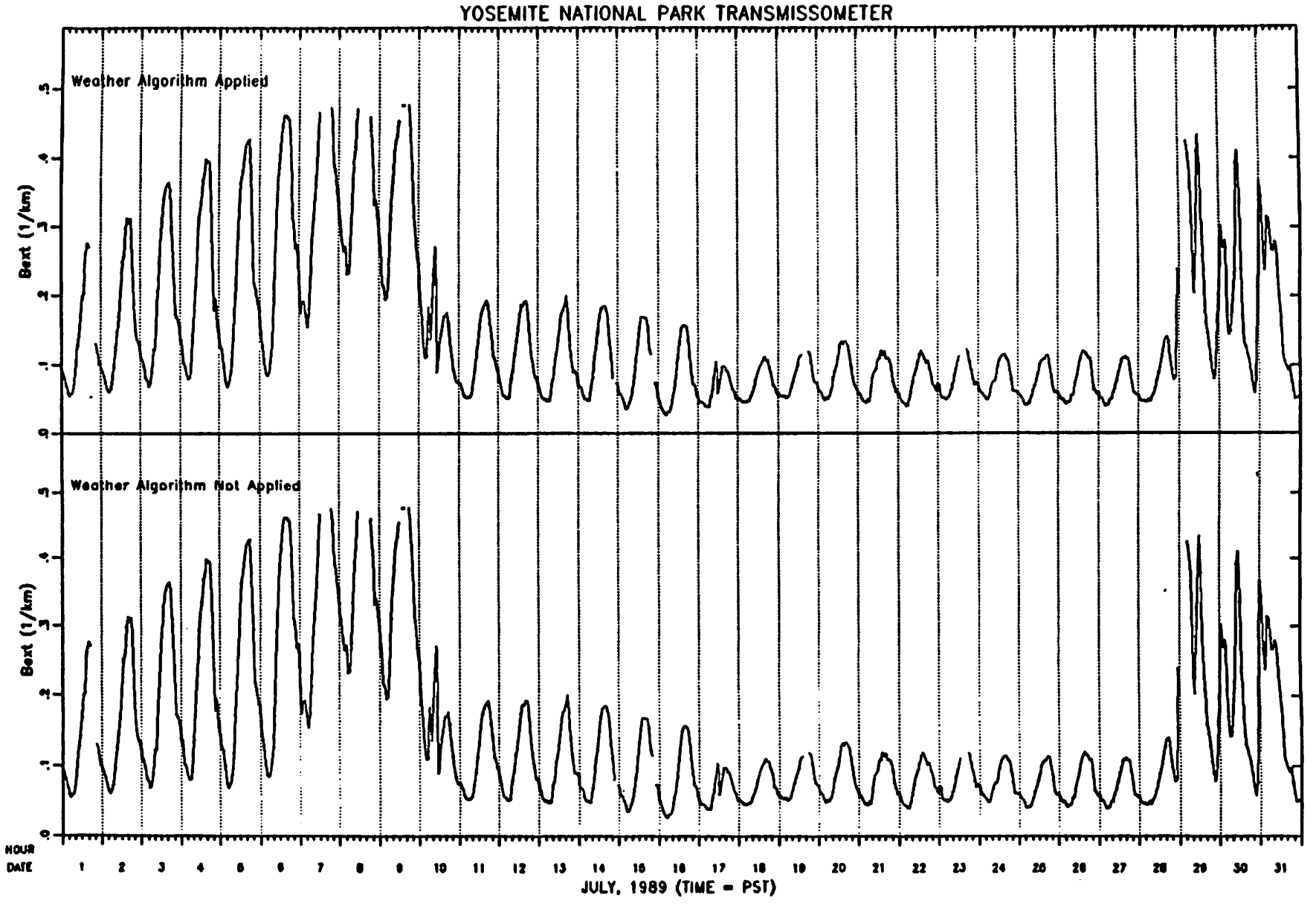


Figure 7.6 Example Weather-Algorithm Plot, Yosemite National Park, July 1989.

# REFERENCES


## Chapter 1

1. Pitchford M.L. and Malm W.C. "Development and applications of a standard visual index," to be published in Atmospheric Environment, 1993.

## Chapter 2

1. Molenar J.V., Cismoski D.S. and Tree R.M. "Intercomparison of ambient optical monitoring techniques," presented at the 84th Annual Meeting of the Air and Waste Management Association Meeting and Exhibition, Kansas City, Mo., June 21-26, 1992.

## Chapter 3

1. Cahill T.A., Eldred R.A. and Feeney P.A. "Particulate monitoring and data analysis for the National Park Service 1982-1985," University of California, Davis, CA, 1986.

2. Chow J.C., Watson J.G., Pritchett L.C., Pierson W.R., Frazier C.A. and Purcell R.G. "The DRI thermal/optical reflectance carbon analysis system: description, evaluation, and applications in U.S. air quality studies," Atmospheric Environment, 1992, in press.

3. Malm W.C., Golestani Y., Gebhart K.A., Cahill T.A., Eldred R.A. and Poirot R. "Estimation of aerosol acidity in the eastern United States," in Proceedings of the 84th Annual Meeting of the Air & Waste Management Association, Vancouver, B.C., 1991.

4. Malm W.C., Sisler J.F. and Mauch L.L. "Assessing the improvement in visibility of various sulfate reduction scenarios," in Proceedings of the 83rd Annual Meeting of the Air and Waste Management Association, Pittsburgh, 1990.

5. Tang I.N., Wong W.T. and Munkelwitz H.R. "The relative importance of atmospheric sulfates and nitrates in visibility reduction," Atmospheric Environment, 15 (12): 2463, 1981.

6. Watson J.G., Chow J.C., Richards L.W., Neff W.D., Andersen S.R., Dietrich D.L. and Olmez I. "The 1987-88 Metro Denver brown cloud study," Desert Research Institute Document No. 8810 1F2, Reno, Nevada, 1988.

## Chapter 4


1. Chow J.C., Watson J.G., Pritchett L.C., Pierson W.R., Frazier C.A. and Purcell R.G. "The DRI thermal/optical reflectance carbon analysis system: description, evaluation, and applications in U.S. air quality studies," Atmospheric Environment, 1992, in press.

2. Eatough E.J., Lewis E.A., Mangelson N.F., Lewis L., Crawford J. and Sun B. "A Comparison of the determination of particulate sulfate and $SO_2$ (g) at Meadview using filter pack and diffusion denuder sampling systems," submitted to Dr. R. Farber, Southern California Edison, Rosemead, Ca., 91770, December, 1991.

3. Turpin B.J., Huntzicker J.J. and Adams K.M. "Intercomparison of photoacoustic and thermal-optical methods for the measurement of atmospheric elemental carbon," Atmospheric Environment, 24A:1831-1835 (7), 1990.


## Chapter 6


1. Hanel G. "The properties of atmospheric aerosol particles as functions of the relative humidity at thermodynamic equilibrium with the surrounding moist air," Advances in Geophysics, 19:73, 1982.

2. NOAA. Climatic Atlas of the United States, ESSA, Department of Commerce - 1968. Reprinted by National Oceanic and Atmospheric Administration, October, 1970.

3. Ouimette J.R. and Flagan R.C. "The extinction coefficient of multicomponent aerosols," Atmospheric Environment, 16:2405, 1982.

4. Sloane C.S. "Change in aerosol optical properties with change in chemical composition," presented at the 78th Annual Meeting of Air Pollution Control Association, 1985.

5. Stelson A.W. and Seinfeld J.H. "Relative humidity and temperature dependence of the ammonium nitrate dissociation constant," Atmospheric Environment 15:983, 1982.

6. Tang I.N., Wong W.T. and Munkelwitz H.R. "The relative importance of atmospheric sulfates and nitrates in visibility reduction," Atmospheric Environment, 15 (12): 2463, 1981.

7. Tsay S., Stephens G.L. and Greenwald T.J. "An investigation of aerosol microstructure on visual air quality," Atmospheric Environment, 25A(56):1039, 1991.

8. vandeHulst H.C. "Light scattering by small particles," Dover Publication, New York, NY, 1981.

9. Wexler A. and Seinfeld J. "Second-generation inorganic aerosol model," Atmospheric Environment, 25A(12):2731, 1991.

10. White W.H. "On the theoretical and empirical basis for apportioning extinction by aerosols: a critical review," Atmospheric Environment, 20:1659, 1986.